AFRPL-TR-73-47

EXPLORATORY DEVELOPMENT FOR THE TECHROLL® SEAL MOVABLE NOZZLE SYSTEM VOLUME I

L.L. SCHOEN
AND
E.B. BAHNSEN, G.E. CONNER, J.L. GRIMSLEY

FINAL REPORT

JUNE 1973

CONTRACT NO. F04611-71-C-0024

AIR FORCE ROCKET PROPULSION LABORATORY

AIR FORCE SYSTEMS COMMAND, UNITED STATES AIR FORCE
EDWARDS, CALIFORNIA, 93523

UTC 2402-FR

EXPLORATORY DEVELOPMENT FOR THE TECHROLL® SEAL MOVABLE NOZZLE SYSTEM VOLUME I

L. L. Schoen
and
E. B. Bahnsen, G. E. Conner, J. L. Grimsley

UTC 2402-FR

FOREWORD

The exploratory development of the TECHROLL® seal (U.S. patent Nos. 3698192 and 3727408) movable nozzle program described herein was conducted by United Technology Center, Sunnyvale, California, under contract No. F04611-71-C-0024. Mr. William F. Payne and Captain Douglas Bailey, MKCC, Air Force Rocket Propulsion Laboratory, were the project officers. This report contains no classified information extracted from other classified documents.

The United Technology Center program manager was Mr. W. B. Grens, and the project engineer was Mr. L. L. Schoen. The United Technology project number is 2402.

This technical report has been reviewed and is approved.

Charles R. Cooke
Chief, Solid Rocket Division
AFRPL/MK

ABSTRACT

The TECHROLL seal is a constant-volume, fluid-filled bearing configured with a pair of rolling convolutes that permits omniaxis deflection of a rocket motor nozzle. The fluid-filled bearing is pressurized by nozzle ejection loads and serves as both the movable nozzle bearing and nozzle seal. The TECHROLL seal is made of a fabric-reinforced elastomeric composite material and does not require complex manufacturing processes or tight tolerances. United Technology Center, under contract to the Air Force Rocket Propulsion Laboratory, has conducted an exploratory development program concerned with the TECHROLL seal. This program consisted of three major phases of technical effort. The first phase included evaluation of candidate seal materials and demonstration of a TECHROLL seal movable nozzle thrust vector control system in tactical missile and strategic missile configurations. The second phase included advanced development of the concept. The third phase was an add-on effort for Naval Weapons Center for the design, fabrication, and test of a TECHROLL movable nozzle with integral actuators capable of omniaxial deflection of 15^{o} and contained within an 8-in.-diameter envelope. The results of this effort will be reported under separate cover later this year. This report covers only phase I and phase II activities. During these two phases, seal material evaluation was completed, and demonstration motor tests of a high-pressure tactical system movable nozzle and a movable nozzle for a second-stage Minuteman motor were conducted at the Air Force Rocket Propulsion Laboratory. Each movable nozzle system was characterized by bench testing prior to firing. Torques, spring rates, and dynamic response characteristics were identified and later verified during static motor tests. In addition, an analytical model describing TECHROLL seal characteristics was developed. All static motor firings were completely successful and verified the performance predictability and low torque characteristics of the TECHROLL seal.

CONTENTS

Section		Page
I	INTRODUCTION AND SUMMARY	1
II	TECHROLL SEAL NOZZLE SYSTEM PERFORMANCE	5
	1. Objectives	5
	2. Background and Description	5
	3. System Characteristics	7
	a. Torque Characteristics	7
	b. Structural Characteristics	11
	4. System Performance	13
	a. Minuteman Second-Stage Nozzle	13
	b. Air-Launched Nozzle (HIPPO)	29
III	TECHROLL SEAL NOZZLE SYSTEM ANALYTICAL MODELING	71
	1. Introduction and Summary	71
	2. Static Firing Simulations	72
	a. Introduction	72
	b. Discussion	72
	c. Limitations	84
	d. Conclusions	86
	3. Movable Nozzle Dynamic Model	86
	a. Introduction	86
	b. Discussion	87
	c. Demonstration	100
	d. Conclusions	127
	4. TECHROLL Parameter Equations	127
	a. Introduction	127
	b. Discussion	127
	c. Limitations and Conclusions	133
IV	EXPLORATORY MATERIALS DEVELOPMENT	135
	1. Objectives	135
	2. Accomplishment Summary	136
	a. Selection Criteria	136
	b. Candidate Materials	138
	c. Material Testing	141
	d. Composite Selection and Testing	155
	e. Testing AFRPL-Furnished Specimens	155
	3. Seal Development	155
	a. Design	155
	b. Fabrication	160
	c. Nondestructive Testing	165
V	COMMERCIAL SOURCE OF SUPPLY	171
	1. Introduction	171
	2. Vendor Selection	171
	3. Fabrication and Test Results	171

CONTENTS (Concluded)

Section		Page
	4. Quantity Manufacturing Costs	175
	5. Fabrication Method	175
VI	CONCLUSIONS AND RECOMMENDATIONS	176
	APPENDIX I: Data Collection and Reduction	179
	APPENDIX II: Equation Derivations	188
	APPENDIX III: Test Methods	205

Unclassified
Security Classification

DOCUMENT CONTROL DATA - R & D

(Security classification of title, body of abstract and indexing annotation must be entered when the overall report is classified)

1. ORIGINATING ACTIVITY (Corporate author)	2a. REPORT SECURITY CLASSIFICATION
United Technology Center	Unclassified
	2b. GROUP

3. REPORT TITLE
Exploratory Development for the TECHROLL® Seal Movable Nozzle System
Volume I

4. DESCRIPTIVE NOTES *(Type of report and inclusive dates)*
Final Report covering the period 15 March 1971 through 30 March 1973

5. AUTHOR(S) *(First name, middle initial, last name)*
L. L. Schoen, E. B. Bahnsen, G. E. Conner, and J. L. Grimsley

6. REPORT DATE	7a. TOTAL NO. OF PAGES	7b. NO. OF REFS
30 June 1973	~~220~~ 236	-

8a. CONTRACT OR GRANT NO.	9a. ORIGINATOR'S REPORT NUMBER(S)
F04611-71-C-0024	UTC 2402 FR
b. PROJECT NO.	
UTC 2402	9b. OTHER REPORT NO(S) *(Any other numbers that may be assigned this report)*
c.	AFRPL-TR-73-47
d.	

10. DISTRIBUTION STATEMENT
This document is subject to special export controls and each transmittal to foreign governments [illegible] with prior approval of AFRPL (RPPR/STINFO), Edwards, California 93523.

11. SUPPLEMENTARY NOTES	12. SPONSORING MILITARY ACTIVITY
	Air Force Rocket Propulsion Laboratory Air Force Systems Command United States Air Force, Edwards, CA 93523

13. ABSTRACT

The TECHROLL seal is a constant-volume, fluid-filled bearing configured with a pair of rolling convolutes that permits omniaxis deflection of a rocket motor nozzle. The fluid-filled bearing is pressurized by nozzle ejection loads and serves as both the movable nozzle bearing and nozzle seal. The TECHROLL seal is made of a fabric-reinforced elastomeric composite material and does not require complex manufacturing processes or tight tolerances. United Technology Center, under contract to the Air Force Rocket Propulsion Laboratory, has conducted a three-phase exploratory development program for the TECHROLL seal. This report covers only phase I and phase II activities. During these two phases, seal material evaluation was completed, and demonstration motor tests of a high-pressure tactical system movable nozzle and a movable nozzle for a second-stage Minuteman motor were conducted at the Air Force Rocket Propulsion Laboratory. Each movable nozzle system was characterized by bench testing prior to firing. Torques, spring rates, and dynamic response characteristics were identified and later verified during static motor tests. In addition, an analytical model describing TECHROLL seal characteristics was developed. All static motor firings were completely successful and verified the performance predictability and low torque characteristics of the TECHROLL seal.

DD FORM 1 NOV 65 1473

Unclassified
Security Classification

14. KEY WORDS	LINK A		LINK B		LINK C	
	ROLE	WT	ROLE	WT	ROLE	WT
movable nozzle						
TECHROLL® seal						
HIPPO						
Minuteman stage 2 motor						
nozzle materials						
omniaxial deflection						
matched-die molding						

ILLUSTRATIONS

Figure		Page
1	TECHROLL Seal Movable Nozzle	6
2	Material and Dimensional Relationships for Minuteman TECHROLL Seal	14
3	TECHROLL Seal Movable Nozzle for Second-Stage Minuteman	15
4	Minuteman TECHROLL Seal Nozzle Hysteresis Torque	19
5	Minuteman TECHROLL Seal Static Firing Torque vs Deflection Angle for Constant Velocity (30.3^{o}/sec)	20
6	Minuteman TECHROLL Seal Hysteresis Torque vs Seal Internal Pressure	21
7	Minuteman TECHROLL Seal Nozzle Axial Movement vs Seal Internal Pressure	22
8	Unacceptable Characteristics Detected by the Axial Spring Test	23
9	Minuteman Motor Chamber Pressure and Seal Internal Pressure vs Time	24
10	Minuteman TECHROLL Seal Bench Test Open Loop Duty Cycle	26
11	Minuteman Nozzle Movements vs Deflection Angle	26
12	Minuteman TECHROLL Seal Total Torque During Bench Test Duty Cycle	27
13	Minuteman Static Firing Duty Cycle, Deflection Angle vs Time	27
14	Minuteman TECHROLL Seal Nozzle Torque During Static Firing	28
15	Minuteman Nozzle Movements During Static Firing	29
16	Prefire View of Minuteman Nozzle Assembly	30
17	Postfire Aft View of Minuteman Nozzle Assembly	30
18	Postfire Front View of Minuteman Nozzle Assembly	30
19	Minuteman Static Test, Expanded Time Plots	31
20	Conventional HIPPO TECHROLL Seal Movable Nozzle Assembly	32
21	HIPPO TECHROLL Seal Configurations	32
22	Material and Dimensional Relationships for the Conventional HIPPO TECHROLL Seal	34
23	Material and Dimensional Relationships for TECHROLL Miniseal	34
24	HIPPO (All-Boost) Hysteresis Torque vs Deflection Angle	38
25	HIPPO (Boost-Sustain) Hysteresis Torque vs Deflection Angle	38

ILLUSTRATIONS (Continued)

Figure		Page
26	HIPPO (High Pressure) Hysteresis Torque vs Deflection Angle	39
27	HIPPO (Miniseal) Hysteresis Torque vs Deflection Angle	39
28	HIPPO (All-Boost) Static Firing, Torque vs Deflection Angle	40
29	HIPPO (Boost-Sustain) Static Firing, Torque vs Deflection Angle	40
30	HIPPO (All-Boost) Axial Displacement vs Seal Internal Pressure	42
31	HIPPO (Boost-Sustain) Axial Displacement vs Seal Internal Pressure	42
32	HIPPO (High Pressure) Axial Displacement vs Seal Internal Pressure	43
33	HIPPO (Miniseal) Axial Displacement vs Seal Internal Pressure	43
34	HIPPO TECHROLL Seal (Boost-Sustain) Lateral Stiffness	44
35	HIPPO TECHROLL Seal (Boost-Sustain) Torsional Stiffness	44
36	HIPPO (All-Boost) Nozzle Static Firing, Chamber Pressure and Seal Internal Pressure vs Time	45
37	HIPPO (Boost-Sustain) Nozzle Static Firing, Chamber Pressure and Seal Internal Pressure vs Time	46
38	HIPPO (Miniseal) Nozzle Static Firing, Chamber Pressure and Seal Internal Pressure vs Time	46
39	HIPPO TECHROLL Seal (All-Boost) Bench Test Duty Cycle	48
40	HIPPO TECHROLL Seal (Boost-Sustain) Bench Test Duty Cycle	48
41	HIPPO TECHROLL Seal (Miniseal) Closed Loop Duty Cycle	49
42	HIPPO (All-Boost and Boost-Sustain) Nozzle Movements vs Deflection Angle	49
43	TECHROLL Seal Lateral Stiffness Effects	50
44	HIPPO TECHROLL (Miniseal) Lateral Stiffness vs Fluid Pressure (Theoretical)	50
45	HIPPO (All-Boost) TECHROLL Seal Total Torque During Bench Test Duty Cycle	52
46	HIPPO (Boost-Sustain) TECHROLL Seal Total Torque During Bench Test Duty Cycle	52
47	HIPPO (Miniseal) $+10^{\circ}$ to -10° Step Response	53
48	HIPPO (Miniseal) -10° to $+10^{\circ}$ Step Response	54
49	HIPPO (Miniseal) 22.2 Hz $\pm 10^{\circ}$ Triangular Wave Response	55

ILLUSTRATIONS (Continued)

Figure		Page
50	HIPPO (Miniseal) 1 through 5 Hz $\pm 3^{o}$ Sine Wave Response	56
51	HIPPO TECHROLL Seal Fluid Damping vs Nozzle Angular Deflection	57
52	All-Boost TECHROLL Seal Nozzle Torque During Static Firing	59
53	Boost-Sustain Nozzle Torque During Static Firing	59
54	HIPPO (Miniseal) Nozzle Torque During Static Firing	60
55	HIPPO (All-Boost) Static Firing, Open Loop Duty Cycle	60
56	HIPPO (Boost-Sustain) Static Firing, Open Loop Duty Cycle	61
57	HIPPO (Miniseal) Static Firing, Closed Loop Duty Cycle	61
58	HIPPO (All-Boost and Boost-Sustain) Nozzle Movements During Static Firing	62
59	Prefire View of HIPPO Nozzle Assembly	62
60	Postfire Aft View of Conventional HIPPO Nozzle Assembly	63
61	Postfire Front View of Conventional HIPPO Nozzle Assembly	63
62	Postfire Aft View of HIPPO Miniseal Nozzle Assembly	64
63	Postfire View of HIPPO Miniseal Nozzle Assembly	64
64	Postfire Front View of HIPPO Miniseal Nozzle Assembly	64
65	All-Boost Static Firing, Expanded Time Plots	65
66	Boost-Sustain Static Firing, Expanded Time Plots	66
67	HIPPO (Miniseal) Static Firing, Expanded Time Plots	67
68	Schematic of TECHROLL Seal Movable Nozzle	72
69	Dynamic Model of TECHROLL Seal Movable Nozzle	74
70	Axial Stiffness of TECHROLL Seal for Minuteman Nozzle	77
71	Rotational Characteristics of TECHROLL Seal for Minuteman Nozzle	77
72	Nozzle Simulation of Minuteman Static Firing	79
73	Nozzle Simulation of Minuteman Static Firing	80
74	Axial Stiffness of TECHROLL Seal for HIPPO Motor	81
75	Rotational Characteristics of TECHROLL Seal for HIPPO Motor	81
76	Nozzle Simulation of HIPPO (All-Boost) Static Firing	82
77	Nozzle Simulation of HIPPO (All-Boost) Static Firing	83
78	Actuator End Stop Stiffness	85

ILLUSTRATIONS (Continued)

Figure		Page
79	Schematic of Baseline Movable Nozzle System	87
80	Movable Nozzle Geometry (Single Axis, Three Degrees of Freedom)	93
81	Movable Nozzle Coordinates (Single Axis, Three Degrees of Freedom)	93
82	Movable Nozzle Dynamic Model (Block Diagram)	101
83	Servovalve Static Flow Gain	103
84	Servovalve Static Pressure Gain	103
85	Servovalve Static Flow Pressure Curves (Model)	104
86	Servovalve Static Flow Pressure Curves (Ideal)	104
87	Servovalve Step Response	105
88	Servovalve Step Response, Flow Limited	105
89	Servoactuator Linearity and Resolution	106
90	Servoactuator Static Friction	106
91	Servoactuator Step Response (Displacement)	107
92	Servoactuator Step Response (Velocity)	107
93	Servoactuator Step Response (Flow)	108
94	Servoactuator Step Response (Pressure)	108
95	Servoactuator Step Response (Pressure)	109
96	Nozzle System Linearity and Resolution	110
97	Nozzle System Rotational Hysteresis and Spring Rate	110
98	TECHROLL Seal Axial Hysteresis and Stiffness	111
99	Nozzle System Step Response (Angular Deflection)	111
100	Nozzle System Step Response, (Angular Velocity)	112
101	Nozzle System Step Response, (Actuation Torque)	112
102	Nozzle System Step Response, (Actuator Displacement)	113
103	Nozzle System Step Response, (Actuator Velocity)	113
104	Nozzle System Step Response, (Actuator Pressure)	113
105	Nominal Parameters	114
106	Amplifier Gain, 10X	115
107	Servovalve Flow Limit, 4X	116
108	Actuator Piston Area, ½X	117

ILLUSTRATIONS (Continued)

Figure		Page
109	Nozzle Inertia, 2X	118
110	Grease Boot Removed	119
111	Seal Hysteresis, 2X	120
112	Rotational Spring Rate (Negative), 2X	121
113	Rotational Spring Rate (Positive), 2X	122
114	Motor Vibration (1 g Axial and Lateral)	123
115	Motor Vibration (2 g Axial and Lateral)	124
116	Motor Vibration (4 g Axial and Lateral)	125
117	Motor Vibration (10 g Axial and Lateral)	126
118	TECHROLL Seal Dimensions	128
119	TECHROLL Seal Shape Coefficient vs Seal Geometry	132
120	Hysteresis Coefficient vs Fabric Thickness	132
121	Material Relationship for TECHROLL Seal	137
122	Elastomer/Reinforcement Fabric Specimen	140
123	Burst Test Fixture for 0.5-In. Convolute	145
124	Flex Cycle Test Fixture	145
125	Burst Strength vs Thickness for Candidate Nylon Fabrics	152
126	Sample of J. P. Stevens Fabric	153
127	Sample of Prodesco Item No. 1 Fabric	153
128	Sample of Prodesco Item No. 2 Fabric	154
129	Sample of Prodesco Item No. 3 Fabric	154
130	Burst Strength vs Thickness for Specimens Furnished by AFRPL	157
131	Burst Specimen Set I	158
132	Burst Specimen, Set II	158
133	Burst Specimen, Set III	159
134	Burst Specimen, Set IV	159
135	Pattern on 45° Bias Flat Stock Fabric	161
136	Cut Fabric and Bead Wires	161
137	Cut Fabric, Bead Wires, and Metal Reinforcement Rings for HIPPO Motor	162
138	Matched-Die Mold	162
139	Fabric Reinforcement Preform	163

ILLUSTRATIONS (Concluded)

Figure		Page
140	Fabric Preform with Reinforcement Ring	163
141	Layup on Mold with Bead Holddown Rings in Place	164
142	Layup Under Vacuum	164
143	Completed Layup Ready for Molding	166
144	Mold Loaded in Heated Hydraulic Press	166
145	Molding the Seal	167
146	Finished Seal Attached to Male Part of Mold	167
147	Finished Seal with Flashing on Outer Surface	168
148	Finished Seal with Flashing on Inner Surface	168
149	TECHROLL Seal for Minuteman and HIPPO Motors	169
150	TECHROLL Seal Assembly, HIPPO Envelope Drawing	172
151	TECHROLL Seal Assembly, Minuteman Envelope Drawing	173

TABLES

Table		Page
I	Test Results	2
II	Torque Equation Coefficients	8
III	Nozzle Structural Characteristics	11
IV	Minuteman Performance Summary	18
V	HIPPO Performance Summary	36
VI	Test Results	70
VII	Minuteman and HIPPO Static Firing Simulation Parameters	75
VIII	Parameters	89
IX	Variables	91
X	Derivatives and Laplace Transforms	95
XI	TECHROLL Geometry Dimensions	129
XII	TECHROLL Material Properties	129
XIII	TECHROLL Seal Parameters	134
XIV	Candidate Materials	139
XV	Effect of Temperature on Tensile Strength and Elongation	142
XVI	Comparison of Manufacturer and UTC Test Data on Tensile Strength and Elongation of Fabric	143
XVII	Effect of Temperature on Burst Strength	144
XVIII	Elastomers: Accelerated Aging and Compatibility with Candidate Fluids - Physical Change	146
XIX	Elastomers: Accelerated Aging and Compatibility with Candidate Fluids - Burst Strength	147
XX	Elastomers: Accelerated Aging and Compatibility with Candidate Greases - Physical Change	148
XXI	Elastomers: Accelerated Aging and Compatibility with Candidate Greases - Burst Strength	149
XXII	Elastomer Material Ranking	150
XXIII	AFRPL-Furnished Specimens	156

ABBREVIATIONS

AFRPL	Air Force Rocket Propulsion Laboratory
DPF	dynamic pressure feedback
DVM	digital voltmeter
EPDM	ethylene-propylene diene monomer
FDT	floating data tape
FM	frequency modulation
HIPPO	high internal pressure producing orifice
ICBM	intercontinental ballistic missile
LVDT	linear variable differential transformer
MEOP	maximum expected operating pressure
N/A	not applicable
NDT	nondestructive test
NWC	Naval Weapons Center
SIP	seal internal pressure
S/N	serial number
TVC	thrust vector control
UTC	United Technology Center

SECTION I

INTRODUCTION AND SUMMARY

This technical report, submitted in accordance with the requirements of item B003, exhibit B to contract No. F04611-71-C-0024, covers activities performed during the period 15 March 1971 through 30 March 1973.

The program for exploratory development of the TECHROLL seal movable nozzle had the following major objectives:

A. Demonstration of a TECHROLL seal movable nozzle TVC system in an ICBM configuration

B. Demonstration of a TECHROLL seal movable nozzle in a tactical missile configuration

C. Development of advanced TECHROLL seal fabrication methods which would result in improved performance, lower costs, and a commercial non-aerospace source for future seal procurement

D. Demonstration of a TECHROLL seal movable nozzle in an 8-in.-diameter configuration for NWC.

The program consisted of three phases. The first phase involved basic seal development in which candidate seal configurations were designed, analyzed, and tested in air-launched tactical missile and ICBM configurations. The second phase was devoted to advanced seal development that included evaluation of seal fabrication and derivation of analytical techniques for future seal design efforts. A third phase add-on provided testweight hardware in an 8-in.-diameter air-launched missile configuration for evaluation by NWC. This phase is the subject of a separate report to be published later this year.

Bench and solid rocket motor testing of the TECHROLL seal movable nozzle were accomplished in all program phases. Bench tests were conducted at UTC; motor firings were conducted at AFRPL and NWC. Table I presents a summary of bench and static test configurations and the test conditions.

This report contains data obtained during the material evaluation activity, bench and static test results of the ICBM-configured TECHROLL seal, and bench and static test results of the three tests of the tactical missile configured nozzle assembly.

The primary objectives of the materials evaluation effort of phase I were to (1) develop the techniques necessary to evaluate quantitatively the acceptability of various seal composite materials for application to the TECHROLL seal system required for air-launched and strategic missile applications and (2) derive a composite seal material capable of satisfying the requirements of the high pressure air-launched motor seal at 75°F. Details of this task are contained in section IV.

TABLE I

TEST RESULTS

Motor Test					
Seal	Chamber Pressure, psia	Duration, sec	Deflection, degrees	Deflection Rate, degrees/sec	Remarks
Minuteman	430 (maximum)	60	±6.5 single axis	30.3	Phase I
Air launch	1,800 (maximum)	20	±12 single axis	58	Phase I
Air launch	1,680/680 (boost/sustain)	20	±11.5 single axis	140	Phase II
Air launch	2,700 (maximum)	20	±6.4 single axis	70	Phase II
Air launch	2,100 maximum (1,600 MEOP TVC)	5.5	±15 omniaxis	762	Phase III

Bench Test					
Seal	Temperature, °F	Chamber Pressure, psia	Deflection, degrees	Deflection Rate, degrees/sec	Remarks
Minuteman	75	1,000	6.5	60	Phase I
Air launch	75	2,000	13	30	Phase I
Air launch	75	2,000	---	---	Tested by Government
Air launch	75	2,000	10.2	60	Subcontractor seal
Air launch	75	2,000	10	140	Phase II (boost-sustain)
Air launch (alternate)	75	3,000	10	---	Phase II
Air launch	75	3,000	10	100	Phase II
Air launch	75	1,600	15	300 to 600	Phase III
Air launch	75	1,600	15	300 to 600	Tested by Government
Air launch	75	20	5 and 10	100 and 30	Phase II (viscous fluids)

Screening tests were performed on elastomers and reinforcement fabrics independently and in combination as composites. The goal was to develop a single seal composite material for use on both the 2,000- and 3,000-psi chamber pressure air-launched motor tests.

The dual seam, high tenacity, nylon-neoprene composite developed during a UTC in-house prototype program was selected for the Minuteman seal material to meet the schedule requirement for a static motor test within 5 months of contract initiation.

The following were the principal results of the phase I materials evaluation:

A. A two-ply nylon-neoprene composite material was developed that was capable of satisfying requirements of the tactical TECHROLL seal configuration at ambient (75°F) temperature.

B. Laboratory test techniques capable of providing seal material comparative ratings were developed and preliminary material design information was obtained.

C. Adequacy of long term aging characteristics of the nylon-neoprene composite material and other composite materials considered for wide temperature range application was verified in conjunction with associated seal fluids and protective greases.

D. A three-ply nylon-neoprene composite material capable of satisfying TECHROLL seal requirements for a tactical motor with 3,000-psi chamber pressure was developed.

E. Data of the relationships between the fabric characteristics (bidirectional strength, weave geometry, etc.) and the general capabilities of a finished seal were obtained.

A TECHROLL seal movable nozzle compatible with a Wing I stage 2 Minuteman motor and a single nozzle aft closure was designed and fabricated. This movable nozzle unit was bench tested at UTC and shipped to AFRPL where it was static tested on the Minuteman motor on 1 October 1971. The Minuteman movable nozzle demonstrated a $\pm 6^{\circ}$ thrust vector deflection at slew rates of 30.3°/sec during a motor burning time of 60 sec.

Similarly, TECHROLL seal movable nozzles were designed in a tactical air-launched configuration for test evaluation on a high pressure HIPPO motor. Two movable nozzle configurations were demonstrated during three motor tests at AFRPL. The first test was conducted on 14 December 1971. A $\pm 10^{\circ}$ nozzle thrust vector deflection at a maximum slew rate of 58°/sec was obtained during a 20-sec all-boost firing at 1,800-psi maximum chamber pressure. A second firing of a similar nozzle on 24 March 1972 demonstrated movable nozzle performance in a boost-sustain motor with a chamber pressure of 1,680 to 700 psi, maximum nozzle deflection of 10°, and maximum slew rate of 142°/sec during the 20-sec test.

The third test demonstrated the TECHROLL seal movable nozzle on an all-boost HIPPO motor operating at a chamber pressure of 2,700 psi for 20 sec. The TECHROLL seal assembly in this unit used a narrow width convolute (miniseal) configuration. The high pressure nozzle demonstrated $\pm 6.4^{\circ}$ deflection at slew rates to 70°/sec during the motor test at AFRPL on 23 March 1973.

The measured TECHROLL seal performance characteristics for all tests compared favorably with pretest predictions.

In conjunction with the experimental data obtained during bench and static testing, a mathematical model of the TECHROLL seal movable nozzle with an open loop control system was developed and is discussed in section III. The model was used to check the performance of each movable nozzle configuration prior to its static test. As bench test and static test firing data became available, nondimensional empirical correction factors were derived to increase model accuracy. The final goal of the analytical effort was to derive expressions for all seal parameters related to actuation torques, nozzle torque characteristics (i.e., inertia, aerodynamics, thrust misalignment, and gravity), and a closed loop servohydraulic actuation system. This goal was met successfully.

The mathematical model is presented in the form of component equations, system equations, functional block diagrams, and analog computer simulations of the TVC systems static test fired during phases I and II.

The phase II effort was devoted to advanced seal development that included further evaluation of seal fabrication methods, evaluation of a commercial source of supply (discussed in section V), derivation of analytical techniques for future seal design efforts, and the 3,000-psi HIPPO motor TECHROLL miniseal test firing.

Phase III provided NWC with testweight hardware for an 8-in.-diameter air-launched missile configuration for both bench and static testing.

Data collection and reduction for bench and static testing are discussed in appendix I. Appendix II presents derivations of equations that were analytically developed to predict some of the key TECHROLL seal parameters. Appendix III outlines the test methods and techniques used to perform bench and static tests for this program.

SECTION II

TECHROLL SEAL NOZZLE SYSTEM PERFORMANCE

1. OBJECTIVES

The objectives of the TECHROLL seal performance evaluation were to (1) characterize and quantify seal motions and torques, (2) demonstrate seal structural integrity during overpressure conditions, and (3) demonstrate system operational characteristics during static test firing conditions. These objectives were achieved through a series of analytical studies, selective bench tests, and static test firings. The data obtained from these studies and tests were used in formulation of the analytical model for each system.

2. BACKGROUND AND DESCRIPTION

A brief description of the TECHROLL seal is presented in this section to orient the reader not familiar with the basic design and operation of this unit.

The TECHROLL seal (figure 1) is a constant volume, fabric reinforced, elastomeric bladder configured with two rolling convolutes that permit omniaxial deflection of a movable nozzle system. The bladder is filled with an incompressible fluid and serves the dual function of movable nozzle bearing and hot gas seal in a rocket motor installation. During nozzle vectoring, the fluid flows around the seal maintaining the constant volume geometry. Unpressurized during storage, the TECHROLL seal is pressurized by nozzle ejection loads produced during firing. The fabric reinforced seal is supported structurally in all areas except at the rolling convolute, and the small width of the convolute allows low tensile forces to occur in the elastomer coated reinforcement cloth. These forces characteristically are less than 500 lb/linear in., which is well within the state of the art of nylon, rayon, or dacron reinforced materials. The elastomeric coating is used as a filler to prevent leakage through the weave in the reinforcing cloth.

A key feature of the TECHROLL seal movable nozzle is its low inherent torque. Lowest seal torques occur when the convolutes are placed on a common plane.

Because of the change in momentum of the gas stream an aerodynamic side force occurs in movable nozzles when they are deflected. The resultant side force is near the throat on conventional nozzles. The TECHROLL seal pivot point may be located at the throat area or at the location of the resultant side force, thereby reducing the aerodynamic torque component due to the very small moment arm. This reduced torque feature contrasts with the conventional elastometallic joint (alternating spherical layers of rubber and metal) where aerodynamic torque ranges are 1 to 5 times greater than for the seal torque. The elastometallic joint design requires the layers of rubber and metal to be compressed to ensure seal integrity. This constraint precludes location of the elastometallic joint pivot point in the throat area and results in high aerodynamic torques.

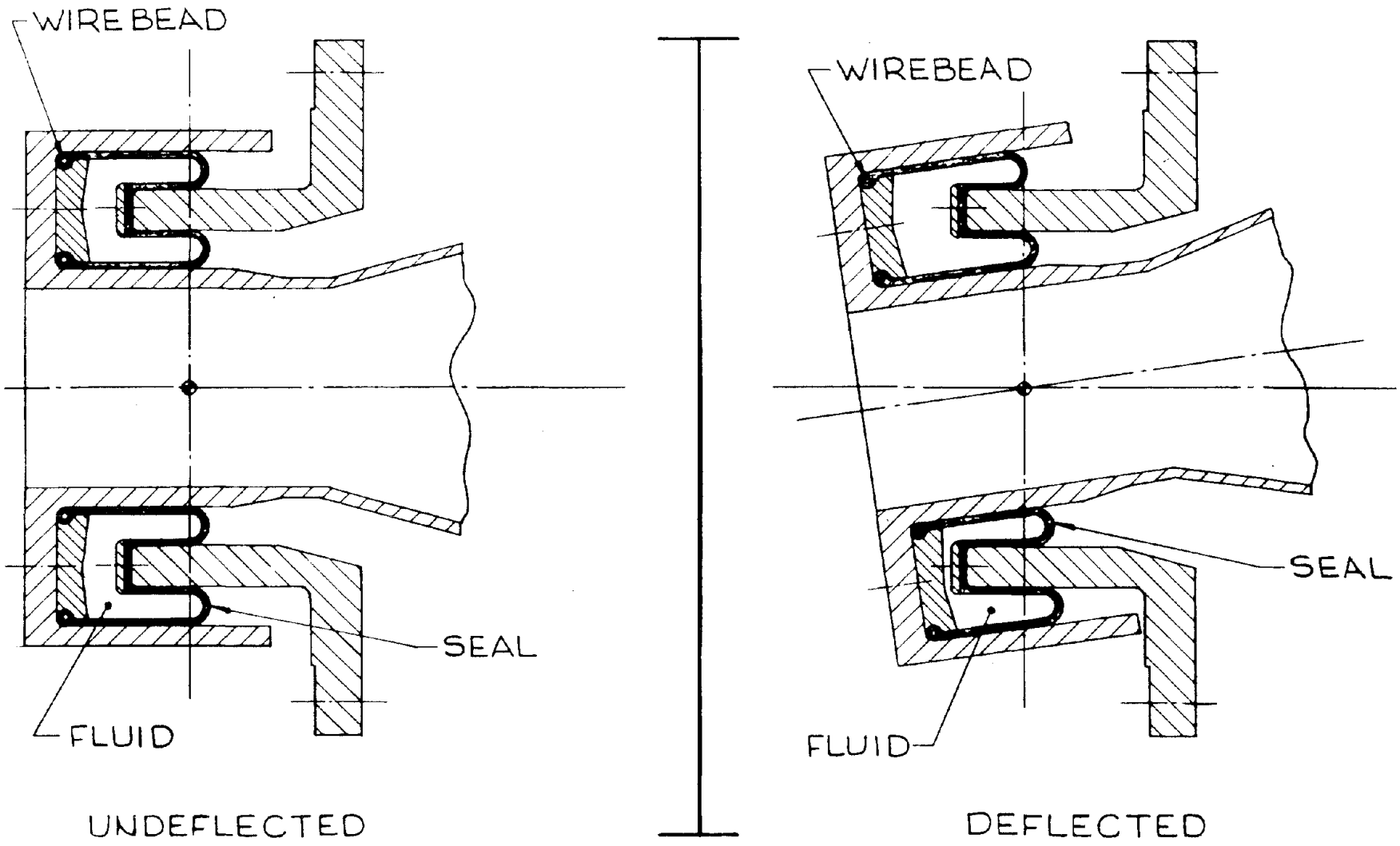

Figure 1. TECHROLL Seal Movable Nozzle

Thermal protection of the TECHROLL seal from the chamber exhaust gases was provided by a barrier of silicone grease retained by a carbon cloth or rubber wiper. A variety of alternate, simplified design approaches are available.

The fluid used in the TECHROLL seal is selected for long term storage compatibility with the seal elastomeric coating. Silicone hydraulic oil has been used successfully in this test program and has industry-proven 10-year compatibility with many rubber coatings. A feature of the silicone oil is the wide range of fluid viscosity available, from 5 to 200,000 centistokes, which allows specific selection to achieve system damping if required. During storage, the potential for the fluid loss in the TECHROLL seal is minimal since the seal is essentially unpressurized.

3. SYSTEM CHARACTERISTICS

A discussion of the torque-associated performance parameters and load-induced movements is presented in this subsection to describe clearly the functional and operational characteristics of the TECHROLL seal as part of a missile control system. The torque required to rotate the movable nozzle over the range of nozzle deflection angle (θ_N), nozzle angular velocity ($\dot{\theta}_N$), and angular acceleration ($\ddot{\theta}_N$) required by the missile guidance system is of primary importance

Additional seal structural characteristics of interest include the seal stiffness (motion resulting from load) when loaded along the centerline (axially), perpendicular to the centerline (laterally), and around the centerline (torsionally); the resulting pivot point location during nozzle actuation; and the pressure generated within the seal cavity in reaction to nozzle loads.

The performance of each of these pertinent system characteristics was evaluated either analytically or experimentally, or by a combination of both techniques, if practical.

a. Torque Characteristics

The angular deflection performance of the TECHROLL seal movable nozzle can be expressed by a general torque equation which identifies coefficients relating static and dynamic nozzle conditions to torque. These coefficients represent inertia, damping, spring rate, friction, and offset torque terms which can be derived analytically and/or experimentally. Table II presents a summary of these terms as they relate to the following torque equation, and shows the method of determination.

$$T_T = I_T\ddot{\theta}_n + B_T\dot{\theta}_N + K_T\theta_N + T_{HT}\left[\frac{\dot{\theta}}{\dot{\theta}}\right] + T_O + T_M + T_{OM} \quad \text{in.-lb}$$

(1) Total Inertia

The total inertia (I_T) is composed of the inertias of the nozzle (I_N), boot (I_B), and TECHROLL seal fluid (I_S). The inertias of the nozzle and boot were determined analytically by calculating the inertias of all movable components about their centers of mass and by translating

TABLE II

TORQUE EQUATION COEFFICIENTS

Coefficient	Description	Method of Determination	Unit
$I_T = I_N + I_B + I_S$	Total inertia	---	in.-lb/sec^2/rad
I_N	Nozzle inertia	Theoretical	in.-lb/sec^2/rad
I_B	Boot inertia	Theoretical	in.-lb/sec^2/rad
I_S	Seal inertia	Theoretical and bench test	in.-lb/sec^{2}rad
$B_T = B_S + B_B + B_{AI} + B_{AE}$	Total damping	---	in.-lb-sec/rad
B_S	Seal damping	Theoretical and bench test	in.-lb-sec/rad
B_B	Boot damping	Static test	in.-lb-sec/rad
B_{AI}	Internal aerodynamic damping	Static test	in.-lb-sec/rad
B_{AE}	External aerodynamic damping	N/A	---
$K_T = K_S + K_B + K_{AI} + K_{AE} + K_M$	Total spring rate	---	in.-lb/degree
K_S	Seal spring rate	Bench test	in.-lb/degree
K_B	Boot spring rate	---	in.-lb/degree
K_{AI}	Internal aerodynamic spring rate	Static test	in.-lb/degree
K_{AE}	External aerodynamic spring rate	N/A	in.-lb/degree
K_M	Mass induced spring rate	Theoretical	in.-lb/degree
T_{HT}	Total seal hysteresis torque	Bench test	in.-lb
T_O	Seal offset torque	Bench test	in.-lb
T_M	Thrust misalignment torque	Static test	in.-lb
T_{OM}	Mass induced offset torque	Theoretical	in.-lb
T_T	Total torque	Static test	in.-lb

that inertia to the assumed or observed pivot point. No experimental verification of nozzle and boot inertias was conducted. The inertia of the seal fluid was determined analytically by the following equation, the derivation of which is contained in appendix II:

$$I_S = \pi K_C K_A \frac{\rho W R^5}{h} \quad \text{in.-lb-sec/rad}$$

where:

K_C = seal cone angle coefficient

K_A = acceleration deflection coefficient

ρ = fluid density, lb-sec^2/in.^{4}

W = seal cavity width, in.

R = seal mean radius, in.

h = seal cavity height, in.

The accuracy of the equation was evaluated by special testing.

(2) Total Damping

The total damping (B_T) is composed of the damping contributed by the TECHROLL seal fluid (B_S), boot (B_B), internal aerodynamics (B_{AI}), and external aerodynamics (B_{AE}). The fluid used to fill the TECHROLL seal fluid was analytically determined by the following equation, the derivation of which is contained in appendix II:

$$B_S = 12\pi K_C K_{S_H} K_V \frac{\mu W R^5}{h^3} \quad \text{in.-lb-sec/rad}$$

where:

K_{SH} = seal shape coefficient

K_V = velocity deflection coefficient

μ = fluid viscosity, lb-sec/in.^{2}

The accuracy of the equation was later verified by special testing. The boot and internal aerodynamic damping were not investigated independently; however, their combined effect was measured during the static tests. (The damping due to external flow around the nozzle did not apply to static test conditions.)

(3) Total Spring Rate

The total spring rate (K_T) is composed of the spring rates of the TECHROLL seal (K_S), boot (K_B), nozzle internal aerodynamics (K_{AI}), nozzle external aerodynamics (K_{AE}), and the mass-induced spring rate (K_M). The TECHROLL seal exhibits the characteristics of a spring due to the nonsymmetrical pressure area relationship when the seal is deflected. The spring rates of the TECHROLL seal and boot were determined independently during bench testing. The nozzle aerodynamic spring rate is due to the change in momentum of the gas stream when the nozzle is deflected. The spring rate due to nozzle internal aerodynamics was measured during static testing. The spring rate due to nozzle external aerodynamics did not apply to static test condition. The mass-induced spring rate (K_M) was derived analytically from the following basic equation:

$$K_M = M_n L_g g_a / 57.3 \text{(in.-lb /degree)}$$

where:

M_n = movable nozzle mass, lb

L_g = pivot point to mass center distance, in.

g_a = axial acceleration field, g

(4) Seal Hysteresis Torque

Due to the static friction inherent in TECHROLL seal materials and the friction between the seal and its confining metal case, torque must be applied before the nozzle deflects. The seal hysteresis torque (T_{HT}) is defined as that amount of torque which must be applied to achieve first motion. This torque was determined experimentally during bench testing.

(5) Seal Offset Torque

Slight nonsymmetries in the TECHROLL seal create a small amount of torque that must be counteracted to hold the nozzle at the null position. This seal offset torque (T_O) was experimentally determined during bench testing.

(6) Thrust Misalignment Torque

Misalignment between the motor grain and the nozzle throat causes the exhaust stream to create a torque which also must be counteracted to hold the nozzle in the null position. This thrust misalignment torque (T_M) was measured during the static firing.

(7) Mass-Induced Offset Torque

When a lateral acceleration field exists between the motor and nozzle, such as in horizontal testing, a torque must be applied to hold the nozzle in the null position. This mass-induced offset torque (T_{OM}) was determined analytically from the following basic equation:

$$T_{OM} = M_n L_g g_L \cos \theta_N \quad \text{in.-lb}$$

where:

M_n = movable nozzle mass, lb

L_g = pivot point to mass center distance, in.

g_L = lateral accelerator field, g

θ_N = nozzle deflection angle, degree

b. Structural Characteristics

The structural characteristics of the TECHROLL seal movable nozzle can be expressed by its axial, lateral, and torsional stiffness and by its internal pressure results from nozzle loading. Table III presents a summary of these terms and identifies the method of determination.

TABLE III

NOZZLE STRUCTURAL CHARACTERISTICS

Coefficient	Description	Method of Determination	Unit
Stiffness	Axial (K_{SA})	Bench test	psi/in.
Stiffness	Lateral (K_{SL})	Bench test	lb/in.
Stiffness	Torsional (K_{ST})	Bench test	in.-lb/degree
Pressure	Seal, internal (P_I)	Theoretical, bench and static tests	psi

(1) Axial Stiffness

The axial stiffness (K_{SA}) relates the axial load, expressed in terms of seal pressure, to the axial movement of the seal. It is defined as:

$$K_{SA} = \frac{P_I}{X_{SA}} \quad \text{psi/in.}$$

where:

P_I = seal internal pressure, psi

X_{SA} = nozzle axial movement, in.

The axial stiffness was determined experimentally during bench and static testing.

(2) Lateral Stiffness

The lateral stiffness (K_{SL}) relates induced nozzle lateral loads to the lateral motion of the nozzle. It is defined as:

$$K_{SL} = \frac{F_L}{X_{SL}}$$

where:

F_L = lateral load, lb

X_{SL} = nozzle lateral movement, in.

The lateral stiffness was determined experimentally during a special bench test.

(3) Torsional Stiffness

The torsional stiffness (K_{ST}) relates any moment applied around the nozzle centerline to the torsional rotation of the nozzle. It is defined as:

$$K_{ST} = \frac{M_T}{\phi}$$

where:

M_T = moment about nozzle centerline, in.-lb

ϕ = nozzle rotation about centerline, degree

The torsional stiffness was determined experimentally by a special bench test.

(4) Seal Internal Pressure

The seal internal pressure (P_I) results from nozzle loads induced by the gas dynamics of the motor. This pressure as derived by the equation presented in appendix II. Static firing data obtained later verified the accuracy of this equation to be within 5%.

4. SYSTEM PERFORMANCE

Two movable nozzle configurations were selected for the evaluation of the TECHROLL seal. One configuration was compatible with the envelope of a Wing 1 stage 2 Minuteman motor with an aft closure modified to accept a single submerged nozzle. The second was typical of a nozzle configuration found in an air-launched missile. These two movable nozzle assemblies, incorporating TECHROLL seals, were fabricated and underwent extensive bench and static testing. A description of the design and performance of each of these units follows:

a. Minuteman Second-Stage Nozzle

(1) Design

An existing, fixed, Air Force Minuteman test nozzle was redesigned to incorporate a TECHROLL seal (figure 2) to provide one plane deflection capability as shown by the nozzle assembly of figure 3.

(a) Changes

The major changes to the existing Air Force test nozzle configuration consisted of:

Steel shell modifications: Addition of a steel housing for the TECHROLL seal, elimination of the flange on the exit cone, and design of a separate steel adapter to attach the nozzle/TECHROLL seal assembly to the test motor aft closure

Monolithic nose cap: The design of a monolithic nose cap to protect the forward face of the seal housing which replaced two separate components (nose cap and entrance ring) in the Air Force design

Insulation: New insulation on the submerged portion of the nozzle to provide thermal protection for the seal housing

Exit cone materials: At the direction of the Air Force project officer, carbon-phenolic tape MX4926 replaced graphite-phenolic tape FM5228 as the throat insert material. The exit cone materials, MX4926 and MXA6012 asbestos-phenolic tape, were those

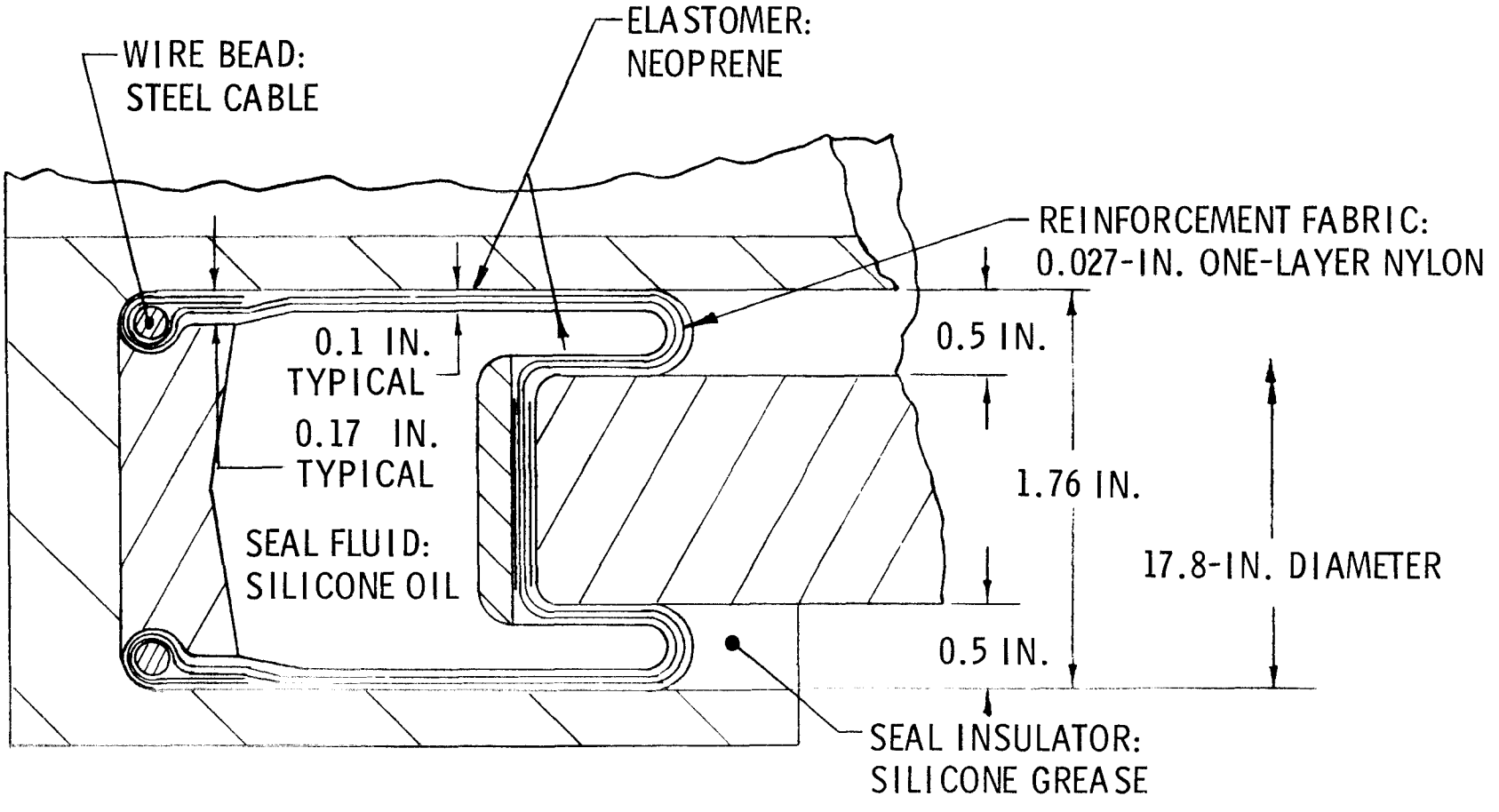

Figure 2. Material and Dimensional Relationships for Minuteman TECHROLL Seal

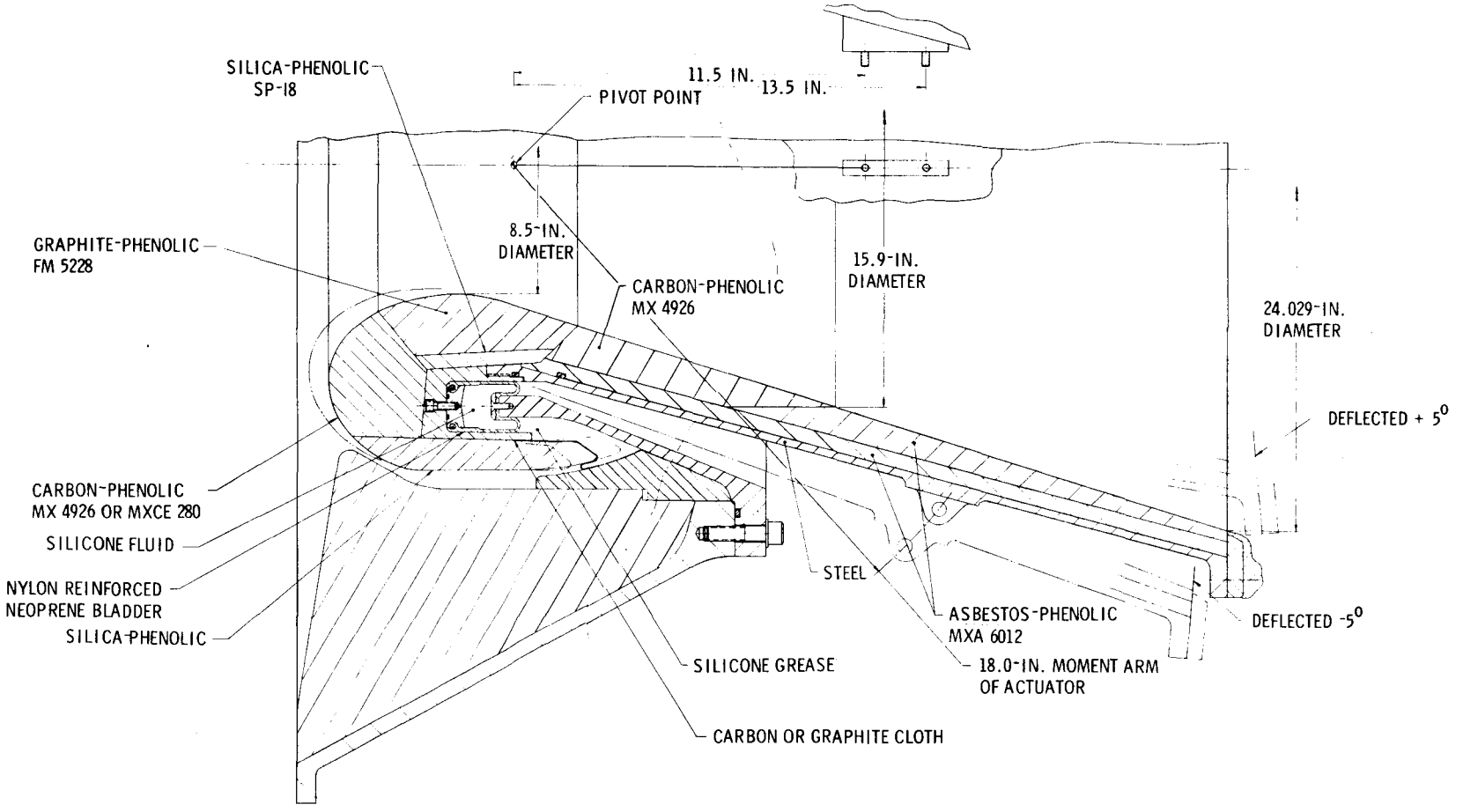

Figure 3. TECHROLL Seal Movable Nozzle for Second-Stage Minuteman

specified in the original design. Throat diameter (8.5 in.), exit cone half-angle (17^{o} 30'), exit cone expansion ratio (8.0), and wrap angles (0^{o} nominal) also remained the same.

(b) New Components

The new components required by addition of the TECHROLL seal consisted of:

Nose cap: The nose cap was fabricated from MXCE-280, an elastomeric modified carbon-phenolic molding compound. The nose cap was bonded to the steel housing using EA913, an epoxy adhesive, and was supported mechanically in a radial direction by a 5^{o} taper on the forward face of the housing.

Insulation: Thermal protection for the seal housing on the submerged side was provided by a silica-phenolic tape, FM5404, wrapped 0^{o} to the nozzle centerline. It was bonded to the seal housing and the nose cap by EA913 adhesive. The forward end of this component provided additional radial support for the nose cap.

Nozzle shell: The shell was designed as a two-piece configuration consisting of (1) a seal housing fabricated from 4340 steel heat treated to 150,000-psi ultimate tensile strength, and (2) an exit cone shell fabricated from 4130 steel heat treated to 120,000-psi ultimate tensile strength. The seal housing was an integral unit attached to the exit cone shell through a threaded joint located slightly aft of the throat plane. This joint location allowed the exit cone to be attached after complete assembly of the seal components to the aft closure adapter. The exit cone shell included an integral thickened ring in the plane of the TVC actuator attach point. This ring limited shell deflection due to actuation loads and prevented strain failure in the exit cone liner materials.

Aft closure adapter: The aft closure adapter was basically a 22^{o} half-angle reverse cone. It adapted the TECHROLL seal nozzle to the aft closure, supported the seal, and transmitted the nozzle ejection loads to the aft closure. It was fabricated from 4340 steel and was heat treated to 150,000-psi ultimate tensile strength.

Adapter insulation: Thermal protection for the submerged side of the aft closure was provided by a component of silica-phenolic tapewrapped 0^{o} to the nozzle centerline. This component was contoured to provide a rolling surface for the grease rentention cloth and support for the grease cavity during assembly of the nozzle to the aft closure. The insulation was bonded to the adapter with EA913 adhesive.

Grease retention cloth: The grease retention cloth was carbon cloth (CCA-1). The cloth acted as a thermal barrier and retained the silica grease placed in the cavity to provide thermal protection for the seal convolute.

(2) Performance

The performance requirements for the Minuteman TECHROLL seal movable nozzle assembly were:

Maximum motor pressure, psia	1,000
Duration, sec	60
Maximum nozzle deflection angle, degree	5
Maximum nozzle velocity, degree/sec	20
Operating temperature, $^{\circ}F$	75

These performance objectives dictated by the Air Force's consideration of the use of a similar configured TECHROLL seal for their C-3 demonstrator program were achieved during a static firing conducted at AFRPL on 1 October 1971. Bench testing prior to the static firing served to verify system readiness for static firing as well as to quantify some of the performance parameters discussed in section III. Table IV presents a summary of the torque equation coefficients and nozzle structural characteristics obtained by analyses, bench, and static test. The following subsections present and discuss the methods by which these coefficients and characteristics were obtained.

(a) Torque coefficients

Total inertia (I_T): The total inertia consisted of the combined nozzle and boot inertias and the seal fluid inertia. The calculated inertia of the combined nozzle and boot ($I_N + I_B$) was 156.3 in.-lb-sec^2, and the inertia of the seal fluid (I_S) was 16.8 in.-lb-sec^2.

Total damping (B_T): The total damping consisted of the combined boot and nozzle internal aerodynamic damping and the seal damping. Damping of the seal (B_S) was calculated to be 176 in.-lb-sec. The combined damping of the boot and nozzle internal aerodynamic ($B_B + B_{AI}$) was obtained by subtracting the seal damping from the total damping measured during the static firing and was 7,659 in.-lb-sec. The nozzle external aerodynamic damping (B_{AE}) did not apply to the static test mode.

Spring rate (K_T): The total spring rate consisted of the seal, boot, and internal aerodynamic spring rates. The spring rate of the seal (K_S) was obtained from the hysteresis torque test data described in the next subsection. This spring rate, represented by the slope of the hysteresis box, was found to be essentially zero on all Minuteman specimens, as shown by the nearly vertical line describing torque as a function for deflection (figure 4).

TABLE IV

MINUTEMAN PERFORMANCE SUMMARY

Item	Value
Motor Firing Test Conditions	
Motor chamber pressure, psi	430
Duration, sec	60
Temperature, ^{o}F	75
Demonstrated TVC	
Maximum deflection, degree	6.5
Maximum velocity, degree/sec	30.3
Torque Equation Coefficients	
I_N, nozzle inertia, in.-lb-sec^2	72.3 bench test
$(I_N + I_B)$, nozzle + boot inertias, in.-lb-sec^2	156.3 static test
I_S, seal fluid inertia, in.-lb-sec^2	16.8
B_S, seal damping, in.-lb-sec	176
$(B_B + B_{AI})$, boot + internal aerodynamic damping, in.-lb-sec	7,659
B_{AE}, external aerodynamic damping, in.-lb-sec	N/A
K_S, seal spring rate, in.-lb/degree	0
$(K_B + K_{AI})$, boot + internal aerodynamic spring rate, in.-lb/degree	527
K_{AE}, external aerodynamic spring rate, in.-lb/degree	N/A
K_M, mass induced spring rate, in.-lb/degree	53.7
T_{HT}, seal hysteresis torque, in.-lb	1,250
T_O, seal offset torque, in.-lb	-160
T_M, thrust misalignment torque, in.-lb	3,230
T_{OM}, mass induced offset torque, in.-lb	3,070
Nozzle Structural Characteristics	
K_{SA} seal axial stiffness, psi/in.	5,220
K_{SL} seal lateral stiffness, lb/in.	Not tested
K_{ST}, seal torsional stiffness, in.-lb/degree	Not tested
P_I, seal internal pressure, psia	1,100 static test 1,600 bench test

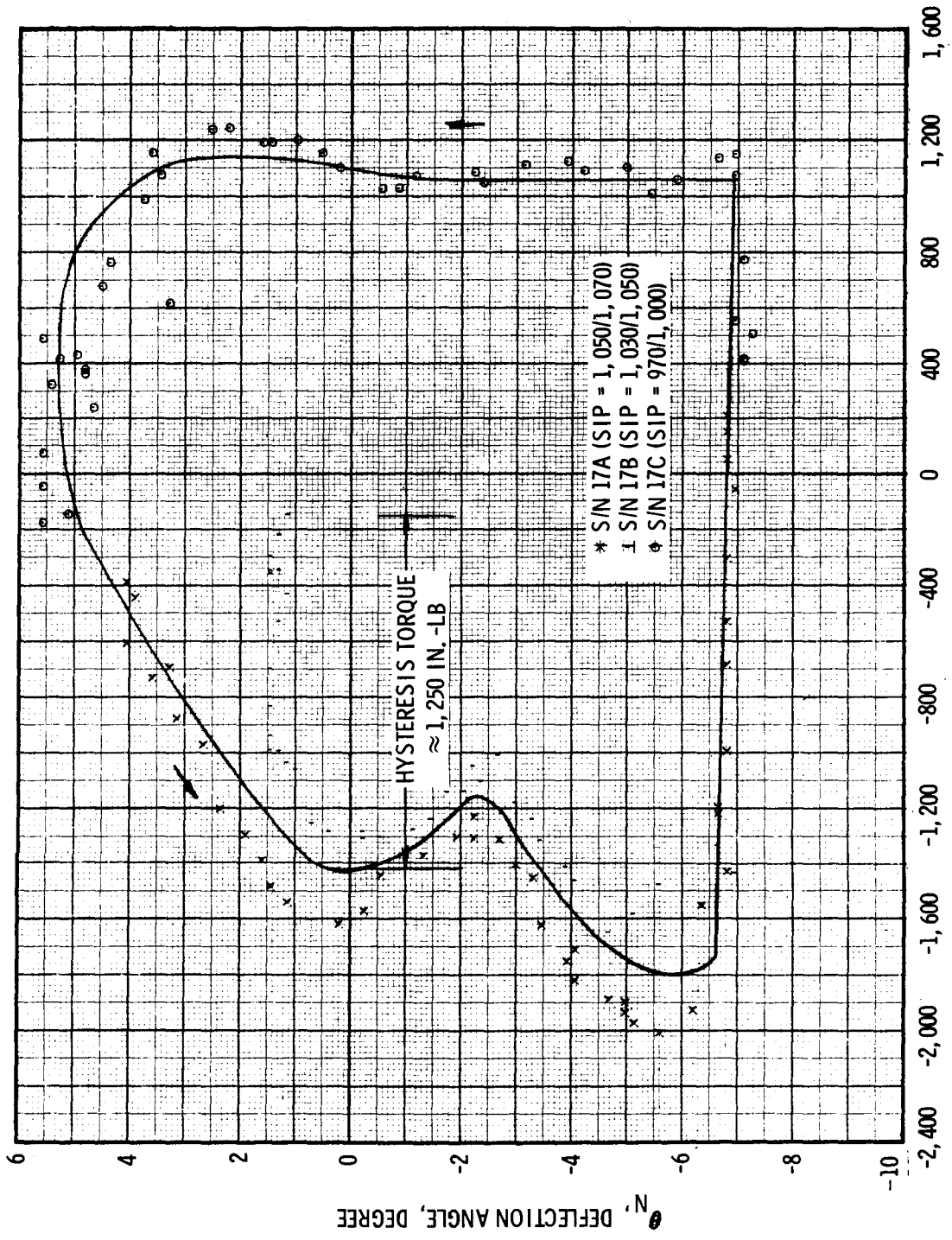

Figure 4. Minuteman TECHROLL Seal Nozzle Hysteresis Torque

The spring rate of the boot (K_B) was assumed to be zero due to the compliant nature of boot materials. This assumption was verified by laboratory investigation of the particular material used. The spring rate due to the nozzle internal aerodynamics (K_{AI}) was obtained by subtracting the spring rate of the seal from the total spring rate measured during the static test, and was found to be 527 in.-lb/^{o}. A comparison between figures 4 and 5 shows this change in the slope of the hysteresis box between bench and static firing conditions. The nozzle external aerodynamic spring rate (K_{AE}) did not apply to the static test mode.

Seal hysteresis torque (T_{HT}): The seal hysteresis torque was obtained by the bench test methods described in appendix III. The results of this test are in the form of a cross-plot of deflection angle (θ_N) as a function of total torque (T_T) as shown in figure 4. The hysteresis torque is defined as the amount of torque which must be applied to achieve first motion, and is equal to 1,250 in.-lb, one half the width of the observed hysteresis box.

The irregularity shown at -2^{o} deflection (figure 4) possibly is due to variations in low deflection velocities during the test. Stiction (static friction) effects present in the TECHROLL seal system can scatter the torque data when the deflection velocities are low. The effect of seal internal pressure on the seal hysteresis torque also was investigated and is shown in figure 6.

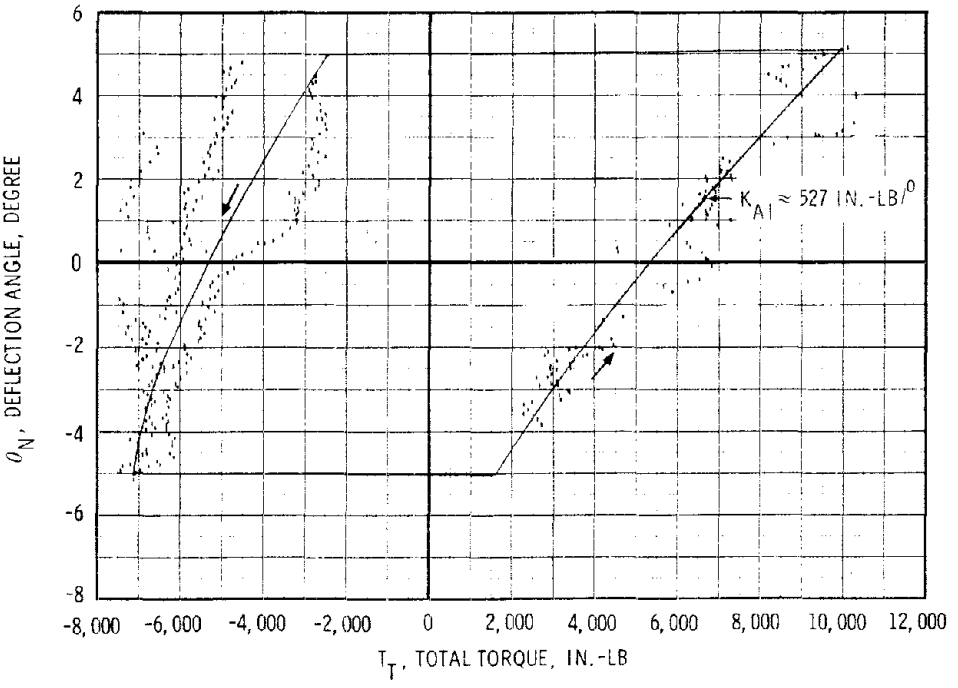

Figure 5. Minuteman TECHROLL Seal Static Firing Torque vs Deflection Angle for Constant Velocity (30.3^{o}/sec)

Seal offset torque (T_O): The seal offset torque is defined as the torque required to maintain null position as a result of slight nonsymmetries in the TECHROLL seal. This torque is represented by the torque offset of the hysteresis box (figure 4), and was -160 in.-lb.

Thrust misalignment torque (T_M): The thrust misalignment torque is the torque required to maintain null position as a result of asymmetrical exhaust flow in the nozzle. This torque was obtained by subtracting the sum of T_O and T_{OM} from the total misalignment torques obtained during the static firing. Figure 5 shows that the total misalignment torques were essentially zero. Therefore, the thrust misalignment torque was -3,020 in.-lb.

Mass-induced offset torque (T_{OM}): The mass induced offset torque was calculated to be 3,230 in.-lb

(b) Structural Characteristics

Seal axial stiffness (K_{SA}): The seal axial stiffness was determined using the test methods described in appendix III. The Minuteman seals had a spring rate of 5,220 psi/in. Figure 7 presents the seal pressure versus axial displacement cross-plots obtained during bench testing.

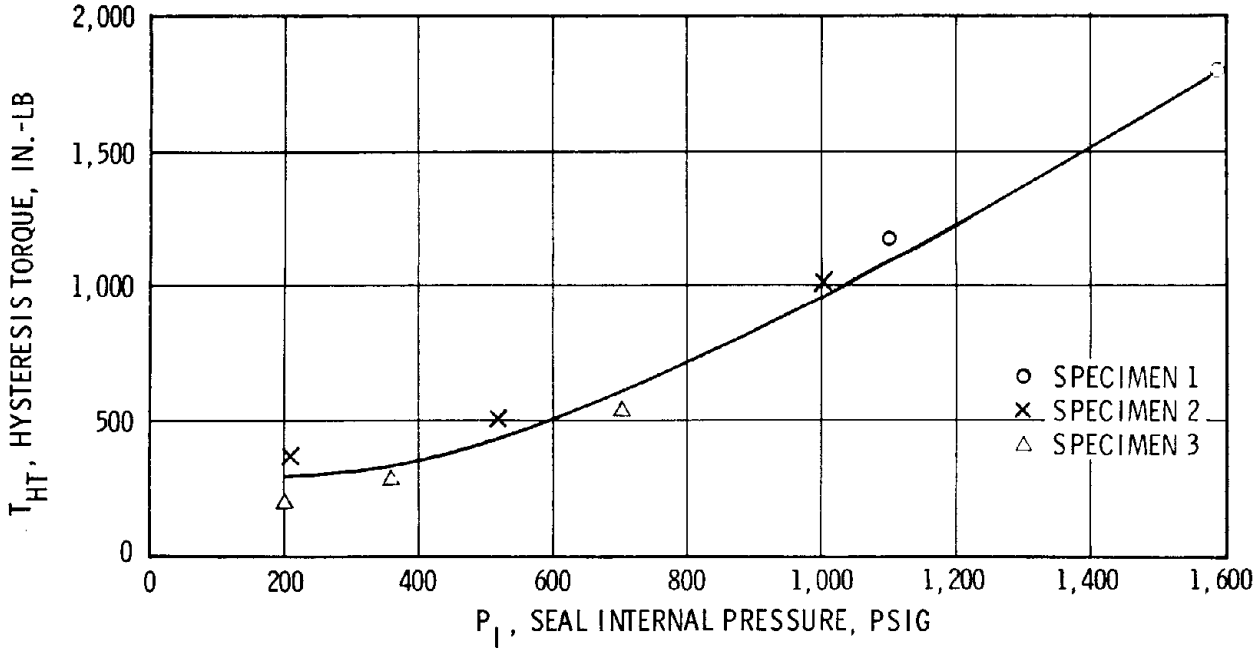

Figure 6. Minuteman TECHROLL Seal Hysteresis Torque vs Seal Internal Pressure

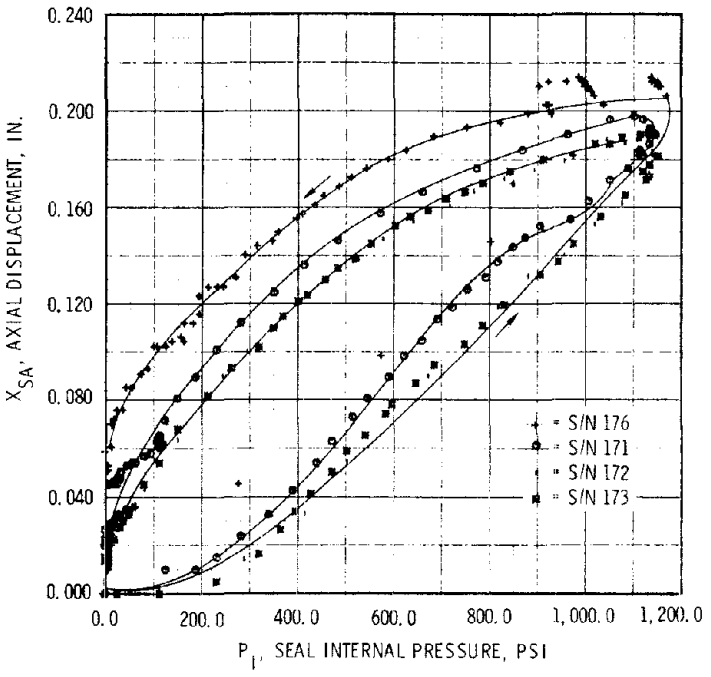

Figure 7. Minuteman TECHROLL Seal Nozzle Axial Movement vs Seal Internal Pressure

Loops are a result of energy losses in the system i.e., the seal is not a perfect spring in the axial direction. The shape of this loop was an indicator of the seal integrity. When a seal exhibited irregularities in spring rate, such as those shown in figure 8 anomalous performance and substandard burst pressure could be predicted. This correlation between axial spring rate change and substandard seal performance was used as partial acceptance criteria.

The axial hysteresis plot in figure 8 also shows that (1) oil leakage was indicated by failure of the nozzle to return to the initial axial location, and (2) air entrapment in the seal was indicated by excessive axial displacements for a given pressure.

Seal lateral stiffness (K_{SL}) and seal torsional stiffness (K_{ST}): The seal lateral and torsional stiffness was not investigated for the Minuteman seals.

Seal internal pressure (P_I): Using the equation derived in appendix II, the seal internal pressure was calculated to be 1,100 psig for a chamber pressure of 450 psig. Figure 9 presents the seal internal and chamber pressures obtained during the static test. Test results agree very closely with calculated values.

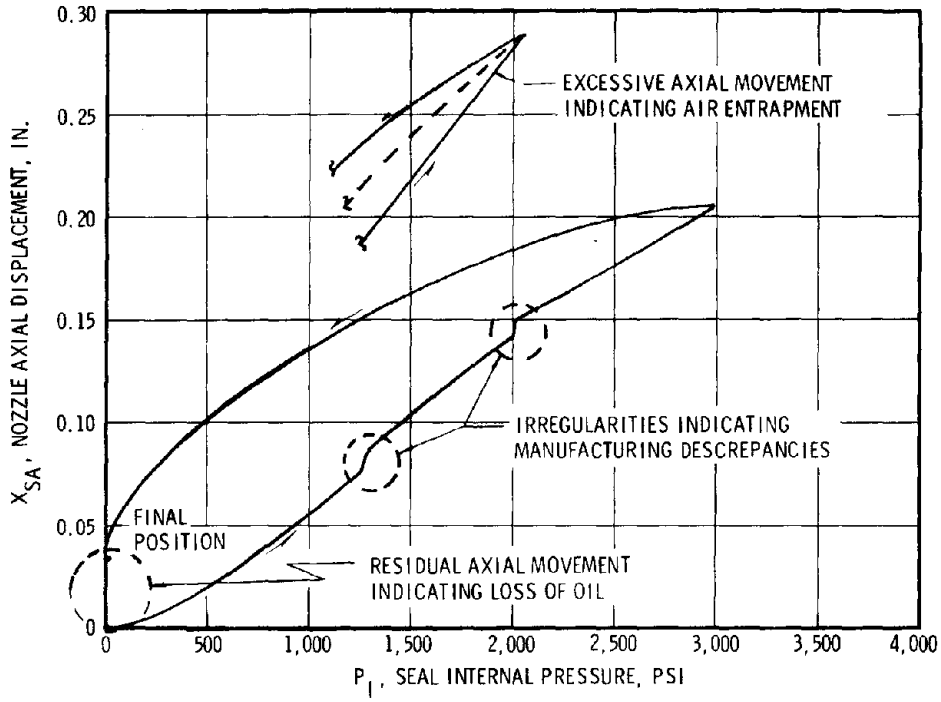

Figure 8. Unacceptable Characteristics Detected by the Axial Spring Test

(c) Bench and Acceptance Tests

Bench and acceptance tests were conducted for the Minuteman TECHROLL seal selected for static motor testing. The objectives were to demonstrate the adequacy and readiness of the TECHROLL seal and its supporting actuation and instrumentation systems for static motor testing. Bench and acceptance test of the TECHROLL seal consisted of:

Ignition shock test: Integrity of the TECHROLL seal during ignition transient was verified for Minuteman seals by raising the seal pressure to MEOP within approximately 500 msec. None of the shock tested seals exhibited anomalous characteristics following this test. The test method is described in appendix III.

Safety margin test: The safety margin was determined by increasing the seal internal pressure until failure occurred. The safety margin was calculated by:

$$\text{Safety margin} = \frac{P_{\text{failure}}}{\text{MEOP}} - 1 \times 100$$

The Minuteman configuration seal was proof tested to 2,000-psi seal internal pressure, the equivalent of 1.82 times MEOP, for 1.5 min prior to failure. Failure at 2,000 psi was characterized by fluid leakage through the interstices of the reinforcement fabric. This seal was designed to sustain internal pressures

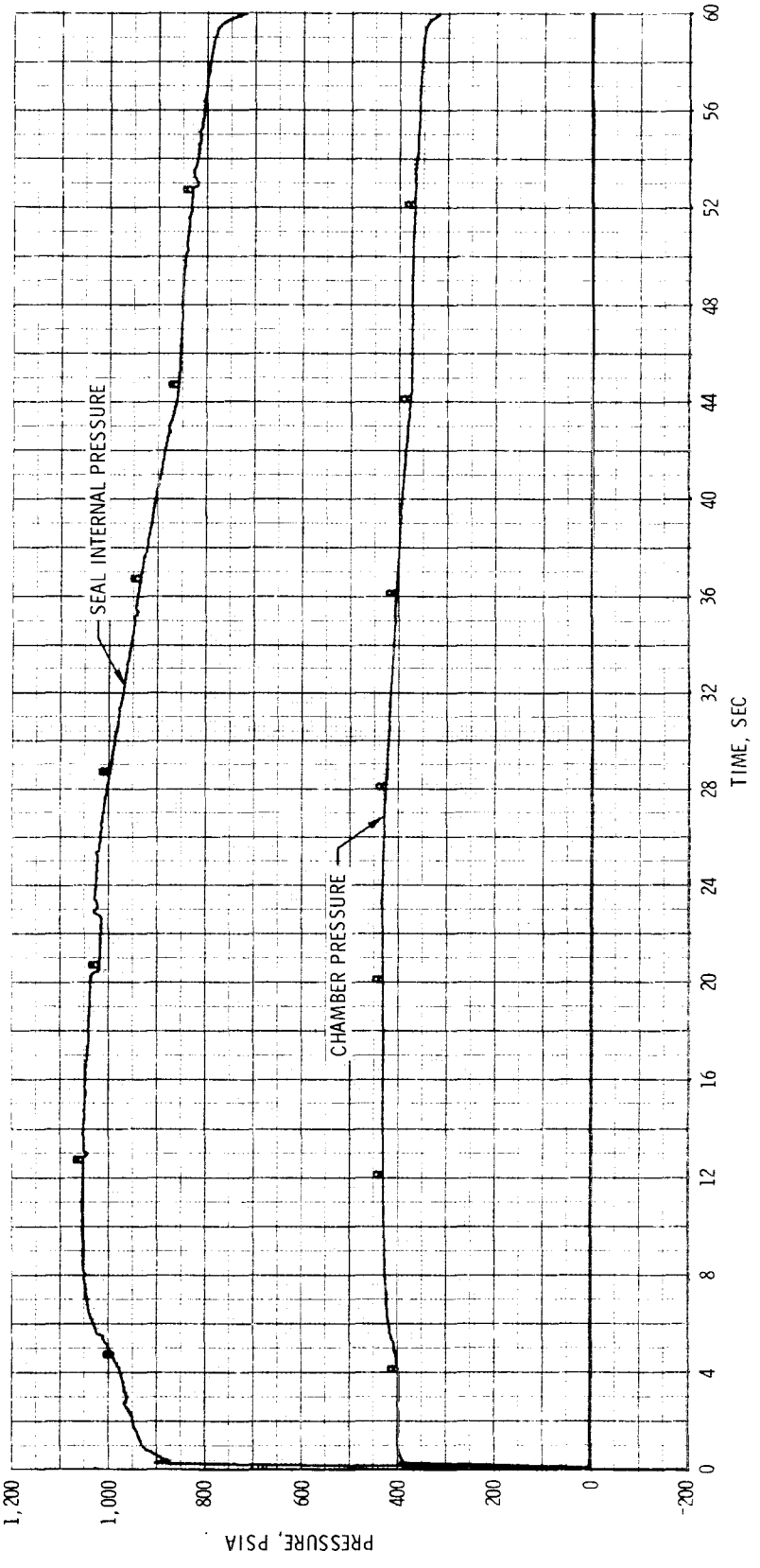

Figure 9. Minuteman Motor Chamber Pressure and Seal Internal Pressure vs Time

equivalent to those experienced by a TECHROLL seal in a first-stage Poseidon (C-3) application operating at 1,000-psi chamber pressure and 1,600-psi seal pressure. The burst pressure factor of safety for the Poseidon (C-3) application is 1.25, which is based on a calculated seal MEOP requirement of 1,600 psig. This requirement was added to qualify the TECHROLL seal for use on the C-3 demonstrator program.

Simulated duty cycle test: This test consisted of loading the nozzle to simulate motor firing conditions and nozzle actuation, as described in appendix III, with the open loop duty cycle (figure 10) planned for motor test use. During the duty cycle, movement of the nozzle in axial and lateral directions and total actuation torque were monitored.

Figure 11 shows a plot of axial and lateral nozzle movements during the duty cycle (figure 10) for the Minuteman nozzle. The nozzle movements are referenced to a theoretical intercept point on the nozzle that is defined as the intersection of the nozzle centerline and the plane of the seal convolute tips at the unpressurized condition and at 0° deflection. The relatively small excursions of the nozzle during the cycle indicate that the true pivot point was very close to the theoretical intercept point.

Figure 12 shows the total actuation torques obtained during the duty cycle bench test of the Minuteman movable nozzle assembly.

(d) Static Test

The Minuteman TECHROLL seal movable nozzle system was successfully static fired at AFRPL in accordance with the test methods described in appendix III, and all objectives were satisfied. The seal pressure was as predicted and no thermal protection degradation was observed.

Total torque: The total nozzle torques measured during the Minuteman static firing duty cycle (figure 13) are shown in figure 14. The differences between these total nozzle torques and the bench test total actuation torques result from the increase in nozzle inertia due to addition of the nozzle abatives and thermal insulation system, and gas flow through the nozzle.

In interpreting the torques measured during the period of acceleration, it must be understood that the values presented are large only because of the excessively high accelerations (approximately 20,000 $^{\circ}/sec^2$) achieved with the open loop actuation systems, and not because of the TECHROLL seal system. For example, if a closed loop actuation system were used to deflect the Minuteman nozzle sinusoidally about null with an amplitude of 5°, the velocity would equal the tested velocity of

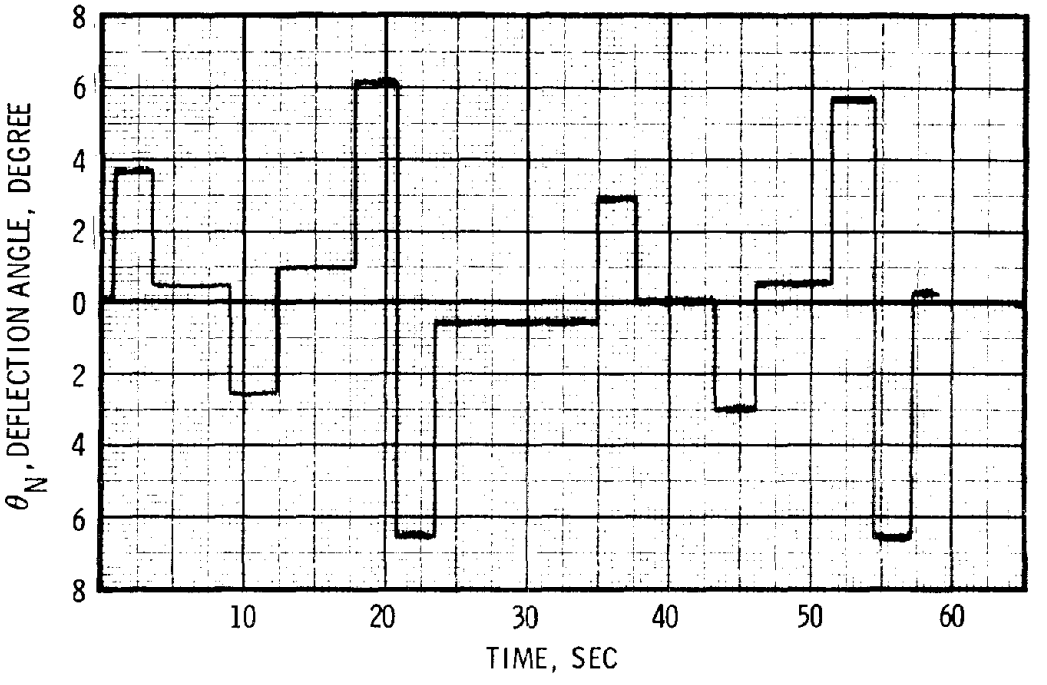

Figure 10. Minuteman TECHROLL Seal Bench Test Open Loop Duty Cycle

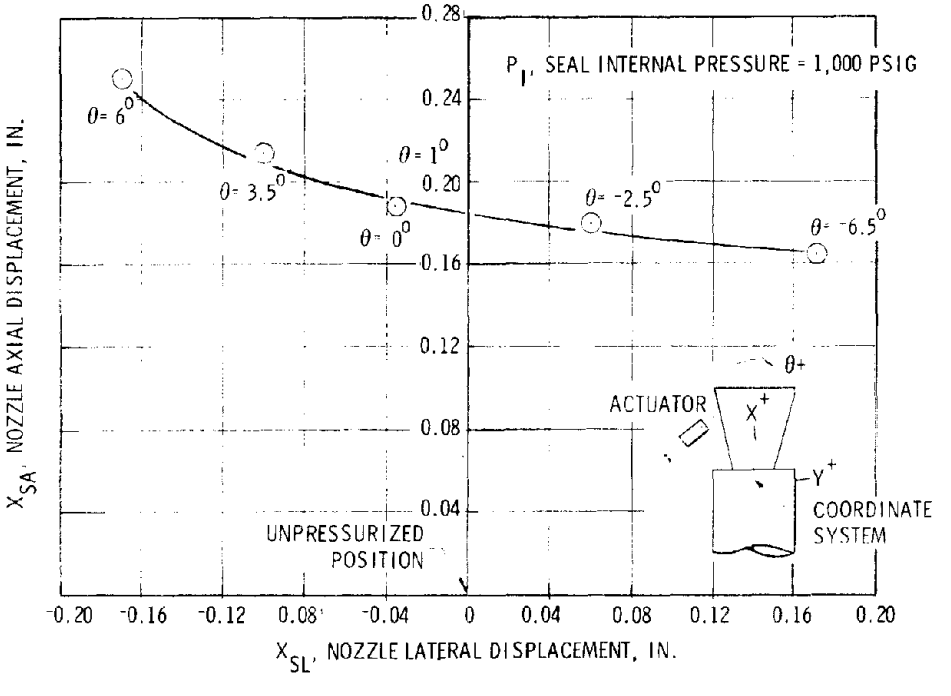

Figure 11. Minuteman Nozzle Movements vs Deflection Angle

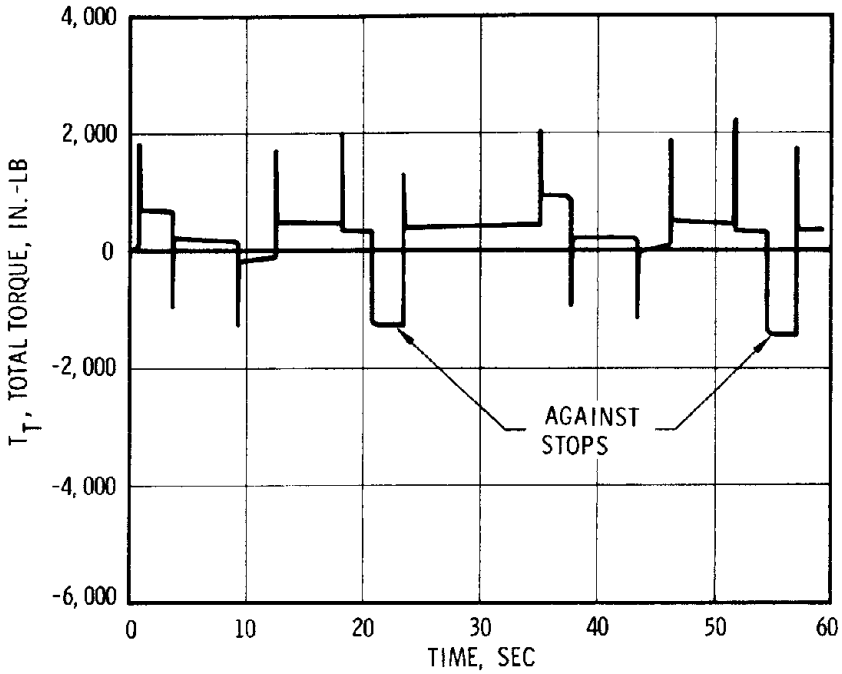

Figure 12. Minuteman TECHROLL Seal Total Torque During Bench Test Duty Cycle

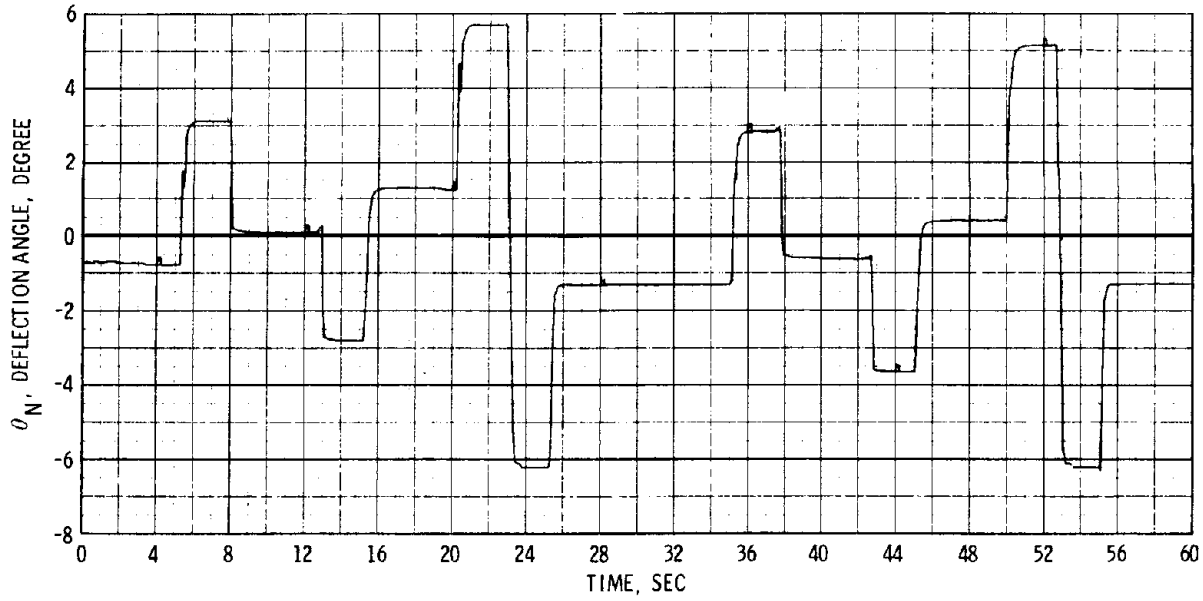

Figure 13. Minuteman Static Firing Duty Cycle, Deflection Angle vs Time

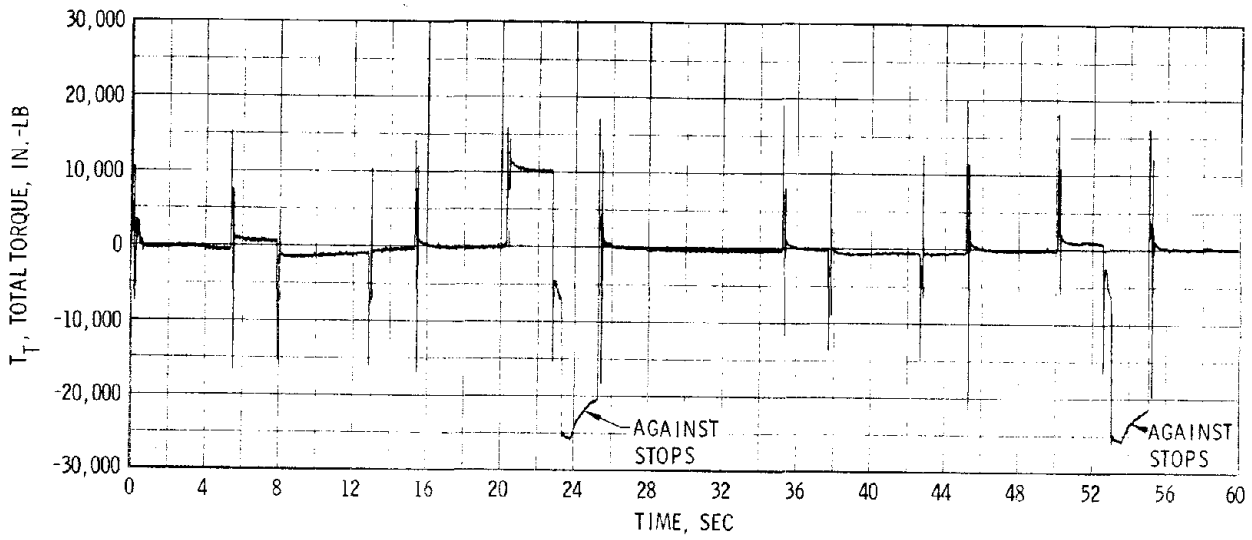

Figure 14. Minuteman TECHROLL Seal Nozzle Torque During Static Firing

30.3°/sec but the acceleration (approximately 10,000°/sec^2) would be only one-half of the tested acceleration. This would reduce the acceleration torques to approximately one-half of the tested values.

Nozzle movements: Figure 15 presents the nozzle movements recorded during the static firing of the Minuteman nozzle. Comparison of this plot to that obtained during bench testing shows no significant differences.

Nozzle insulation performance: All ablatives eroded as predicted for the 60-sec firing. No measurable amount of insulative grease was consumed. The graphite cloth grease retention device remained intact and experienced very little flame effects. The prefired nozzle (figure 16), postfired aft view (figure 17), and postfired front view (figure 18) indicate the condition of the ablatives. Since no posttest ablative analysis was required under this contract, the nozzle was not disassembled.

Expanded time plots: Figure 19 shows expanded time plots of the Minuteman nozzle axial deflection, lateral deflection, deflection angle, and seal torque during an early portion of the static firing.

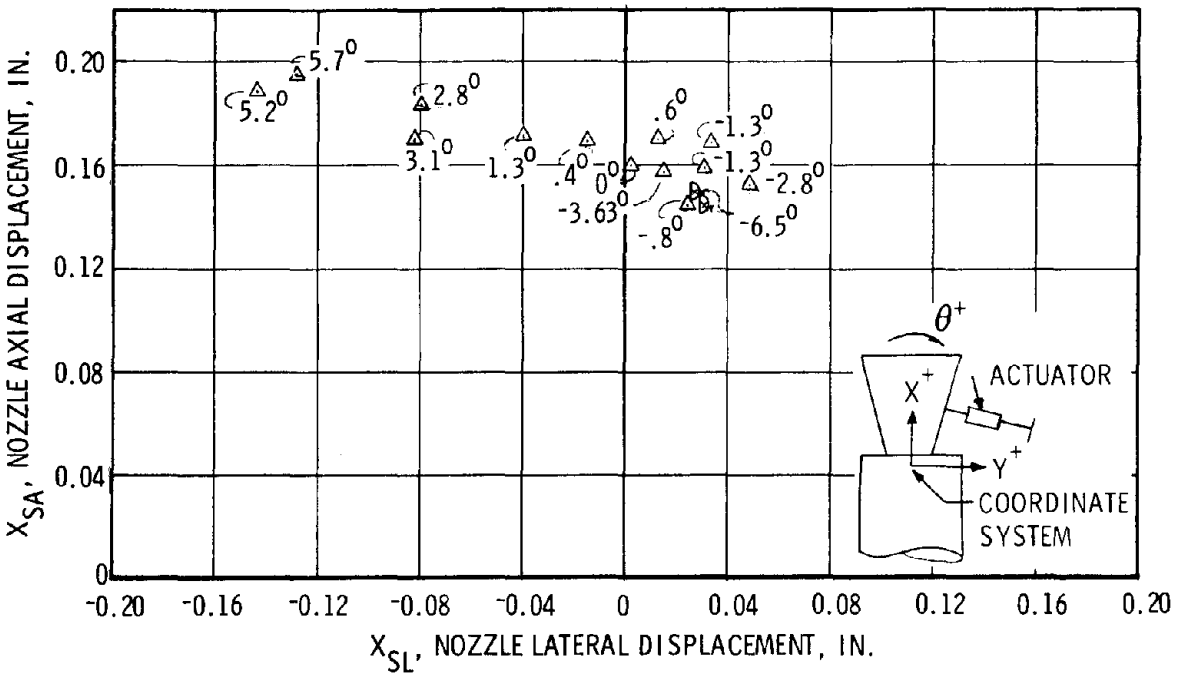

Figure 15. Minuteman Nozzle Movements During Static Firing

b. Air-Launched Nozzle (HIPPO)

(1) Design

The air-launched TECHROLL seal nozzle assembly, (figures 20 and 21) used the nozzle ablative design developed under contract No. F04611-69-C-0065, Development of High Performance Materials for High Pressure Rocket Motors. Modifications to this basic design allowed for incorporation of a TECHROLL seal to provide a 10° deflection capability in a single plane. One nozzle assembly was used for all three air-launched configuration firings with a slight modification necessary to properly house the miniseal.

(a) The major changes to the existing high pressure test nozzle configuration consisted of:

Nozzle: Adapting the existing nozzle (from contract No. F04611-69-C-0065) required that the nozzle shell be recontoured; however, the thickness of the shell was maintained at or about the original design thickness. This was possible because the insulation components of the existing nozzle were thicker than required by this program and could be reduced without sacrificing structural or thermal integrity of the nozzle. The forward end of the shell also was redesigned to incorporate a steel housing integral with the shell to support the TECHROLL seal.

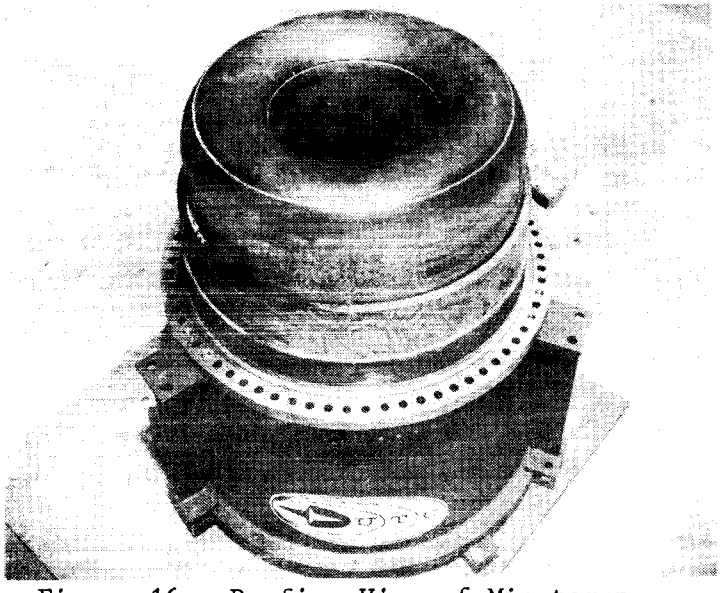

Figure 16. Prefire View of Minuteman Nozzle Assembly

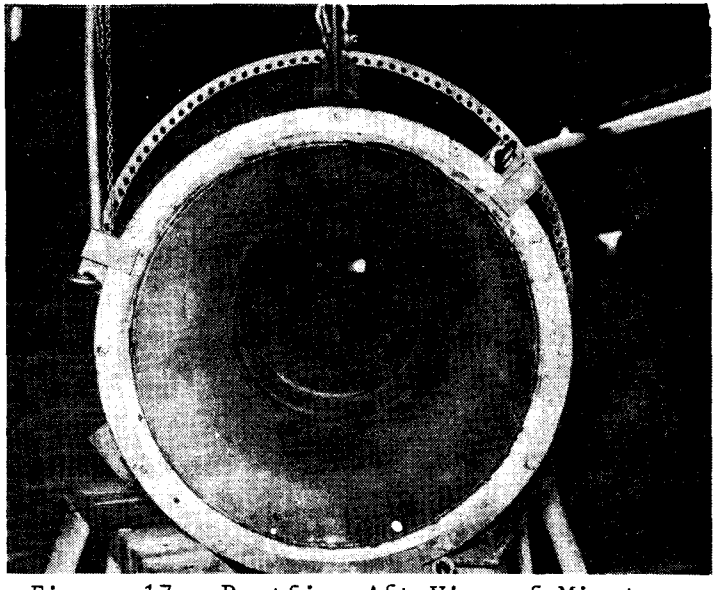

Figure 17. Postfire Aft View of Minuteman Nozzle Assembly

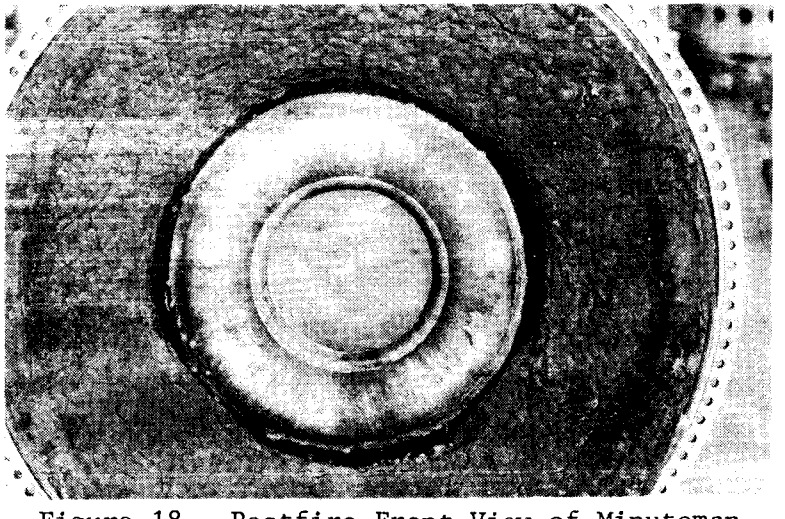

Figure 18. Postfire Front View of Minuteman Nozzle Assembly

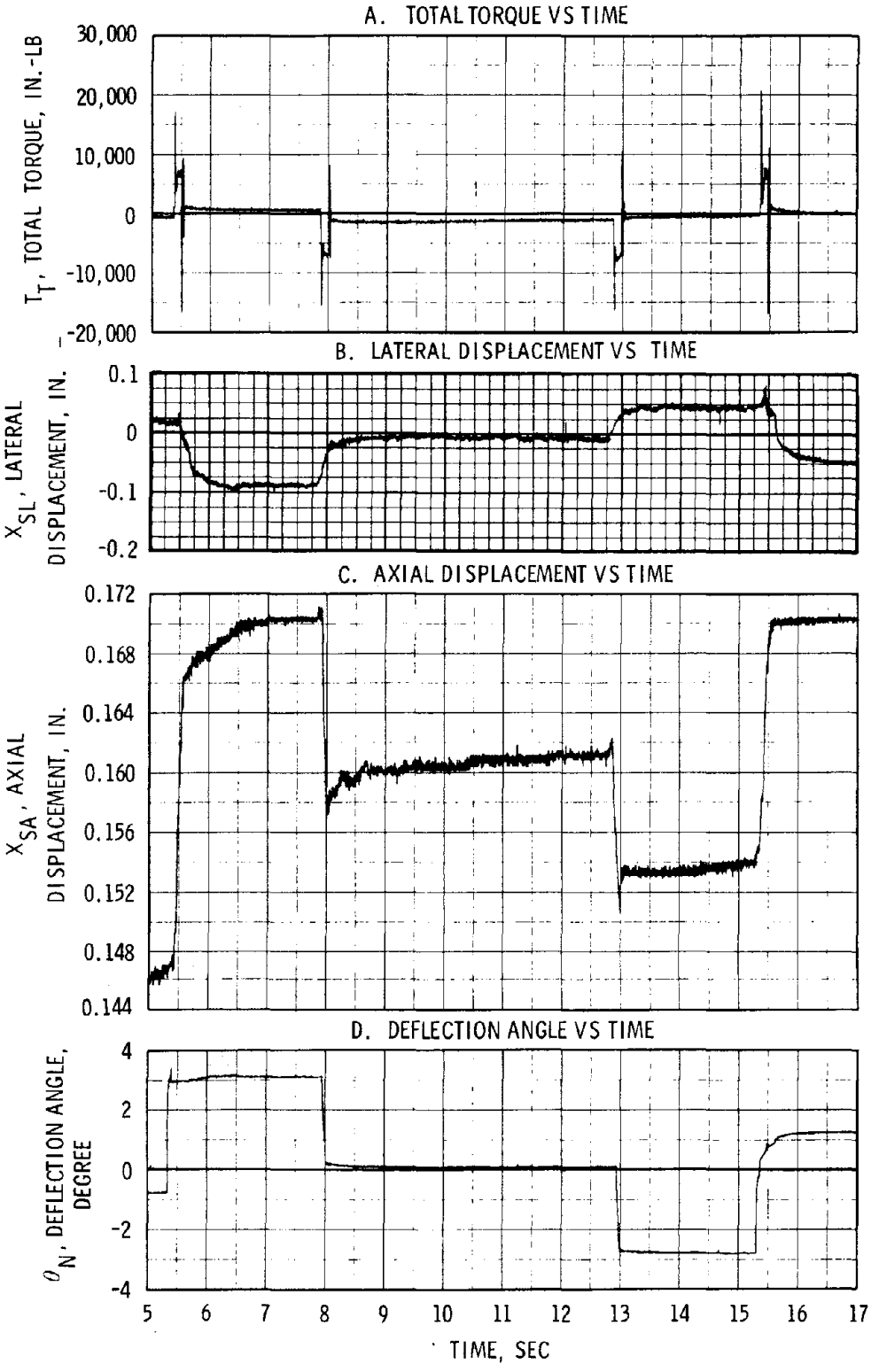

Figure 19. Minuteman Static Test, Expanded Time Plots

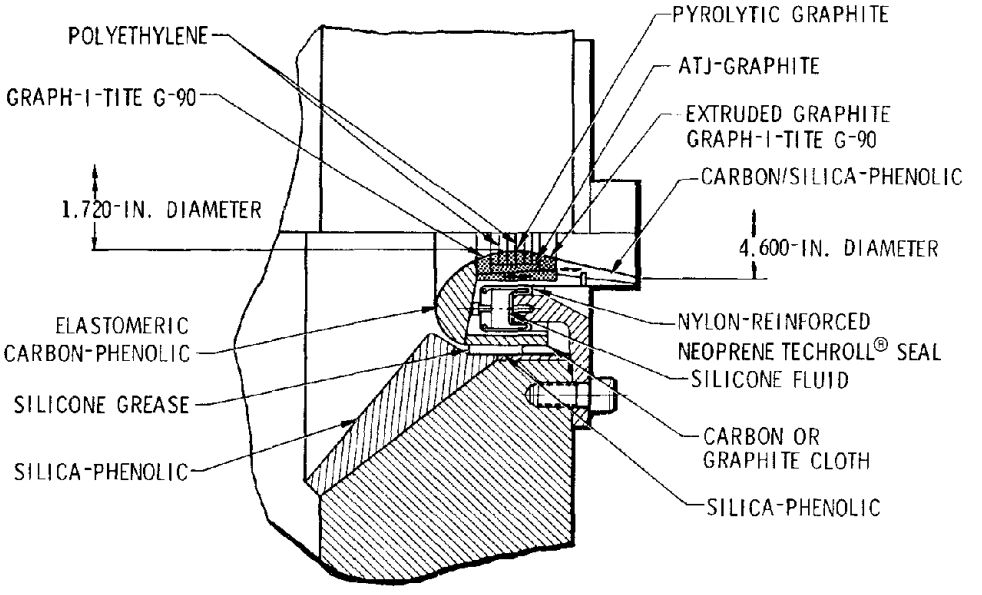

Figure 20. Conventional HIPPO TECHROLL Seal Movable Nozzle Assembly

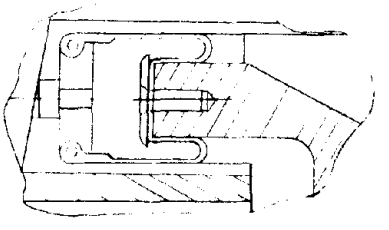

A. Conventional Seal
(2,000-psi chamber pressure)

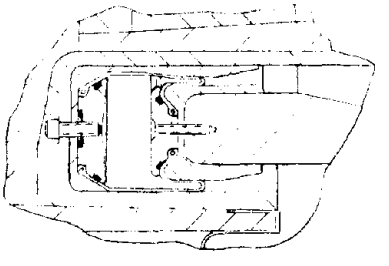

B. Miniseal
(3,000-psi chamber pressure)

Figure 21. HIPPO TECHROLL Seal Configurations

Insulative components: New insulative components were designed to provide thermal protection for the seal housing.

Adapter: A conical steel adapter was required to support the aft side of the seal and to adapt the nozzle assembly to the modified HIPPO motor aft closure in a submerged configuration.

(b) New Components

The new components required by the addition of the TECHROLL seal consisted of:

Nose cap: The nose cap was fabricated from MXCE-280, a carbon molding compound, and was bonded to the steel housing with EA913 adhesive.

Insulation: Thermal protection for the seal housing on the submerged side was provided by silica-phenolic tape, FM5404, wrapped 0° to the nozzle centerline. It was bonded to the seal housing using EA913 adhesive.

Nozzle shell: The shell was designed as an integral unit fabricated of 4340 steel and was heat treated to 150,000-psi ultimate tensile strength. The actuator was attached to a threaded ring on the aft end of the nozzle shell.

Aft closure adapter: The aft closure adapter was a flanged cylinder which adapted the nozzle to the modified HIPPO aft closure, supported the seal, and transmitted the nozzle ejection loads to the aft closure. It was fabricated from 4340 steel, and was heat treated to 150,000-psi tensile strength ultimate.

Carbon cloth: The carbon cloth (CCA-1) was bonded between the aft end of the seal housing and the aft closure adapter and formed a cavity which was filled with silicone grease (DC40) to provide thermal protection for the seal. The cloth was bonded to the seal housing with EA913 adhesive and fastened to the aft closure adapter by a steel ring, phenolic tube assembly. This tube assembly supported the grease cavity and assured that the carbon cloth was not pinched or otherwise restricted during assembly.

(c) Configuration

The all-boost and boost-sustain nozzle assemblies (figures 20 and 21A) were identical, using the conventional TECHROLL seal shown in figure 22. The high pressure seal used a three-layer conventional TECHROLL seal (figure 22) with the same external dimensions as the all-boost and boost-sustain seals; therefore, this seal could be tested in the existing hardware. To accommodate the miniseal, it was necessary to add removable spacers within the seal housing and to fabricate a new set of retaining rings as shown in figures 21B and 23.

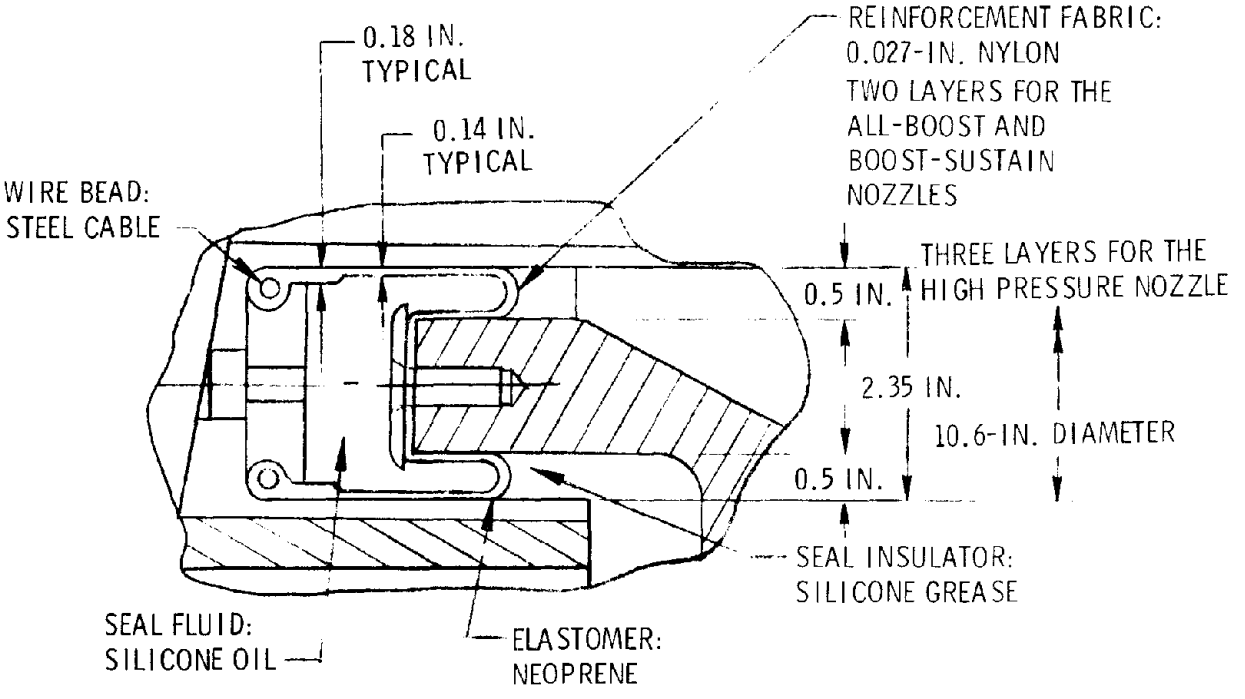

Figure 22. Material and Dimensional Relationships for the Conventional HIPPO TECHROLL Seal

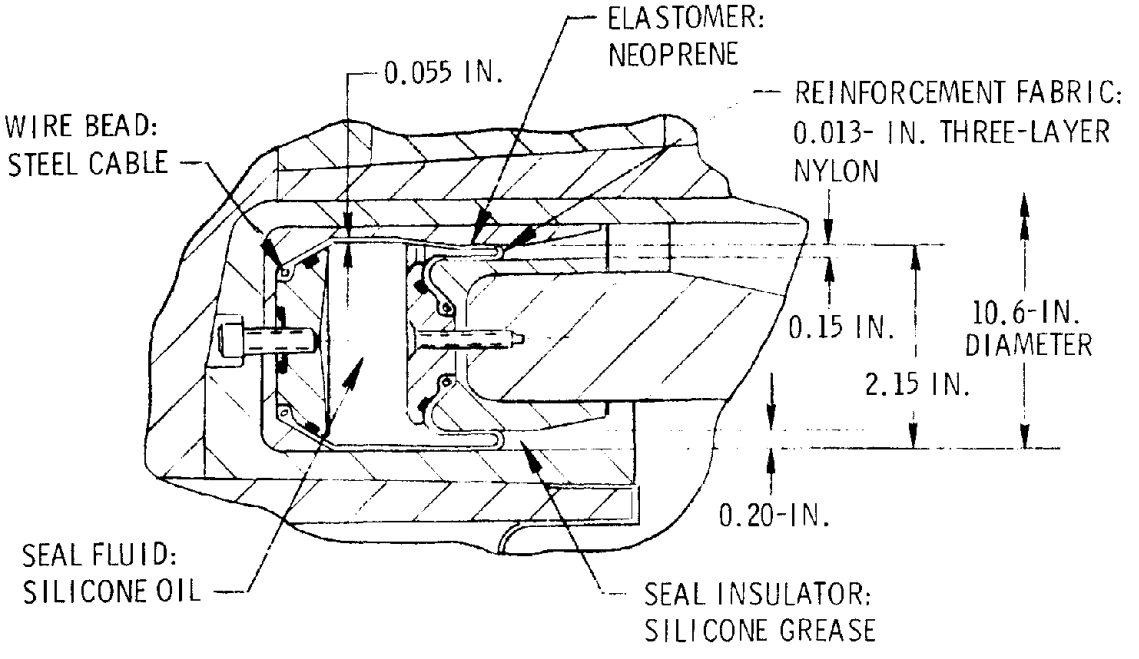

Figure 23. Material and Dimensional Relationships for TECHROLL Miniseal

(2) Performance

The performance requirements for the HIPPO TECHROLL seal movable nozzle assemblies were:

	Performance Requirement		
	All-Boost	Boost-Sustain	High Pressure Seal
Maximum motor pressure, psia	2,000	2,000	3,000
Duration, sec	20	20	20
Maximum nozzle deflection angle, degree	10	10	10
Maximum nozzle velocity, degree/sec	30	300	30
Operating temperature, ^{o}F	75	75	75

Two seals, a three-ply conventional seal and a miniseal were competitively evaluated for performance through a limited series of bench tests prior to selection for high pressure static firing. Evaluation consisted of comparing the seal margin of safety, nozzle axial stiffness, and seal hysteresis torque. The results as presented in table V, led to selection of the miniseal. Bench tests served to verify system readiness for the static firing as well as to quantify some of the performance parameters discussed in section III. Table V presents a summary of the torque equation coefficients and nozzle structural characteristics obtained by analysis, bench, and static tests. The following paragraphs discuss the methods by which these coefficients and characteristics were obtained.

(a) Torque coefficients

Inertia (I_T): The calculated combined inertia of the nozzle and boot ($I_N + I_B$) was 9.10 in.-lb-sec^2. The inertia of the seal fluid (I_S) was highest for the miniseal due to the smaller size of the fluid cavity and varied for the three nozzles as follows:

All-boost	$I_S = 0.41$ in.-lb-sec^2
Boost-sustain	$I_S = 0.41$ in.-lb-sec^2
Miniseal	$I_S = 0.68$ in.-lb-sec^2

Damping (B_T): Damping of the seal (B_S) was calculated to be 2.38 in.-lb-sec for the all-boost nozzle, 2.38 in.-lb-sec for the boost-sustain nozzle, and 6.64 in.-lb-sec for the miniseal nozzle. The combined damping of the boot and internal aerodynamics ($B_B + B_{AI}$) was obtained by subtracting the seal damping obtained in bench tests from the total damping measured during the static firings. The combined damping was 2,579 in.-lb-sec for the all-boost nozzle, 1,862 in.-lb-sec for the boost-sustain nozzle, and 1,880 in.-lb-sec for the miniseal nozzle. The nozzle external aerodynamic damping (B_{AE}) did not apply to the static test mode.

TABLE V

HIPPO PERFORMANCE SUMMARY

Item	All-Boost	Boost-Sustain	Miniseal	Conventional High Pressure
Test Conditions				
Motor chamber pressure, psia	1,800	1,680	2,700	---
Duration, sec	25	22	20	---
Temperature, ^{o}F	50	50	50	---
Demonstrated TVC				
Maximum deflection, degree	12	11.5	6.4	10
Maximum velocity, degree/sec	58	140	65	---
Torque Equation Coefficient				
I_N, nozzle inertia, in.-lb-sec^2	4.35	4.35	4.35	4.35
$I_N + I_B$, nozzle + boot inertia, in.-lb-sec^2	9.1	9.1	9.1	9.1
I_S, seal fluid inertia, in.-lb-sec^2	0.41	0.41	0.68	0.41
B_S, seal damping, in.-lb-sec	2.38	2.38	6.64	2.38
$(B_B + B_{AI})$, boot and aerodynamic damping, in.-lb-sec	2,579	1,862	1,880	---
B_{AE}, external aerodynamic damping, in.-lb-sec	N/A	N/A	N/A	N/A
K_S, seal spring rate, in.-lb/degree	62.5	62.5	138	488
$(K_B + K_{AI})$ boot + internal aerodynamic spring rate, in.-lb/degree	0	37	52	---
K_{AE}, external aerodynamic spring rate, in.-lb/degree	N/A	N/A	N/A	N/A
K_M, mass induced spring rate, in.-lb/degree	0	0	0	0
T_{HT}, seal hysteresis torque, in.-lb	1,450	1,000	2,300	3,500
T_O, seal offset torque, in.-lb	750	450	-725	-500
T_M, thrust misalignment torque, in.-lb	-250	-100	-250	---
T_{OM}, mass induced offset torque, in.-lb	0	0	0	0
Nozzle Structural Characteristics				
K_{SA}, seal axial stiffness, psi/in.	14,650	14,650	14,500	50,600
K_{SL} seal lateral stiffness, psi/in.	26,000	---	---	---
K_{ST}, seal torsional stiffness range, psi/in.	5,200 to 25,000	---	---	---
P_I, seal internal pressure, psi	2,850	2,620	4,200	4,800

Spring rate (K_T): The spring rate of the seal (K_S) was obtained from hysteresis test data. This spring rate is represented by the slope of the hysteresis box and was 62.5 in.-lb/^{o} for the all-boost nozzle, 62.5 in.-lb/^{o} for the boost-sustain nozzle, 138 in.-lb/^{o} for the miniseal nozzle, and 488 in.-lb/^{o} for the high pressure nozzle, as shown by the centerline slopes of figure 24 through 27. The spring rate of the boot (K_B) was assumed to be zero due to the compliant nature of boot materials. This assumption was verified by laboratory investigation of the particular material used. The spring rate due to nozzle internal aerodynamics (K_{AI}) was obtained by subtracting the spring rate of the seal from the total measured spring rate during the static tests. The spring rate was essentially 0 in.-lb/^{o} for the all-boost nozzle, 37 in.-lb/^{o} for the boost-sustain nozzle, and 52 in.-lb/^{o} for the miniseal nozzle. Figures 28 and 29 show this change in the slope of the hysteresis box during static firing conditions of the all-boost nozzle and boost-sustain nozzle, respectively. The pronounced change in slope at the hardover position was due to the holddown ring bottoming out against the seal wall. This effect was pronounced since inaccuracies in the open loop actuation system caused the nozzle to deflect more than the intended 10^{o} maximum. The nozzle external aerodynamic spring rate (K_{AE}) did not apply to the static test mode.

Seal hysteresis torque (T_{HT}): The seal hysteresis torque was obtained by the bench test methods described in appendix III. The result of these tests are in the form of a cross-plot of deflection angle (θ_N) as a function of total torque (T_T) and are shown in figures 24 through 27 for the four configurations tests. The hysteresis torque is defined as that torque which must be applied to achieve first motion, and is equal to one-half the width of the hysteresis box. This torque equaled 1,450 in.-lb for the all-boost nozzle, 1,000 in.-lb for the boost-sustain nozzle, 2,300 in.-lb for the miniseal nozzle, and 3,500 in.-lb for the high pressure nozzle.

Seal offset torque (T_O): The seal offset torque is defined as that torque required to maintain the nozzle in the null position as a result of any asymmetry existing in the TECHROLL seal. This torque is represented by the torque offset of the hysteresis boxes (figures 24 through 27) and was found to be 750 in.-lb for the all-boost nozzle, 450 in.-lb for the boost-sustain nozzle, -725 in.-lb for the miniseal nozzle, and -500 in.-lb for the high-pressure nozzle.

Thrust misalignment torque (T_M): The thrust misalignment torque is defined as the torque required to maintain the nozzle in the null position as a result of asymmetrical exhaust flow in the nozzle. This torque was obtained by subtracting the seal offset torque from the total misalignment torque obtained during the

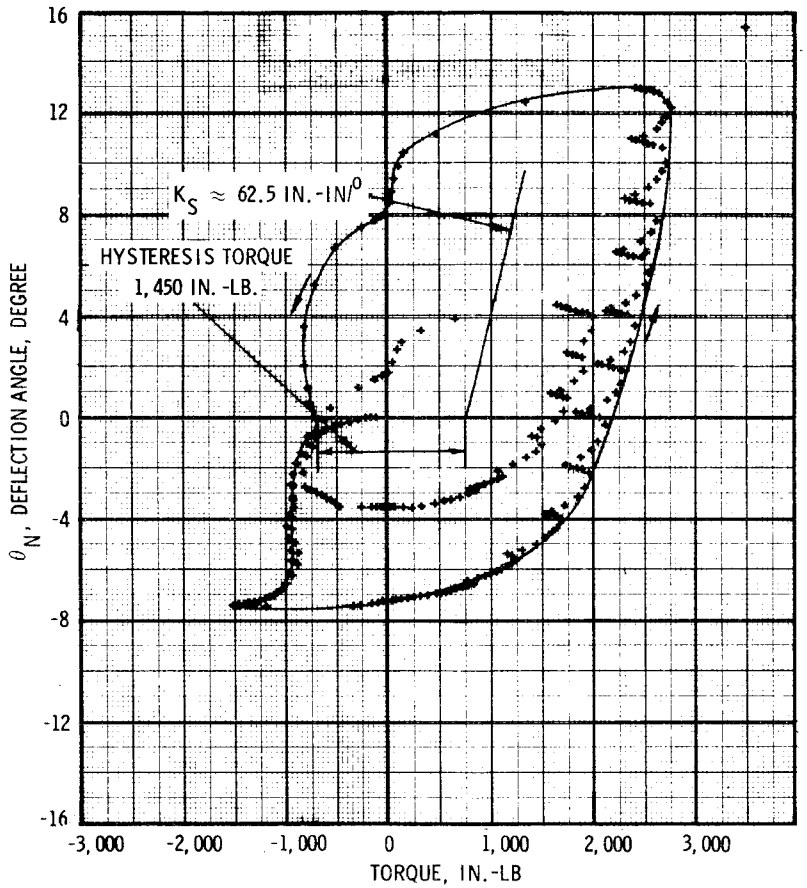

Figure 24. HIPPO (All-Boost) Hysteresis Torque vs Deflection Angle

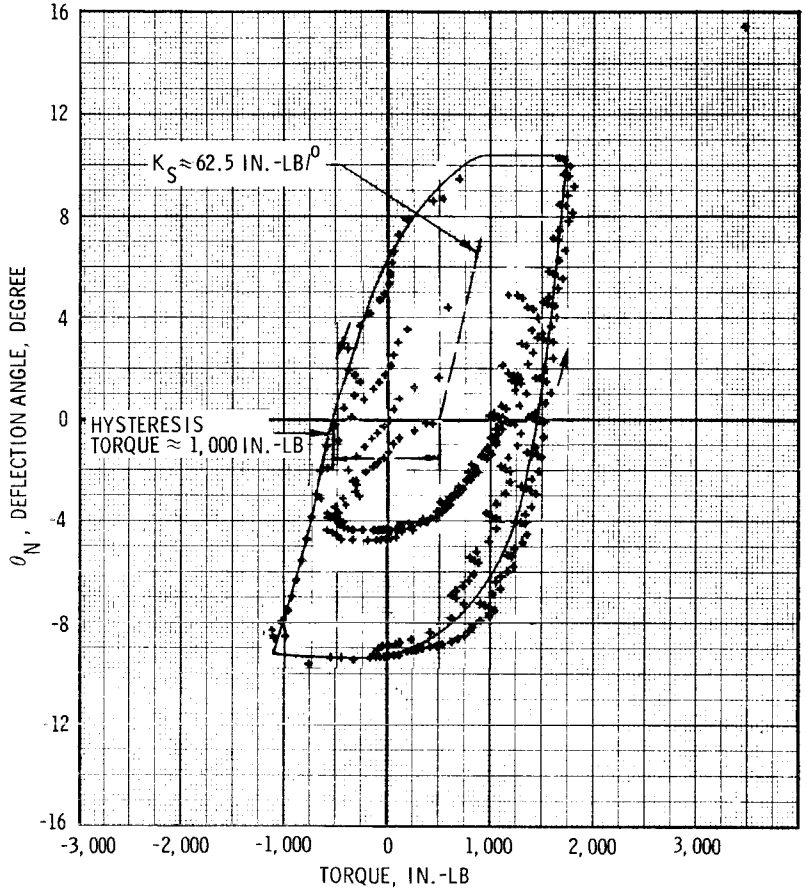

Figure 25. HIPPO (Boost-Sustain) Hysteresis Torque vs Deflection Angle

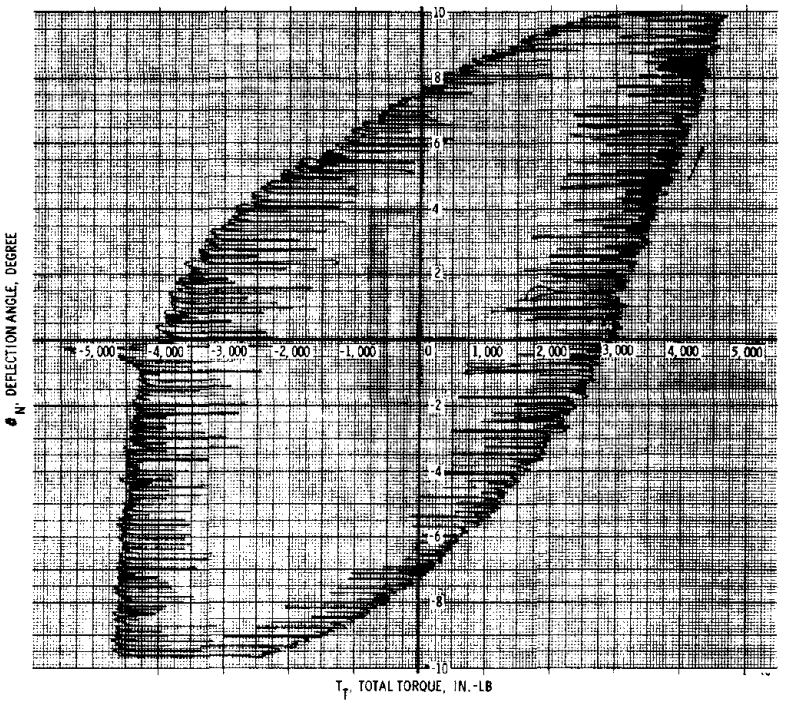

Figure 26. HIPPO (High Pressure) Hysteresis Torque vs Deflection Angle

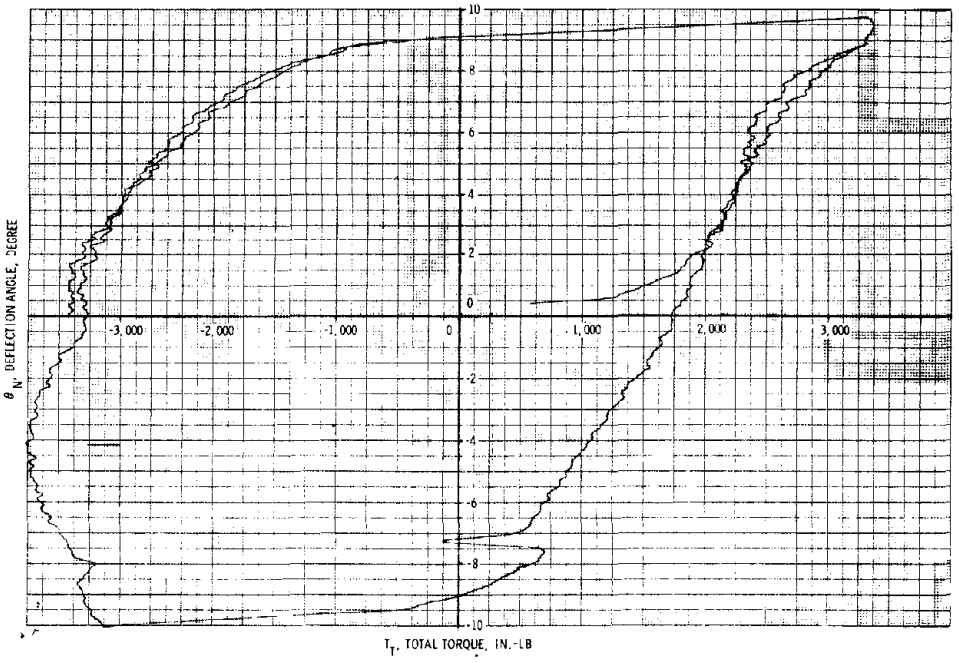

Figure 27. HIPPO (Miniseal) Hysteresis Torque vs Deflection Angle

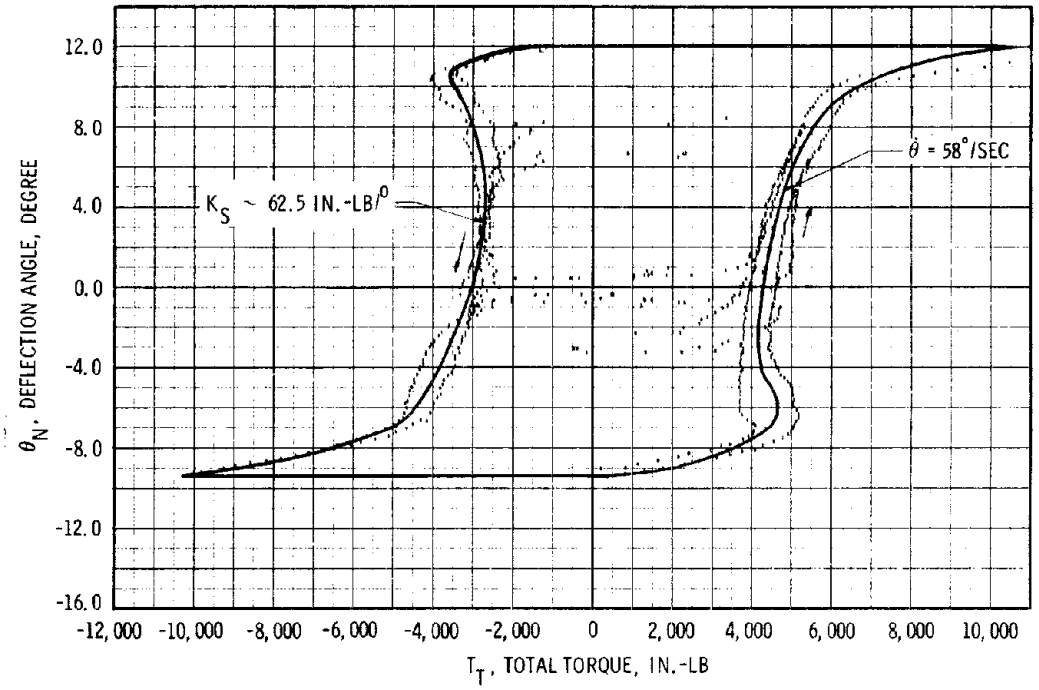

Figure 28. HIPPO (All-Boost) Static Firing, Torque vs Deflection Angle

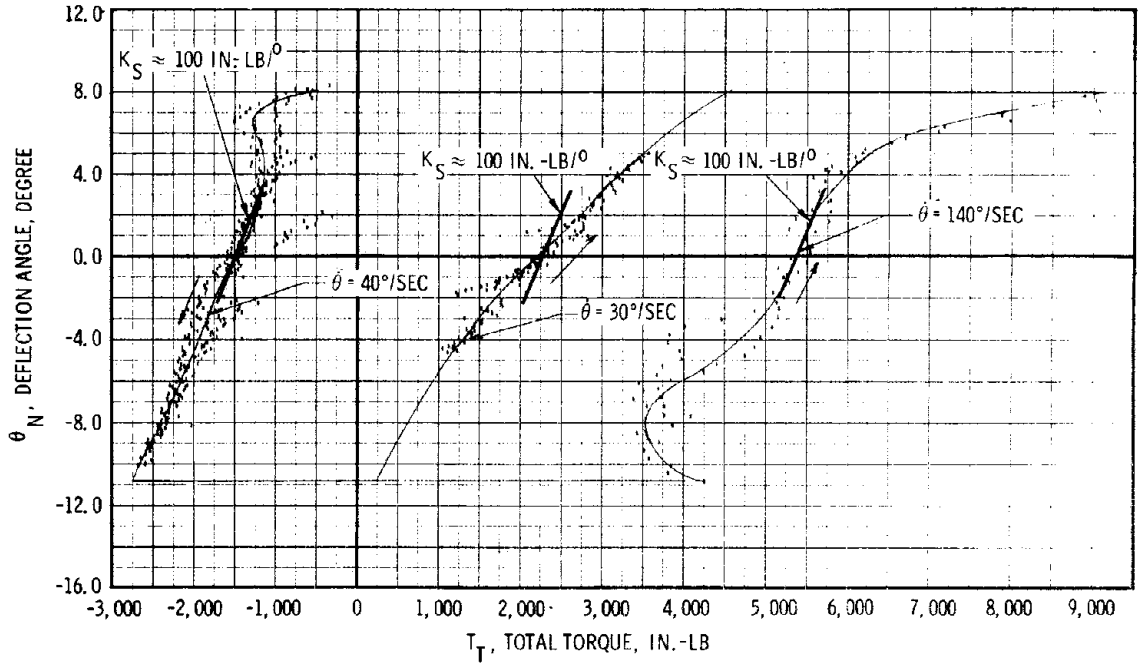

Figure 29. HIPPO (Boost-Sustain) Static Firing, Torque vs Deflection Angle

static firing. The thrust misalignment torque was -250 in.-lb for the all-boost nozzle, and -250 in.-lb at T_M -0 for the miniseal nozzle.

Mass-induced offset torque (T_{OM}): The mass-induced offset torque was zero due to the vertical orientation of the nozzles during static test.

(b) Structural Characteristics

Seal axial stiffness (K_{SA}): Using the test methods described in appendix III, the HIPPO seals had axial spring rates of 14,650 psi/in. for the all-boost and boost-sustain nozzles, 14,500 psi/in. for the high pressure nozzle, and 50,600 psi/in. for the miniseal nozzle. Figures 30 through 33 show the seal pressure and axial displacement cross-plots obtained for the four seals, respectively. The highest axial stiffness was achieved by the miniseal.

Seal lateral stiffness (K_{SL}): Using the test methods described in appendix III, the seal lateral stiffness for the all-boost nozzle seal was 26,000 lb/in. Figure 34 shows a cross-plot of lateral force versus lateral displacement. No lateral stiffness data were obtained for the miniseal.

Seal torsional stiffness (K_{ST}): Using the test method described in appendix III, the torsional stiffness of the all-boost nozzle seal was 5,200 in.-lb/^{o} for angles of less than 1^{o}, and 25,000 in.-lb/^{o} for angles between 1^{o} and 1.8^{o}. Figure 35 shows the torque. No torsional stiffness data were obtained for the miniseal.

Seal internal pressure (P_I): Using the equation derived in appendix II, the seal internal pressure was calculated to be almost the same as those recorded during the three static tests. Test results were 2,850-psi seal pressure for a 1,800-psi chamber pressure for the all-boost nozzle, 2,620-psi seal pressure for a 1,680-psi chamber pressure for the boost-sustain nozzle, and 4,200-psi seal pressure for a 2,700-psi chamber pressure for the miniseal nozzle, as shown in figures 36, 37, and 38, respectively.

(c) Bench and Acceptance Tests

Bench acceptance tests were conducted on the HIPPO TECHROLL seals selected for the all-boost nozzle, boost-sustain nozzle, and miniseal nozzle static motor firings. The high pressure conventional seal was not acceptance tested. The objectives and the procedures were identical to those of the Minuteman tests discussed previously.

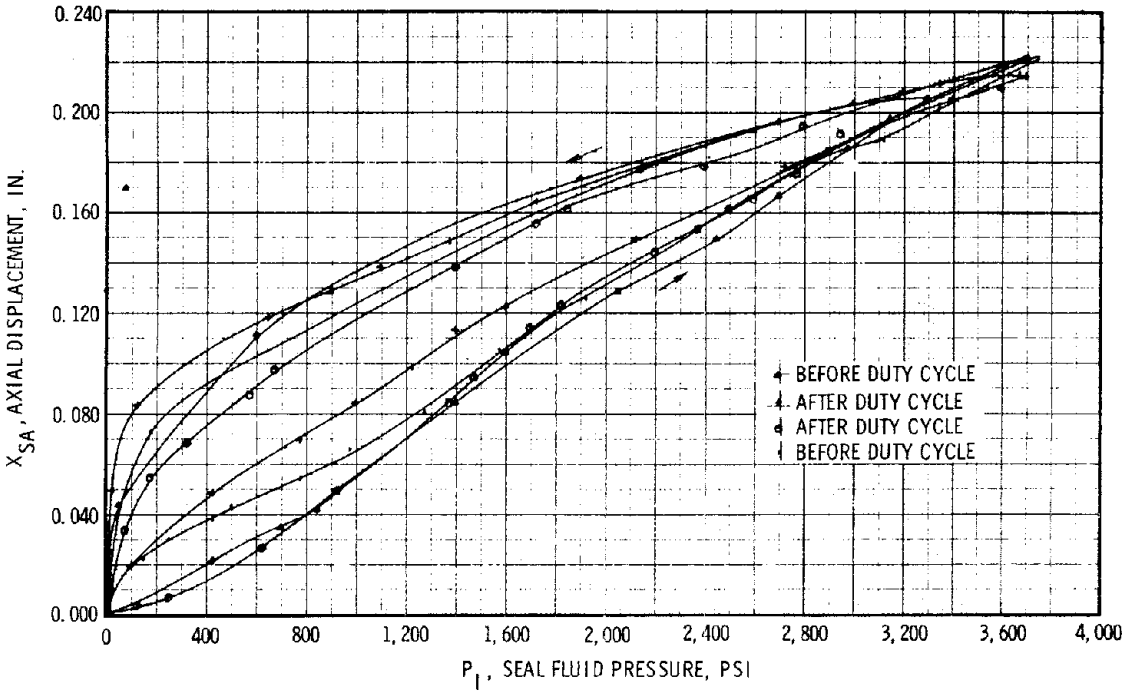

Figure 30. HIPPO (All-Boost) Axial Displacement vs Seal Internal Pressure

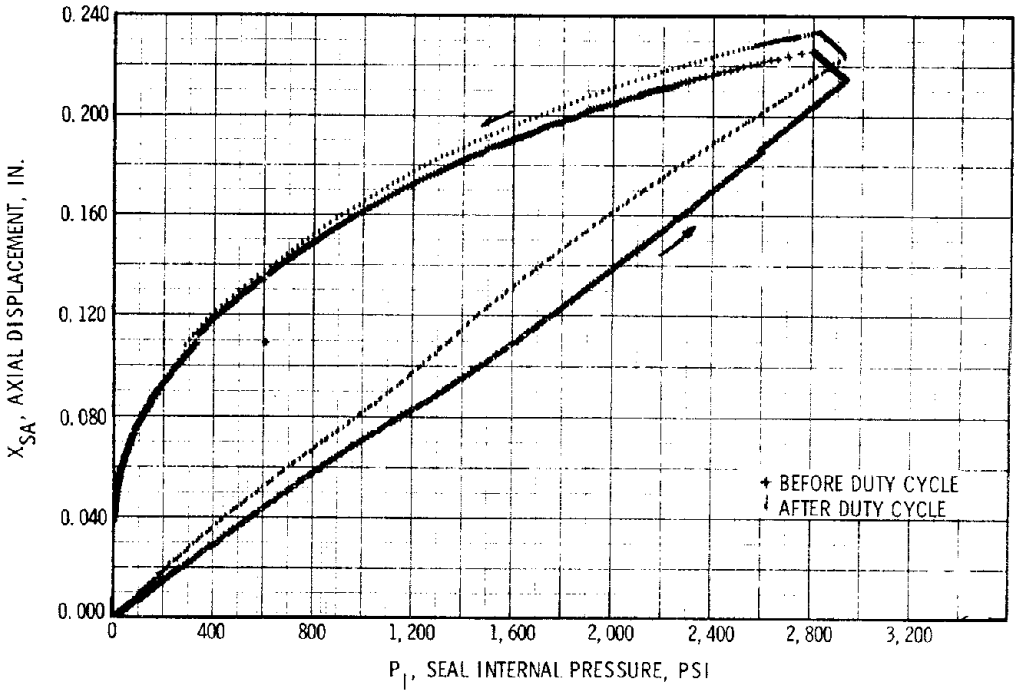

Figure 31. HIPPO (Boost-Sustain) Axial Displacement vs Seal Internal Pressure

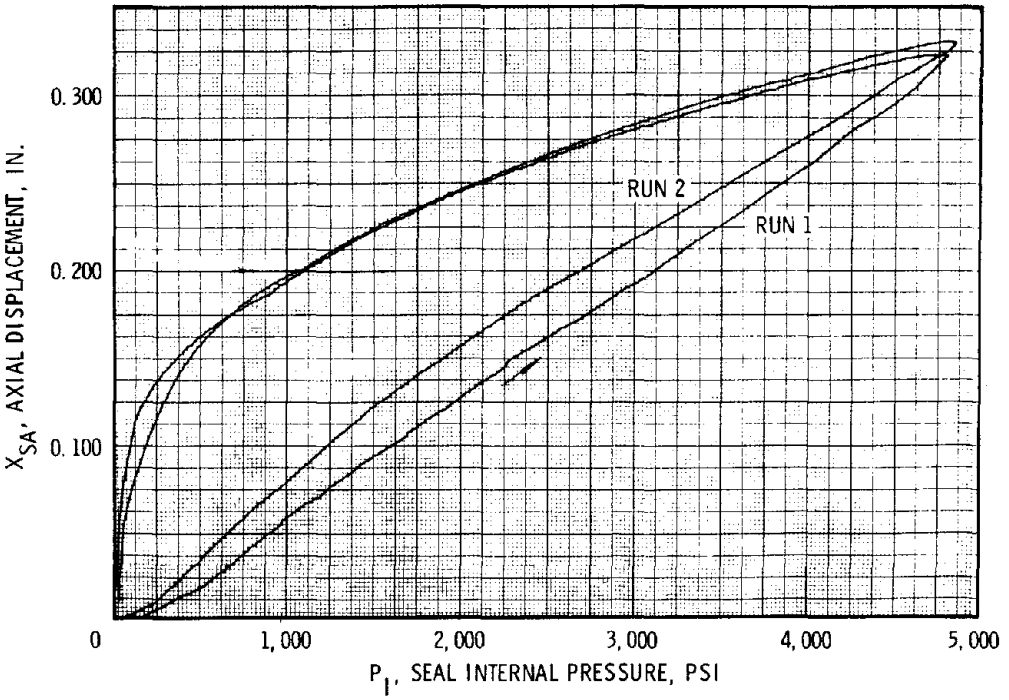

Figure 32. HIPPO (High Pressure) Axial Displacement vs Seal Internal Pressure

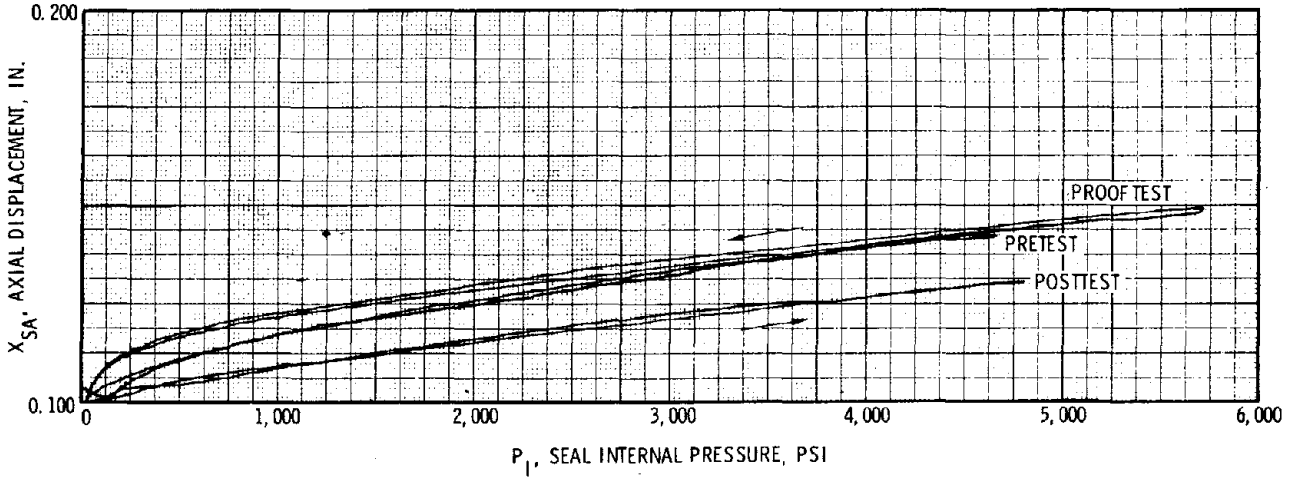

Figure 33. HIPPO (Miniseal) Axial Displacement vs Seal Internal Pressure

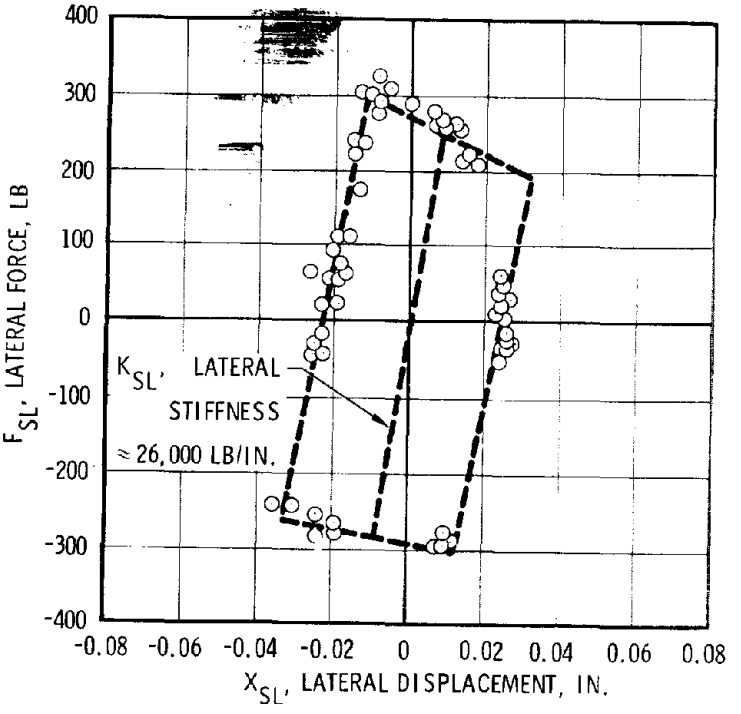

Figure 34. HIPPO TECHROLL Seal (Boost-Sustain) Lateral Stiffness

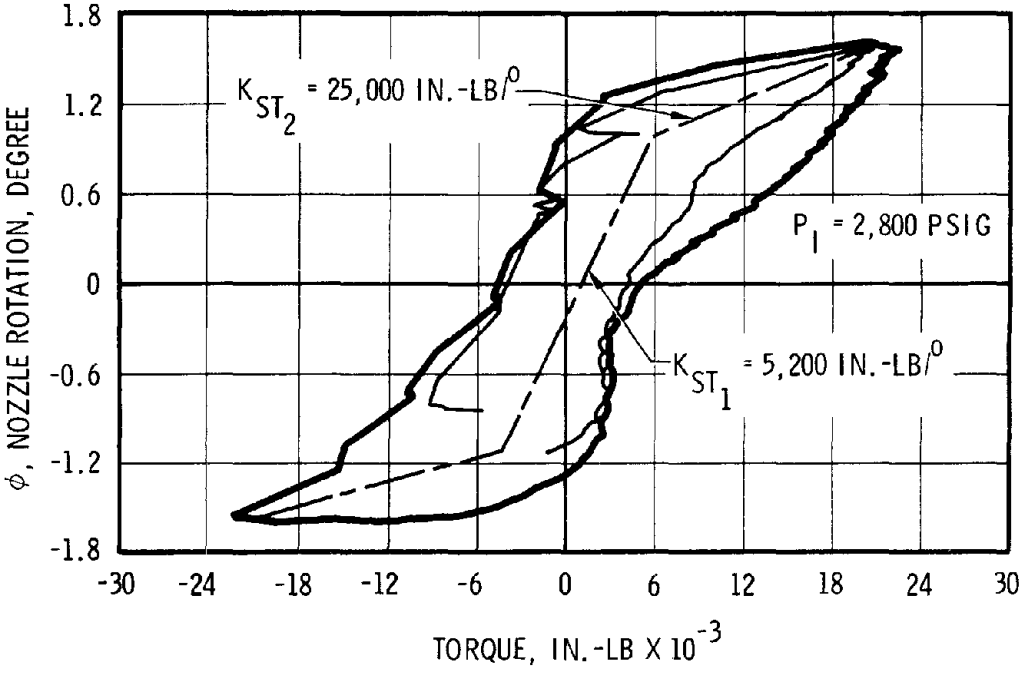

Figure 35. HIPPO TECHROLL Seal (Boost-Sustain) Torsional Stiffness

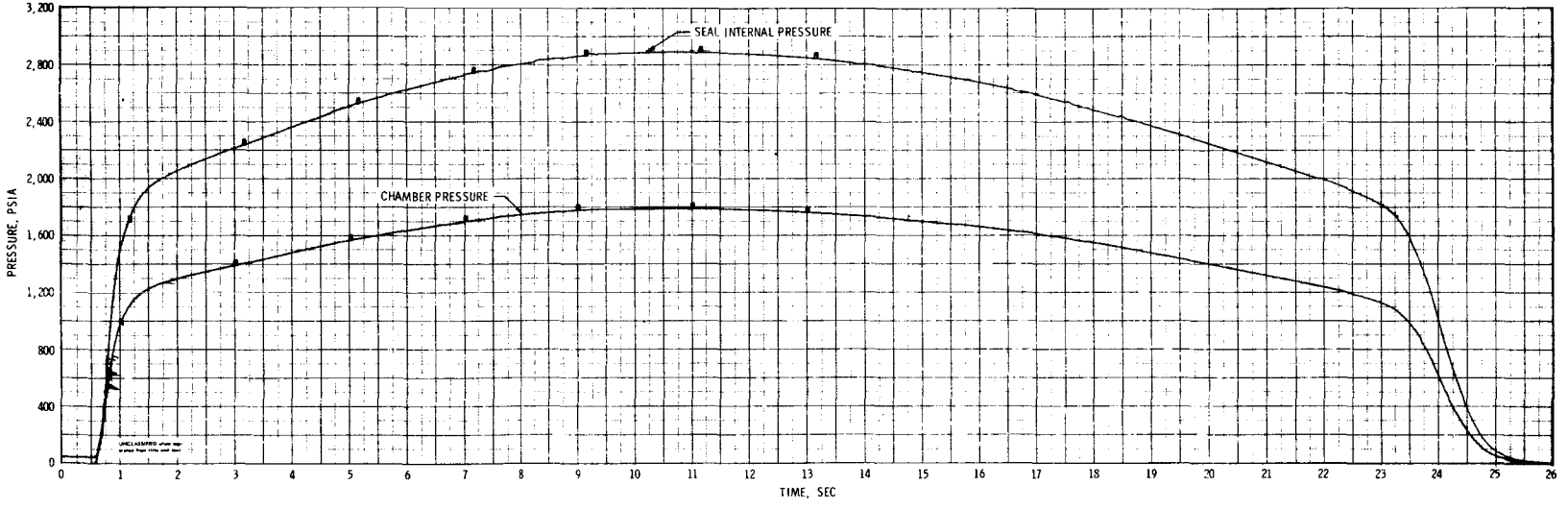

Figure 36. HIPPO (All-Boost) Nozzle Static Firing
Chamber Pressure and Seal Internal Pressure vs Time

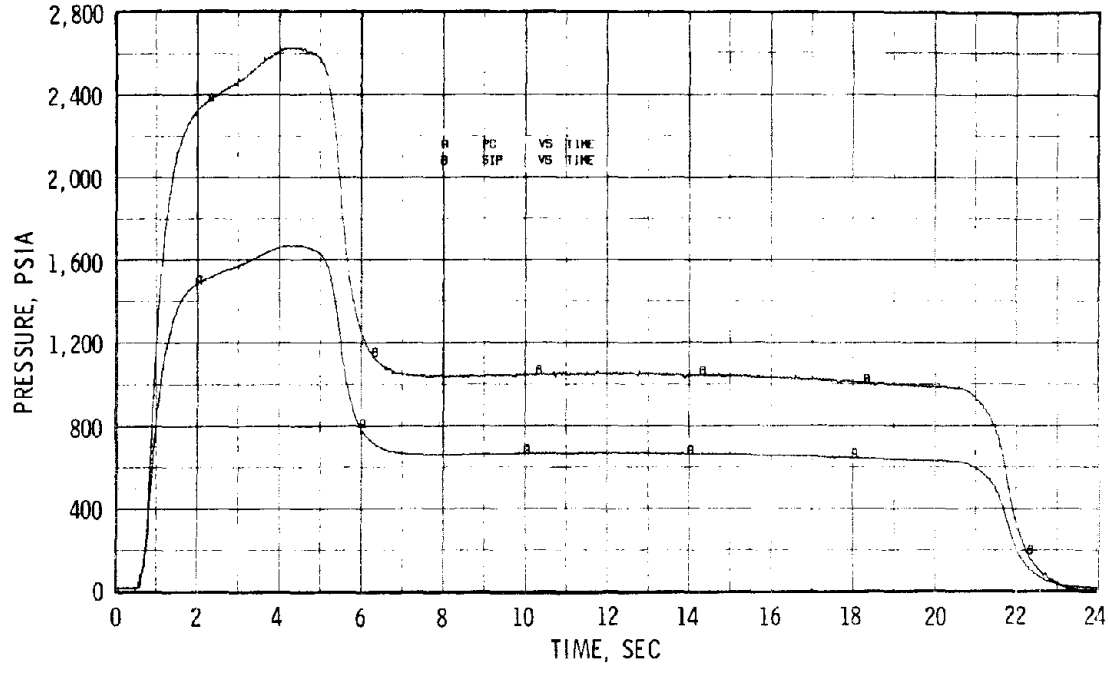

Figure 37. HIPPO (Boost-Sustain) Nozzle Static Firing, Chamber Pressure and Seal Internal Pressure vs Time

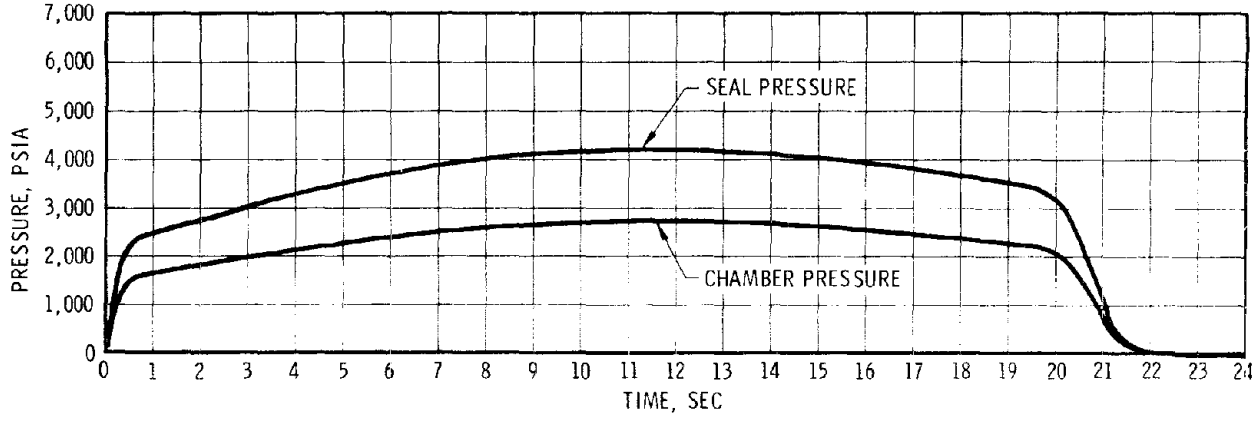

Figure 38. HIPPO (Miniseal) Nozzle Static Firing, Chamber Pressure and Seal Internal Pressure vs Time

Ignition shock test: These tests were conducted to simulate the ignition transient effects. Both conventional HIPPO seals (tested by raising the seal pressure to MEOP within approximately 500 msec) exhibited no anomalous characteristics. Based on previous favorable results, this test was not repeated for the HIPPO miniseal.

Safety margin test: The two-layer conventional HIPPO seals were tested similarly to the Minuteman seal. These seals survived 120 sec at 3,700-psi chamber pressure prior to failure. The failure mode was structural failure of the composite. This test demonstrated a factor of safety of 1.28 based on a HIPPO test motor MEOP of 2,000-psia and a maximum seal pressure of 2,900 psia. Figure 33 shows the proof pressure test on the HIPPO miniseal in which the seal was held at 5,700 psig for 10 sec without failure.

Simulated duty cycle test: The open loop duty cycles for the all-boost and boost-sustain nozzle tests were similar (figures 39 and 40). During the open loop duty cycles, the movement of the nozzle in the axial and lateral directions and the total actuation torque were monitored. The closed loop duty cycle for bench testing the miniseal nozzle (figure 41) was conducted in segments due to command source limitations. Nozzle motion and torque data were recorded. Figure 42 shows a plot of axial and lateral movements of the conventional all-boost and boost-sustain nozzles. Both nozzles exhibited small excursions during the duty cycle.

The first series of bench testing the miniseal nozzle resulted in an inner-half seal failure. All mechanical interference problems and nonconcentricities of the hardware were discounted as the cause. Inadequate lateral stiffness of the seal was suspected and investigated analytically.

Under certain conditions of seal geometry and high pressure, the lateral stiffness (spring rate) can become negative. If this condition exists, a small disturbance can drive the seal to its extreme lateral displacement. This lateral bottoming could cause both pinching and overstressing of the convolute of the seal (figure 43) and could lead to failure.

Because of the unexplained inner convolute failures on the two-layer HIPPO miniseals, an investigation was conducted to determine whether lateral stiffness effects were the cause. Analytically, the miniseals (two layers of fabric on both the inner and outer convolute) showed a negative lateral stiffness (nonrestoring) at the operating pressure (figure 44). Negative lateral stiffness would result from pinching the inner convolute at one point (with a force exceeding 700 lb at MEOP) and overstressing the inner convolute at another point (at least 33% over the the design stress). Experimentally, a negative lateral stiffness

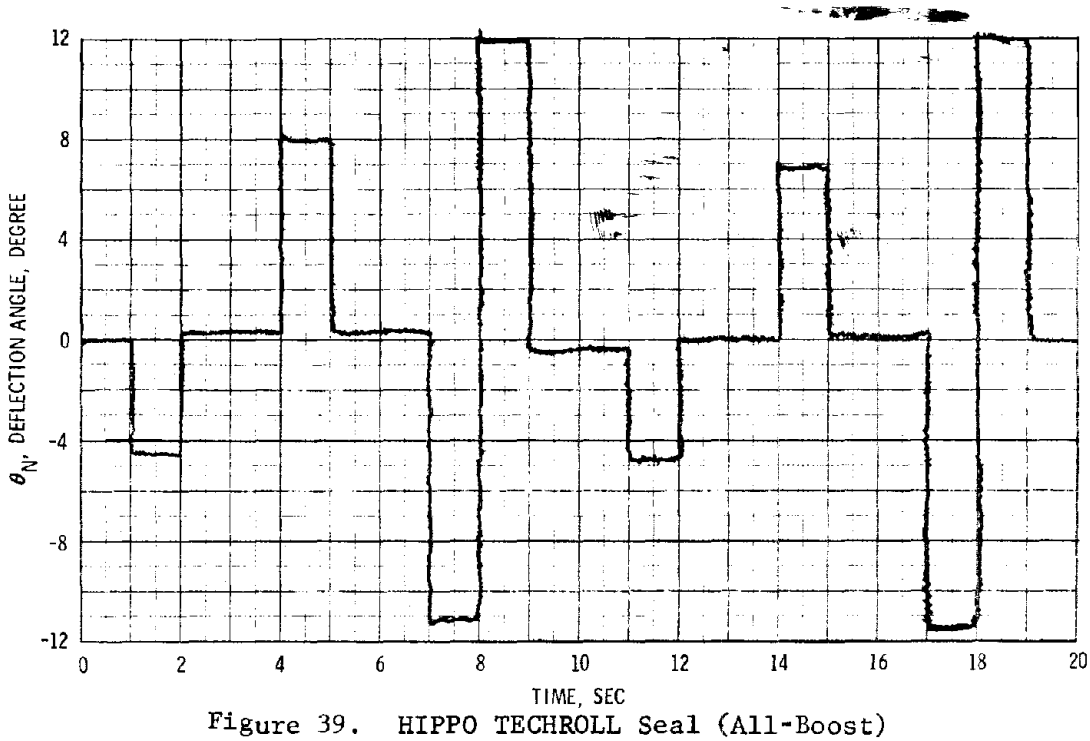

Figure 39. HIPPO TECHROLL Seal (All-Boost)
Bench Test Duty Cycle

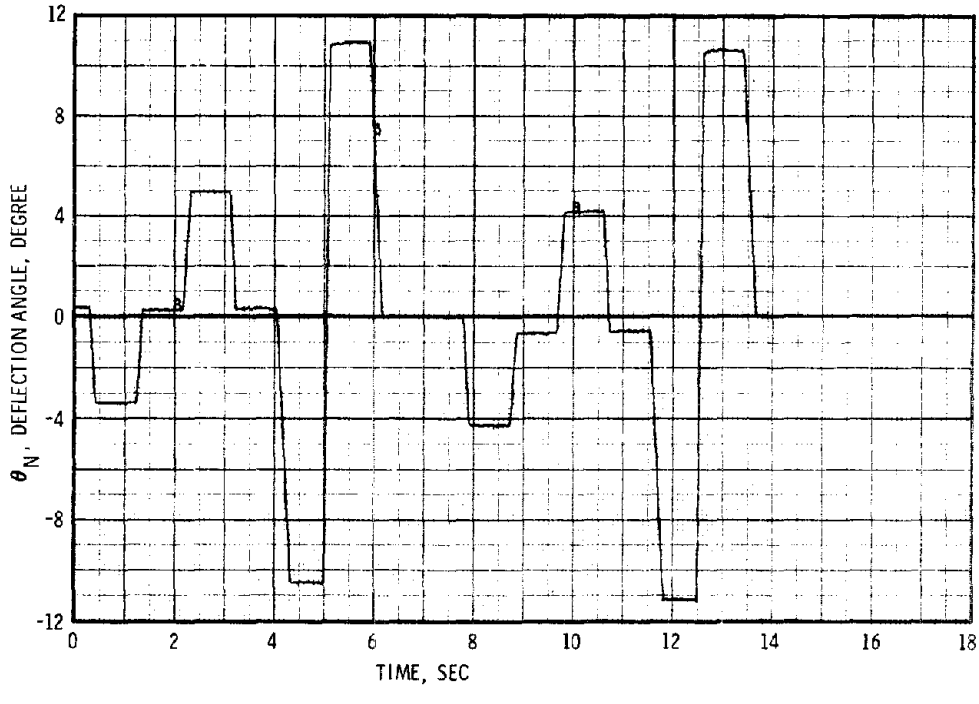

Figure 40. HIPPO TECHROLL Seal (Boost-Sustain)
Bench Test Duty Cycle

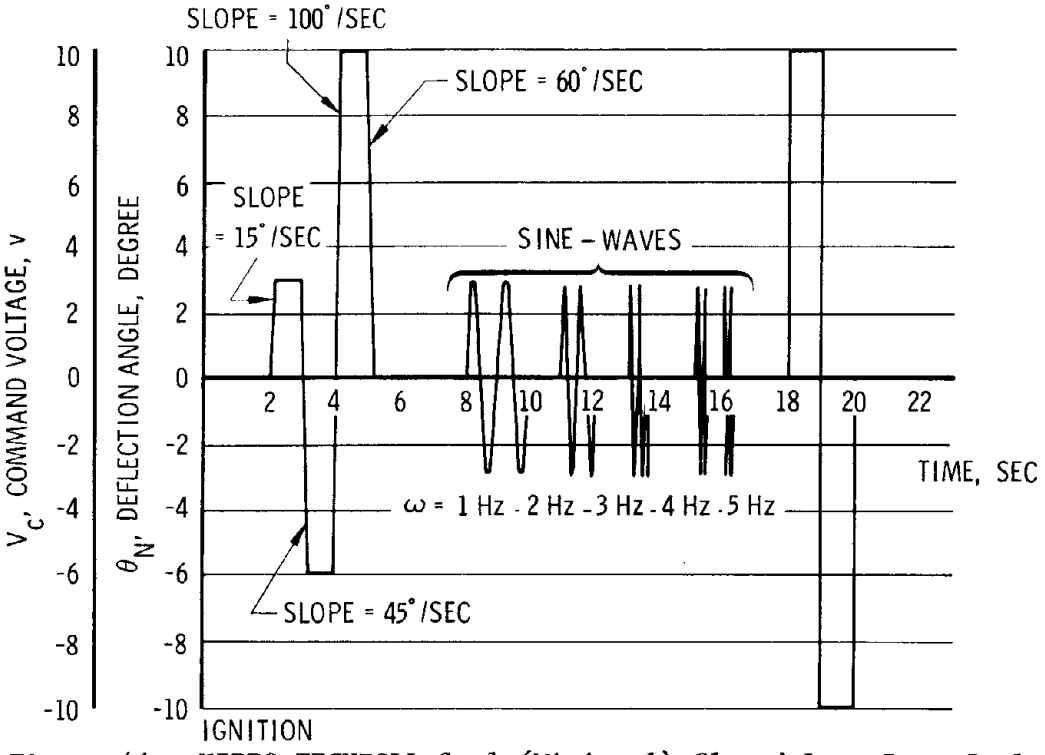

Figure 41. HIPPO TECHROLL Seal (Miniseal) Closed Loop Duty Cycle

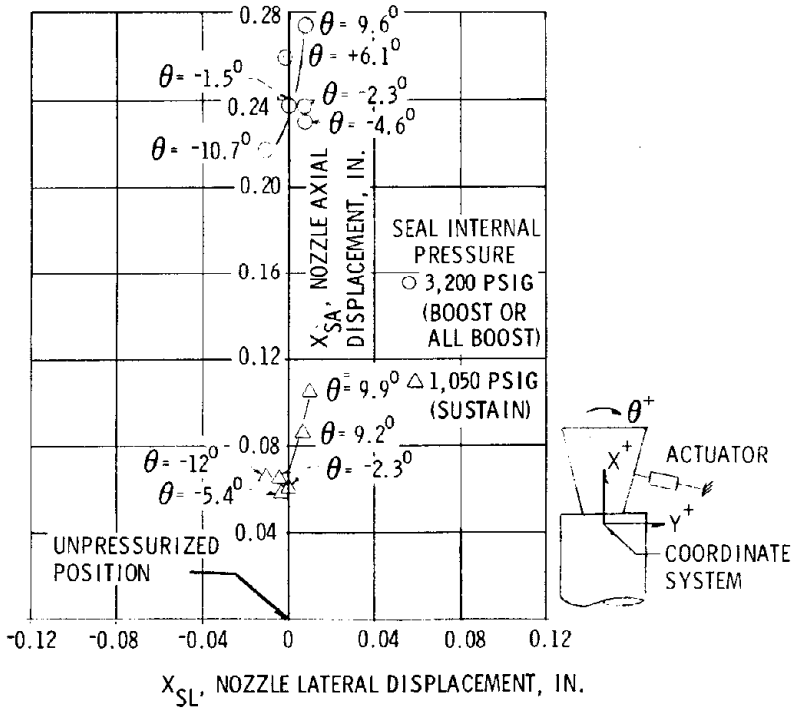

Figure 42. HIPPO (All-Boost and Boost-Sustain) Nozzle Movements vs Deflection Angle

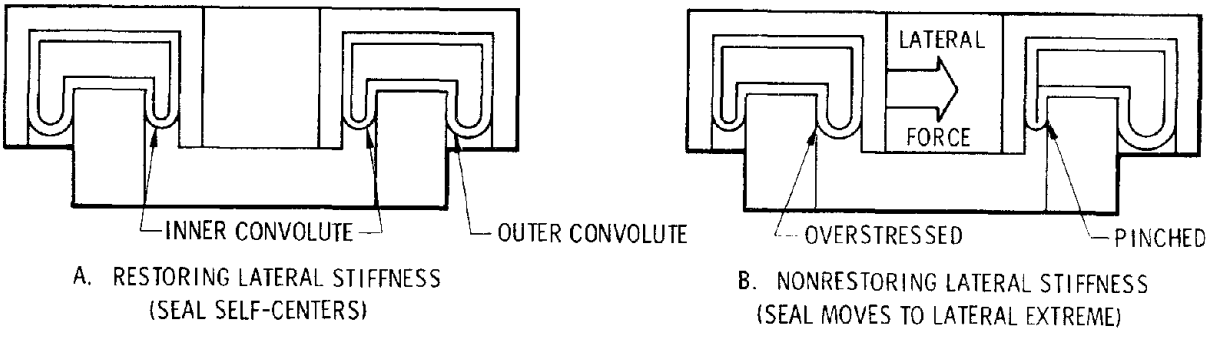

Figure 43. TECHROLL Seal Lateral Stiffness Effects

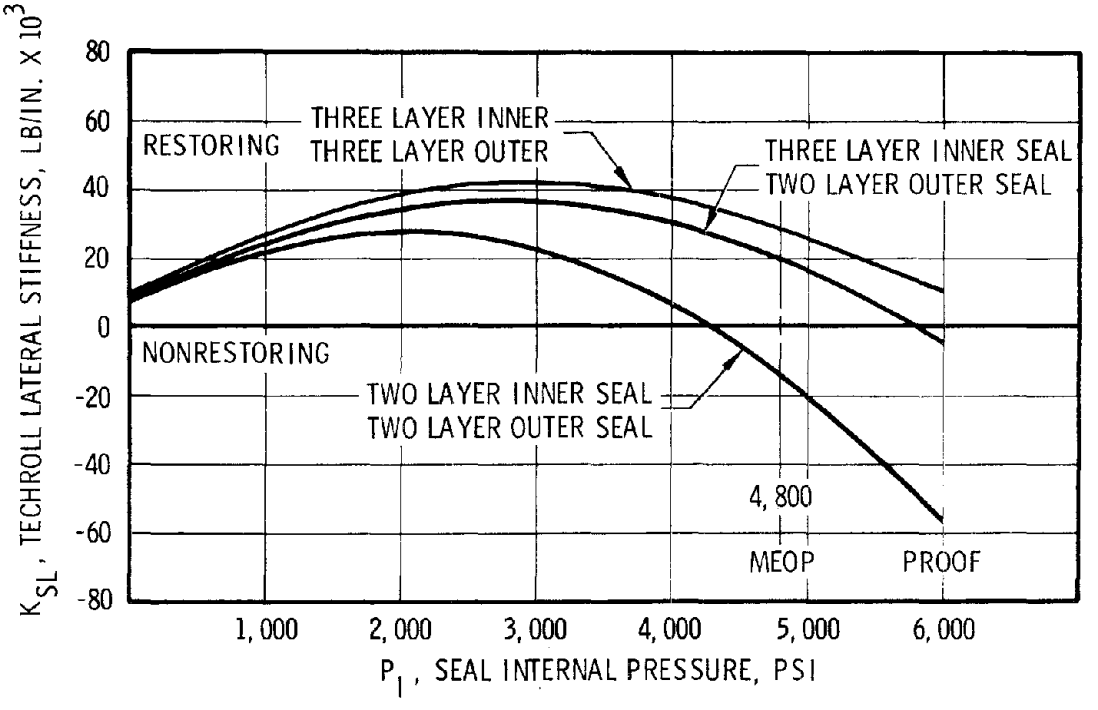

Figure 44. HIPPO TECHROLL (Miniseal) Lateral Stiffness vs Fluid Pressure (Theoretical)

has not been verified conclusively; however, there are indications that the condition exists, including observed abrasion of the inner convolutes, and or unusually large offset torques. A lateral stiffness deficiency was a probable cause of the initial miniseal failures. Analysis indicated that condition could be corrected by increasing total fabric thickness. By adding a third fabric layer of the same thickness (0.013 in.) to the inner seal and eventually to the outer seal, an increased lateral stiffness was achieved (figure 39) and bench testing was completed successfully.

Figures 45 and 46 show the total actuation torques obtained during the open loop duty cycles of the two conventional HIPPO nozzles. Figures 47 through 50 show the total actuation torques obtained during the closed loop duty cycle of the HIPPO miniseal nozzle. Figures 47 and 48 show the HIPPO miniseal response to full amplitude step commands. Figures 47 and 48 show that the total peak actuation torque required was 5,000 in.-lb to achieve a peak nozzle velocity of approximately 420°/sec. Figure 49 depicts the nozzle response to a 2.2-Hz ±10° triangle wave. As anticipated, the velocity was approximately 90°/sec. Figure 50 shows the nozzle response to a 1- through 5-Hz sine wave of amplitude ±3°. Again, the resulting response was as anticipated. Using a liquid filled hydrotest fixture as in the Minuteman test sequence, the bench test technique added additional viscous drag torque components to the total actuation torque. The difference is not apparent at high nozzle velocities, as indicated in a comparison of torques (figures 47, 48, and 22).

(d) Viscous Fluids Special Test

Fluid damping: The flow of fluid in the seal as the nozzle is deflected adds damping to the system. For small tactical systems this additional damping could contribute the actuation torque required to move the nozzle. Initially, this coefficient was derived analytically as described earlier. However, a special test was inserted into the bench test phase of the HIPPO (boost-sustain) nozzle to verify the analytical technique. Experimental values of TECHROLL seal fluid damping were obtained for three seal fluid viscosities at various nozzle deflection angles and velocities. These results are plotted in figure 51 with the theoretical relationships. Valid data were obtained for the high viscosity (60,000 centistoke) fluid where seal damping becomes measurable relative to other seal and actuator parameters. Available test data seem to support the validity of the analytically derived equation for predicting TECHROLL seal damping. Figure 51 shows experimental data for the high viscosity fluid agree with the theoretical data over approximately 75% of

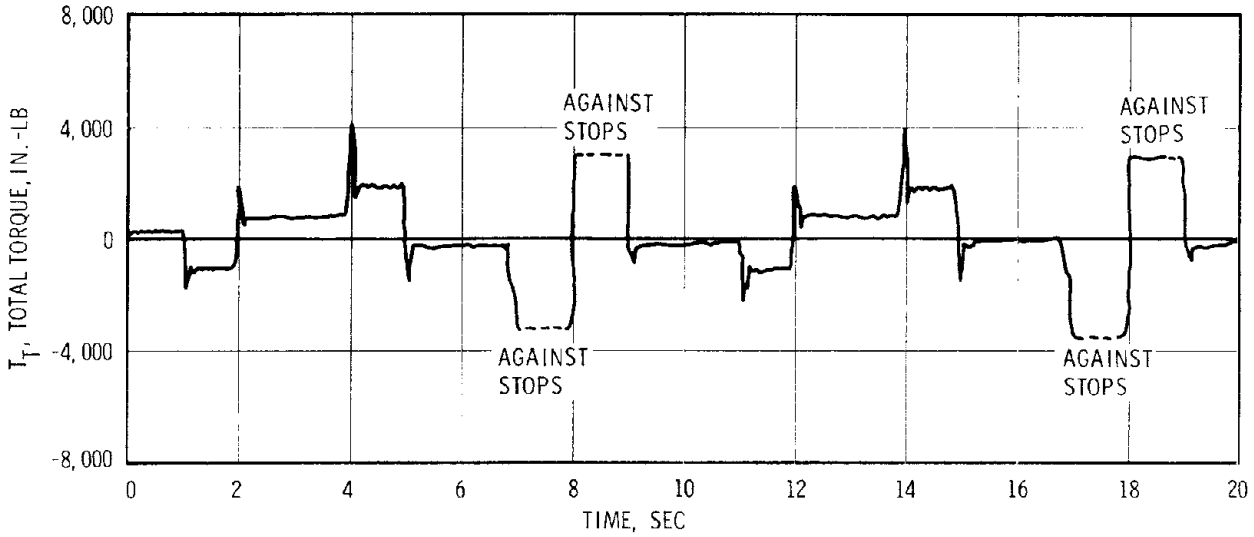

Figure 45. HIPPO (All-Boost) TECHROLL Seal Total Torque During Bench Test Duty Cycle

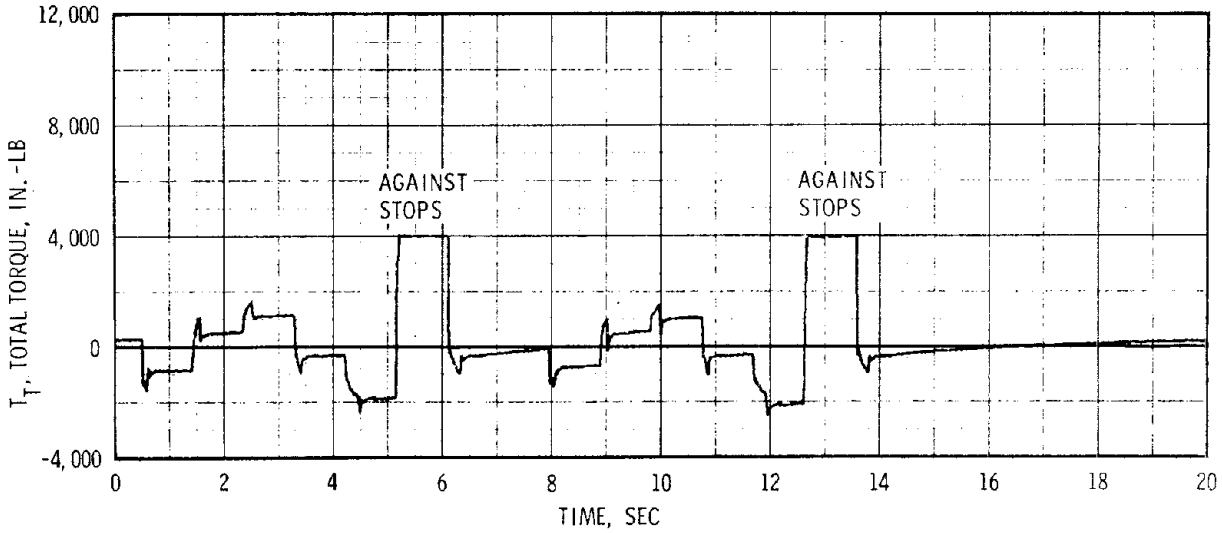

Figure 46. HIPPO (Boost-Sustain) TECHROLL Seal Total Torque During Bench Test Duty Cycle

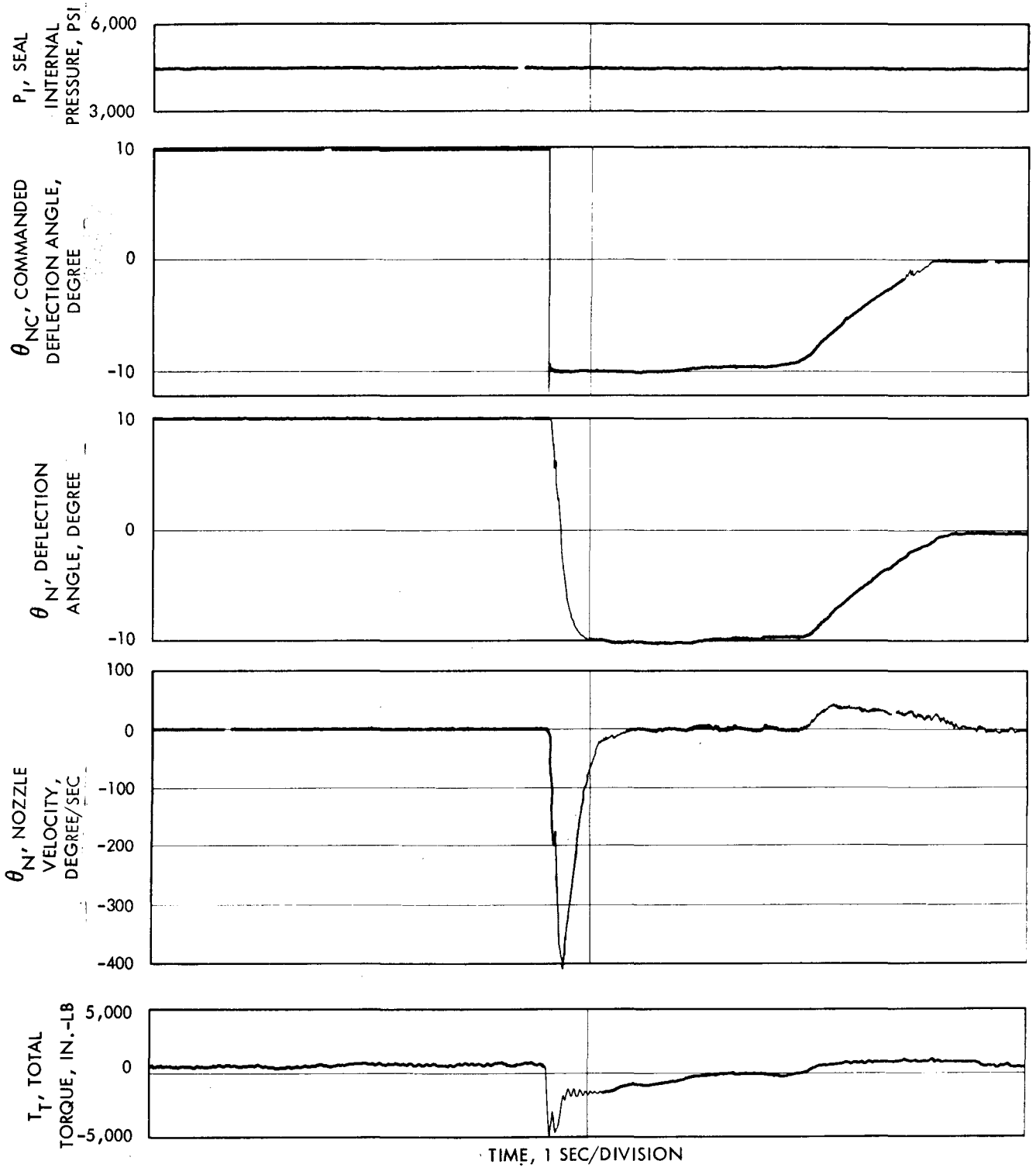

Figure 47. HIPPO (Miniseal) $+10^{o}$ to -10^{o} Step Response

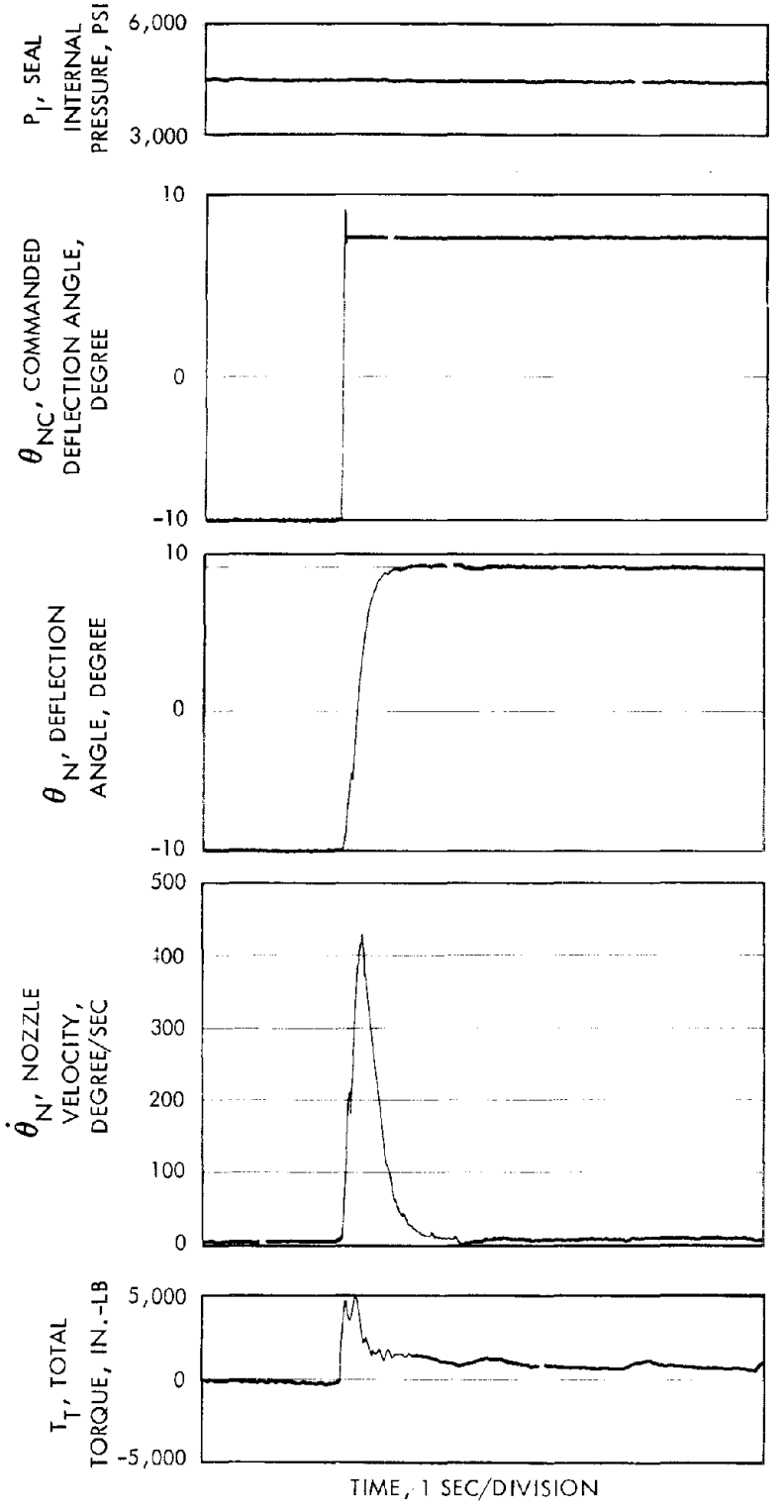

Figure 48. HIPPO (Miniseal) -10^{o} to $+10^{o}$ Step Response

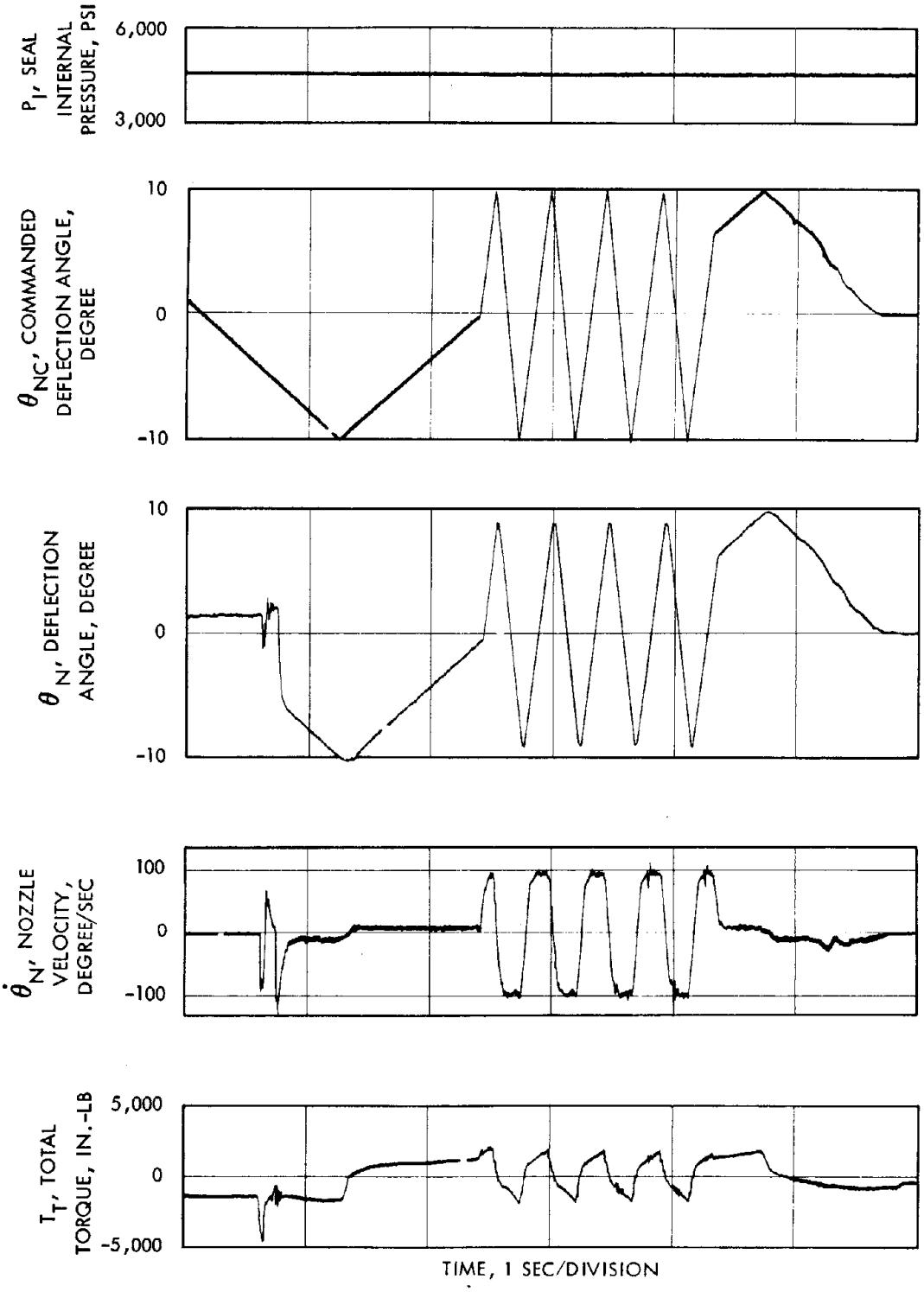

Figure 49. HIPPO (Miniseal) 22.2 Hz $\pm 10^{o}$ Triangular Wave Response

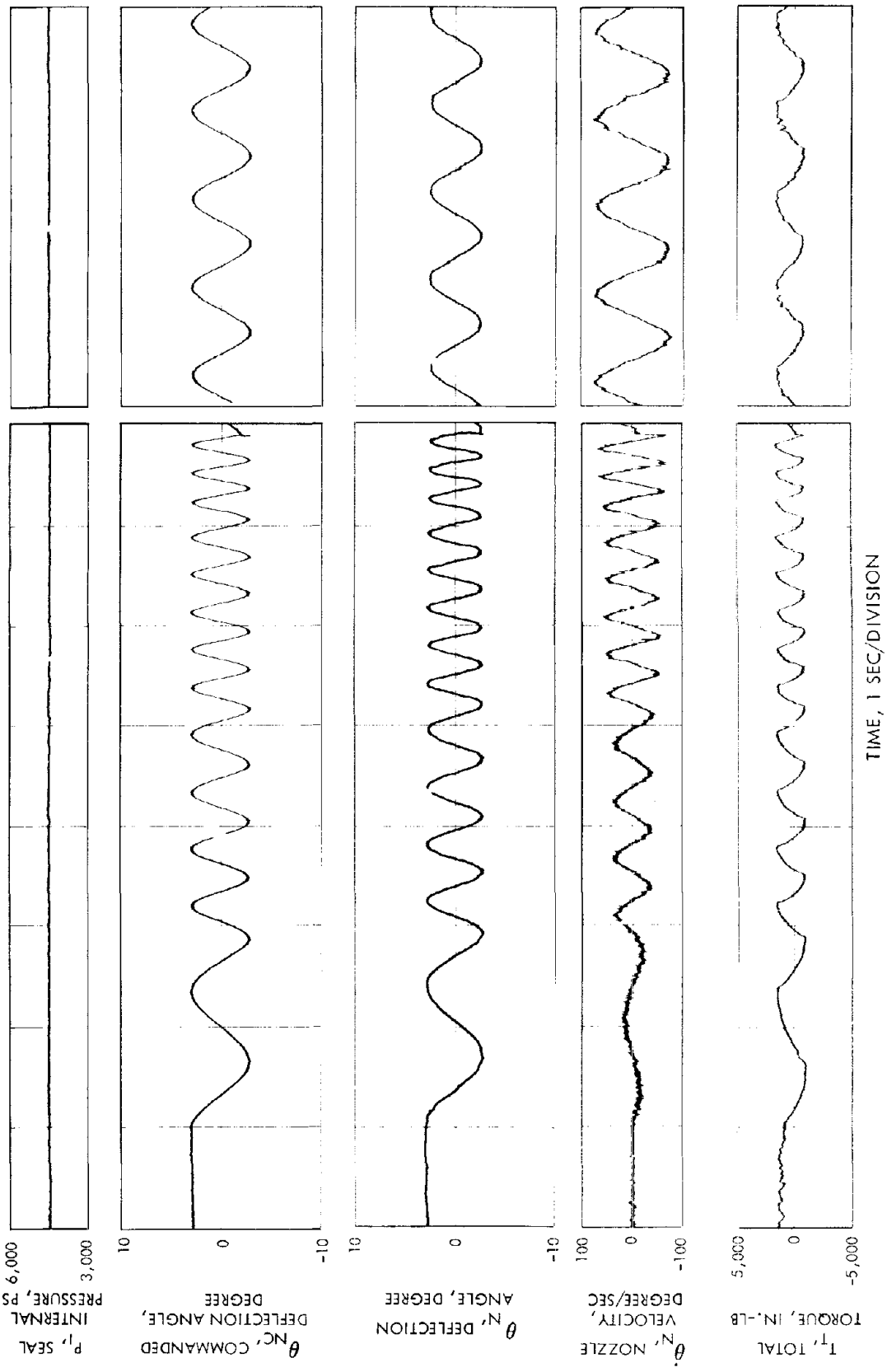

Figure 50. HIPPO (Miniseal) 1 through 5 Hz $\pm 3^{o}$ Sine Wave Response

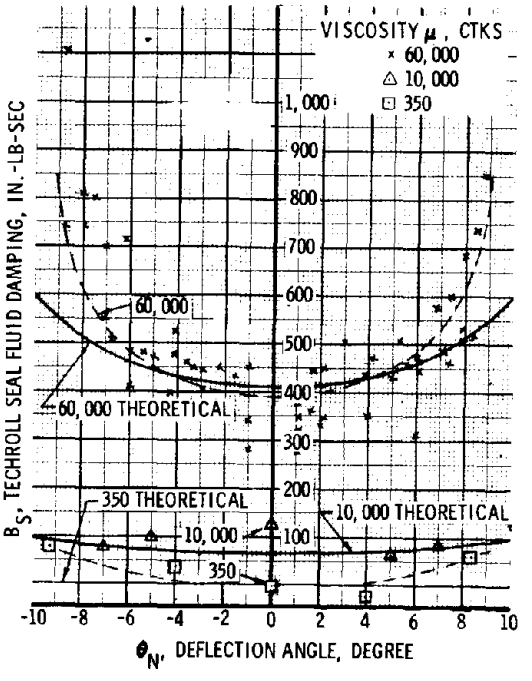

Figure 51. HIPPO TECHROLL Seal Fluid Damping vs Nozzle Angular Deflection

the deflection range to within a ±20% tolerance; however, at extreme deflection angles experimental damping exceeds the theoretical. Damping data for the two lower fluid viscosities are sufficiently accurate to substantiate the predicted proportionality between damping and viscosity.

Experimental seal damping data were obtained with difficulty for the three test fluids (figure 47); however, data accuracy is roughly proportional to the viscosity of the fluid used in the test. At one extreme, damping values for the high viscosity fluid should be reasonably accurate (within approximately ±10%), while values for the low viscosity fluid may be accurate only within an order of magnitude. At the high slew rates required for these tests, it was discovered (analytically) that the actuator introduced considerable apparent damping caused by pressure drops between the cylinder cavities and their respective pressure transducers. Furthermore, due to the nonsymmetrical nature of the actuator, actuator damping coefficients were different for positive and negative velocities.

Fluid inertia: Because the fluid must be accelerated from rest, the fluid mass adds inertia to the movable nozzle. For large accelerations, its contribution to the actuation torque may be large. This test attempted to determine the coefficient I_F in the torque equation but was unsuccessful. No valid experimental data were obtained from the seal fluid inertia tests. This result was a consequence of a combination of the following effects:

A. The HIPPO seal geometry and available fluid densities result (theoretically) in extremely small inertia values for the seal relative to other torque-related parameters (especially nozzle inertia and seal hysteresis).

B. The existing HIPPO open loop actuator produced significant start-stop torque transients during large accelerations (when inertia measurements should be made).

C. The digital data reduction system could not compute instantaneous values of angular acceleration with sufficient accuracy. Three sampling rates were attempted: 100, 500, and 1,600 samples/sec.

(e) Static Test

Three HIPPO TECHROLL seal movable nozzle systems, the all-boost, boost-sustain, and miniseal, were successfully static fired, in accordance with the test methods detailed in appendix III. All objectives were satisfied.

Total nozzle torques: The total actuation torques are shown in figures 52, 53, and 54 for the all-boost, boost-sustain, and the miniseal tactical air-launched configured nozzles occurring during their respective static firing duty cycles which are shown in figures 55, 56, and 57. The differences between total actuation torques and total bench test torques result from the increase in nozzle inertia due to addition of the nozzle ablatives, thermal insulation system, and gas flow through the nozzle.

Nozzle movements: Figure 58 shows the nozzle movements recorded during the combined static firings of the HIPPO all-boost and HIPPO boost-sustain nozzles. Comparison of these plots to those obtained during bench testing shows no significant difference. Miniseal nozzle movement data were not obtained due to channel cross-talk signals generated within the digital recording equipment during the static test.

Nozzle insulation performance: Figure 59 shows an external view of the HIPPO conventional seal and the HIPPO miniseal nozzle assembly prior to firing. A postfire visual inspection showed that the ablatives and grease retention cloth performed as predicted for the HIPPO conventional seals (figures 60 and 61) and

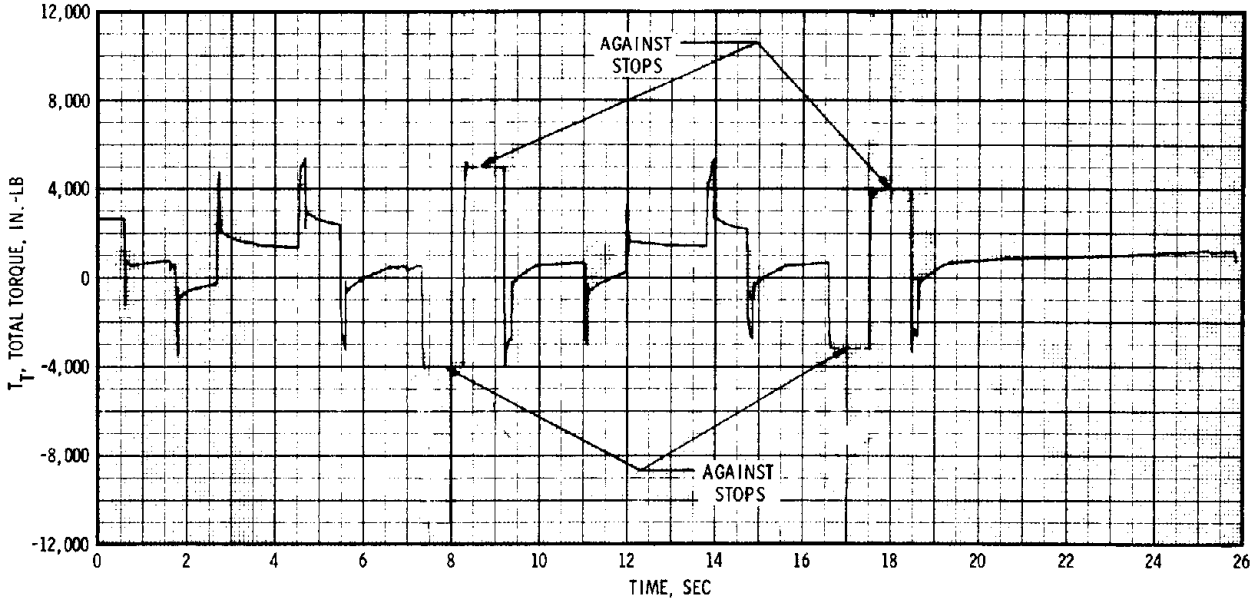

Figure 52. All-Boost TECHROLL Seal Nozzle Torque During Static Firing

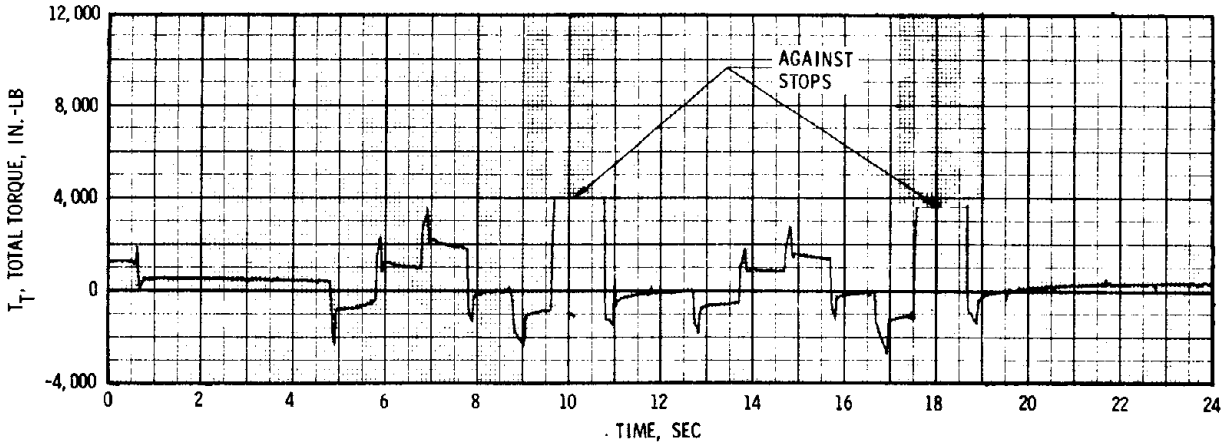

Figure 53. Boost-Sustain Nozzle Torque During Static Firing

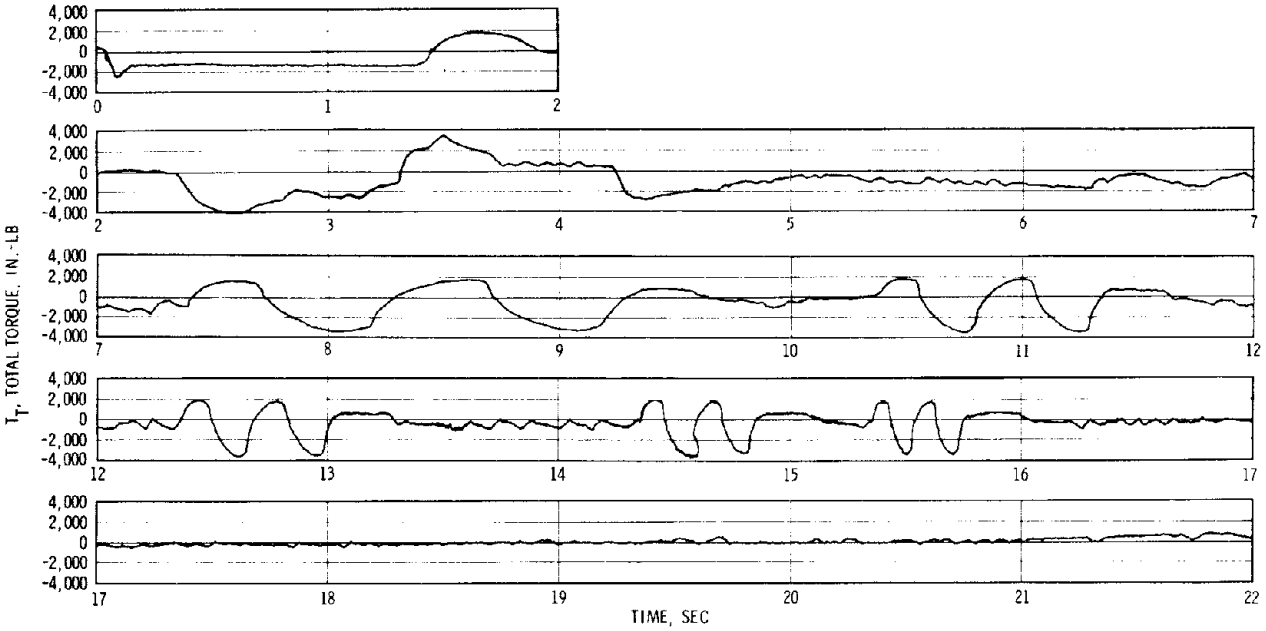

Figure 54. HIPPO (Miniseal) Nozzle Torque During Static Firing

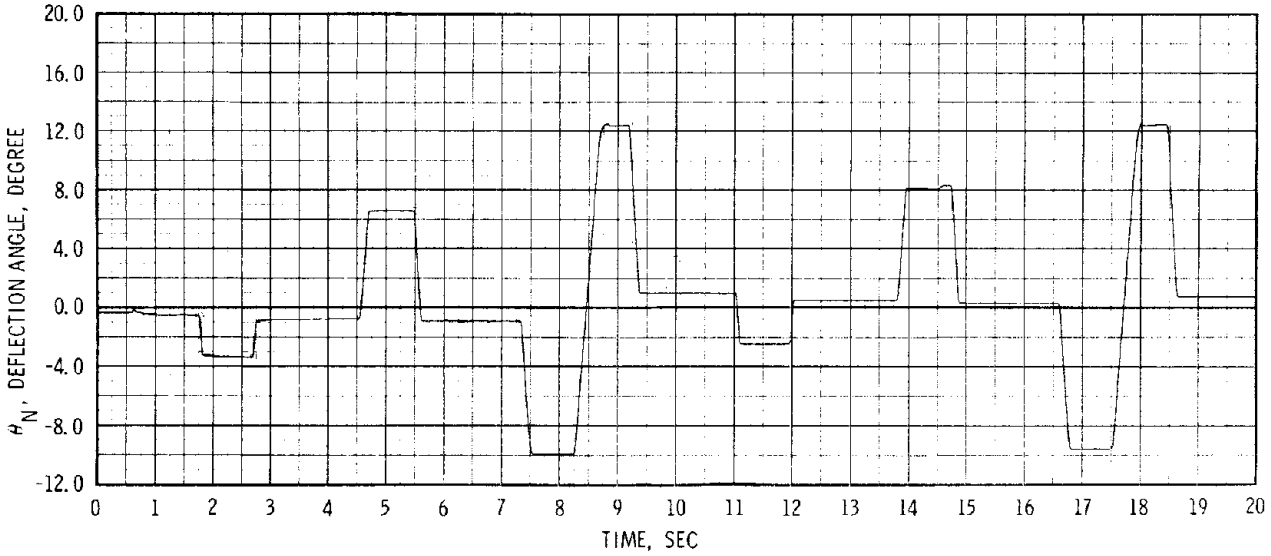

Figure 55. HIPPO (All-Boost) Static Firing, Open Loop Duty Cycle

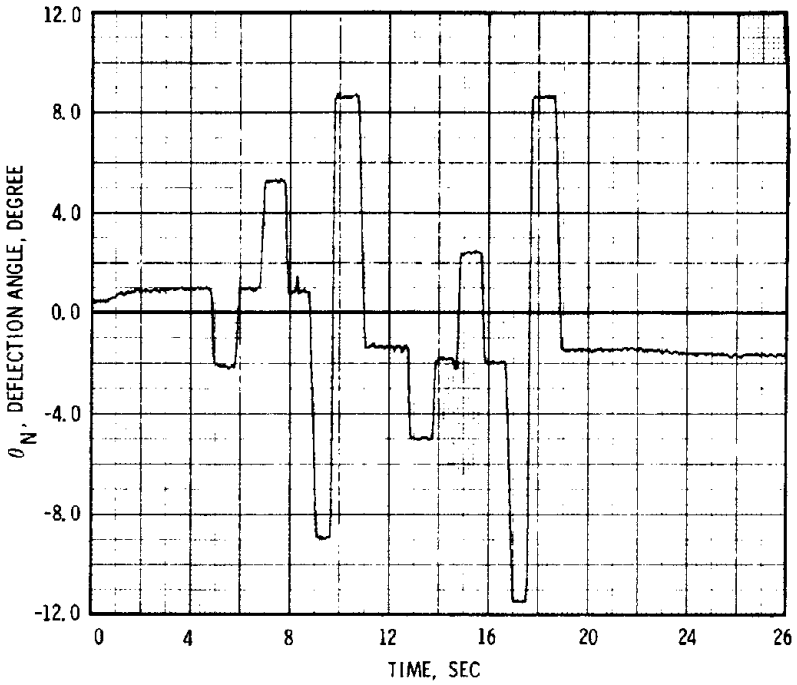

Figure 56. HIPPO (Boost-Sustain) Static Firing, Open Loop Duty Cycle

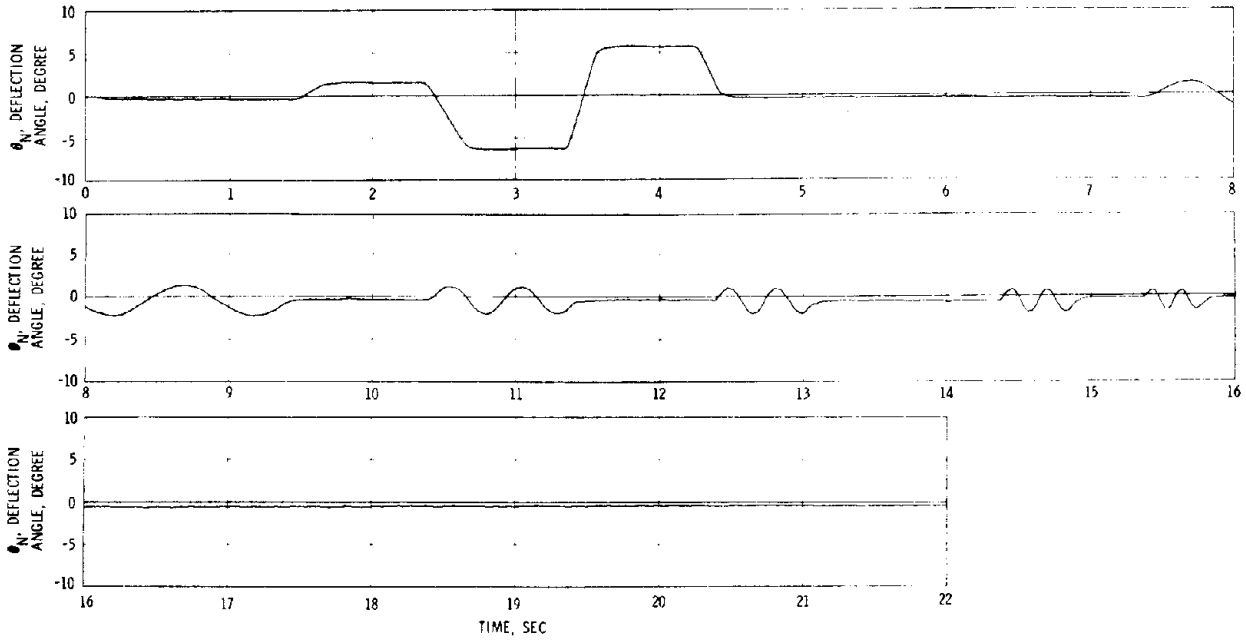

Figure 57. HIPPO (Miniseal) Static Firing, Closed Loop Duty Cycle

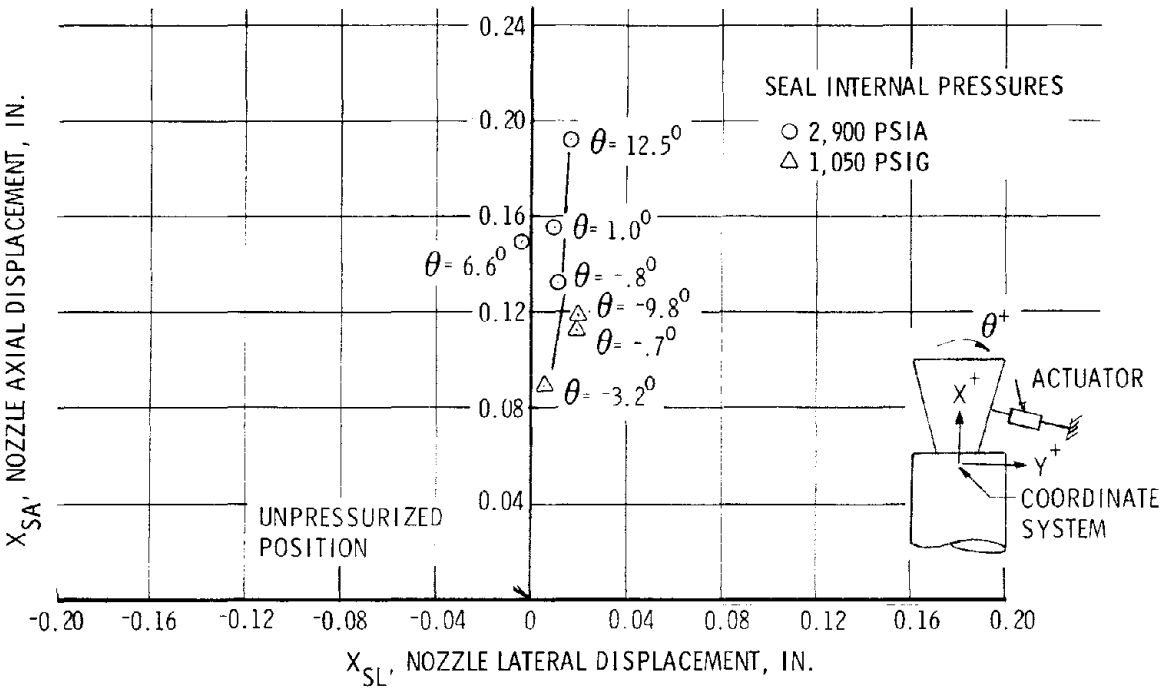

Figure 58. HIPPO (All-Boost and Boost-Sustain) Nozzle Movements During Static Firing

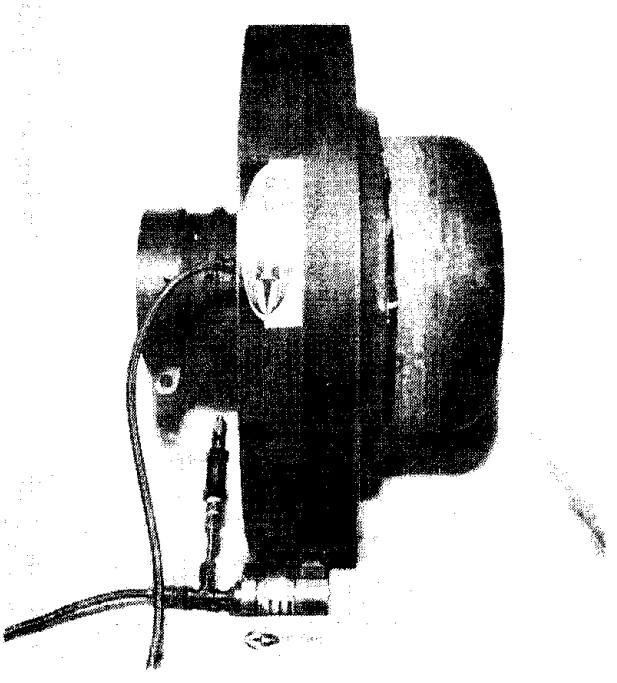

Figure 59. Prefire View of HIPPO Nozzle Assembly

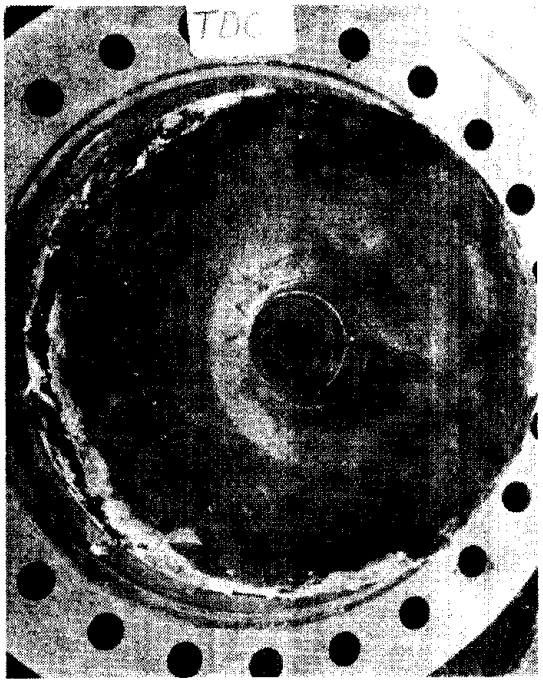

Figure 60. Postfire Aft View of Conventional HIPPO Nozzle Assembly

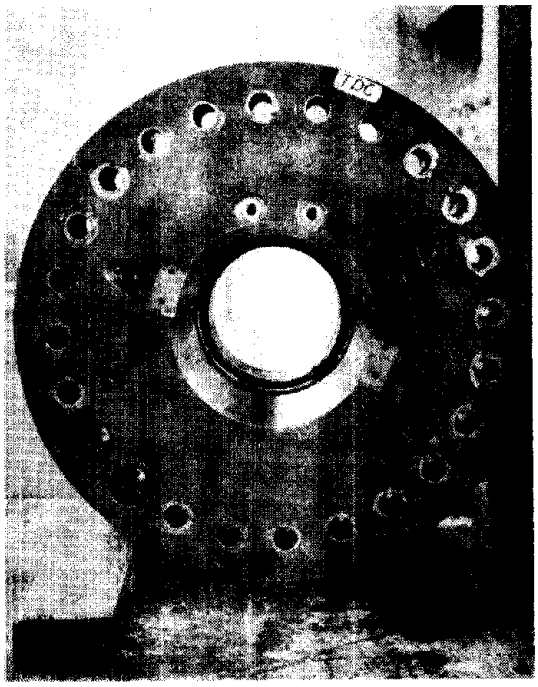

Figure 61. Postfire Front View of Conventional HIPPO Nozzle Assembly

for the HIPPO miniseals (figures 62, 63, and 64). In addition, no measurable grease loss was apparent. No provision was made in the program for postfire analyses and, therefore, no postfire ablation char data were recorded. After the first two firings, the nozzle assembly was disassembled and prepared for the next use. After the third firing, the nozzle assembly was left intact.

Expanded time plots: Figures 65 and 66 show expanded time plots of portions of the TVC duty cycles of the HIPPO all-boost and boost-sustain nozzle deflection angle, axial displacement, lateral displacement angular velocity, and seal torque during their respective static firings.

Figure 67 shows similar data for the miniseal nozzle. The firing of the miniseal seal was nominal. However, the data revealed a nozzle deflection command reduction during the duty cycle resulting a maximum deflection of less than the intended 10^{o}. The anomaly resulted from a malfunction in the facility command instrumentation and not within any test hardware. Evidence in support of this conclusion was verified by the loss of some of the digital output data and by the command levels monitored by by the ''quick-look'' oscillograph.

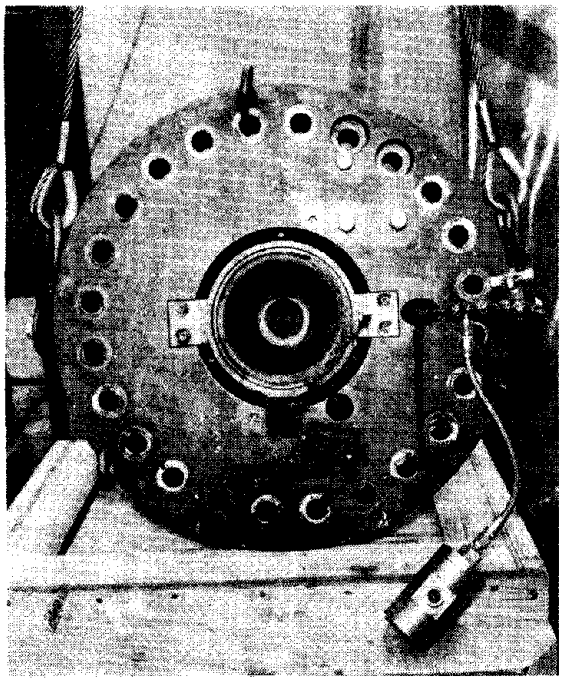

Figure 62. Postfire Aft View of HIPPO Miniseal Nozzle Assembly

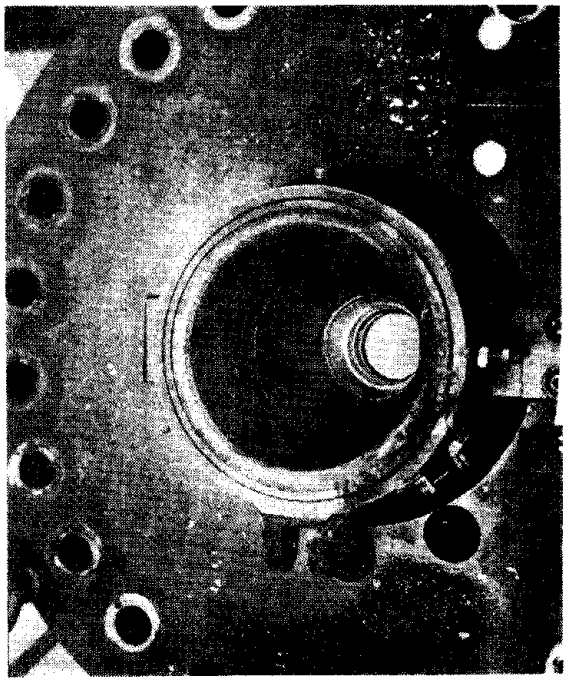

Figure 63. Postfire View of HIPPO Miniseal Nozzle Assembly

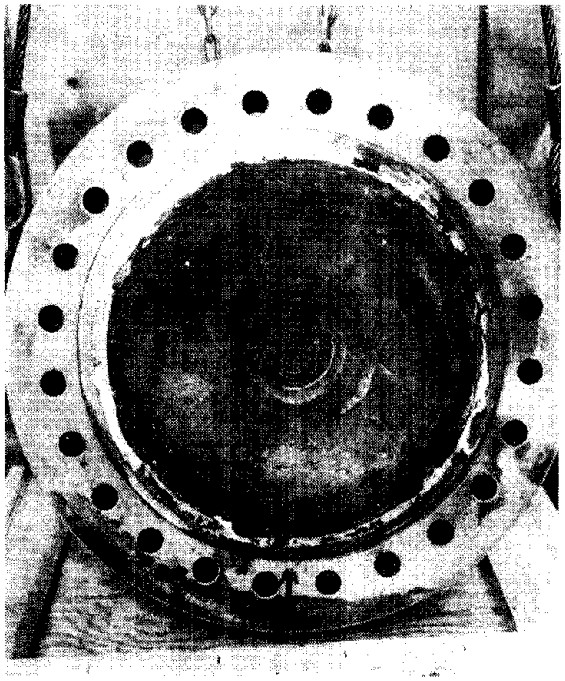

Figure 64. Postfire Front View of HIPPO Miniseal Nozzle Assembly

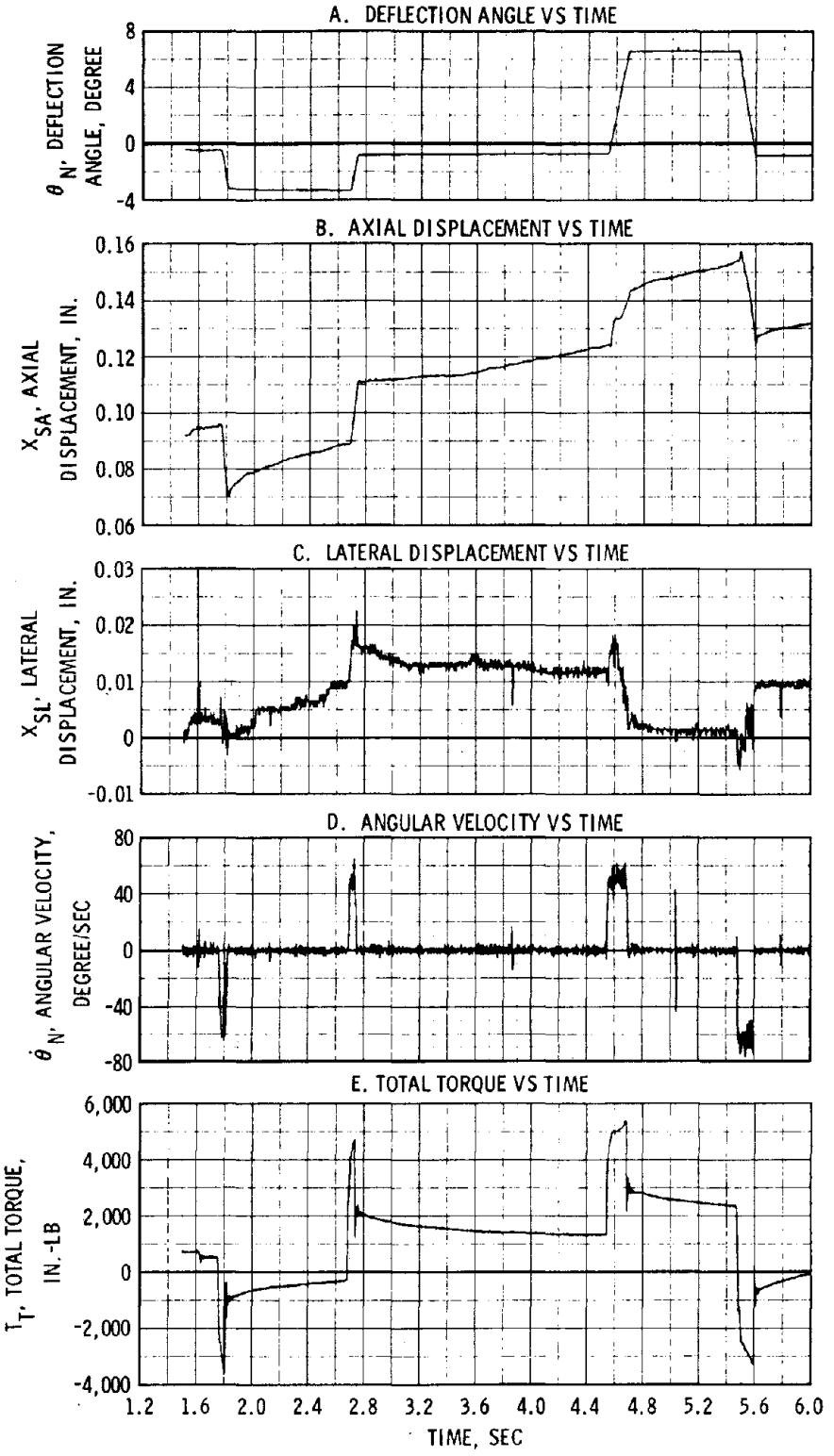

Figure 65. All-Boost Static Firing, Expanded Time Plots

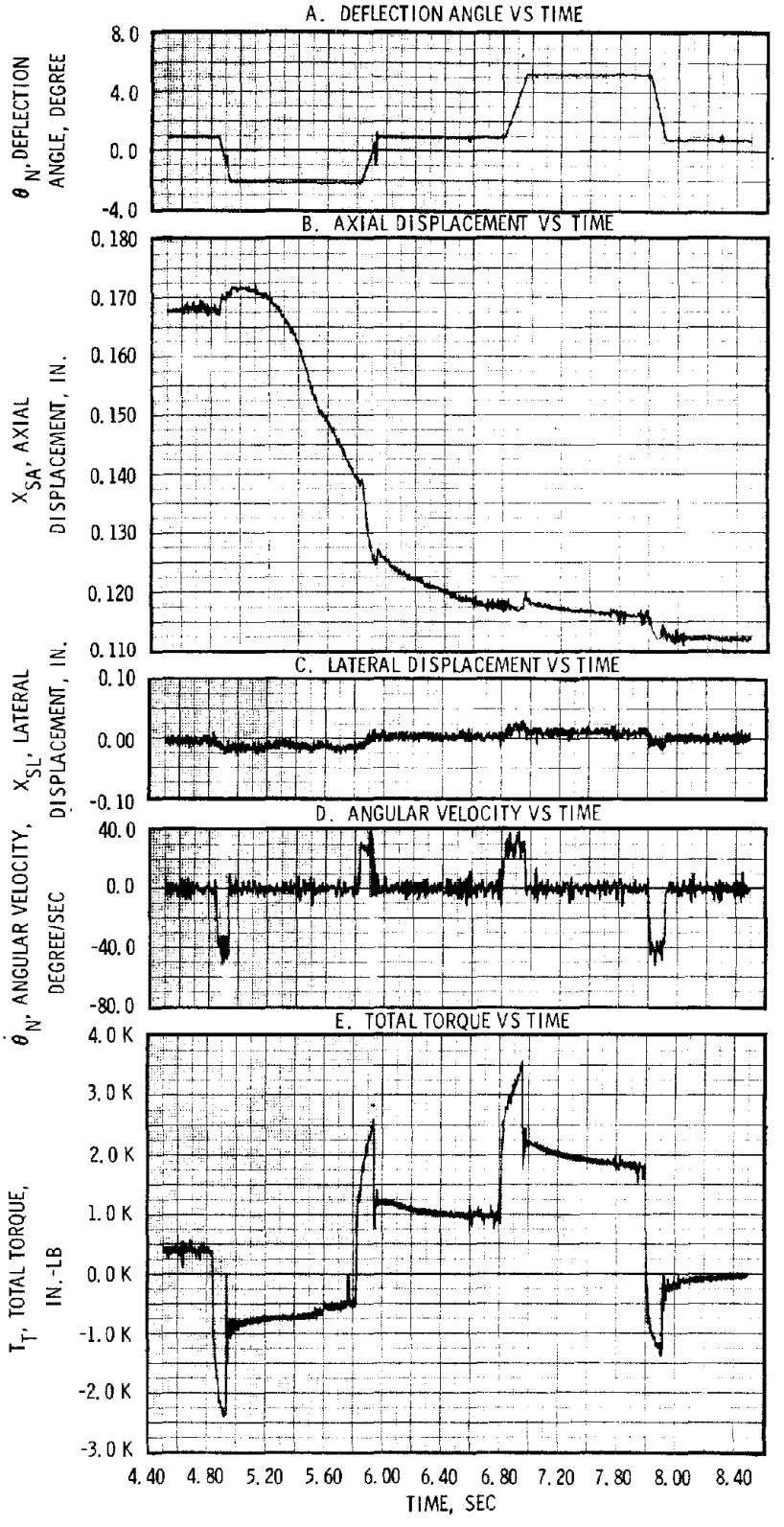

Figure 66. Boost-Sustain Static Firing, Expanded Time Plots

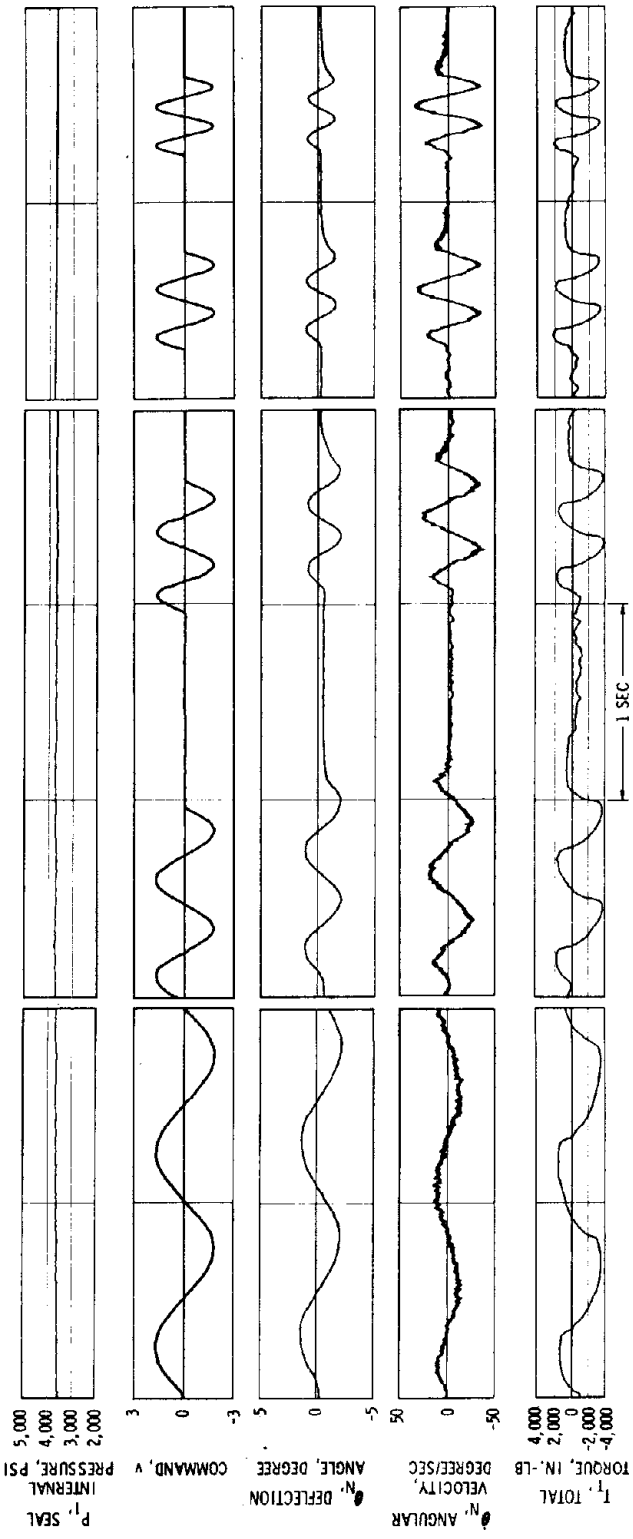

Figure 67. HIPPO (Miniseal) Static Firing, Expanded Time Plots (Sheet 1 of 2)

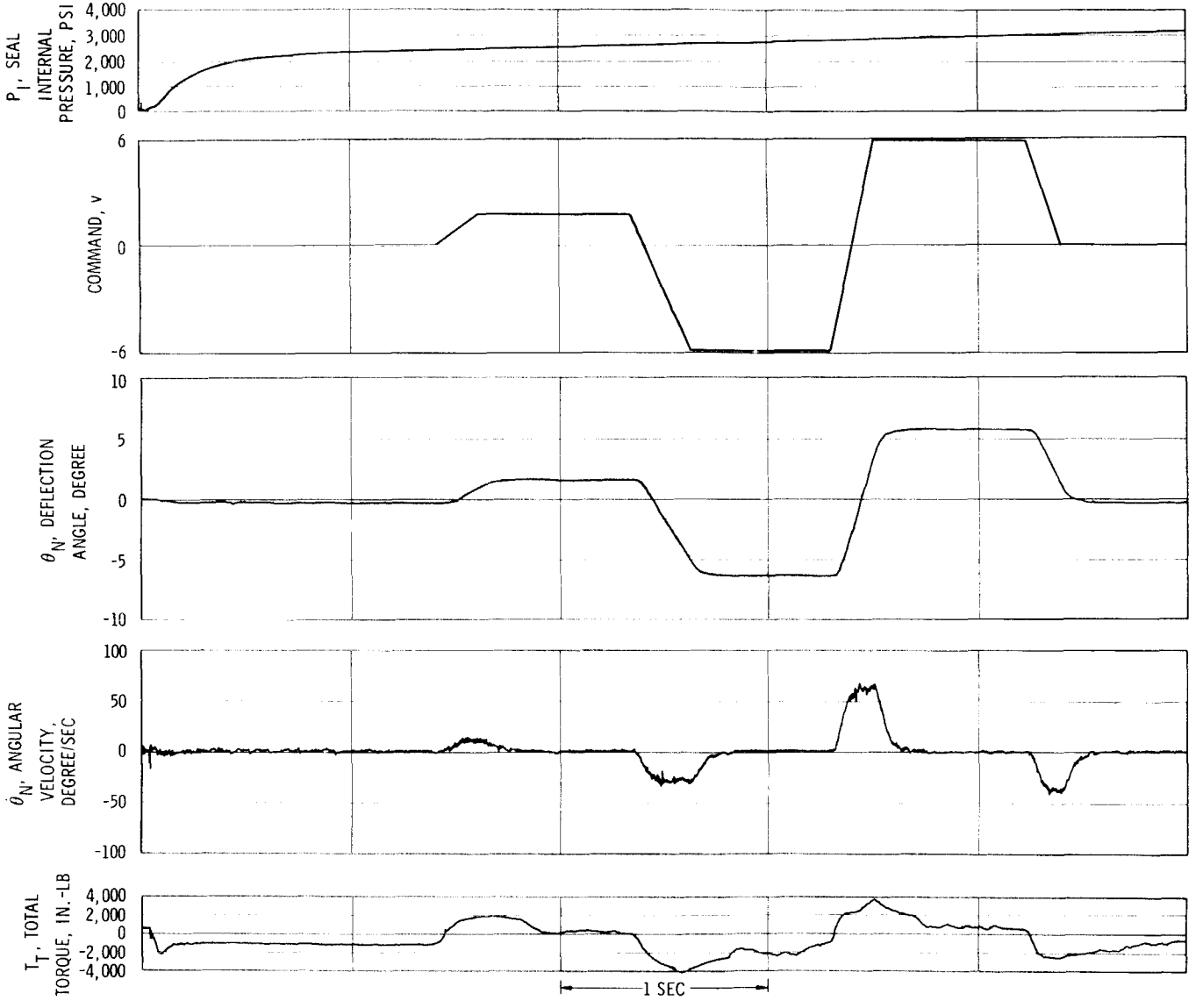

Figure 67. HIPPO (Miniseal) Static Firing, Expanded Time Plots
(Sheet 2 of 2)

(3) Performance Summary

Table VI summarizes the test results described in the preceding subsections. The test series conducted during phases I and II show that the state of the art of the TECHROLL seal as adaptable to both ICBM and air-launched systems is:

	Angle Deflection, degree	Slew Rate, degree/sec	Seal Pressure, psi
ICBM	±6	>30	>2,000
Air launch	>±10	>140	>6,000

TABLE VI

TEST RESULTS

Motor Test					
Seal	Chamber Pressure, psia	Duration, sec	Deflection, degrees	Deflection Rate, degrees/sec	Remarks
Minuteman	430 (maximum	60	±6.5 single axis	30.3	Phase I
Air launch	1,800 (maximum)	20	±12 single axis	58	Phase I
Air launch	1,680/680 (boost/sustain)	20	±11.5 single axis	140	Phase II
Air launch	2,700 (maximum)	20	±6.4 single axis	70	Phase II
Air launch	2,100 maximum (1,600 MEOP TVC)	5.5	±15 omniaxis	762	Phase III

Bench Test					
Seal	Temperature, °F	Chamber Pressure, psia	Deflection, degrees	Deflection Rate, degrees/sec	Remarks
Minuteman	75	1,000	6.5	60	Phase I
Air launch	75	2,000	13	30	Phase I
Air launch	75	2,000	---	---	Tested by Government
Air launch	75	2,000	10.2	60	Subcontractor seal
Air launch	75	2,000	10	140	Phase II (boost-sustain)
Air launch (alternate)	75	3,000	10	---	Phase II
Air launch	75	3,000	10	100	Phase II
Air launch	75	1,600	15	300 to 600	Phase III
Air launch	75	1,600	15	300 to 600	Tested by Government
Air launch	75	20	5 and 10	100 and 30	Phase II (viscous fluids)

SECTION III

TECHROLL SEAL NOZZLE SYSTEM ANALYTICAL MODELING

1. INTRODUCTION AND SUMMARY

Data from the bench and static tests described in this section together with the materials data discussed in section IV were analytically integrated into a preliminary TECHROLL seal movable nozzle mathematical model through an interative process of analytical methods refinement. This process produced a functional analytical model accurately depicting system performance characteristics and is the subject of this section.

Analytical modeling for the TECHROLL seal development program was divided into three phases with a major activity identified for completion at the end of each phase. The primary task I activity consisted of conducting analog computer simulations of the first two static firings of Minuteman and HIPPO (2,000 psi) nozzles. These simulations contained static and dynamic characteristics of the TECHROLL seal, movable nozzle, and hydraulic actuation system. The simulations were useful because they provided confidence in the performance of each system prior to the static motor firing and provided a firm base for the development of a generalized mathematical model in task II. The Minuteman and HIPPO simulations are documented in subsection 2, using bench test and static firing parameters.

Task II activities, which emphasized the development of a generalized movable nozzle dynamic model, included (1) an explicit definition of geometries, coordinate systems, and parameters and (2) the derivation of component performance and system interaction equations. The analytical model that was formulated should be useful for future analog, digital, and hybrid computer simulations of movable nozzle systems. The complete model was checked out using a large capacity analog computer at NASA Ames Research Center. The details of the model and typical outputs are presented in subsection 3.

A major activity throughout the program consisted of formulating analytical expressions for the prediction of important TECHROLL seal parameters related to structural stiffness and actuation torque. Both theoretical derivation and empirical correlation techniques were used to obtain these expressions. Additional data from the C-3 demonstrator and 8-in.-diameter demonstrator tests were used to update the parameter expression. Parameter equations are given in subsection 4.

Some parameter values used in the simulations of the Minuteman and HIPPO static motor firings (subsection 2) and the demonstration simulation of the closed-loop Minuteman nozzle (subsection 3) may not agree exactly with reported test data and final analytical predictions (subsection 4). This reflects an improvement in data reduction techniques and analytical prediction capabilities between the time these simulations were made and the end of the program. However, these inconsistencies were not of sufficient magnitude to warrant rerunning the simulations.

2. STATIC FIRING SIMULATIONS

a. Introduction

As part of the task I analytical modeling activity, both the Minuteman and the HIPPO TECHROLL seal nozzle systems were simulated in their static firing configurations. These simulations contain essential characteristics of the nozzle, seal, and actuation system. As shown in figure 68, the movable nozzle system is represented by a rigid body with three degrees of freedom of motion within a single axis. The effects of chamber pressure (blowoff loads) and gas dynamics are included. The TECHROLL seal also has three degrees of motion: rotational (θ_N), axial (X_{SA}), and lateral (X_{SL}). The actuation system (with motion X_A) represents an open-loop, solenoid-controlled, hydraulic cylinder. Local deformation of the actuator support structure is included. The motor case can accelerate axially (G_A) and laterally (G_L). As a comparison to bench test data, $X_{NA} = X_{SA}$ for nozzles when $\theta_N = 0$.

b. Discussion

(1) Coordinate Systems

Prior to a discussion of the model itself, it is important to understand the definition of the coordinate systems and sign conventions used. Referring to figure 68, two sets of coordinate axes can be

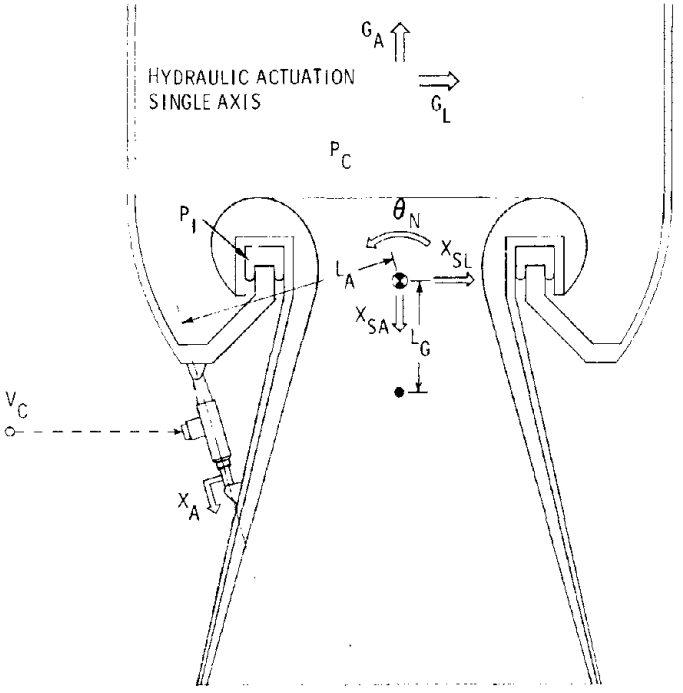

Figure 68. Schematic of TECHROLL Seal Movable Nozzle

considered, one attached to the nozzle and one attached to the motor case. Each set of axes nominally has its origin at a point determined by the intersection between the motor case centerline and the plane of the TECHROLL seal convolutes. One axis of each set (axial) points aft along the centerline of the related component. Another axis (lateral) is perpendicular to the respective centerline of each component. With this definition of coordinate systems, the motion of every point on nozzle can be mapped with respect to every point on the motor case (if necessary).

For each parameter, its derivatives with respect to time, and related forces or torques, the positive direction is shown according to the arrows shown on figure 68. For example, a positive command voltage (Vc) creates a positive actuator force (F_A) which tends to extend the actuator in a positive direction (X_A). The positive actuator force, in turn, creates a positive torque on the nozzle (T_T) which tends to create positive nozzle acceleration (θ_N), velocity (θ_N), and deflection (θ_N).

(2) Dynamic Model

A block diagram of the basic movable nozzle dynamic model is shown in figure 69. The model can be broken into four distinct areas. The hydraulic actuation components are located at the left and center of the diagram; the movable nozzle and TECHROLL seal characterizations are shown at the right of the diagram; rotational characteristics are shown in the central portion of the diagram, axial characteristics in the upper portion, and lateral characteristics in the lower portion.

(3) Parameters

Each symbol used on figure 69 is defined in table VII. Also, numerical values for each parameter are listed as they relate to the Minuteman and HIPPO nozzles in their static firing configurations. The source of each numerical value for the constant parameters is listed in the right-hand column. Using the block diagram presented in figure 69 and the list of parameter values given in table VIII, an analog computer simulation was constructed for both the Minuteman and HIPPO nozzles. These simulations were magnitude-scaled to obtain variable parameters within the ±10-v range of the computer (EAI TR-48) and time-scaled to operate at 1/100 of real time.

(4) Minuteman Simulation

Figure 70 shows TECHROLL seal fluid pressure versus seal axial displacement. This represents an idealized characteristic which can be compared with actual bench test results. Figure 71 represents rotational spring rate and hysteresis characteristics. This was obtained at near zero velocity including the effects of gas dynamics in the nozzle (internal aerodynamic spring rate). The magnitude of the seal hysteresis torque correlates with that obtained on the bench test.

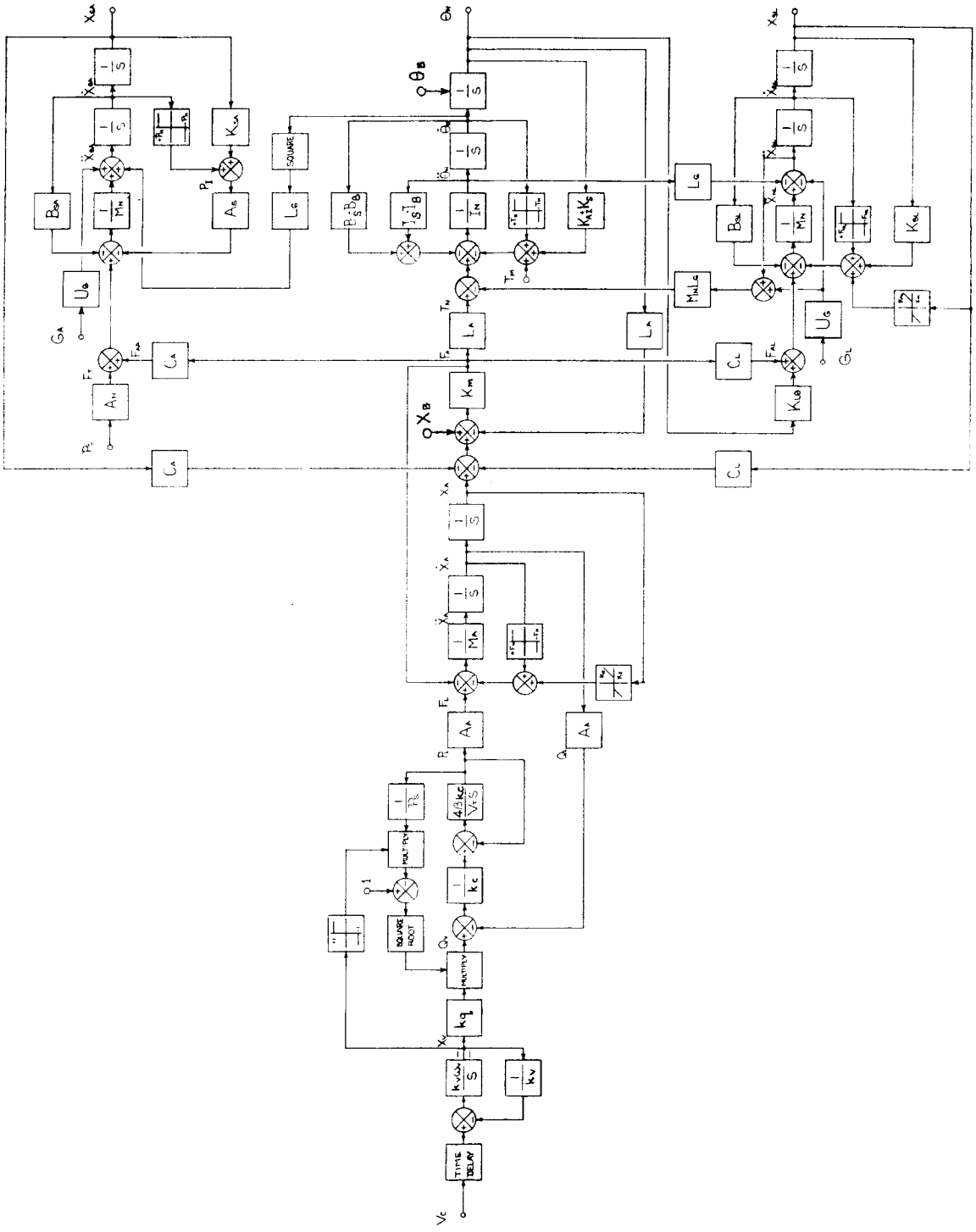

Figure 69. Dynamic Model of TECHROLL Seal Movable Nozzle

TABLE VII

MINUTEMAN AND HIPPO STATIC FIRING SIMULATION PARAMETERS (Sheet 1 of 2)

Constants	Symbol	Values		Unit	Source*
		Minuteman	HIPPO		
Nozzle inertia, about pivot point	I_N	156	4.35	in.-lb-sec^2	A
Seal fluid inertia	I_S	16.7	0.308	in.-lb-sec^2	A
Boot fluid inertia	I_B	1.5	0.028	in.-lb-sec^2	A
Seal fluid damping	B_S	177	7.26	in.-lb-sec	A
Boot fluid damping	B_B	10,900	3,243	in.-lb-sec	S
Seal rotational spring rate	K_S	0	11,450	in.-lb/rad	B
Internal aerodynamic spring rate	K_{AI}	11,450	0	in.-lb/rad	S
Seal hysteresis torque	T_{HT}	1,200	750	in.-lb	B
Seal offset torque	T_O	200	750	in.-lb	B
Thrust misalignment torque	T_M	0	250	in.-lb	S
Nozzle mass, movable portion	M_N	0.972	0.202	lb-sec^2/in.	A
Seal axial damping	B_{SA}	109	78.2	lb-sec/in.	E
Seal lateral damping	B_{SL}	55.4	28.7	lb-sec/in.	E
Seal axial stiffness	K_{SA}	5,000	15,600	psi/in.	B
Seal lateral stiffness	K_{SL}	78,900	101,800	lb/in.	A
Seal lateral limit stiffness	K_{ML}	10^3	10^3	lb/in.	E
Lateral load/rotational coefficient	$K_{L\theta}$	-8,640	-2,040	lb/rad	A
Seal lateral displacement limit, at null	X_M	0.3	0.25	in.	G
Seal axial hysteresis pressure	P_{HA}	200	400	psi	B
Seal lateral hysteresis force	F_{HL}	3,160	2,610	lb	E
Seal ring area	A_S	61.0	47.4	in.^{2}	A
Nozzle blowoff area, effective	A_N	149	76.3	in.^{2}	A
Nozzle pivot point to center of gravity distance	L_G	8.18	0.25	in.	A
Actuator moment arm, at null	L_A	18.0	9.0	in.	G
Actuator axial coefficient, at null	C_A	0.629	0.259	---	G
Actuator lateral coefficient, at null	C_L	0.777	0.966	---	G
Gravity units conversion factor	U_G	386	386	in./sec^2/g	---
Structural stiffness actuator mounting	K_m	10^5	10^5	lb/in.	E
Valve displacement gain	k_v	0.00357	0.00357	in./v	E
Valve flow gain	k_q	67.8	71.2	in.^{3}/sec/in.	A
Valve flow-pressure coefficient	k_c	$4x10^{-5}$	$4x10^{-5}$	in.^{3}/sec/psi	A
Actuator end stop stiffness	k_E	7,200	7,200	lb/in.	B
Actuator end stop displacement	X_E	1.80	1.63	in.	G
Actuator effective mass, movable portion	M_A	0.003	0.003	lb-sec^2/in.	A

TABLE VII

MINUTEMAN AND HIPPO STATIC FIRING SIMULATION PARAMETERS (Sheet 2 of 2)

Constants	Symbol	Values: Minuteman	Values: HIPPO	Unit	Source*
Hydraulic fluid effective bulk modulus	β	10^5	10^5	psi	E
Actuator total entrapped fluid volume	V_T	3.0	3.0	$in.^3$	G
Actuator piston area	A_A	0.626	0.626	$in.^2$	G
Hydraulic supply pressure, net	P_S	3,000	3,000	psi	---
Actuator static friction	F_H	20	20	lb	E
Valve break frequency	ω_V	500	500	rad/sec	E
Actuator displacement bias	X_B	0.113	0.042	in.	G
Nozzle angle initial bias	θ_B	0.0063	0.0047	rad	G
Variables					
Nozzle angular deflection, relative to motor	θ_N	0.1135 (±6.5)	0.209 (±12)	rad (degree)	---
Nozzle angular velocity, relative to motor	$\dot{\theta}_N$	0.523 (±30)	1.045 (±60)	rad/sec (degree/sec)	---
Nozzle angular acceleration, relative to motor	$\ddot{\theta}_N$	±100 (±5,730)	±300 (±17,200)	rad/sec^2 ($degree/sec^2$)	---
Nozzle total torque	T_T	±33,800	±15,920	in.-lb	---
Actuator force, net	F_A	±1,880	±1,880	lb	---
Actuator piston displacement, relative to cylinder	X_A	±2.04	±1.88	in.	---
Actuator piston velocity, relative to cylinder	$\dot{X}_A$	±9.42	±9.42	in./sec	---
Actuator piston acceleration, relative to cylinder	$\ddot{X}_A$	±1,800	±3,150	$in./sec^2$	---
Valve command voltage	V_C	±28	±28	v	---
Valve solenoid displacement	X_V	±0.1	±0.1	in.	---
Actuator load flow rate	Q_L	±5.89	±5.80	$in.^3/sec$	---
Actuator load pressure, differential	P_L	±3,000	±3,000	psi	---
Actuator load force, gross	F_L	±1,880	±1,880	lb	---
Motor chamber pressure	P_C	±430	±1,800	psi	---
Chamber pressure rate	$\dot{P}_C$	±20,000	±30,000	psi/sec	---
Seal internal pressure	P_I	±1,050	±2,900	psi	---
Motor axial acceleration, relative to ground	G_A	0	±1	g	---
Motor lateral acceleration, relative to ground	G_L	-1	0	g	---
Actuator axial force, component	F_{AAA}	±1,180	±487	lb	---
Actuator lateral force, component	F_{AL}	+1,460	+1,820	lb	---
Nozzle axial displacement, relative to motor	X_{SA}	±0.170	±0.160	in.	---
Nozzle lateral displacement, relative to motor	X_{SL}	±0.015	±0.010	in.	---

* A = Analysis G = Geometry S = Static firing
B = Bench test E = Estimate

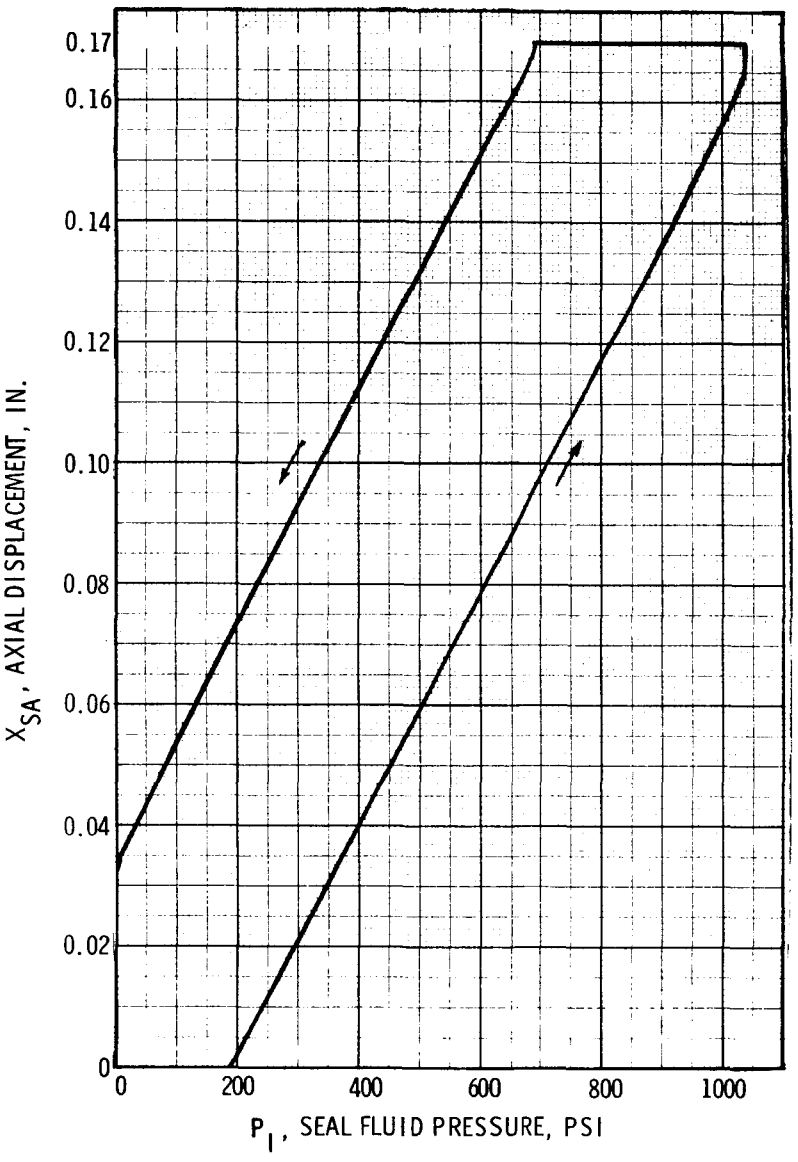

Figure 70. Axial Stiffness of TECHROLL Seal for Minuteman Nozzle

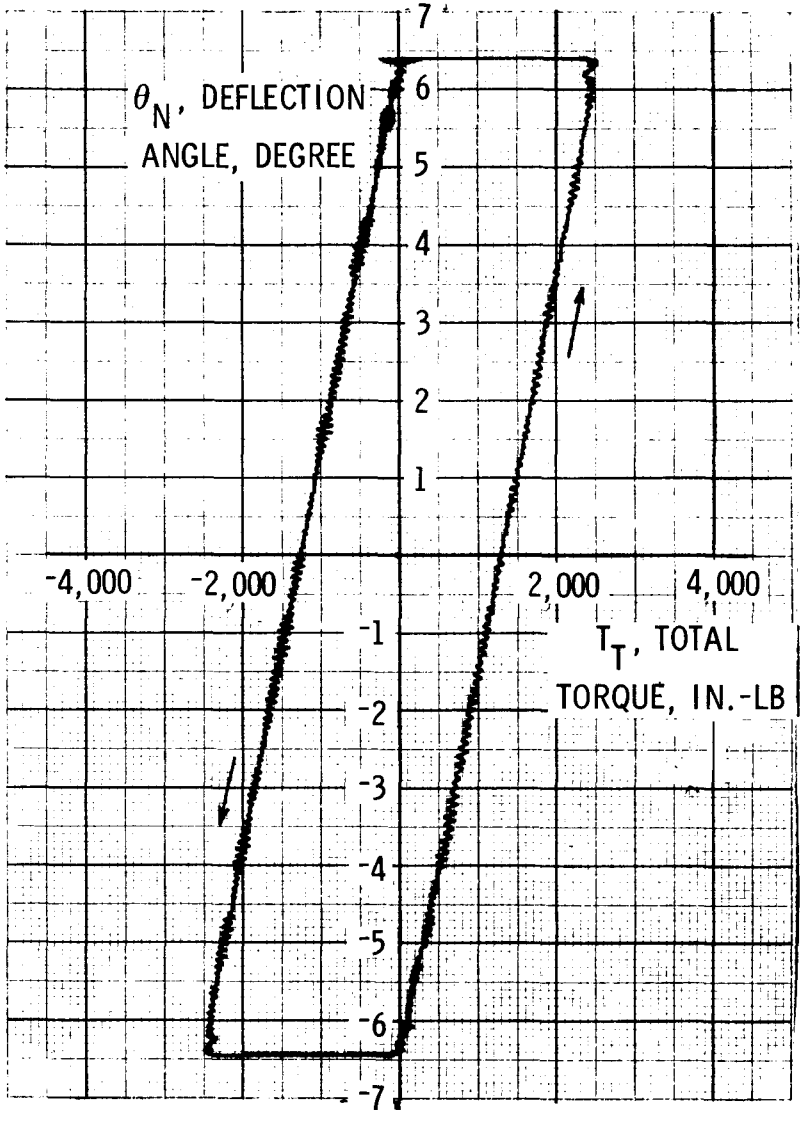

Figure 71. Rotational Characteristics of TECHROLL Seal for Minuteman Nozzle

Figures 72 and 73 represent a partial simulation of the static firing duty cycle. Nine parameters are plotted versus time: (1) nozzle angular deflection, (2) nozzle angular velocity, (3) nozzle actuation torque, (4) TECHROLL seal actuation torque, (5) seal axial displacement, (6) seal lateral displacement, (7) seal fluid pressure, (8) motor chamber pressure, and (9) actuator command voltage. The TECHROLL seal torque (T_S) is defined as that torque due only to the TECHROLL seal; it is expressed as $T_S = I_S \ddot{\theta}_N + B_S \dot{\theta}_N + K_S \theta_N T_{HT} \dot{\theta}_N + T_O$. Events simulated include motor ignition at time zero, a 0^o to 3^o deflection between 0.2 and 0.3 sec, a 3^o to 0^o deflection between 0.5 and 0.6 sec, a 0^o to -3^o deflection between 0.8 and 0.9 sec, and a -3^o to 0^o deflection between 1.1 and 1.2 sec. This essentially duplicates the ignition transient and the first two duty cycle events of the static firing, but on a different time base. Torques, pressures, and displacements can be compared with the static firing data plots, taking into account some simplifications and idealizations required in the model.

Simulated and actual test data for nozzle actuation torque are comparable. Seal torque, broken out separately for the simulation, is quite low compared to total torque. Minuteman nozzle actuation torques are dominated by the inertia of the nozzle and by a viscous torque attributed to the grease in the thermal insulation boot.

Simulated and test results for axial and lateral seal motion do not compare exactly. The reason for the difference may be the lack of a measured value of lateral stiffness and subtle changes in seal volume with deflection (not included in the simulation). More investigation in this area is required.

Simulated chamber and seal pressures compare with test data. However, following the ignition transient, chamber pressure remains constant in the simulation due to computer limitations. (Note the slight ripple on the seal pressure trace when actuation occurred.)

(5) HIPPO Simulation

Simulation of the HIPPO nozzle closely parallels that of the Minuteman. Figure 74 shows seal pressure versus axial displacement. (Note the idealization as compared to the bench test plot shown in figure 30.) Figure 75 represents a low velocity plot of torque versus rotation. This is essentially a pure seal characteristic as the internal aerodynamic spring rate for the HIPPO is nearly zero. Thus, it can be compared with the bench test hysteresis plot (figure 24). Because of limitations in computer size, it was not possible to include the actual nonlinear spring rate characteristic in the simulation.

Figures 76 and 77 represent a simulation of a portion of the static firing duty cycle. Included are the ignition transient, a deflection to 10^o and then to 12^o in the opposite direction.

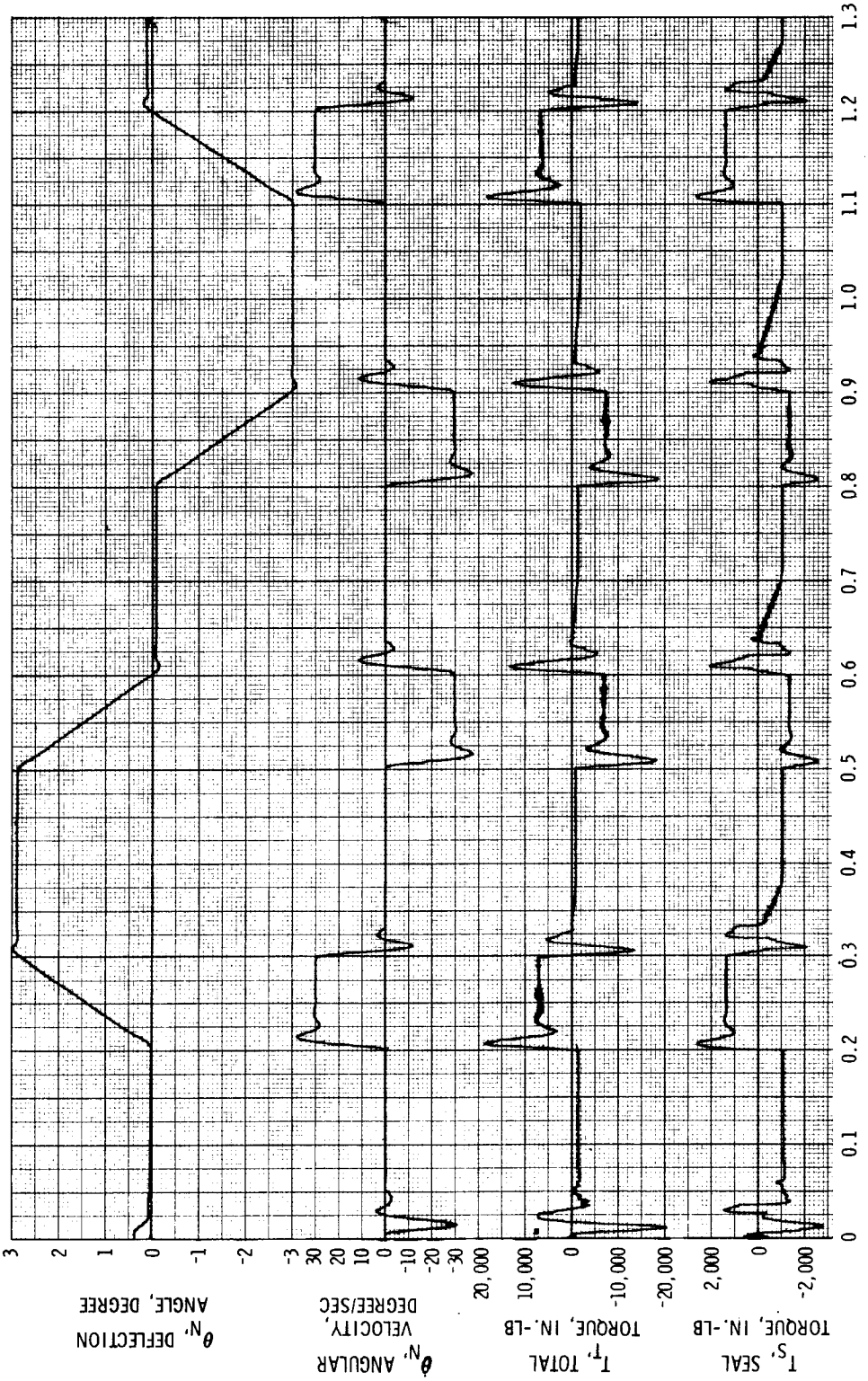

Figure 72. Nozzle Simulation of Minuteman Static Firing

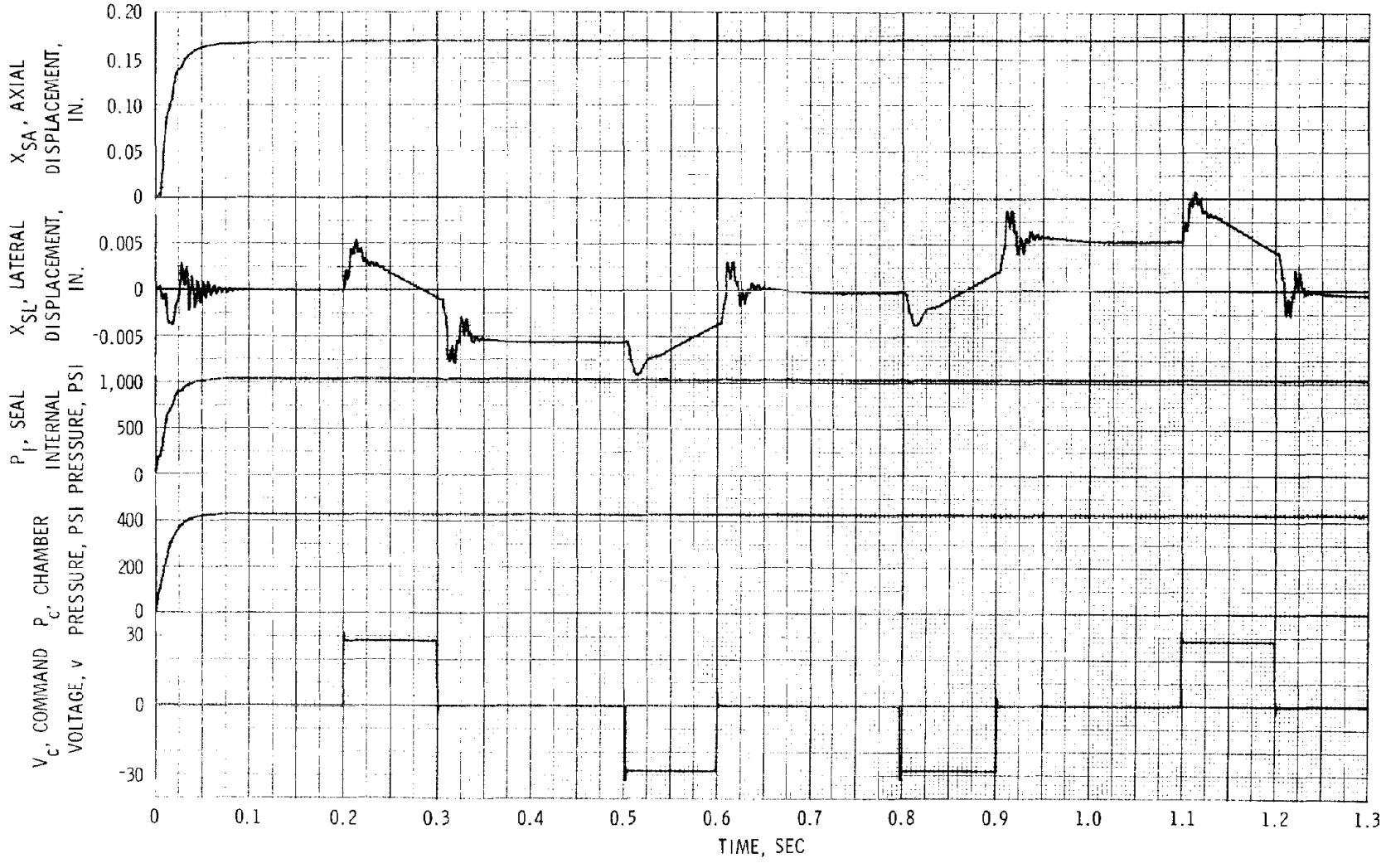

Figure 73. Nozzle Simulation of Minuteman Static Firing

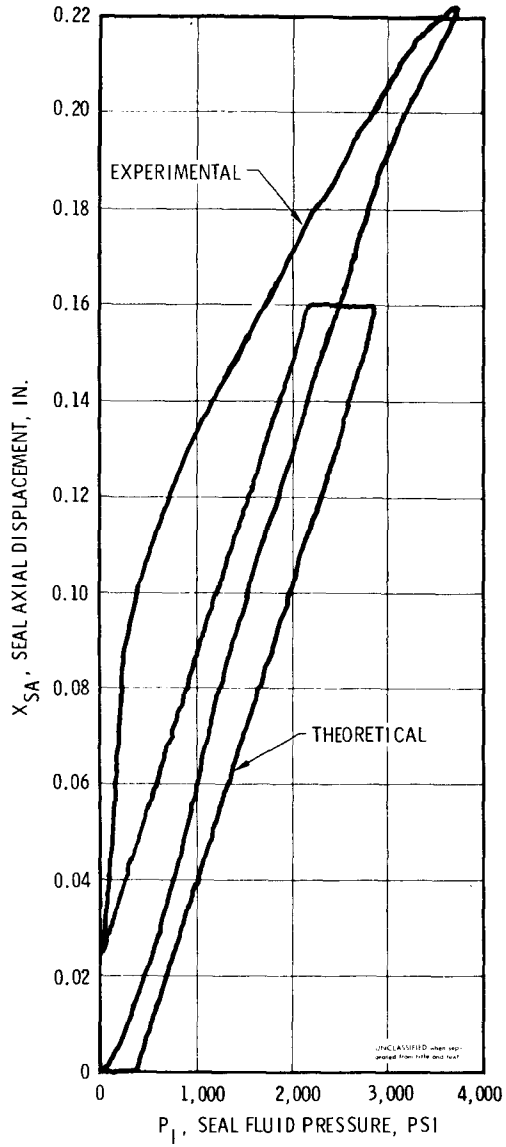

Figure 74. Axial Stiffness of TECHROLL Seal for HIPPO Motor

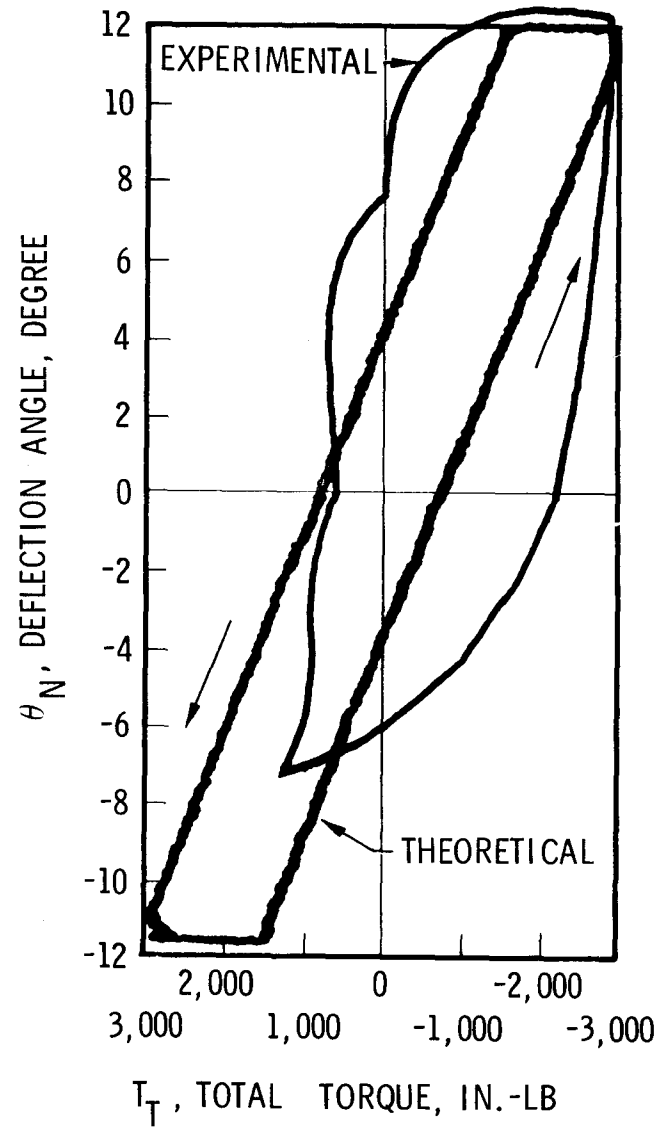

Figure 75. Rotational Characteristics of TECHROLL Seal for HIPPO Motor

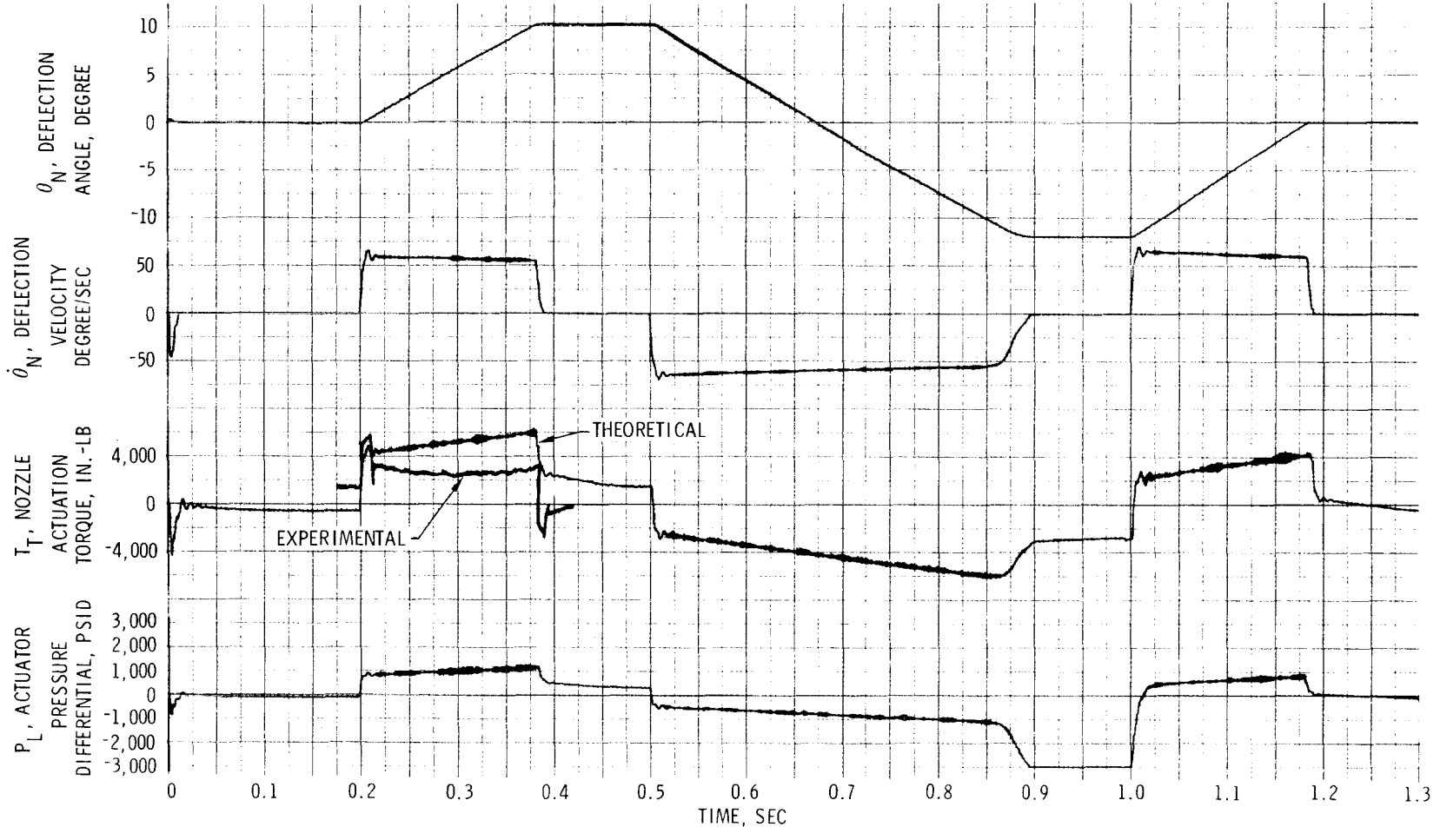

Figure 76. Nozzle Simulation of HIPPO (All-Boost) Static Firing

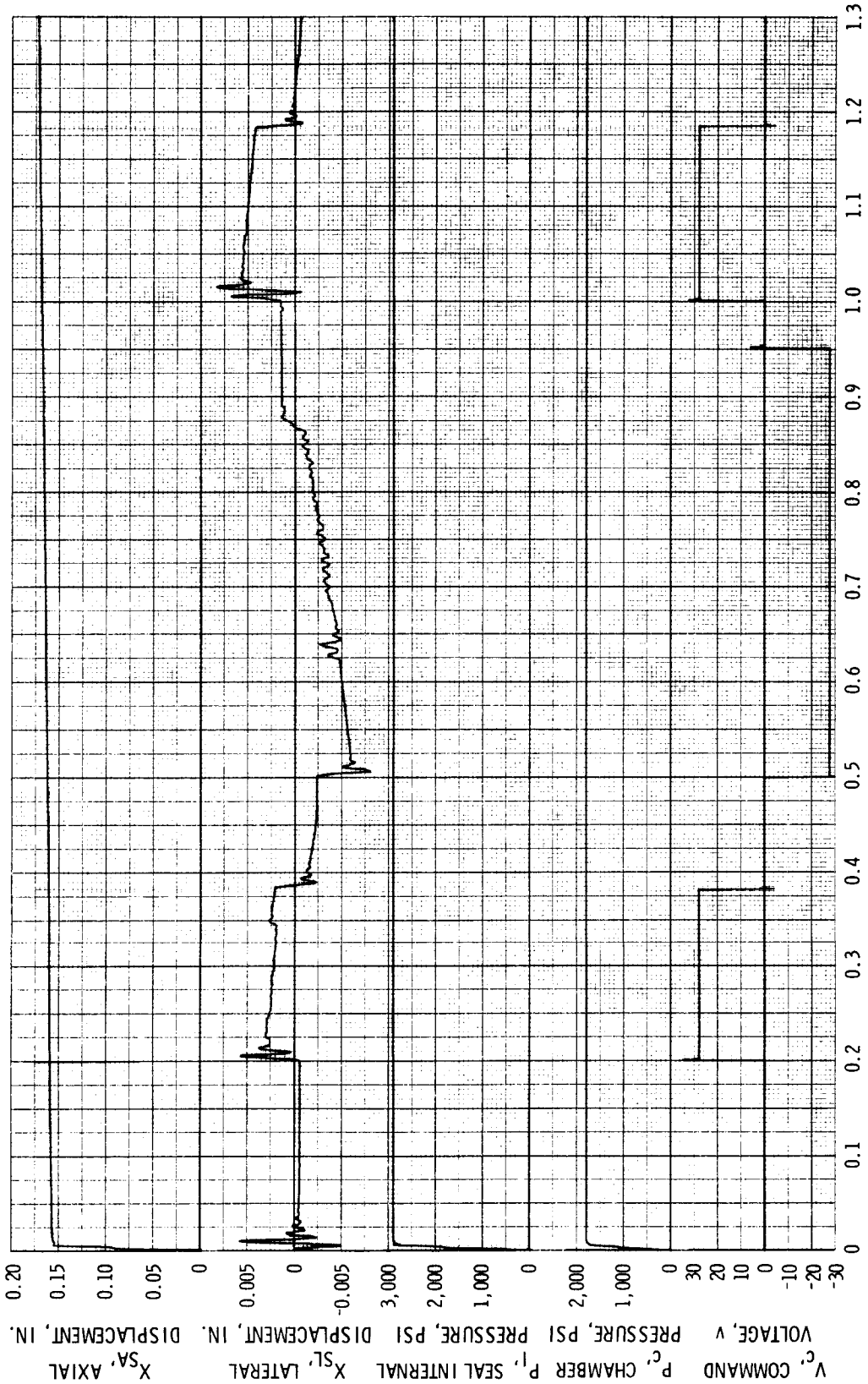

Figure 77. Nozzle Simulation of HIPPO (All-Boost) Static Firing

Simulated results (figure 76) and test results (figure 45) for nozzle actuation torques for the all-boost HIPPO nozzle are not comparable on a one-to-one basis because for large deflections in the static test; either the seal bottoms out at 10^{o} (unintentional), or the actuator bottoms out at 12^{o} (intentional). In either case, torque, which is computed from actuator differential pressure on the static firing, is somewhat misleading at large deflections. Simulated differential pressure is plotted along with torque on figure 76. There is a discrepancy at the 12^{o} deflection when the actuator is bottomed out. The shape of the simulated torque curve should actually be compared with the shape of a static firing torque curve of lower amplitude (figure 65E). Such investigation indicates that HIPPO actuation torques are dominated by three effects: seal spring rate, seal hysteresis, and grease boot damping. Unlike the Minuteman, nozzle inertia has a negligible contribution to torque, at least at these low slew rates.

As on the Minuteman, axial and lateral motions of the HIPPO seal do not correlate exactly between simulated and test results. The lateral motion difference can be explained partially by the analytically predicted lateral stiffness value used in the simulation. A bench test conducted after the simulation effort indicated a lower lateral stiffness value than that predicted.

Simulated chamber and seal fluid pressures (figure 77) agree favorably with static test data. Following the ignition transient (figure 36), simulated chamber pressure was held constant because of computer limitations.

Figure 78 shows the simulated end stop characteristics of the hydraulic actuator. This characteristic, which closely approximates the real hardware, affects nozzle dynamics and actuation torques when the actuator bottoms out at large nozzle deflection angles. An example of this bottoming phenomenon occurs during the 12^{o} deflection of the HIPPO motor.

c. Limitations

Every characteristic shown in the block diagram of figure 69 could not be included in the analog computer simulation because of machine limitations. Therefore, the following less significant characteristics were omitted from both the Minuteman and HIPPO simulations: (1) the solenoid valve time delay, (2) centrifugal force effects on nozzle axial dynamics, (3) seal lateral hysteresis force, and (4) seal lateral limiting. Also for the HIPPO simulation, a constant seal rotational spring rate was used instead of the nonlinear rotational characteristics evident from the bench tests. In addition, seal offset and thrust misalignment torques, which are peculiar to each seal and nozzle fabrication, were omitted from both simulations for clarity.

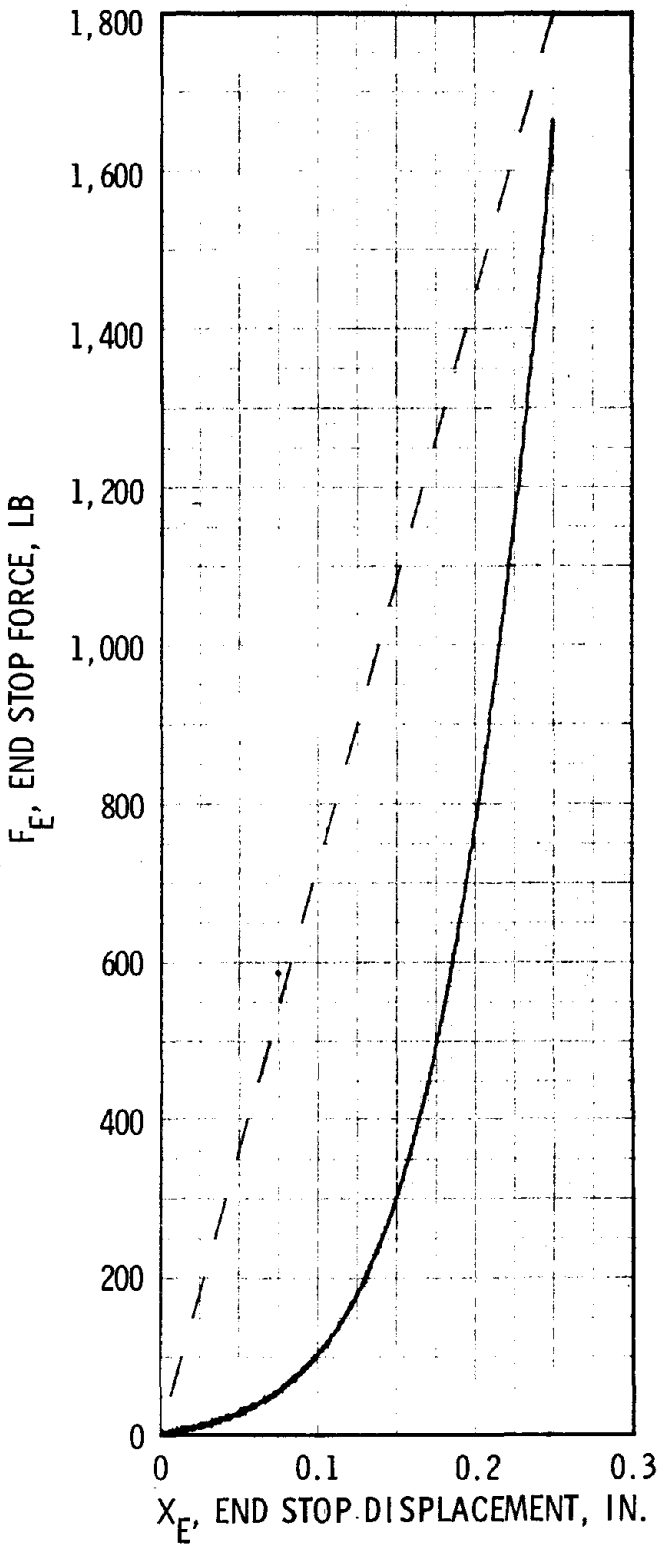

Figure 78. Actuator End Stop Stiffness

d. Conclusions

In general, the results of the Minuteman and HIPPO simulations correlate well with static firing data. Nozzle angular deflections and velocities duplicate closely the static firing results. Also, simulated actuation torques correspond well with static data in both shape and magnitude. Simulated chamber pressure produces realistic axial and rotational nozzle dynamics and TECHROLL seal pressures. However, simulated seal lateral motion is small compared to static firing data. This is probably due to a higher predicted seal lateral stiffness than that which actually exists.

3. MOVABLE NOZZLE DYNAMIC MODEL

a. Introduction

In conjunction with task II modeling activities, a generalized movable nozzle dynamic model was developed. Features of the model include (1) single axis, (2) three degrees of freedom, (3) TECHROLL seal, (4) thermal boot, (5) hydraulic servoactuator, (6) flexible structure, and (7) closed-loop control system. Details of this model including definitions, equations, schematics, and diagrams, are presented in this subsection.

This model has been developed as an analytical tool for studying the dynamic and static characteristics of movable nozzle TVC systems. The model is useful for verifying component sizing, conducting stability analyses, and studying system performance. It has been, and will continue to be, the basis for analog and digital computer simulations of TECHROLL seal movable nozzle systems. To date, simulations have been performed for the following static motor firings: (1) Minuteman; (2) HIPPO (boost); (3) supersonic splitline, subscale (boost and sustain); (4) supersonic splitline, full-scale (boost and sustain); (5) 8-in.-diameter TECHROLL seal demonstrator; and (6) C4 third stage. In addition, a simulation of a Minuteman motor with a hypothetical closed-loop electrohydraulic actuation system has been conducted to check out the complete model. Results are included at the end of this subsection.

The model, as presented herein, is configured for a static motor firing and with some modifications, can simulate bench tests. Given the proper vehicle interfaces (i.e., chamber pressure, nozzle external aerodynamic loading, and vehicle axial and lateral accelerations), the model also can simulate flight test environments.

Components that are fundamental to the model include (1) an all-movable nozzle, (2) the TECHROLL seal, and (3) a single, external, closed-loop hydraulic actuator. However, the model has been constructed for ease of modification to alternate components, such as (1) supersonic splitline nozzle, (2) flexseal, (3) gimbal ring, (4) internal hydraulic actuator, (5) electromechanical actuator, (6) turbopneumatic actuator, (7) servonozzle actuation (gas or liquid injection), and (8) multiple or redundant actuators.

The model with a single axis and three degrees of freedom, presented in this section, will eventually be expanded to two axes and six degrees of freedom. Also, it is intended to develop a fundamental vehicle dynamic model to interface with the movable nozzle dynamic model to assess the effects of vehicle accelerations and aerodynamics on the movable nozzle system. A hydraulic power supply dynamic model is also envisioned to determine its interaction with the nozzle actuation system.

Development details for the basic, generalized, single axis model are discussed in the following subsections.

b. Discussion

(1) Model Composition

The baseline movable nozzle system used to develop the model is shown schematically in figure 79. Major components consist of (1) the all-movable nozzle, (2) the TECHROLL seal, (3) the thermal boot, (4) the hydraulic actuator, (5) the flexible actuator attachment structure, and (6) the closed loop control system. Model inputs consist of the command voltage (Vc), motor chamber pressure (P_c), and vehicle axial and lateral accelerations (G_A and G_L). Model outputs include nozzle angular deflection (θ_N) and seal axial and lateral motions relative to the motor case (X_{SA} and X_{SL}). The model has been developed to provide a large number of internal variables, such as actuation

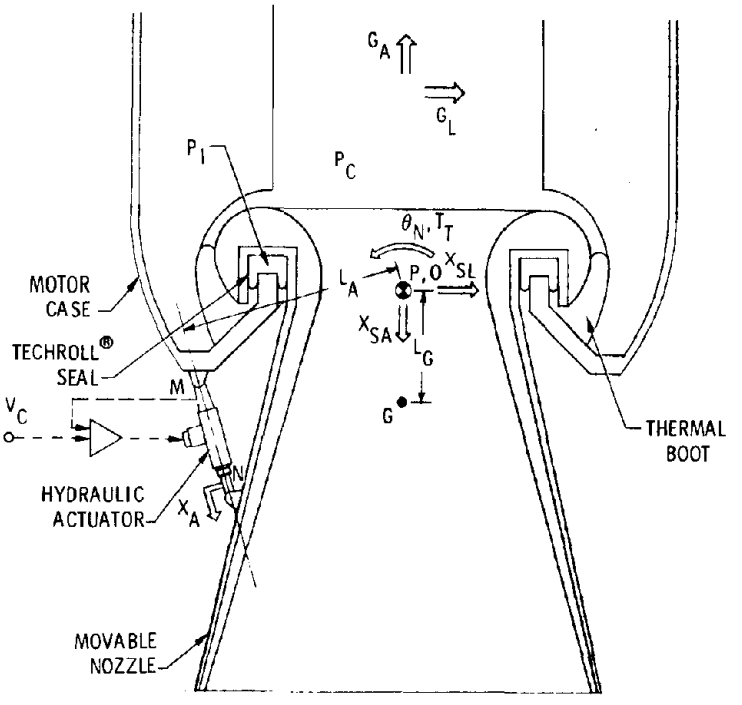

Figure 79. Schematic of Baseline Movable Nozzle System

torque (T_T) and TECHROLL seal internal fluid pressure (P_I). The model assumes a hydraulic power supply with a constant supply pressure (P_S), not shown on the schematic.

Point P on figure 79, which is fixed relative to the nozzle, represents the nominal pivot point of the seal. Point O, fixed relative to the motor, is coincident with point P under some set of conditions (normally no load on the nozzle). Point G represents the center of gravity of the movable portion of the nozzle. The nozzle centerline passes through points P and G. The distance L_G is measured between these two points. Points M and N represent the actuator attach points to the motor case and movable nozzle, respectively. The actuator centerline passes through points M and N. The moment arm (L_A) is the perpendicular distance between the actuator centerline and point P.

Given this brief overview of the composition of the model (inputs, outputs, major components, and the interaction of these components as a system), all technical details are contained in the following subsections.

(2) Parameters

Table VIII contains a complete list of parameters. Included for each parameter is a symbol, definition, typical units, and a numerical value unique to the demonstration system. It is important to note that parameter values must be put into the model; the model does not generate its own parameters. These values come from three sources: (1) analytical/empirical predictions, (2) bench test data, and (3) static firing results. Normally, parameters are considered to be constants. However, certain parameters may actually be functions of one or more variables, or of time. Examples are the geometry parameters L_A, C_A, and C_L which are discussed below. For a specific simulation based on this model, a decision must be made as to those parameters which cannot be considered constant and to those parameters which can be omitted as unimportant. Such decisions are usually based on the following constraints: (1) movable nozzle system characteristics, (2) solution accuracy requirements, (3) simulation time, (4) simulation budget, (5) computer capacity and capability, and (6) computer operating cost. Subscripts R, A, and L refer to rotational, axial, and lateral motions. They are added to describe a multidegree of freedom model.

(3) Variables

Table IX contains a list of all variables, including symbols, definitions, typical units, and maximum/minimum values unique to the demonstration system. It is important to understand the definitions of the various motion variables. Figures 79, 80, and 81 may be useful in locating these variables. Nozzle angular deflection (θ_N) is the angle measured between the respective centerlines of the movable nozzle and motor case. Seal axial and lateral displacements (X_{SA} and X_{SL}) are measured between point P fixed to the nozzle and point O

TABLE VIII

PARAMETERS
(Sheet 1 of 2)

Definition	Value
Nozzle inertia, about pivot point (I_N), in.-lb-sec^2	156
Seal rotational inertia (I_{SR}), in.-lb-sec^2	16.7
Boot rotational inertia (I_{BR}), in.-lb-sec^2	1.5
Seal rotational damping (B_{SR}), in.-lb-sec	177
Boot rotational damping (B_{BR}), in.-lb-sec	10,900
Internal aerodynamic damping (B_{AI}), in.-lb-sec	241
Seal rotational spring rate (K_{SR}), in.-lb/rad	~0
Internal aerodynamic spring rate (K_{AI}), in.-lb-/rad	11,450
Seal rotational hysteresis torque (T_{HT}), in.-lb	1,200
Nozzle mass, movable portion (M_N), lb-sec^2/in.	0.972
Seal axial damping (B_{SA}), lb-sec/in.	~0
Boot axial damping (B_{BA}), lb-sec/in.	109
Seal lateral damping (B_{SL}), lb-sec/in.	~0
Boot lateral damping (B_{BL}), lb-sec/in.	55.4
Seal axial stiffness (K_{SA}), psi/in.	5,000
Seal lateral stiffness (K_{SL}), lb/in.	78,900
Rotational/lateral load coefficient (K_{RL}), lb/rad	-8,640
Seal lateral limit stiffness (K_{ML}), lb/in.	10^5
Seal lateral displacement limit, null (X_{ML}), in.	0.3
Seal axial hysteresis pressure (P_{HA}), psi	200
Seal lateral hysteresis force (F_{HL}), lb	316
Seal ring area (A_S), in.^{2}	61
Nozzle blowoff area, effective (A_N), in.^{2}	149
Actuator moment arm, null (L_A), in.	18
Nozzle pivot point to center-of-gravity distance(L_G), in.	8.18
Actuator axial coefficient, null (C_A)	0.629
Actuator lateral coefficient, null (C_L)	0.777
Gravity units conversion factor (U_G), in./sec^2/g	386
Potentiometer feedback gain (K_F), v/in.	3.18
Amplifier current gain (k_I), ma/v	8.84

TABLE VIII

PARAMETERS
(Sheet 2 of 2)

Definition	Value
Valve torque motor sensitivity (K_{TM}), in.-oz/ma	1.0
Valve feedback spring stiffness (K_V), in.-oz/in.	1,000
Valve flow gain (K_Q), $in.^3$/sec/in	475
Valve flow-pressure coefficient (K_C), $in.^3$/sec/psi	4×10^4
Valve break frequency (ω_V), rad/sec	660
Dynamic pressure feedback gain (K_P), in.-oz/psi	---
DPF break frequency (ω_P), rad/sec	---
Hydraulic fluid bulk modulus, effective (β), psi	10^5
Actuator leakage coefficient (C_T), $in.^3$/sec/psi	10^{-6}
Hydraulic fluid entrapped volume, total (V_T), $in.^3$	1.0
Hydraulic supply pressure (P_S), psi	3,000
Actuator piston area (A_A), $in.^2$	0.222
Actuator piston mass, effective (M_A), lb-sec^2/in.	0.003
Actuator static friction (F_F), lb	20
Actuator end stop stiffness (K_E), lb/in.	10^5
Actuator end stop displacement (X_E), in.	2.0
Structural stiffness, effective (K_{STR}), lb/in.	10^5
Actuator structural stiffness (K_{STA}), lb/in.	---
Nozzle structural stiffness (K_{STN}), lb/in.	---
Motor structural stiffness (K_{STM}), lb/in.	---
Motor point O to M distance (L_M), in.	---
Nozzle point P to N distance, (L_N), in.	---

TABLE IX

VARIABLES
(Sheet 1 of 2)

Definition	Value
Nozzle angular deflection, (θ_N), rad	±0.105
Nozzle angular velocity, ($\dot{\theta}_N$), rad/sec	±0.523
Nozzle angular acceleration ($\ddot{\theta}_N$), rad/sec^2	±80
Nozzle initial offset angle (θ_o), rad	+0.0063
Actuation torque, total (T_T), in.-lb	±12,000
Nozzle torque, total (T_N), in.-lb	±2,450
Seal torque, total (T_S), in.-lb	±1,200
Boot torque, total (T_B), in.-lb	±5,700
External aerodynamic torque (T_{AE}), in.-lb	---
Thrust misalignment torque (T_M), in.-lb	---
Seal offset torque (T_o), in.-lb	---
Seal axial displacement, relative to motor (X_{SA}), in.	+0.17
Seal axial velocity ($\dot{X}_{SA}$), in./sec	---
Seal axial acceleration ($\ddot{X}_{SA}$), in./sec^2	---
Nozzle axial acceleration, relative to ground ($\ddot{X}_{NA}$), in./sec^2	---
Actuator axial force (F_{AA}), lb	±629
Chamber pressure axial force (F_{CA}), lb	64,100
Nozzle axial force, total (F_{NA}), lb	---
Seal axial force, total (F_{SA}), lb	---
Boost axial force, total (F_{BA}), lb	---
Seal internal pressure (P_I), psi	+1,050
Motor chamber pressure (P_C), psi	+430
Chamber pressure rate ($\dot{P}_C$), psi/sec	+20,000
Motor axial acceleration, relative to ground (G_A), g	±4
Seal lateral displacement, relative to motor (X_{SL}), in.	±0.3
Seal lateral velocity ($\dot{X}_{SL}$), in./sec	---
Seal lateral acceleration ($\ddot{X}_{SL}$), in./sec^2	---
Nozzle lateral acceleration, relative to ground ($\ddot{X}_{NL}$) in./sec^2	---
Actuator lateral force (F_{AL}), lb	±518
Chamber pressure lateral force (F_{CL}), lb	±6,710

TABLE IX

VARIABLES
(Sheet 2 of 2)

Definition	Value
Rotational/lateral load force (F_{RL}), lb	±950
Nozzle lateral force, total (F_{NL}), lb	---
Seal lateral force, total (F_{SL}), lb	---
Boot lateral force, total (F_{BL}), lb	---
Seal lateral limit force (F_{ML}), lb	---
Motor lateral acceleration, relative to ground (G_L), g	±4
Seal normal acceleration, relative to ground ($\ddot{X}_{SN}$), in./sec^2	---
Actuator piston displacement, relative to cylinder (X_A), in.	±1.89
Actuator piston velocity ($\dot{X}_A$), in./sec	±9.42
Actuator piston acceleration ($\ddot{X}_A$), in./sec^2	±1,400
Actuator displacement bias (X_B), in.	+0.113
Actuator motion due to nozzle rotation (X_R), in.	±1.89
Strutural displacement (X_{STR}), in.	±0.12
Actuator output force, net (F_A), lb	±666
Actuator load force, gross (F_L), lb	±666
Actuator end stop force (F_E), lb	---
Actuator load pressure, differential (P_L), psi	±3,000
Load pressure rate ($\dot{P}_L$), psi/sec	---
DPF network pressure, differential (P_P), psi	---
Valve load flow rate (Q_L), in.^{3}/sec	±4.75
Actuator piston flow rate (Q_A), in.^{3}/sec	±4.75
Torque motor torque (T_{TM}), in.-oz	±10
Valve spool feedback torque (T_V), in.-oz	±10
DPF network feedback torque (T_P), in.-oz	---
Valve spool displacement (X_V), in.	±0.01
Valve spool velocity ($\dot{X}_V$), in./sec	---
Amplifier current (I_A), ma	±10
Potentiometer feedback voltage (V_F), v	±6
Command voltage (V_C), v	±6

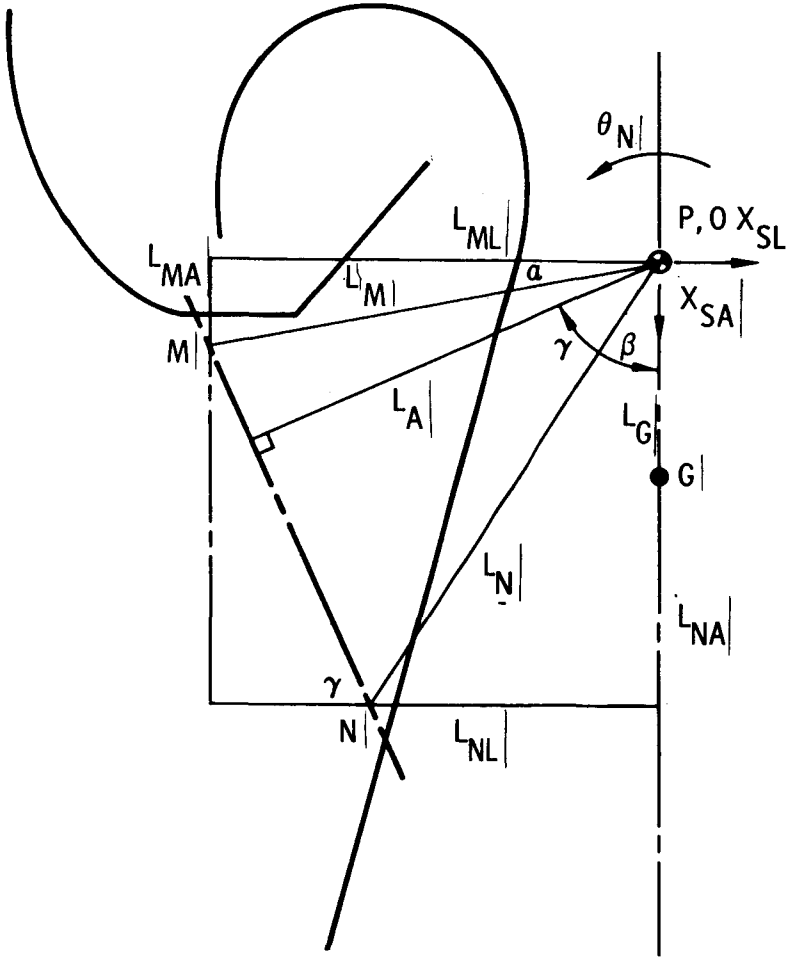

Figure 80. Movable Nozzle Geometry
(Single Axis, Three Degrees of Freedom)

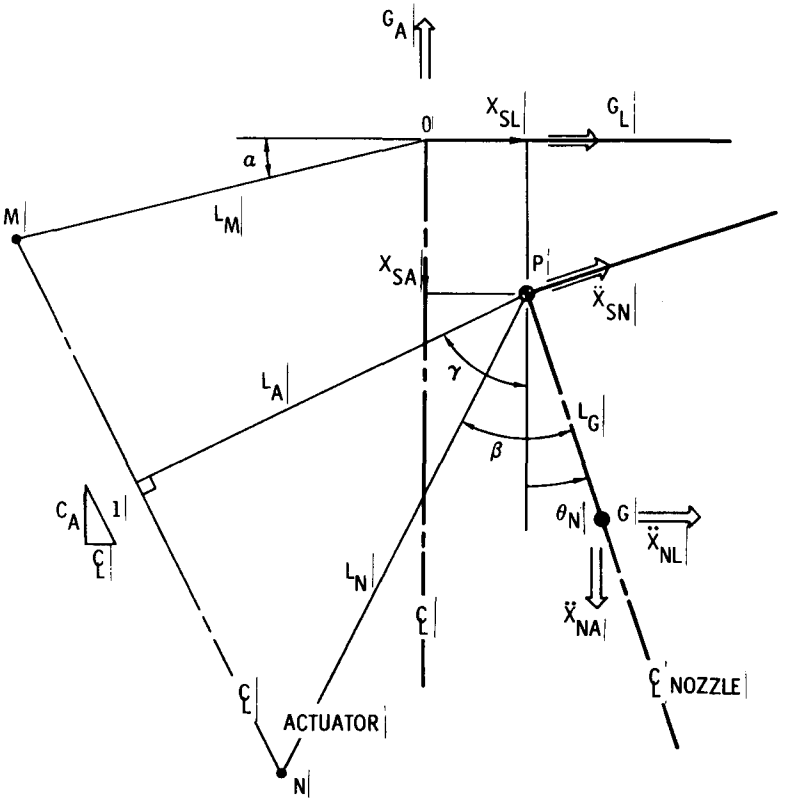

Figure 81. Movable Nozzle Coordinates
(Single Axis, Three Degrees of Freedom)

fixed to the motor. The designation ''axial'' means parallel to the motor axis (or centerline), while ''lateral'' means perpendicular to the motor centerline. Variables $\ddot{X}_{NA}$ and $\ddot{X}_{NL}$ refer to the axial and lateral components of the acceleration of point G, on the nozzle, relative to ground. Seal normal acceleration ($\ddot{X}_{SN}$) represents the component of the acceleration of point P, relative to ground, which is normal to the nozzle centerline. Motor accelerations, G_A and G_L, represent the axial and lateral components of the acceleration of point O on the motor relative to ground (i.e., inertial space).

(4) Derivatives

Table X lists derivatives of variables both in the time domain and the frequency domain and the Laplace transformation which relates the two domains. The differential equations of subsections (5) and (6) are presented in the time domain while the block diagram represents a Laplace transformation of these equations into the frequency domain. No attempt has been made to use different symbols for different domains. For example, $\dot{\theta}_N$ in the equations implies $\dot{\theta}_N(t)$ in the time domain, while $\dot{\theta}_N$ on the block diagram implies $\dot{\theta}_N(s)$ in the frequency domain.

(5) Component Equations

Component equations which describe the performance of each significant component in the movable nozzle system are listed below.

A. Nozzle

1. Rotational

$$T_N = I_N\ddot{\theta}_N\ B_{AI}\dot{\theta}_N + K_{AI}\theta_N + T_{AE} \pm T_M + M_N L_G \ddot{X}_{SN}$$

2. Axial

$$F_{CA} = A_N P_C \cos \theta_N$$

$$F_{NA} = M_N \ddot{X}_{NA}$$

3. Lateral

$$F_{CL} = A_N P_C \sin \theta_N$$

$$F_{NL} = M_N \ddot{X}_{NL}$$

TABLE X

DERIVATIVES AND LAPLACE TRANSFORMS

First Derivative With Respect to Time	Second Derivative With Respect to Time
Time Domain (Component and System Equations)	
$[\dot{\ }](t) = \frac{d[\ ]}{dt}$	$[\ddot{\ }](t) = \frac{d^2[\ ]}{dt^2}$
$\dot{\theta}_N(t) = \frac{d\theta_N}{dt}$	$\ddot{\theta}_N(t) = \frac{d^2\theta_N}{dt^2}$
$\dot{X}_{SA}(t) = \frac{dX_{SA}}{dt}$	$\ddot{X}_{SA}(t) = \frac{d^2X_{SA}}{dt^2}$
$\dot{X}_{SL}(t) = \frac{dX_{SL}}{dt}$	$\ddot{X}_{SL}(t) = \frac{d^2X_{SL}}{dt^2}$
$\dot{X}_A(t) = \frac{dX_A}{dt}$	$\ddot{X}_A(t) = \frac{d^2X_A}{dt^2}$
$\dot{X}_V(t) = \frac{dX_V}{dt}$	$\ddot{X}_{NA}(t) = \frac{d^2X_{NA}}{dt^2}$
$\dot{P}_L(t) = \frac{dP_L}{dt}$	$\ddot{X}_{NL}(t) = \frac{d^2X_{NL}}{dt^2}$
$\dot{P}_C(t) = \frac{dP_C}{dt}$	$\ddot{X}_{SN}(t) = \frac{d^2X_{SN}}{dt^2}$
Frequency Domain (Block Diagram)	
$[\dot{\ }](s) = s[\ ]$	$[\ddot{\ }](s) = s^2[\ ]$
$\dot{\theta}_N(s) = s\theta_N$	$\ddot{\theta}_N(s) = s^2\theta_N$
$\dot{X}_{SA}(s) = sX_{SA}$	$\ddot{X}_{SL}(s) = s^2X_{SL}$
$\dot{X}_{SL}(s) = sX_{SL}$	$\ddot{X}_{SL}(s) = s^2X_{SL}$
$\dot{X}_A(s) = sX_A$	$\ddot{X}_A(s) = s^2X_A$
$\dot{X}_V(s) = sX_V$	$\ddot{X}_{NA}(s) = s^2X_{NA}$
$\dot{P}_L(s) = sP_L$	$\ddot{X}_{NL}(s) = s^2X_{NL}$
$\dot{P}_C(s) = sP_C$	$\ddot{X}_{SN}(s) = s^2X_{SN}$
LaPlace Transforms (Time Domain to Frequency Domain)	
$\mathcal{L}\left\{\frac{d[\ ]}{dt}\right\} = s[\ ](s)$	$\mathcal{L}\left\{\frac{d^2[\ ]}{dt^2}\right\} = s^2[\ ](s)$
$- [\ ](t)_{t=0^+}$	$- s[\ ](t)_{t=0^+} - [\dot{\ }](t)_{t=0^+}$
LaPlace variable, s	
Time, t	

B. TECHROLL Seal

1. Rotational

$$T_S = I_{SR}\ddot{\theta}_N + B_{SR}\dot{\theta}_N + K_{SR}\theta_N + T_{HR}\frac{\dot{\theta}_N}{|\dot{\theta}_N|} \pm T_O$$

2. Axial

$$P_I = K_{SA}X_{SA} + P_{HA}\frac{\dot{X}_{SA}}{|\dot{X}_{SA}|}$$

$$F_{SA} = B_{SA}\dot{X}_{SA} + A_S P_I \cos\theta_N$$

3. Lateral

$$F_{RL} = K_{RL}\tan\theta_N$$

$$F_{SL} = B_{SL}\dot{X}_{SL} + K_{SL}X_{SL} + F_{HL}\frac{\dot{X}_{SL}}{|\dot{X}_{SL}|} + F_{ML} + A_S P_I \sin\theta_N$$

$$F_{ML} = \begin{cases} 0 & |X_{SL}| \leqslant X_{ML} \\ \left(K_{ML}X_{SL} - X_{ML}\right) & \text{for} \quad X_{SL} \geqslant X_{ML} \\ K_{ML}\left(X_{SL} + X_{ML}\right) & \text{for} \quad X_{SL} \leqslant -X_{ML} \end{cases}$$

C. Thermal Boot

1. Rotational

$$T_B = I_{BR}\ddot{\theta}_N + B_{BR}\dot{\theta}_N$$

2. Axial

$$F_{BA} = B_{BS}\dot{X}_{SA}$$

3. Lateral

$$F_{BL} = B_{BL}\dot{X}_{SL}$$

D. Servoactuator

1. Amplifier

$$I_A = K_I(V_C - V_F)$$

2. Servovalve

$$T_{TM} = K_{TM}I_A$$

$$T_{TM} = \left(\frac{K_V}{\omega_V}\right)_V + T_V + T_P$$

$$T_V = K_V X_V$$

$$Q_L = K_Q \sqrt{1 - \frac{X_V}{X_V}\frac{P_L}{P_S}}\, X_V - K_C P_L$$

3. Dynamic pressure feedback

$$P_P = \frac{1}{\omega_P}\left[\dot{P}_L - \dot{P}_P\right]$$

$$T_P = K_P P_P$$

4. Actuator

$$Q_L = Q_A + C_T P_L + \frac{V_T}{4\beta}\dot{P}_L$$

$$Q_A = A_A \dot{X}_A$$

$$F_L = A_A P_L$$

$$F_L = M_A \ddot{X}_A + F_F \frac{\dot{X}_A}{|\dot{X}_A|} + F_E + F_A$$

$$F_E = \begin{cases} 0 & \text{for} \quad |X_A| \leq X_E \\ K_E (X_A - X_E) & \text{for} \quad X_A \geq X_E \\ K_E (X_A + X_E) & \text{for} \quad X_A \leq -X_E \end{cases}$$

5. Potentiometer

$$V_F = K_F X_A$$

E. Structure

$$F_A = K_{STR} X_{STR}$$

$$K_{STR} = \frac{1}{\frac{1}{K_{STA}} + \frac{1}{K_{STN}} + \frac{1}{K_{STM}}}$$

These components include (1) the movable portion of the nozzle, (2) the TECHROLL seal, (3) the thermal protection grease boot, (4) the hydraulic servoactuator, and (5) the actuator attachment structure. For the nozzle, seal, and boot, the equations are divided into the three degrees of freedom: axial, lateral, and rotational. The electrohydraulic servoactuator is subdivided into its components. The amplifier is a linear gain current driver with no electronic compensation. The servovalve is a two- or three-stage flow control valve. Square root flow-pressure characteristics and static pressure sensitivities are included. The valve has a built-in dynamic pressure feedback option with a variable gain and break frequency. The actuator (hydraulic cylinder) is an externally mounted, balanced area, push-pull type. Fluid compressibility, friction, end stop, and mass characteristics are included. The potentiometer (or equivalent, such as LVDT and demodulator) has a linear gain. The structure includes the actuator body, the motor case in the vicinity of the actuator cylinder-end attachment, and the nozzle in the vicinity of the actuator rod-end attachment.

(6) System Equations

The system equations listed below interrelate the component equations of the previous section when those components are assembled into the basic movable nozzle system.

A. Motion interaction

1. $X_A = X_R + X_{STR} - X_B + C_A X_{SA} + C_L X_{SL}$

   where: $X_R = L_A \theta_N$

B. Load interaction

1. $T_T = L_A F_A = T_N + T_S + T_B$ (rotational)

2. $F_{CA} + F_{AA} = F_{NA} + F_{SA} + F_{BA}$ (axial)

   where: $F_{AA} = C_A F_A$

3. $F_{CL} + F_{AL} + F_{RL} = F_{NL} + F_{SL} + F_{BL}$ (lateral)

   where: $F_{AL} = C_L F_A$

C. Acceleration interaction

1. $\ddot{X}_{SN} = (U_G G_A - \ddot{X}_{SA}) \sin \theta_N + (U_G G_L + \ddot{X}_{SL}) \cos \theta_N$ (normal)

2. $\ddot{X}_{NA} = \ddot{X}_{SA} - U_G G_A + L_G \ddot{\theta}_N \sin \theta_N - L_G \dot{\theta}_N^2 \cos \theta_N$ (axial)

3. $\ddot{X}_{NL} = \ddot{X}_{SL} + U_G G_L + L_G \ddot{\theta}_N \cos \theta_N - L_G \dot{\theta}_N^2 \sin \theta_N$ (lateral)

The first equation relates actuator linear displacement (X_A) to equivalent rotational (X_R), axial ($C_A X_{SA}$), and lateral ($C_L X_{SL}$) motions of the nozzle-seal-boot assembly. An actuator bias (X_B) represents an adjustment of the rod length external to the cylinder. It is used to offset the effect of axial motion for a particular chamber pressure. Normally ($C_A X_{SA} - X_B$) = 0 at MEOP. The structural deflection (X_{STR}) accounts for local deformation due to actuator loading.

(7) Geometry

As mentioned previously, the geometry parameters L_A, C_A, and C_L are not actually constants although they are normally treated that way. The geometry equations listed below define these three parameters as a function of nozzle rotational, axial, and lateral motions.

$$L_M = \sqrt{L_{MA}^2 + L_{ML}^2}$$

$$L_N = \sqrt{L_{NA}^2 + L_{NL}^2}$$

$$\alpha = \tan^{-1}\left(\frac{L_{MA}}{L_{ML}}\right)$$

$$\beta = \tan^{-1}\left(\frac{L_{NL}}{L_{NA}}\right)$$

$$\gamma = \tan^{-1}\left(\frac{L_N \cos(\beta - \theta_N - L_M \sin\alpha + X_{SA}}{L_M \cos\alpha - L_N \sin(\beta - \theta_N) + X_{SL}}\right)$$

$$C_A = \sin\gamma$$

$$C_L = \cos\gamma$$

$$L_A = L_N \cos(\gamma + \theta_N - \beta)$$

Figures 80 and 81 illustrate the geometry symbols for the undeflected and deflected nozzles. Mechanizing these equations is much easier for digital than for analog computer simulations.

(8) Block Diagram

The block diagram shown in figure 82 represents the focal point of the analytical modeling effort. The diagram represents the performance of a movable nozzle system and the interaction of its components. All the component and system equations of subsections (5) and (6) have been transformed into the frequency domain and incorporated on the diagram. Small angle approximations were made for nozzle angular deflection θ_N: $\sin\theta_N \approx \theta_N$, $\tan\theta_N \approx \theta_N$, and $\cos\theta_N \approx 1$. The servo-actuator characteristics appear on the left and central portions of the diagram. The nozzle, seal, and boot characteristics appear on the right-hand portion of the diagram. These characteristics are not separated by component but are grouped into the three degrees of freedom: rotational, axial, and lateral.

c. Demonstration

A major task II modeling activity included demonstrating the generalized movable nozzle dynamic model by conducting an analog simulation for a typical solid rocket application. Minuteman movable nozzle, TECHROLL seal, and thermal boot characteristics were selected. However, a hypothetical, optimum size, closed-loop, hydraulic actuation system was substituted for the test-weight, open-loop actuator used for the static firing. Because UTC did not possess adequate analog computing capacity, several outside facilities were considered. The analog/hybrid computing facility at NASA Ames Research Center was selected because of its capacity and convenience to UTC.

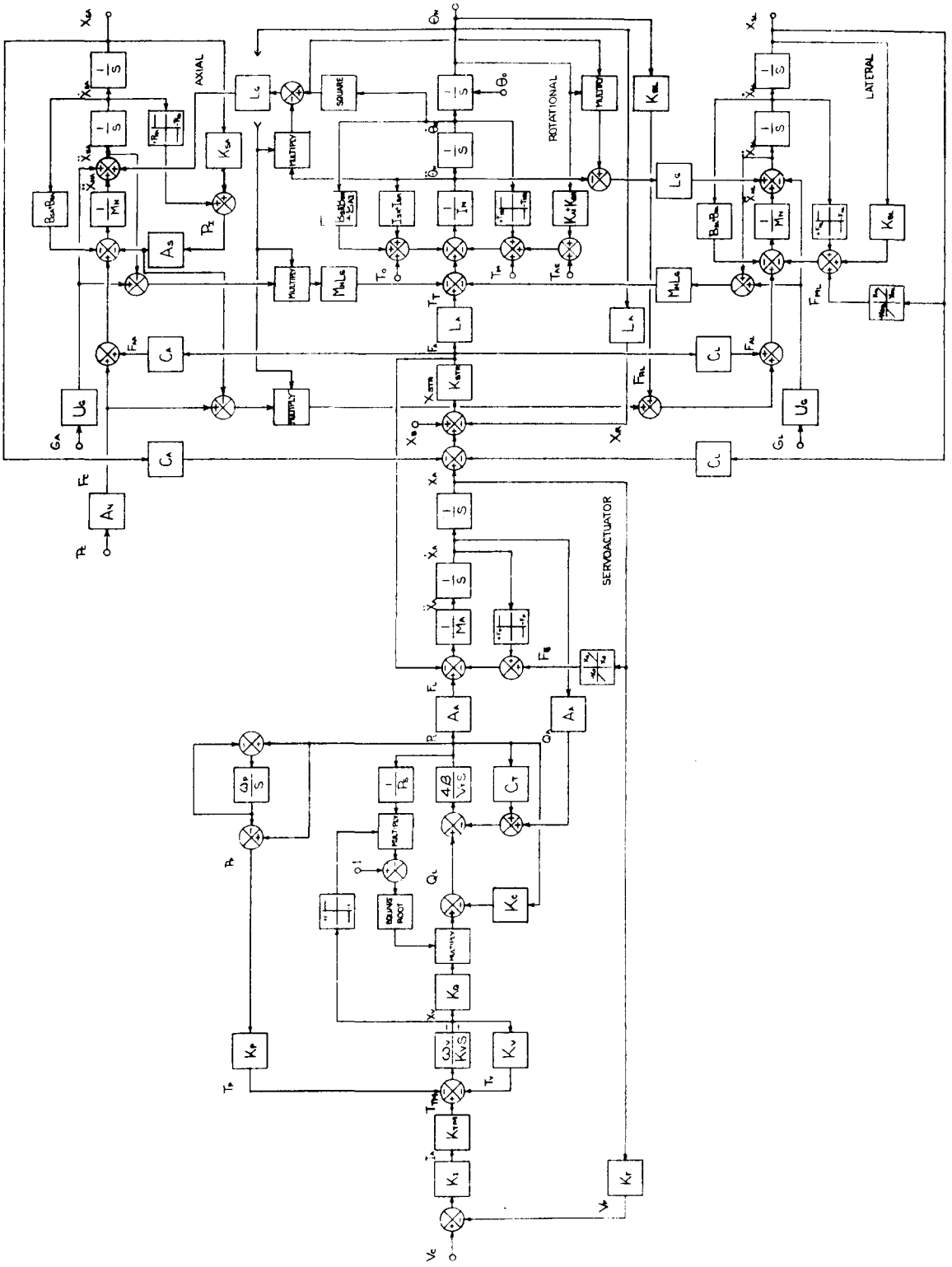

Figure 82. Movable Nozzle Dynamic Model (Block Diagram)

(1) Facility

Two UTC engineers conducted the demonstration simulation at the Ames Research Center facility over a 2-week period. Air Force program directors witnessed the work in progress during that time. The following equipment was used for the study: (1) EAI 8800 analog/hybrid computer (100 v, solid state), (2) EAI variplotter (X-Y), (3) EAI oscilloscope, and (4) Brush pen recorders (16 channels). NASA provided the computing equipment, staff support (for machine familiarization), hardware maintenance, and materials. UTC was responsible for its own programming, patching, and computer operation.

(2) Program

An analog computer diagram was created based on the model block diagram (figure 100) and the simulation parameters and variables (tables VIII and IX). The simulation was magnitude-scaled to utilize the ±100-v operating range of the computer, and time-scaled to operate at 1/100 of real time (for the sake of the recording equipment and operators). The computer was programmed and checked out with relative ease considering a lack of prior familiarity with the equipment.

(3) Results

Runs were documented according to (1) servovalve characterization, (2) servo-actuator characterization, (3) TECHROLL nozzle system characterization, (4) parametric variations, and (5) motor vibration (figures 83 through 117).

Only selected runs are included as figures. Servovalve characteristics were obtained by disconnecting the valve from the actuator. Ideal and model flow-pressure characteristics differ by the incorporation of spool leakage effects in the model.

Servoactuator characteristics were obtained by operating the closed-loop actuator without the movable nozzle, TECHROLL seal, and thermal boot.

Step responses were recorded at six different amplitudes (1 v of command corresponds to one degree of nozzle deflection) for comparison with the same variables after the load was attached.

System characteristics were obtained for a simulated static motor firing. Note the impact of the presence of the TECHROLL nozzle load on the displacement, velocity, and pressure responses of the actuator.

Numerous component parameter variations were made to determine the effect of each on stability, deflection, slew rate, actuation torque, step response, and motor pressurization. A standard duty cycle (both for chamber pressure and nozzle commands) was used for each run for ease

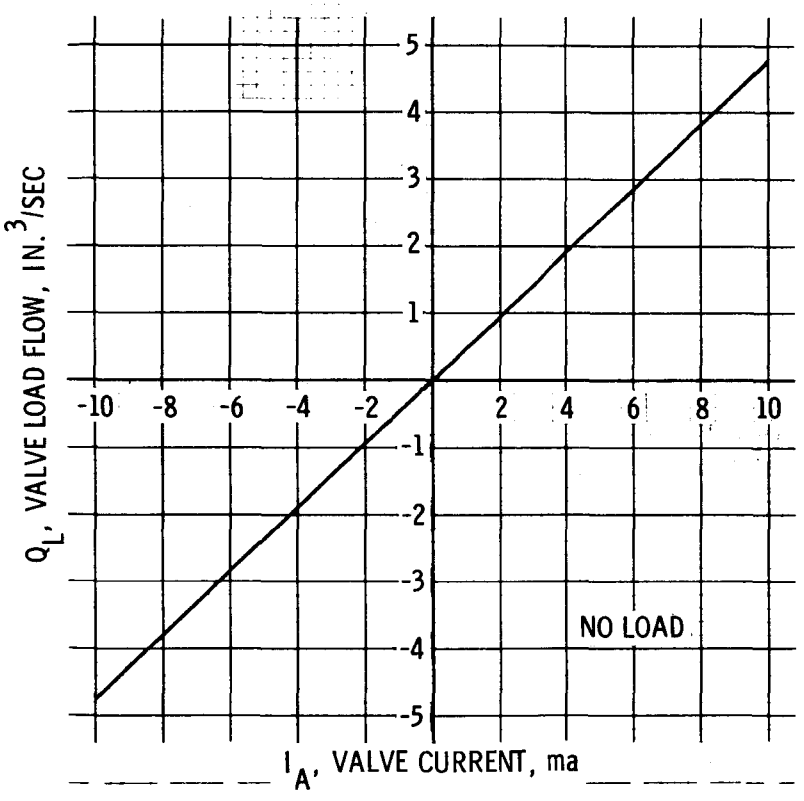

Figure 83. Servovalve Static Flow Gain

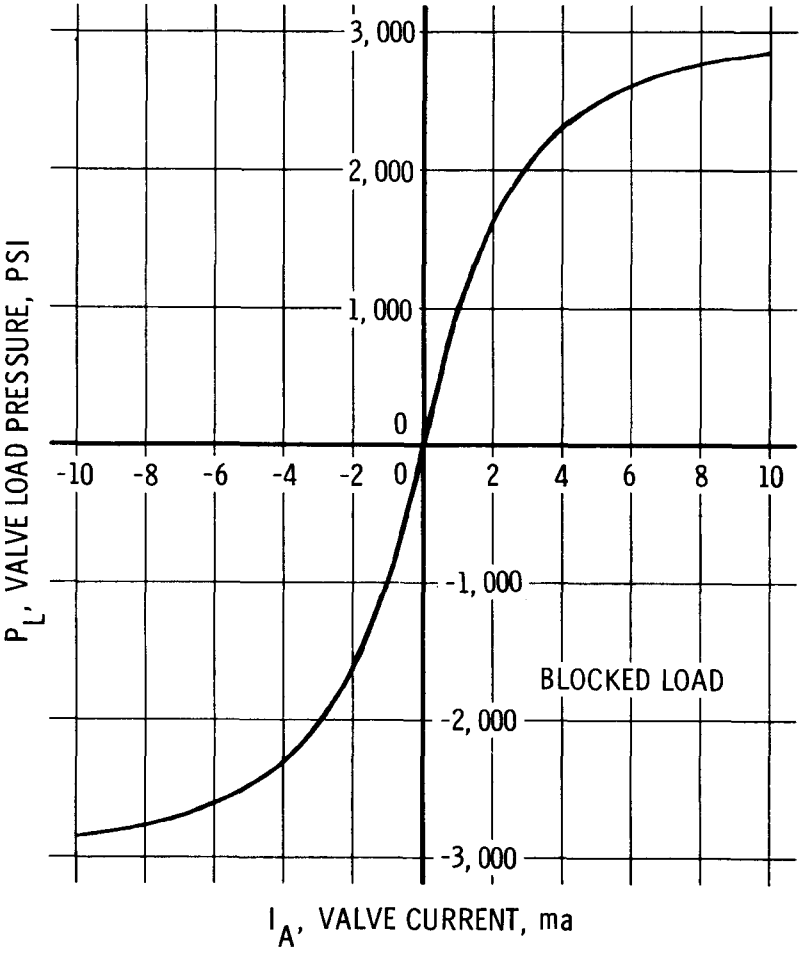

Figure 84. Servovalve Static Pressure Gain

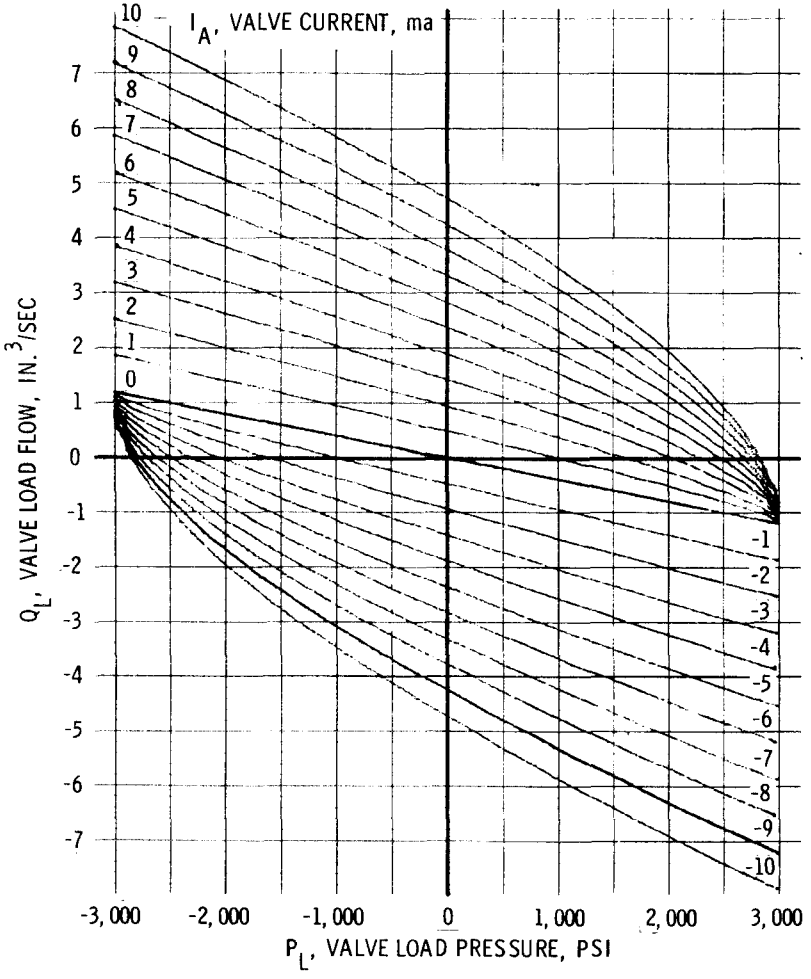

Figure 85. Servovalve Static Flow Pressure Curves (Model)

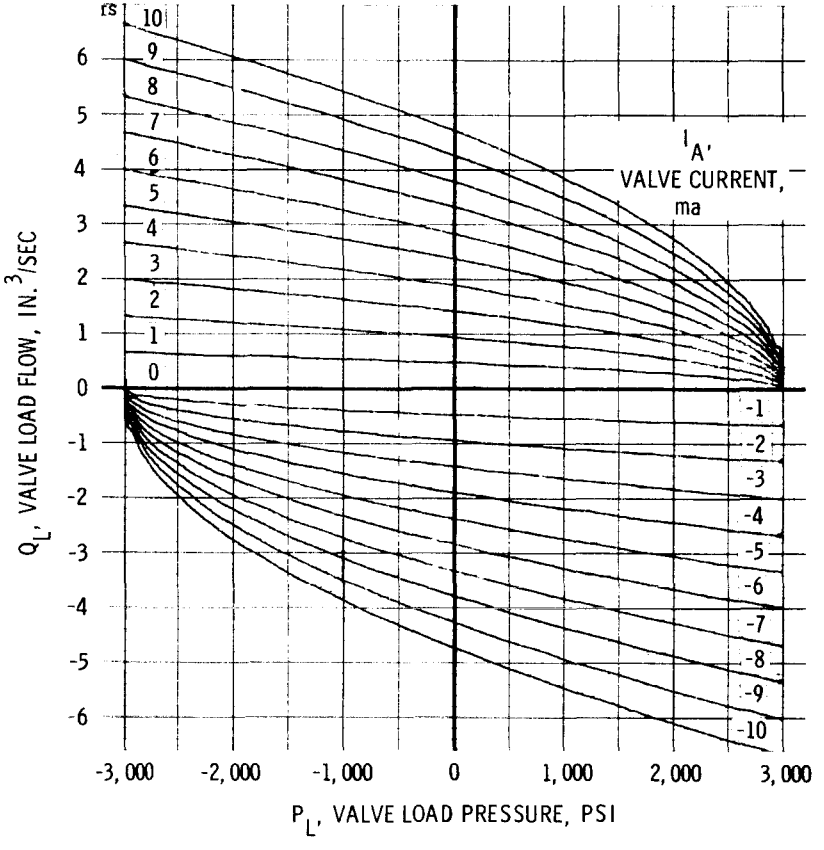

Figure 86. Servovalve Static Flow Pressure Curves (Ideal)

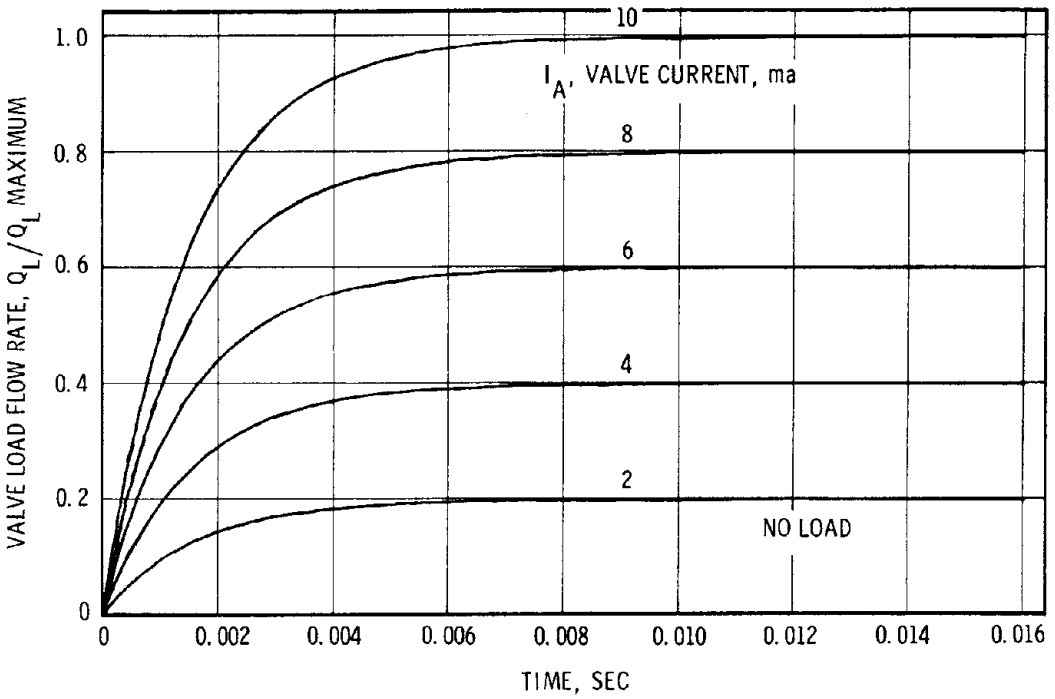

Figure 87. Servovalve Step Response

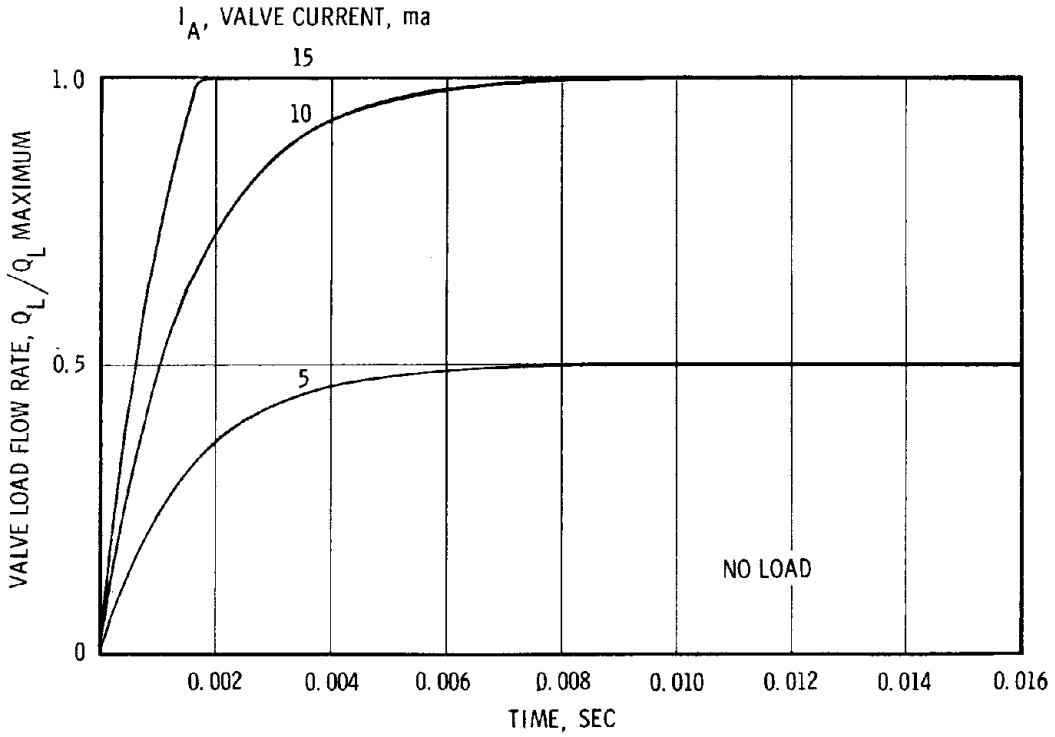

Figure 88. Servovalve Step Response, Flow Limited

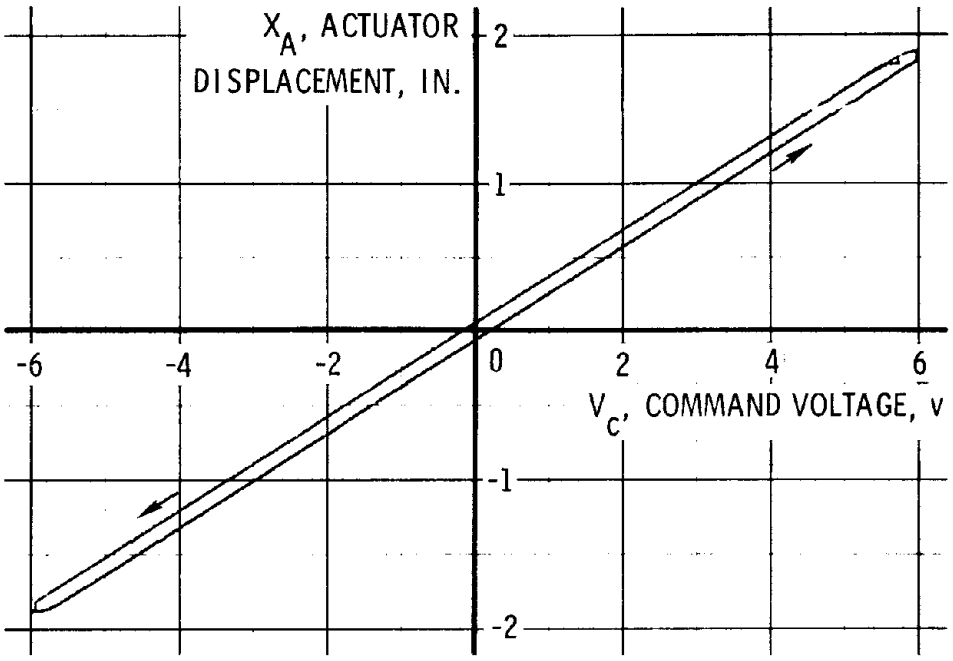

Figure 89. Servoactuator Linearity and Resolution

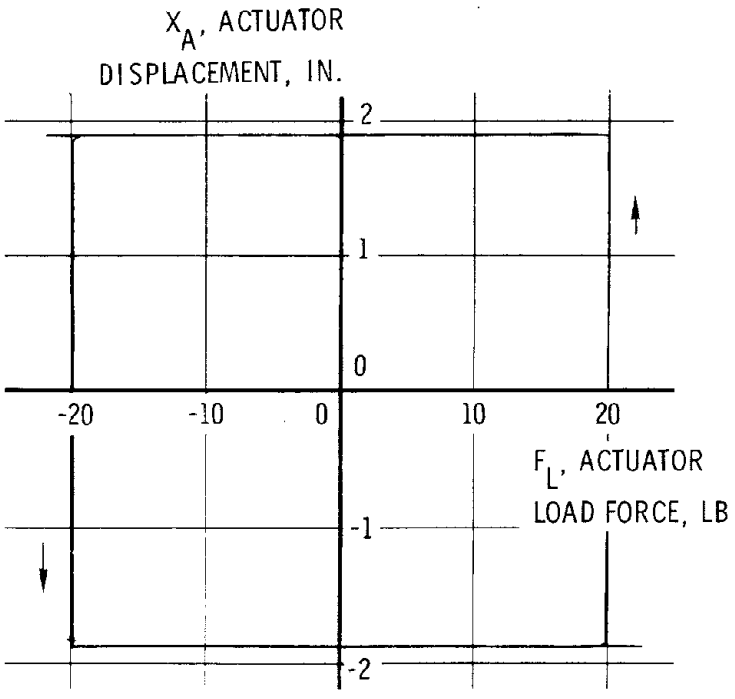

Figure 90. Servoactuator Static Friction

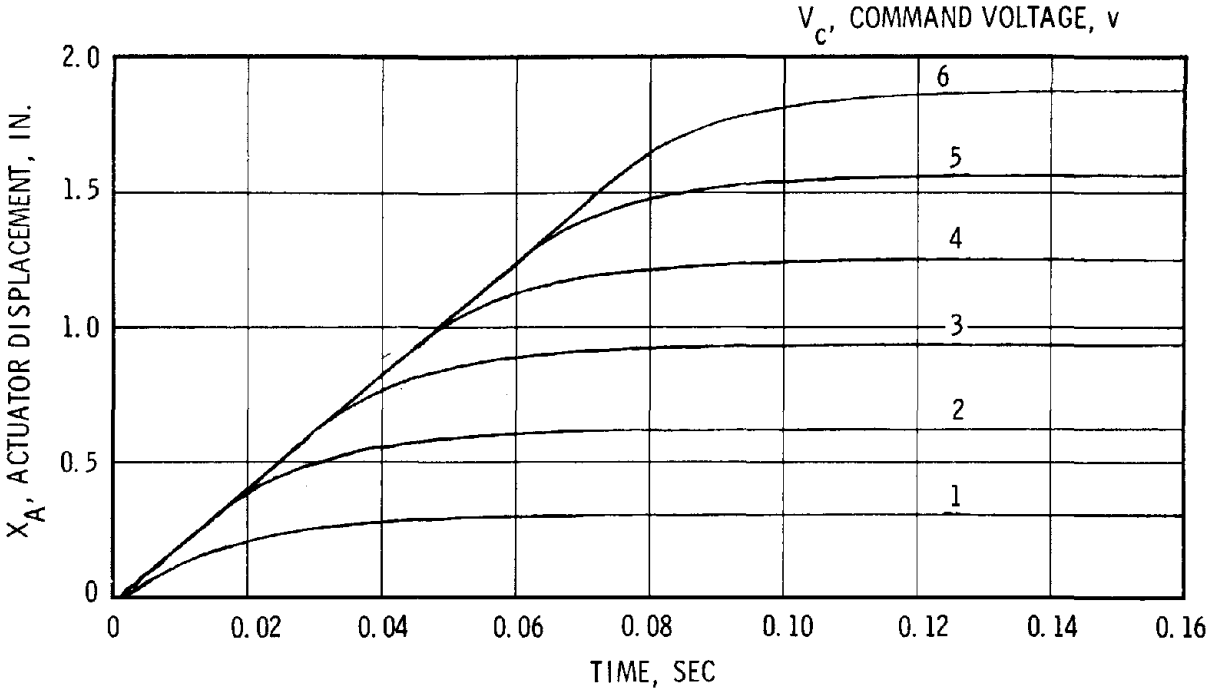

Figure 91. Servoactuator Step Response (Displacement)

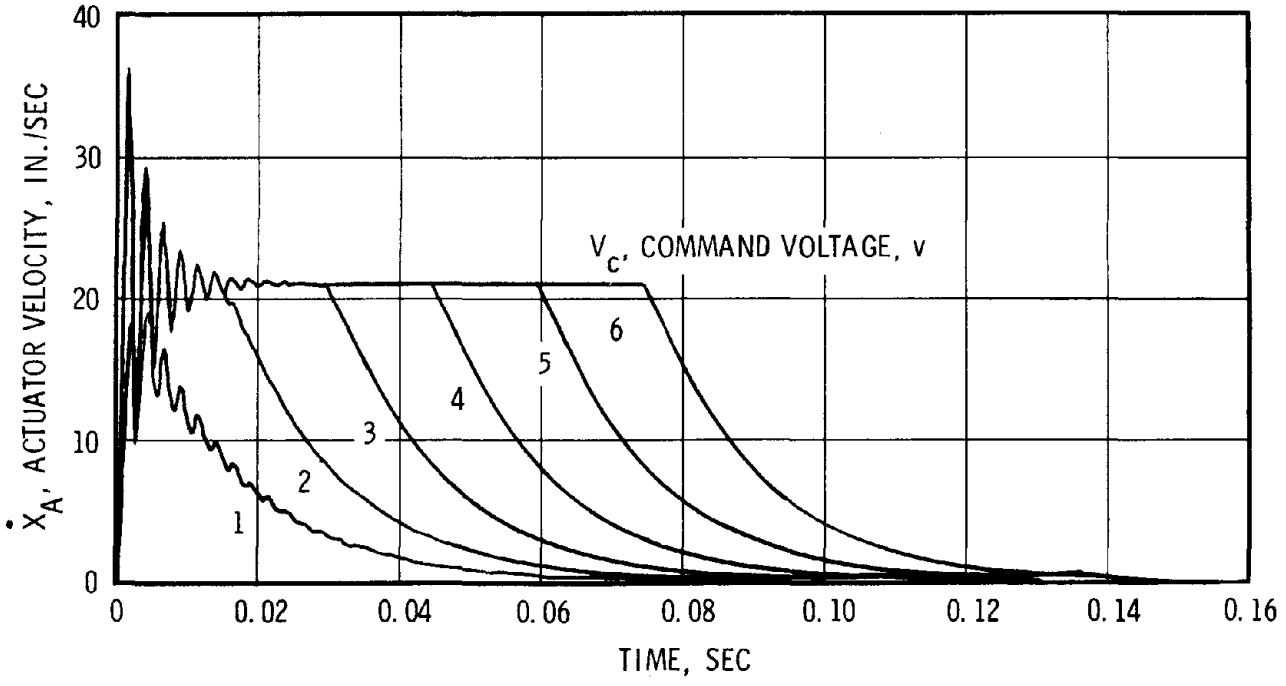

Figure 92. Servoactuator Step Response (Velocity)

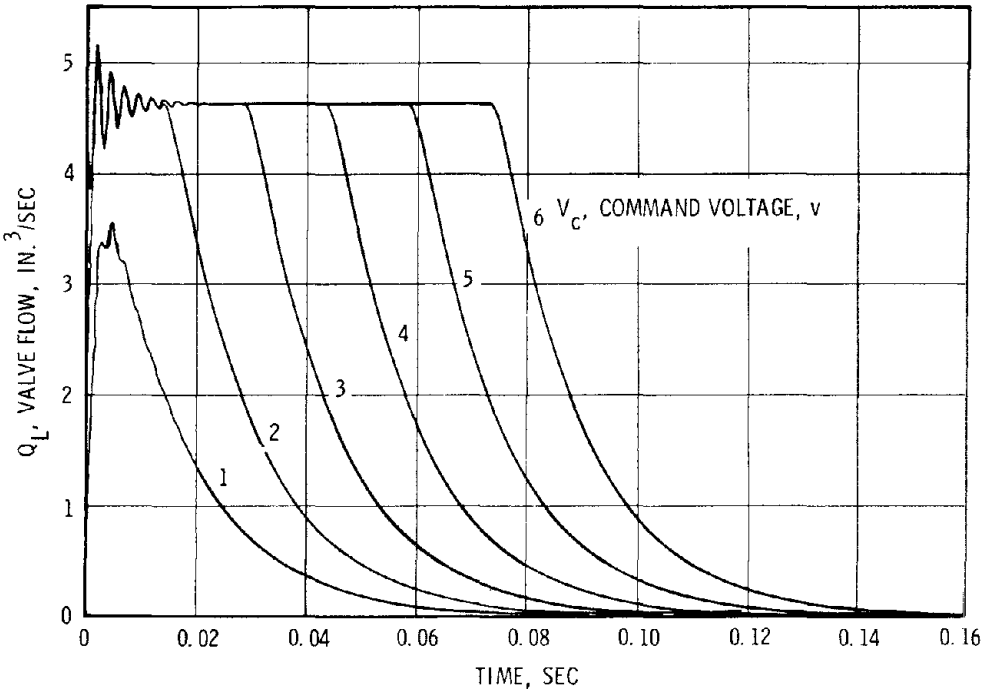

Figure 93. Servoactuator Step Response (Flow)

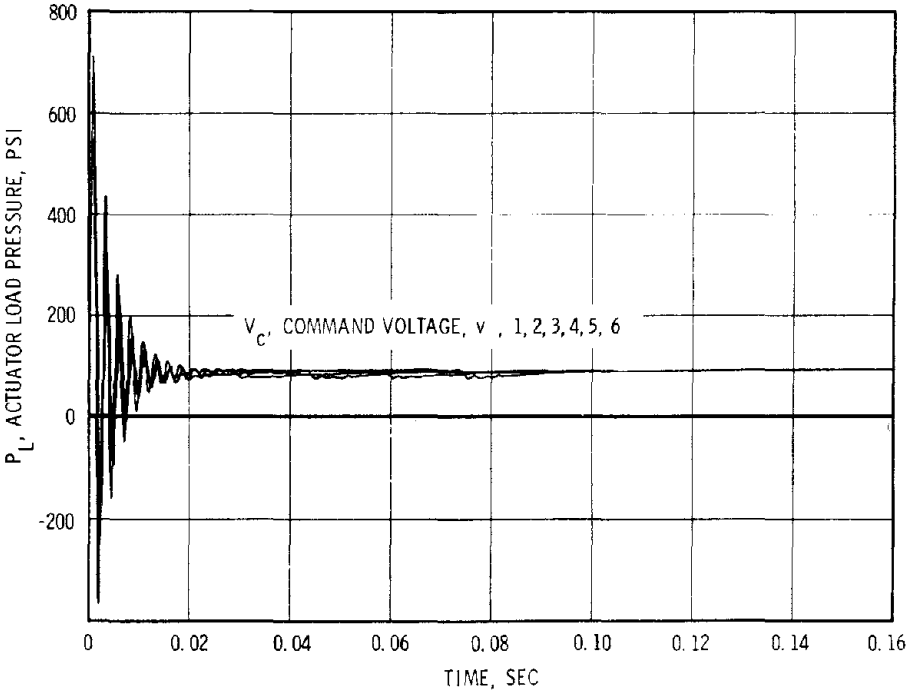

Figure 94. Servoactuator Step Response (Pressure), 1, 2, 3, 4, 5, 6 v

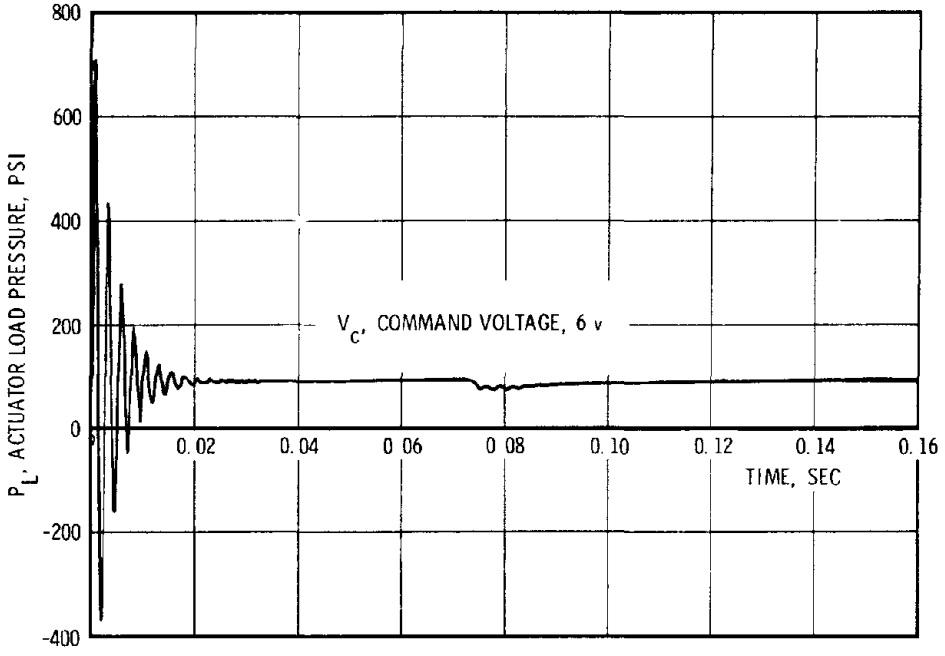

Figure 95. Servoactuator Step Response (Pressure), 6 v

of comparison (see figure 105). The run with 10X amplifier gain indicates a low margin for stability (11.2X was the limit). A 4X servovalve flow rating increases slew rate, but not proportionally, because of the dominance of boot grease damping effects. Half the nominal piston area could vector this system adequately, but at a reduced rate. Doubling the hysteresis reduces slew rate slightly. An interesting comparison can be made of the effects of a negative and positive spring rate of the same magnitude (both twice nominal).

A study of motor vibration effects was convenient because the computer used has a built-in random noise generator. Four levels of vibration are included. The creep in axial displacement at the higher levels was caused by the nozzle g loads overcoming the axial hysteresis of the seal. Hysteresis, a characteristic which the TECHROLL exhibits in all six degrees of freedom, acts like nonlinear damping.

The lateral displacements shown in all the illustrations in this section are incorrect (too large); however, this should have a minimal effect on other recorded data because of the magnitudes involved. Because of the demonstration activity, this problem was traced to an omission of a second-order term (involving sin Θ) in one of the component equations. The equations and block diagram of this report include that term.

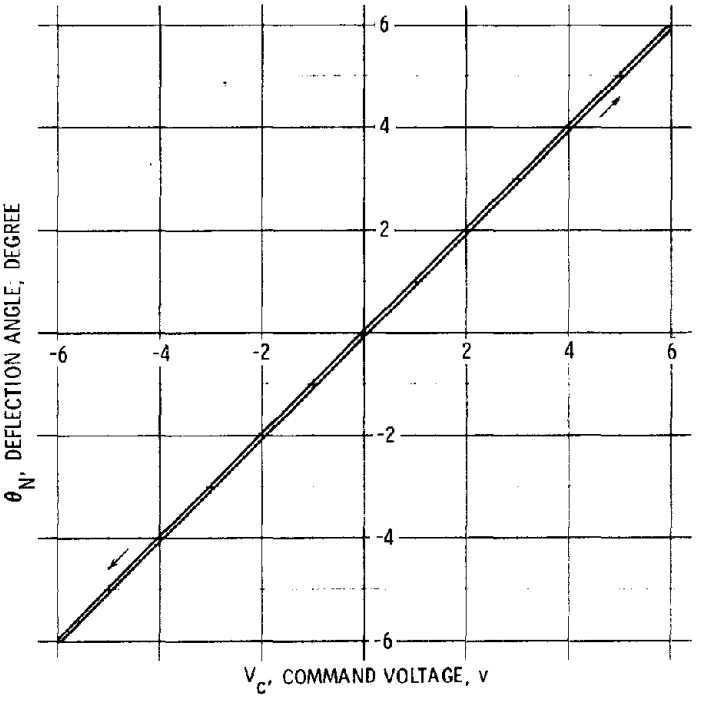

Figure 96. Nozzle System Linearity and Resolution

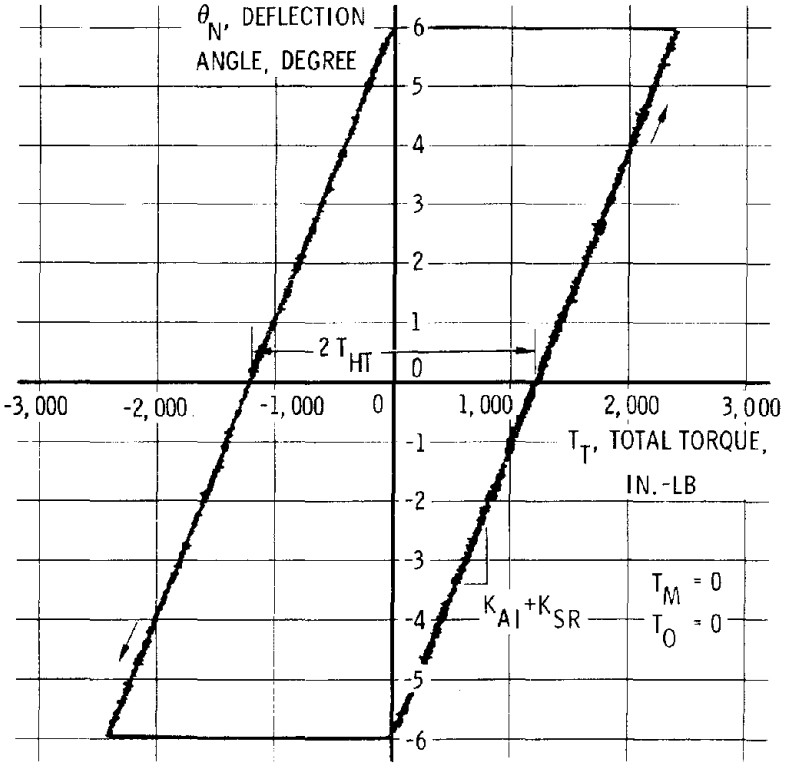

Figure 97. Nozzle System Rotational Hysteresis and Spring Rate

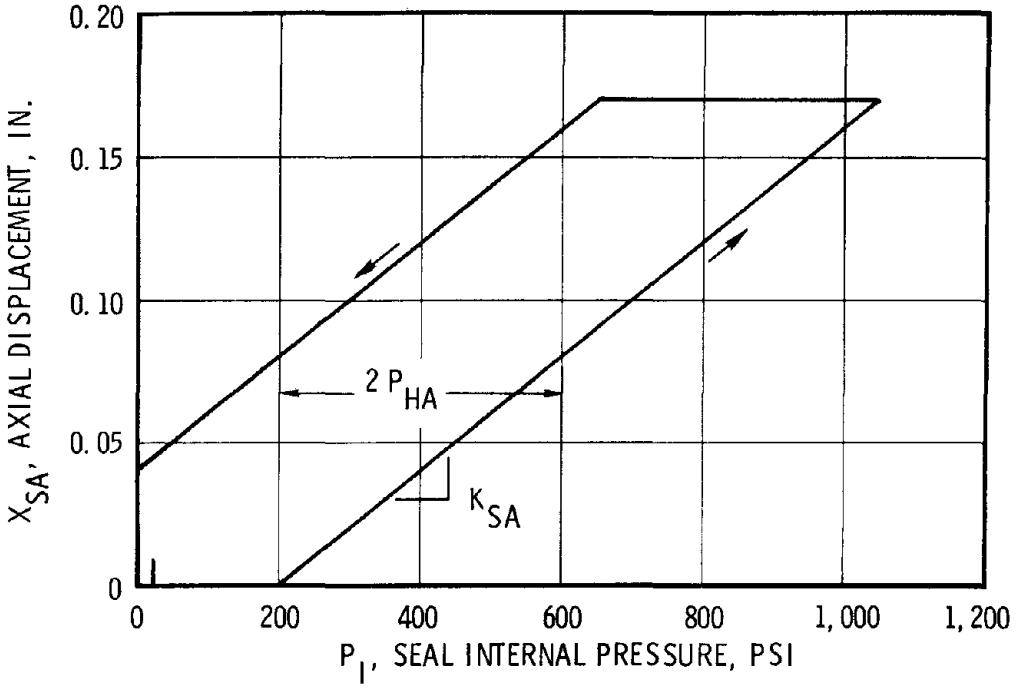

Figure 98. TECHROLL Seal Axial Hysteresis and Stiffness

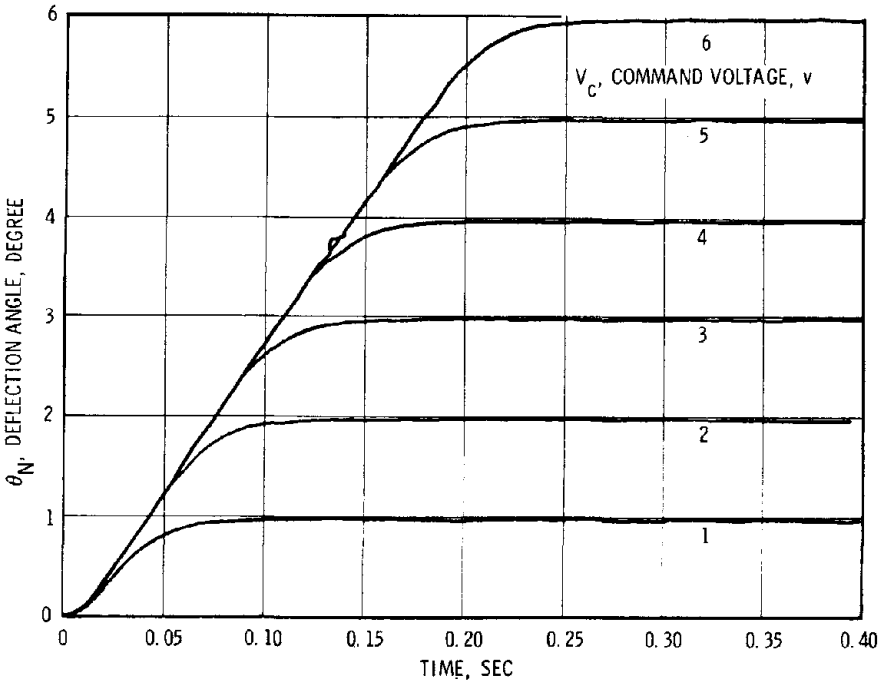

Figure 99. Nozzle System Step Response (Angular Deflection)

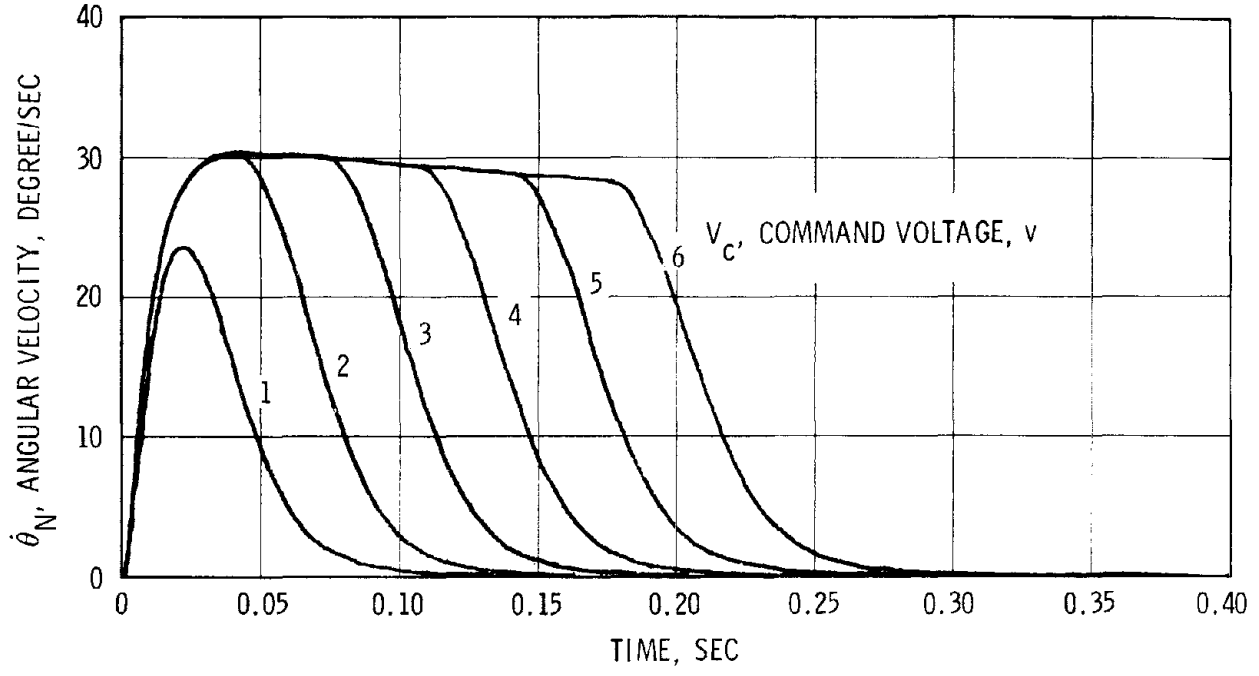

Figure 100. Nozzle System Step Response (Angular Velocity)

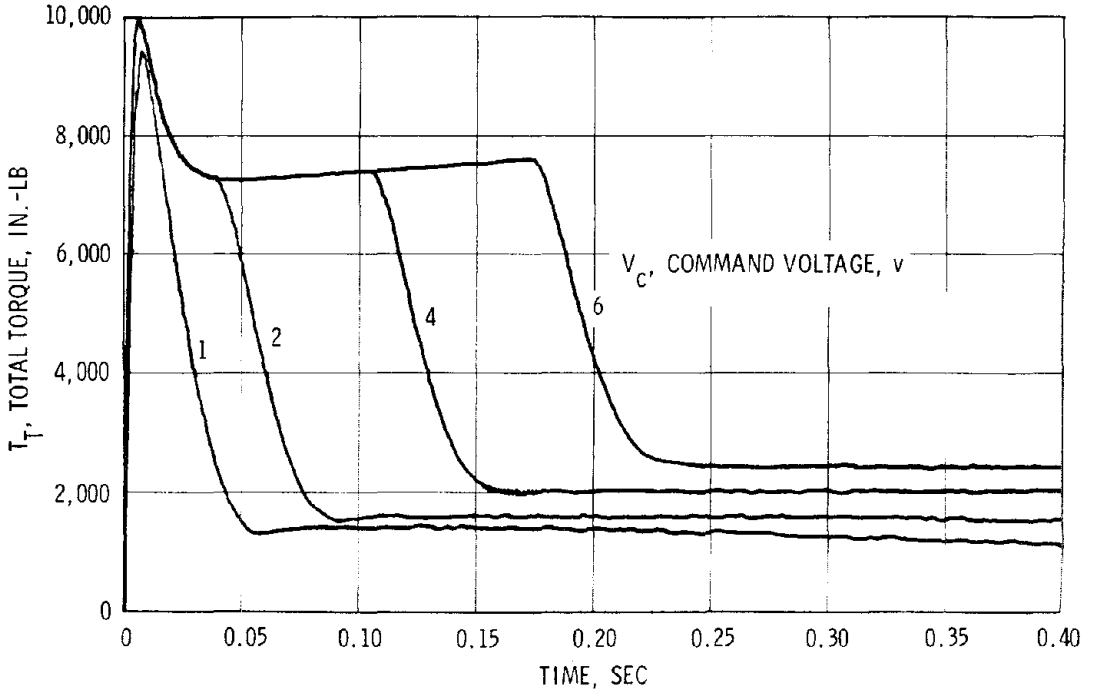

Figure 101. Nozzle System Step Response (Actuation Torque)

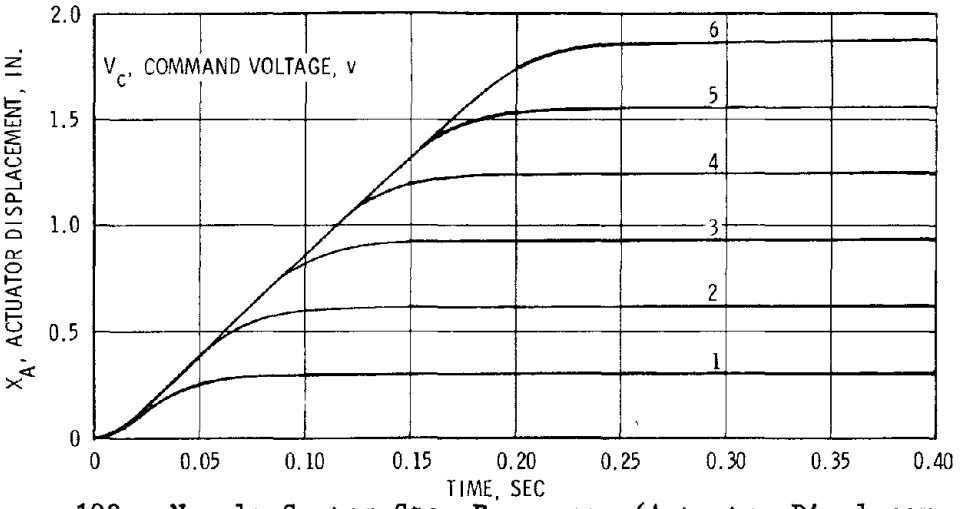

Figure 102. Nozzle System Step Response (Actuator Displacement)

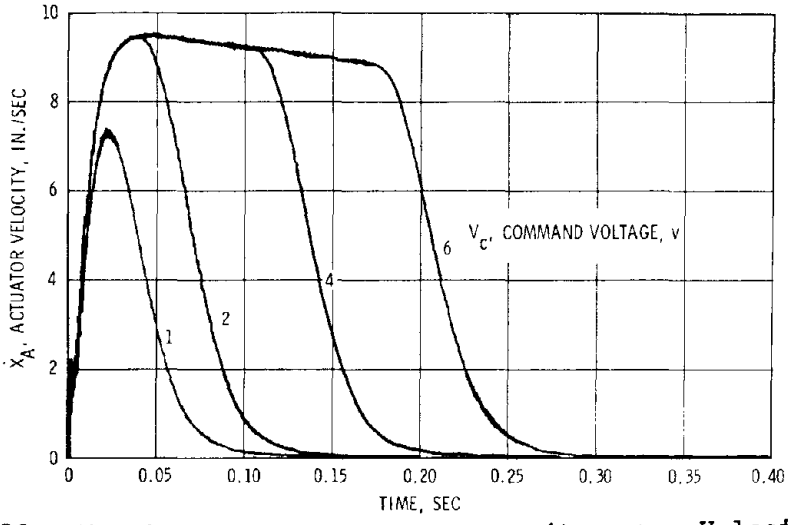

Figure 103. Nozzle System Step Response (Actuator Velocity)

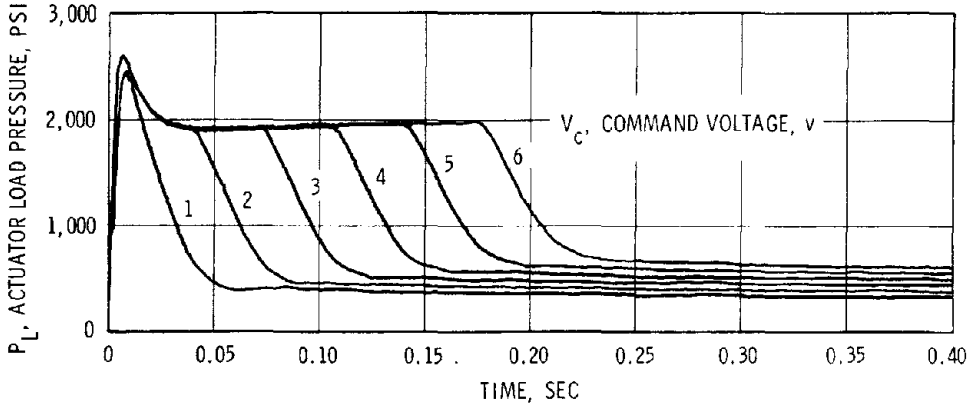

Figure 104. Nozzle System Step Response (Actuator Pressure)

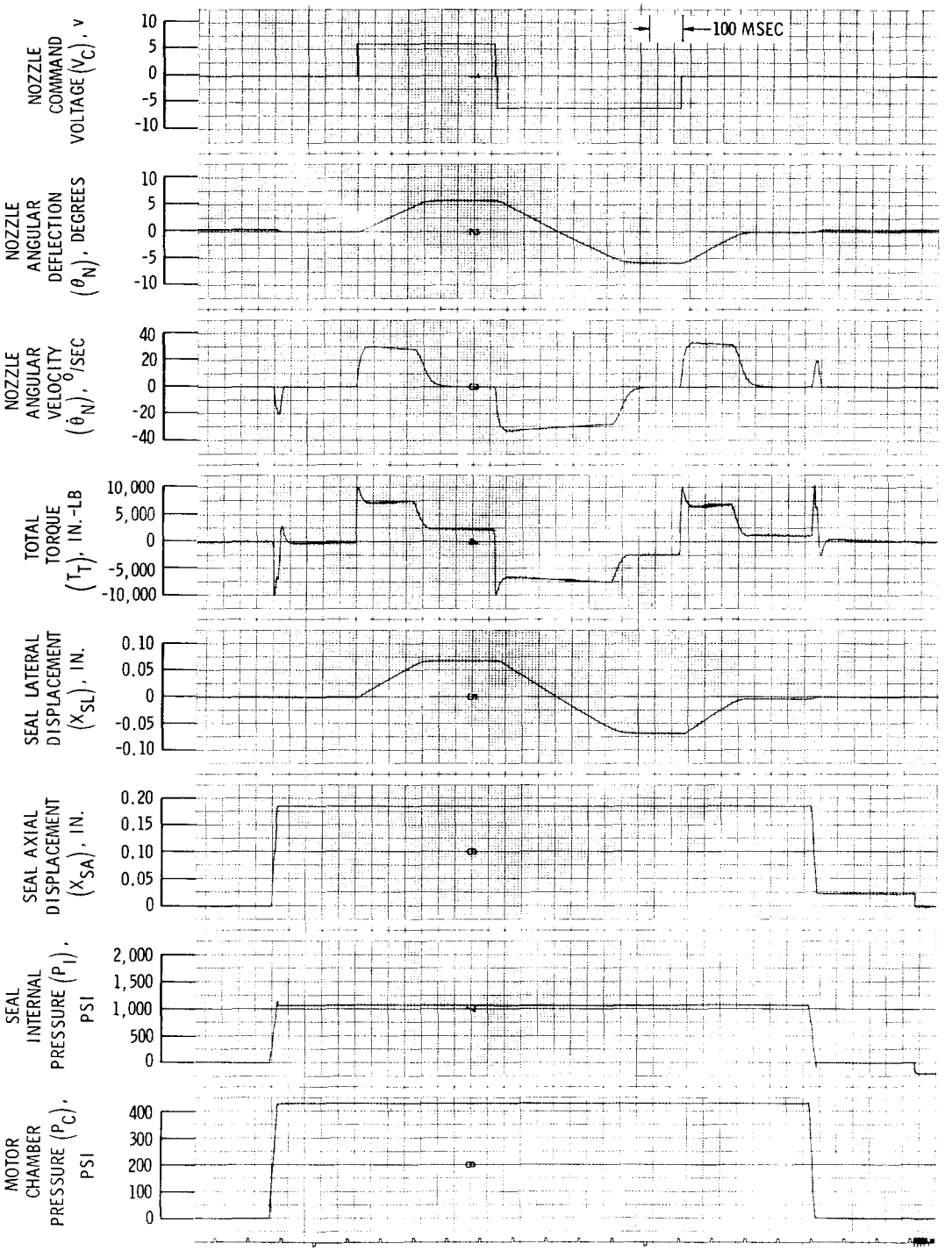

Figure 105. Nominal Parameters

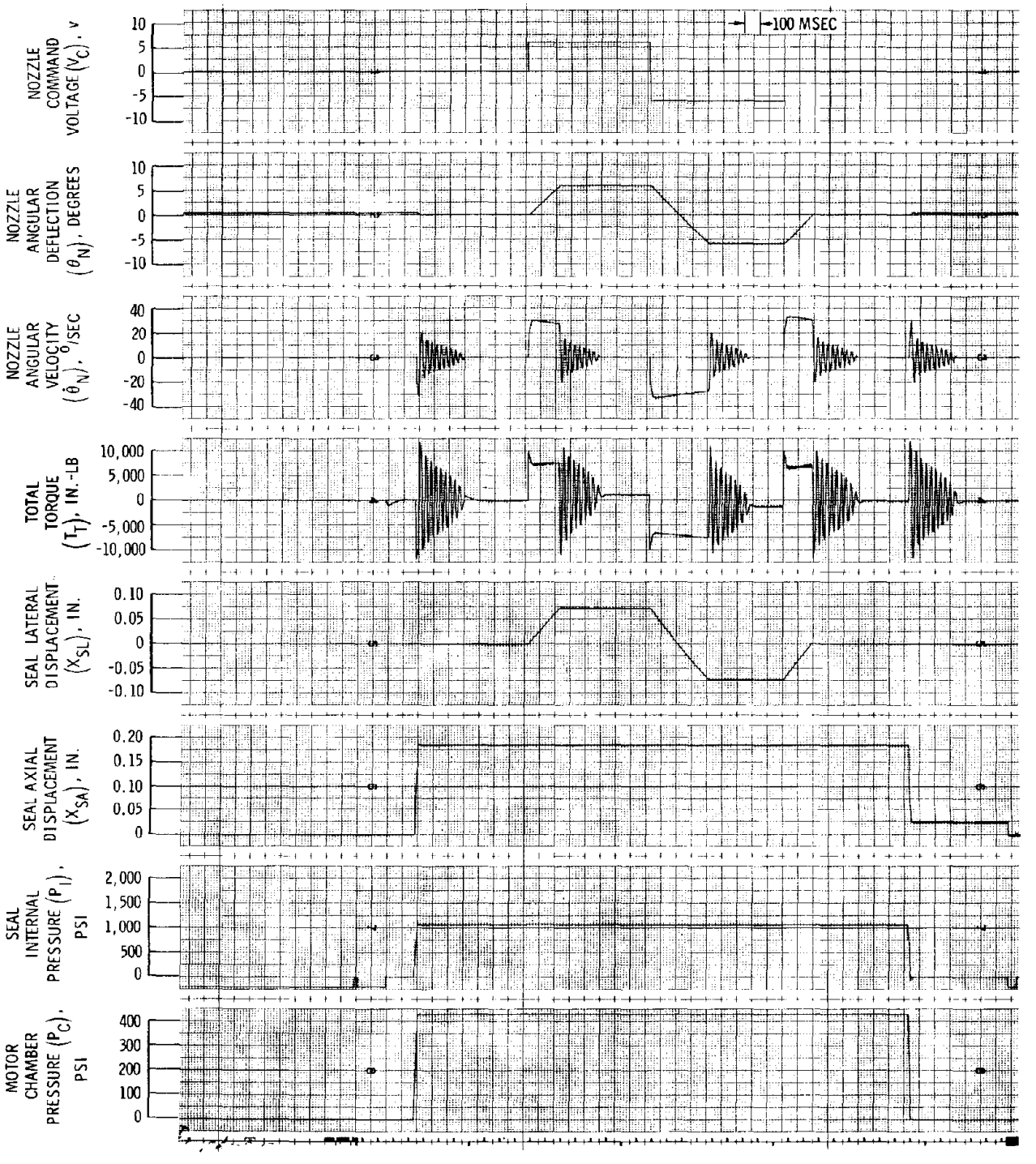

Figure 106. Amplifier Gain, 10X

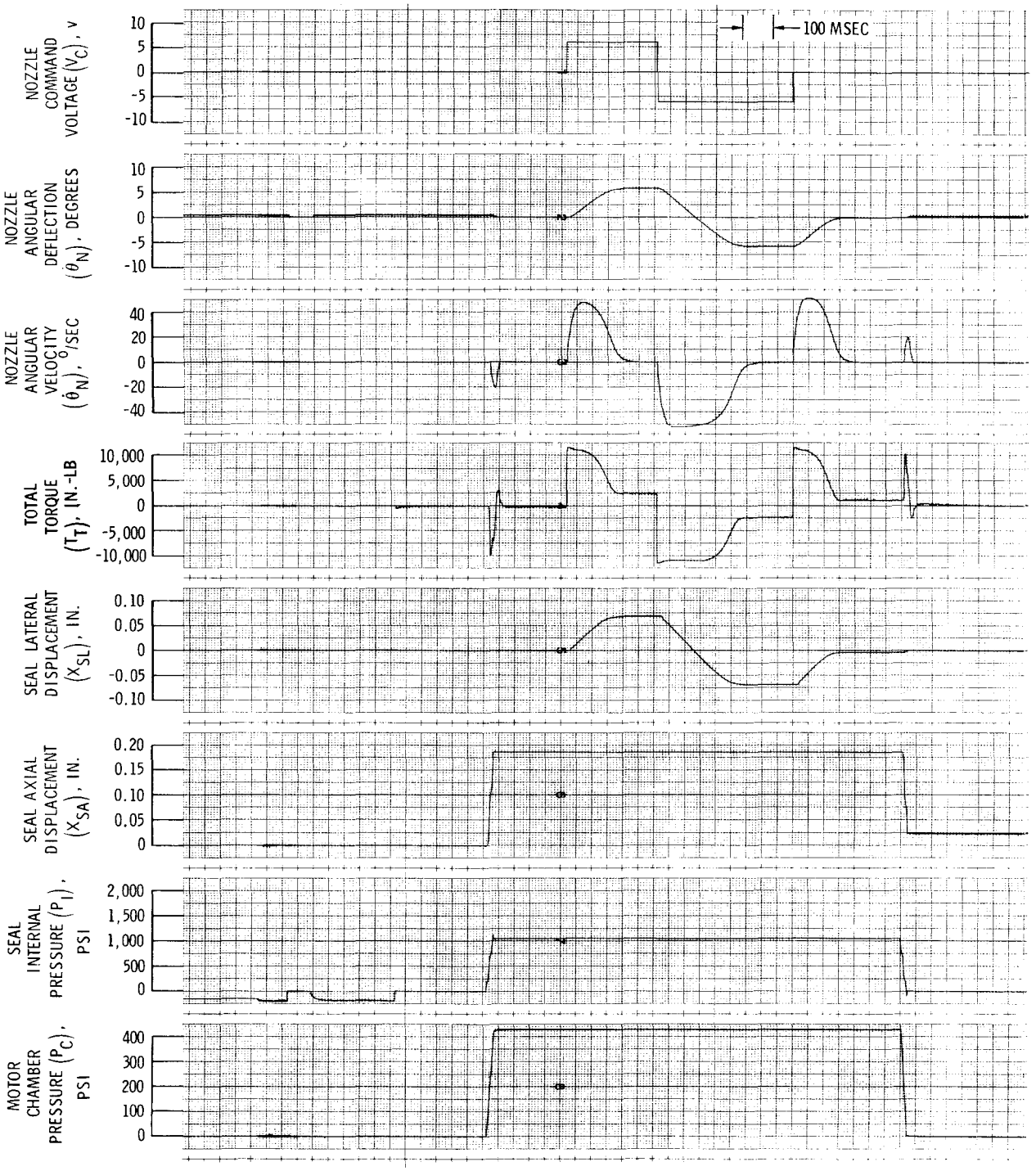

Figure 107. Servovalve Flow Limit, 4X

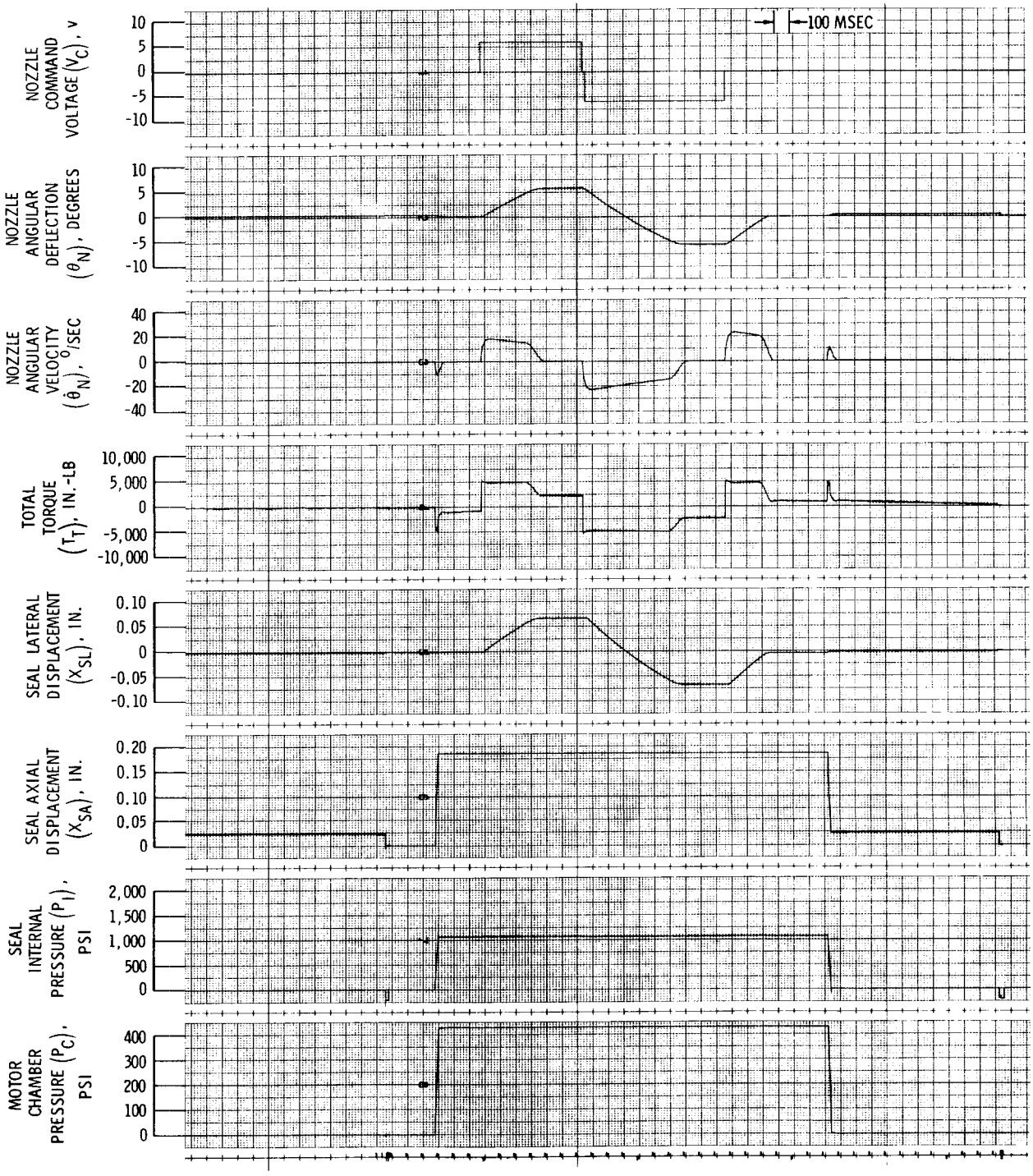

Figure 108. Actuator Piston Area, ½X

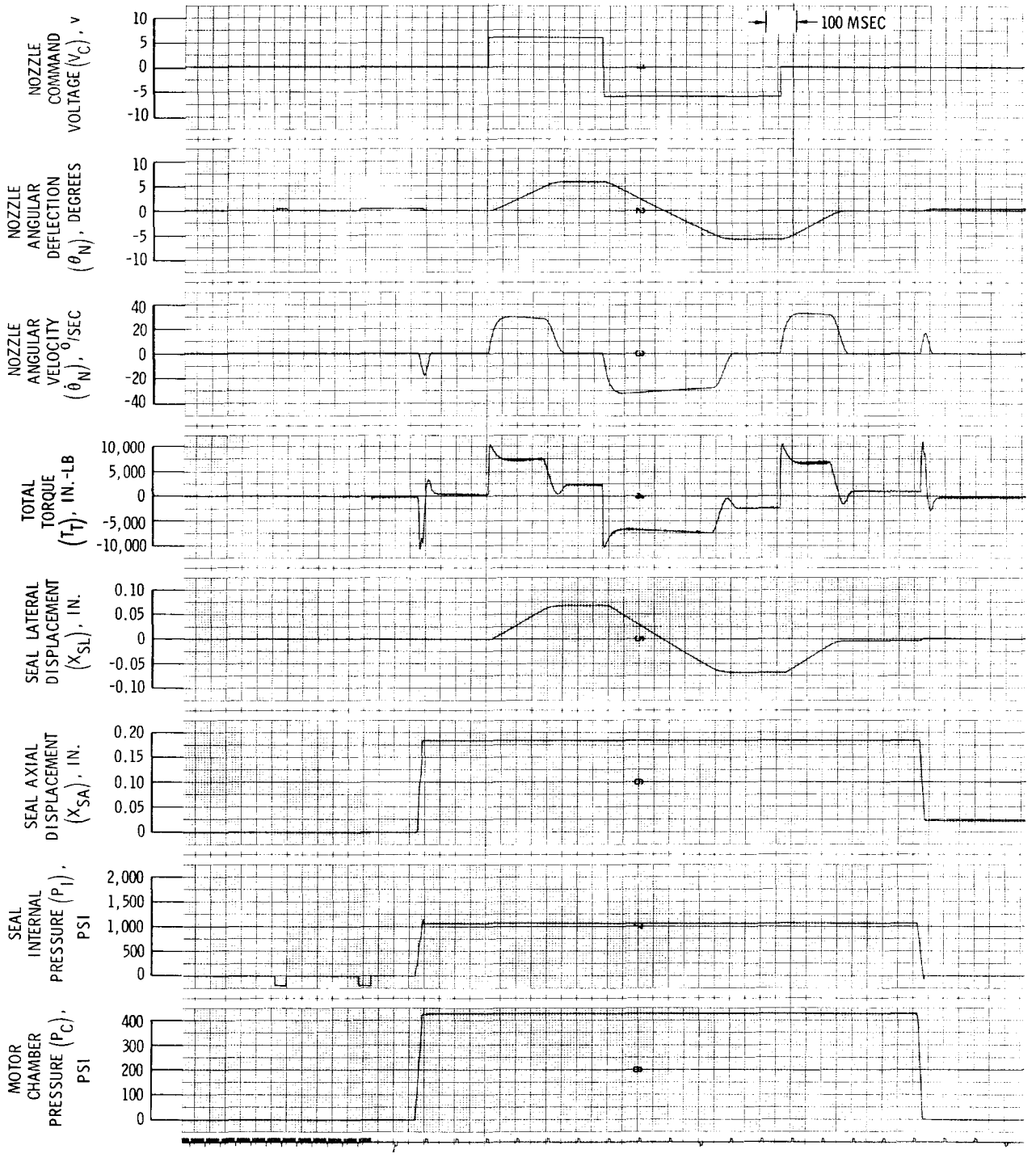

Figure 109. Nozzle Inertia, 2X

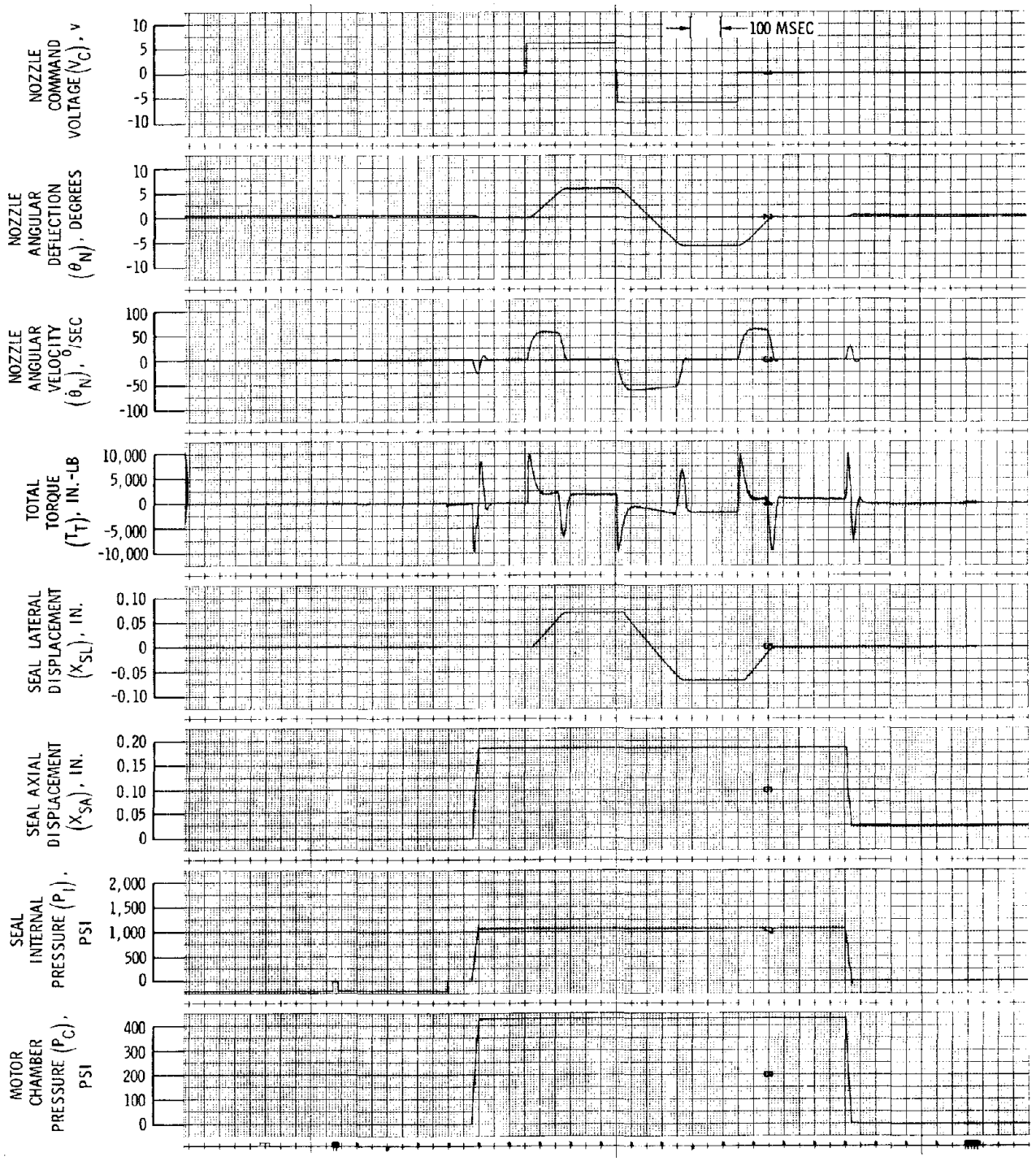

Figure 110. Grease Boot Removed

Figure 111. Seal Hysteresis, 2X

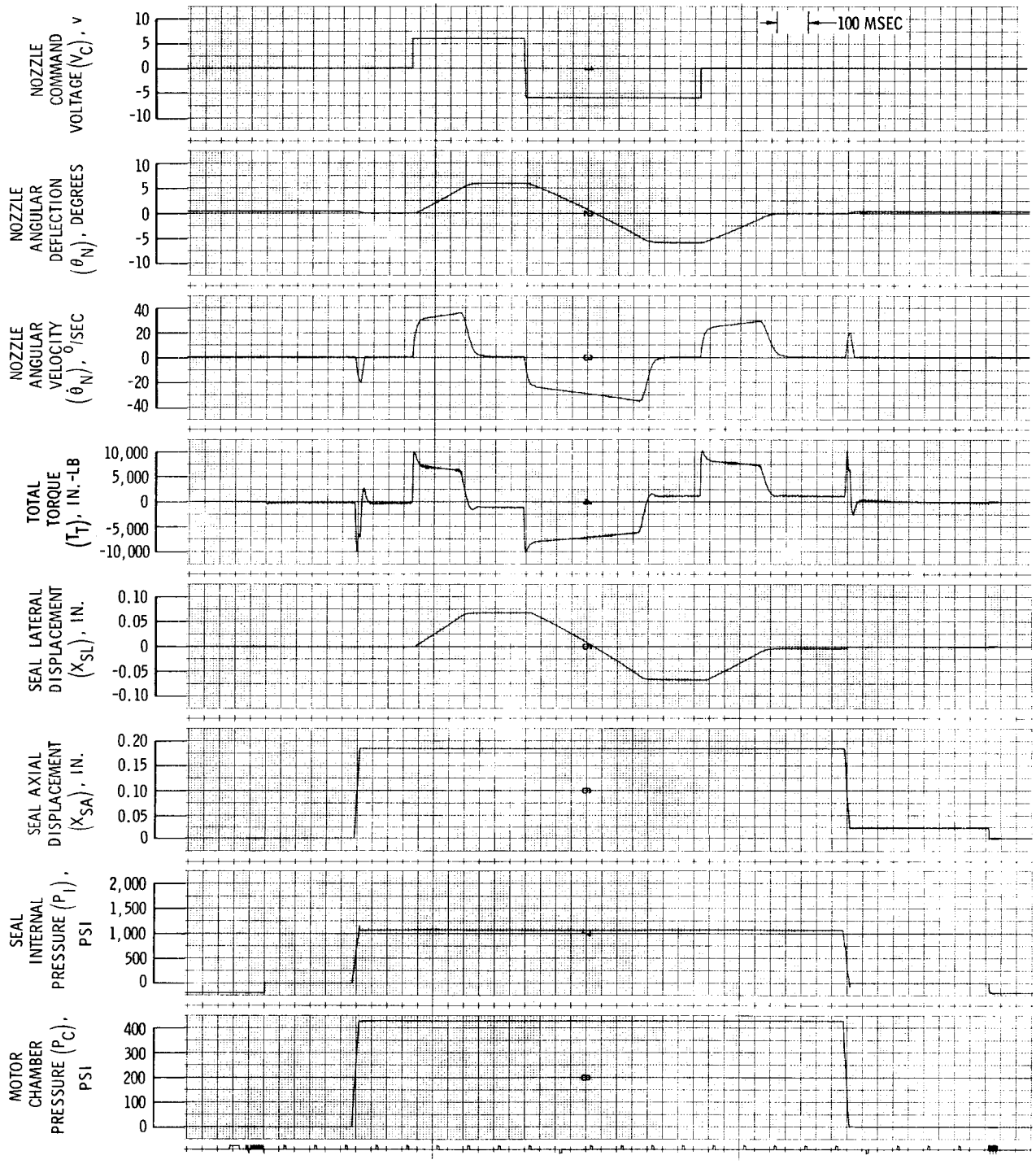

Figure 112. Rotational Spring Rate (Negative), 2X

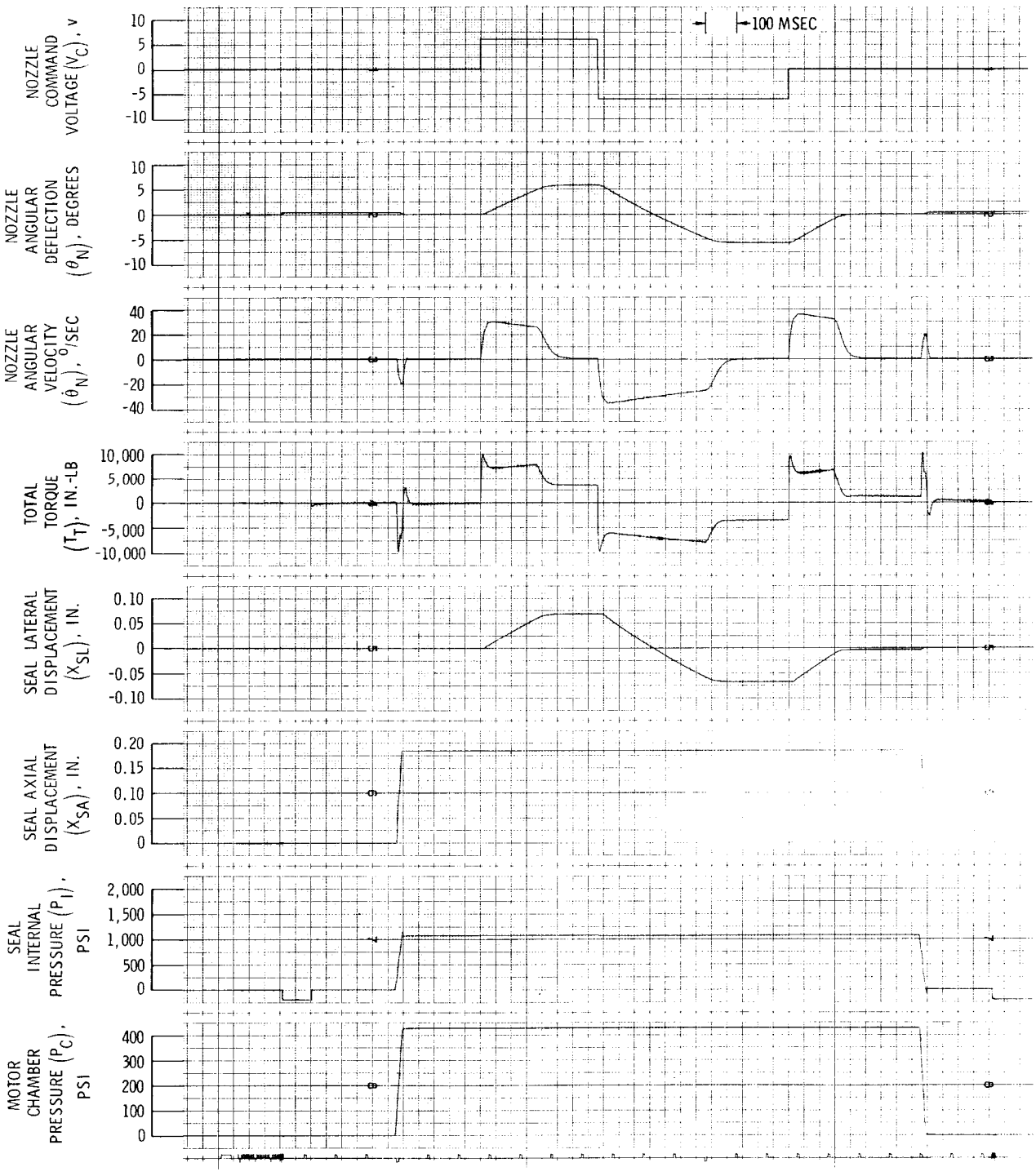

Figure 113. Rotational Spring Rate (Positive), 2X

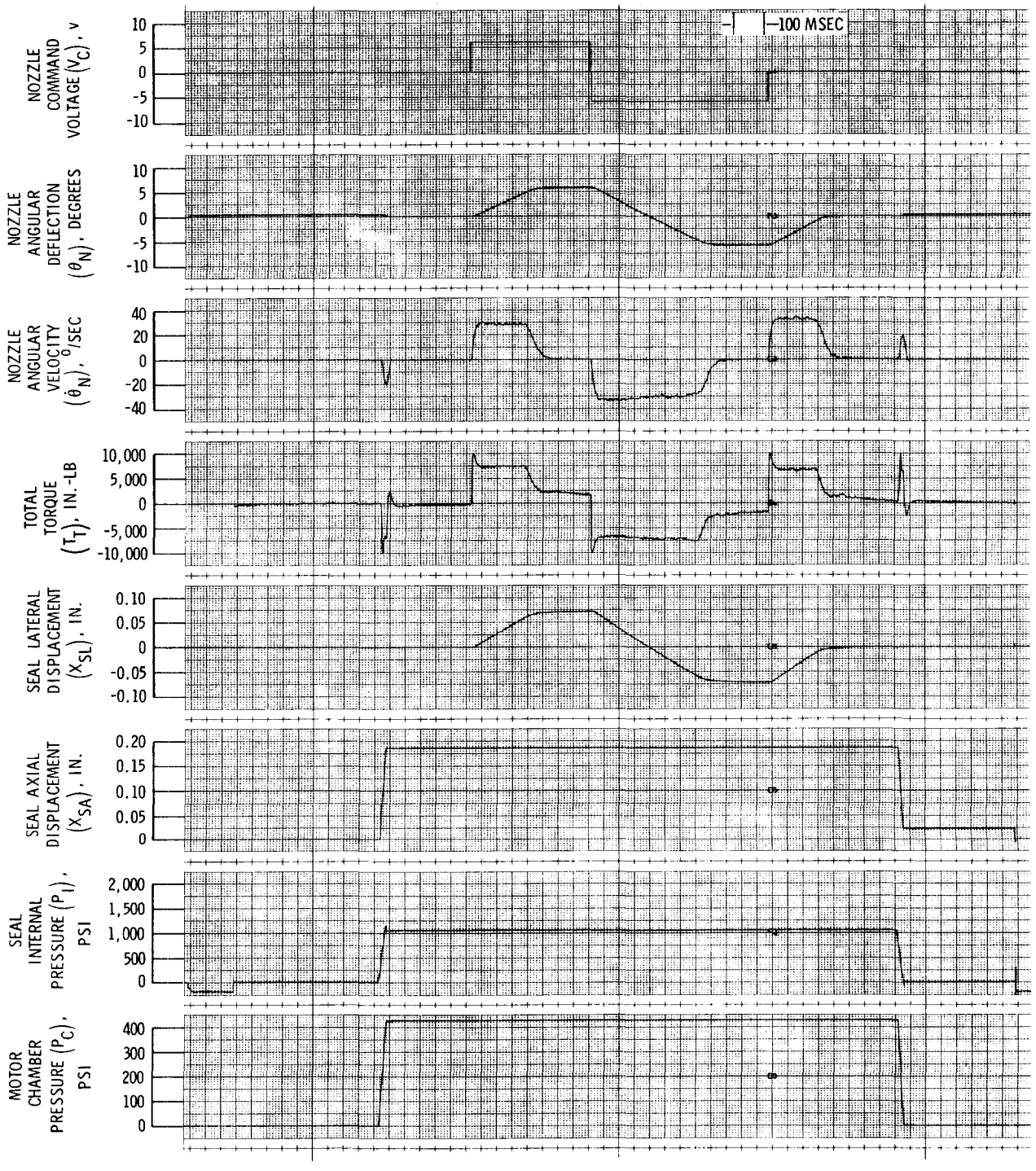

Figure 114. Motor Vibration (±1 g Axial and Lateral)

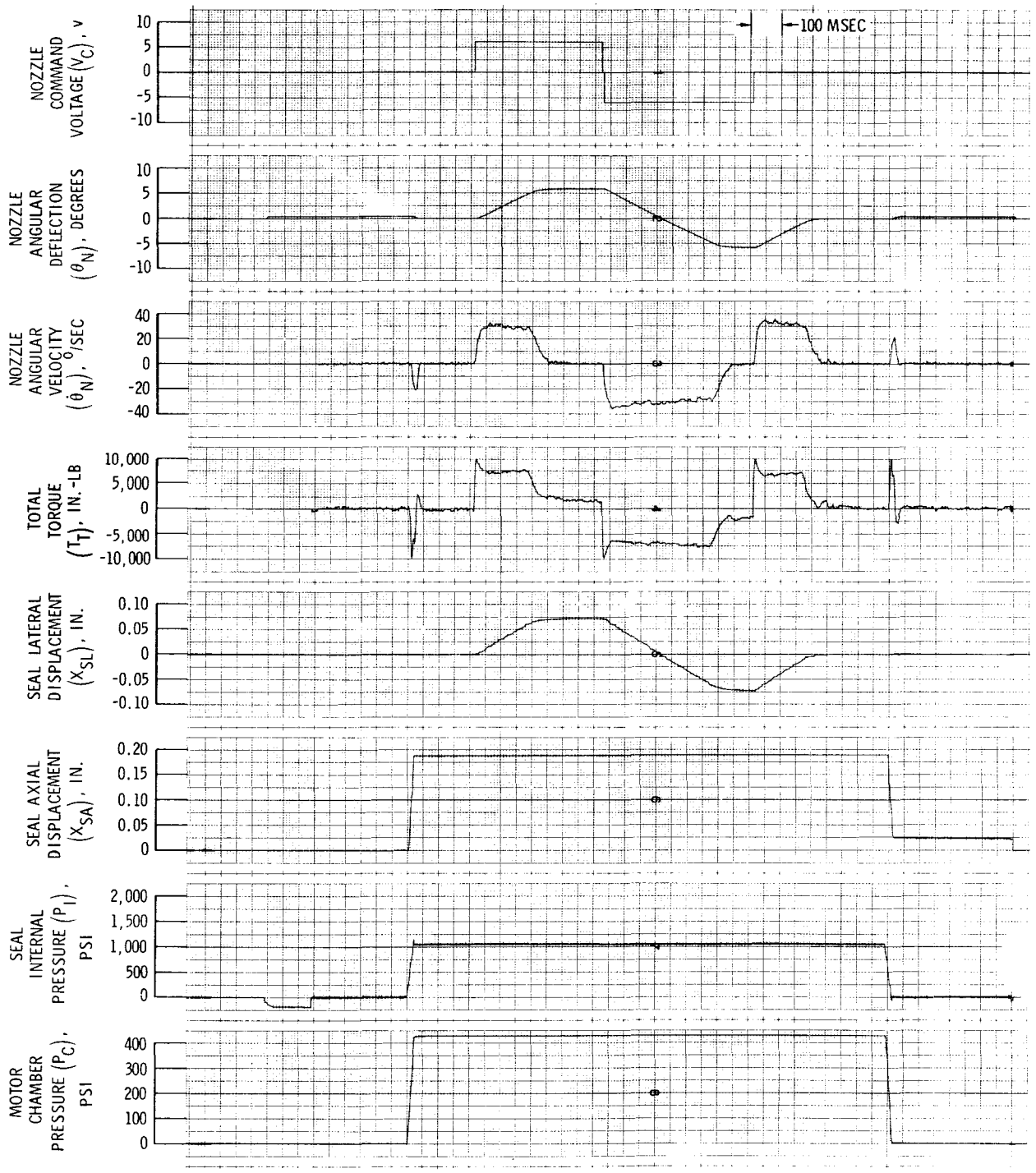

Figure 115. Motor Vibration (±2 g)

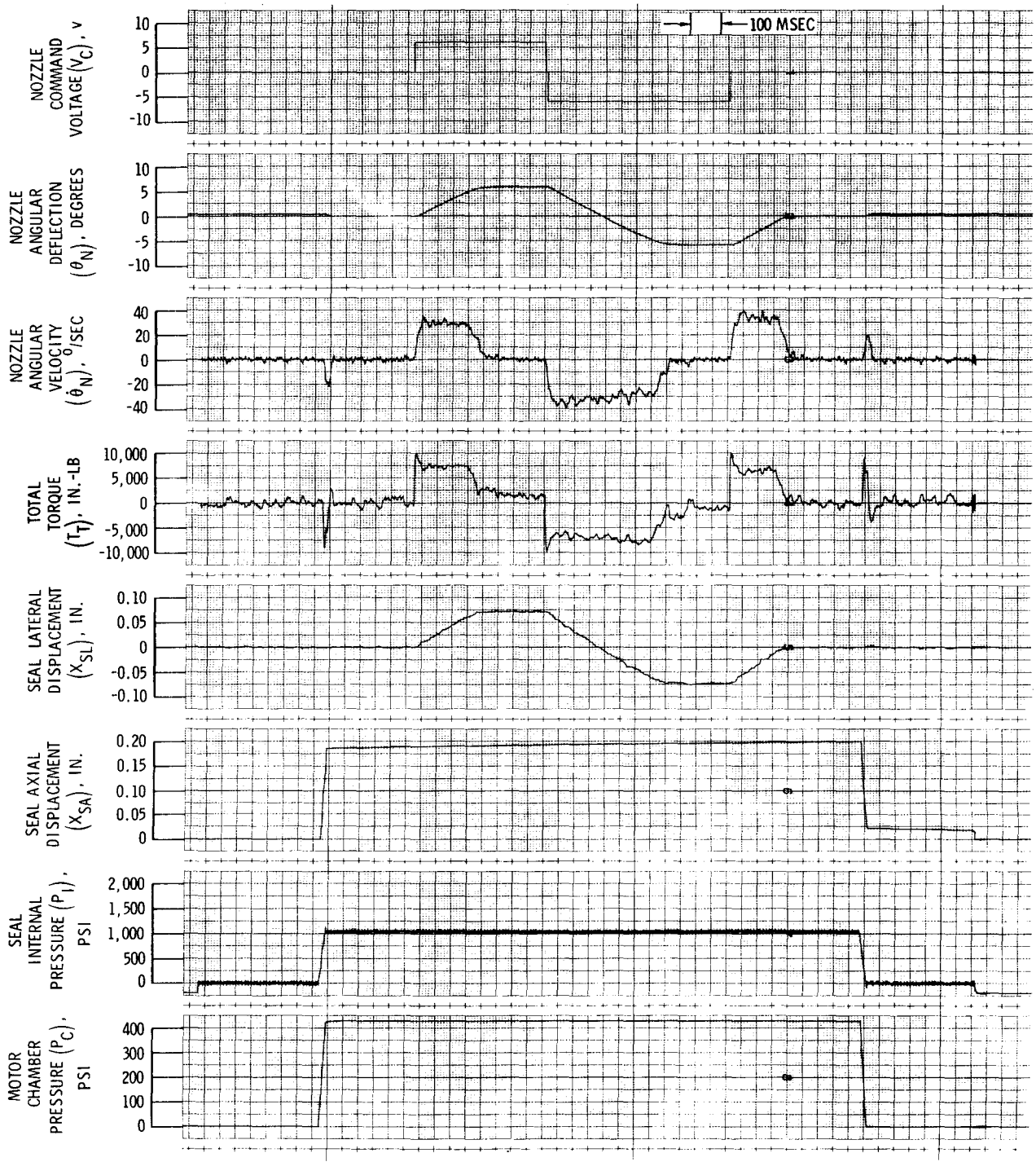

Figure 116. Motor Vibration (±4 g)

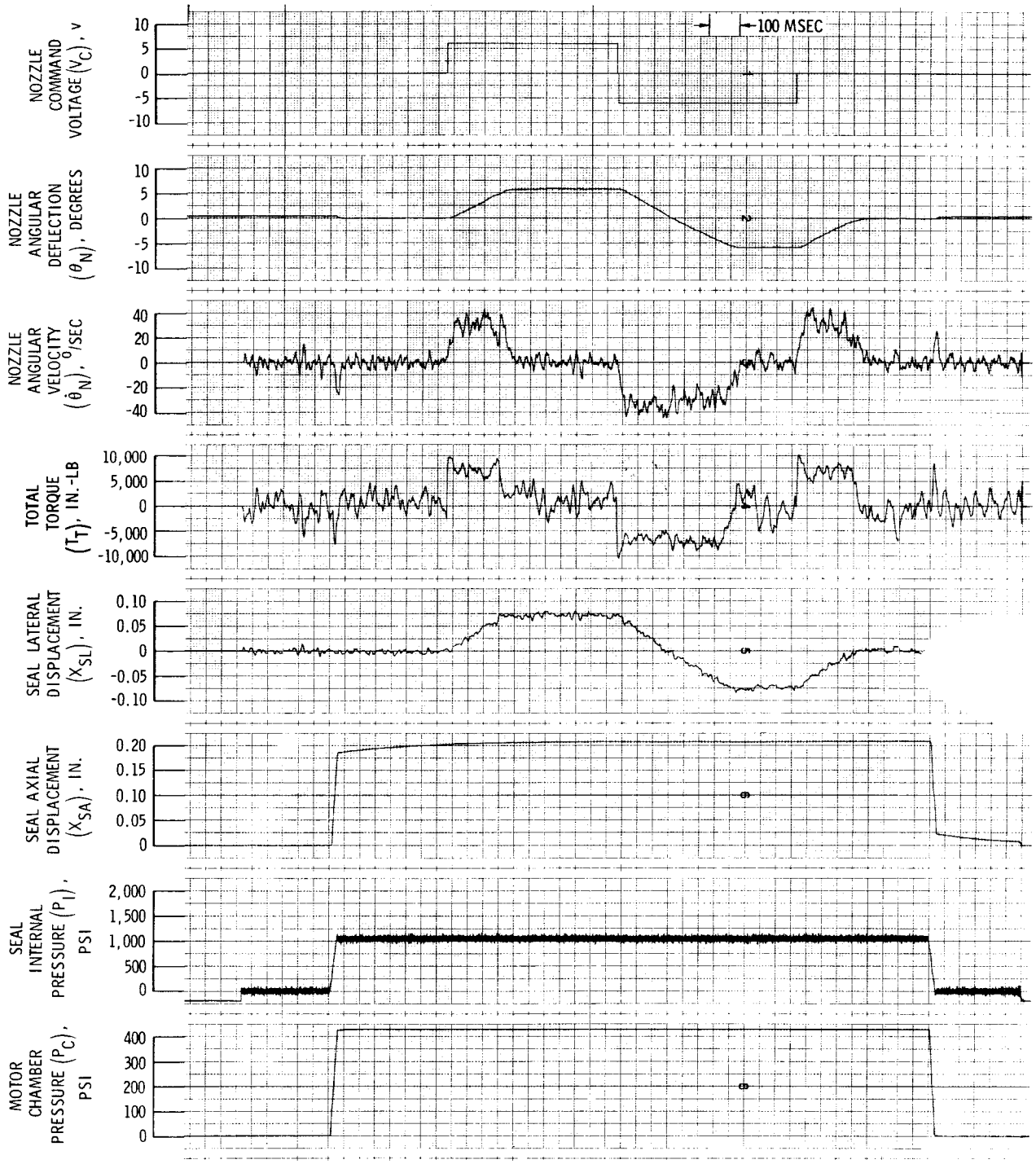

Figure 117. Motor Vibration (±10 g)

d. Conclusions

The model described has been the basis for both analog and digital computer simulations of real movable nozzle systems. Analog (or analog/hybrid) computer patching diagrams are derived directly from the model block diagram (or variations thereof). Parameters and variables are magnitude-scaled to stay within the machine's voltage range. Solutions are normally time-scaled for the readout equipment. Multichannel pen recordings, X-Y plots, oscilloscope photographs, and DVM readouts are available as documentation. The demonstration simulation underscores the usefulness of analog/hybrid computers for solving complex dynamic system problems. Programming flexibility, hands-on access, and operating costs are the greatest assets of this approach; however, analog facilities are not always available and their purchase can represent a significant investment.

Digital simulations are based directly on the model's component and system equations (or variations). No magnitude scaling is required. Solutions are iterated in machine time, which has no relationship to real time. Computer printouts and plots are available as documentation. Digital computers of sufficient capacity are readily available to most engineers; however, operating costs can be prohibitive if a simulation becomes too complex. Digital simulations permit the inclusion of more nonlinear and multivariable interaction effects.

4. TECHROLL PARAMETER EQUATIONS

a. Introduction

A major portion of task III analytical modeling activities included formulation of prediction equations for each TECHROLL seal parameter: (1) rotational inertia, (2) rotational damping, (3) rotational spring rate, (4) rotational hysteresis, (5) rotational offset, (6) axial stiffness, (7) lateral stiffness, and (8) torsional stiffness. These expressions were to result from a combination of theoretical derivation and empirical data correlation techniques. A goal of this activity was to be able to predict these parameters within a ±20% accuracy. The following six static motor firings were used both as a data base and as a comparison for predicted parameters: (1) Minuteman, (2) HIPPO boost, (3) HIPPO boost-sustain, (4) HIPPO high pressure, (5) 8-in.-diameter demonstrator motor, and (6) Poseidon C-3. The 8-in.-diameter and Poseidon C-3 motor firings were not directly covered by this program, but were included to expand the data base to a wider range of seal sizes. Also, bench test data from an alternate HIPPO high pressure seal design were included although the design was never fired.

b. Discussion

A discussion of the useful output of this activity is presented in the following paragraphs. Included are definitions of seal dimensions and material properties, a listing of the analytically and empirically derived TECHROLL parameter equations, and a comparison of predictions versus test data.

(1) Definitions

A cross section of a generalized straight-sided TECHROLL seal is shown in figure 118. Table XI defines all the dimensions shown on the figure, plus additional derived dimensions. Table XII defines related seal material properties, with some typical values.

(2) Equations

The parameter equations listed below were either originated or updated during this program.

Rotational inertia (theoretical)

$$I_{SR} = \pi\rho\left(\frac{w_c^2}{wh}\right)R_S^5\left[2\left[\frac{1-\left(1-\left(\frac{R_S\theta_N}{h}\right)^2\right)^{\frac{1}{2}}}{\left(\frac{R_S\theta_N}{h}\right)^2}\right]\right]$$

~ 1 for small θ_N

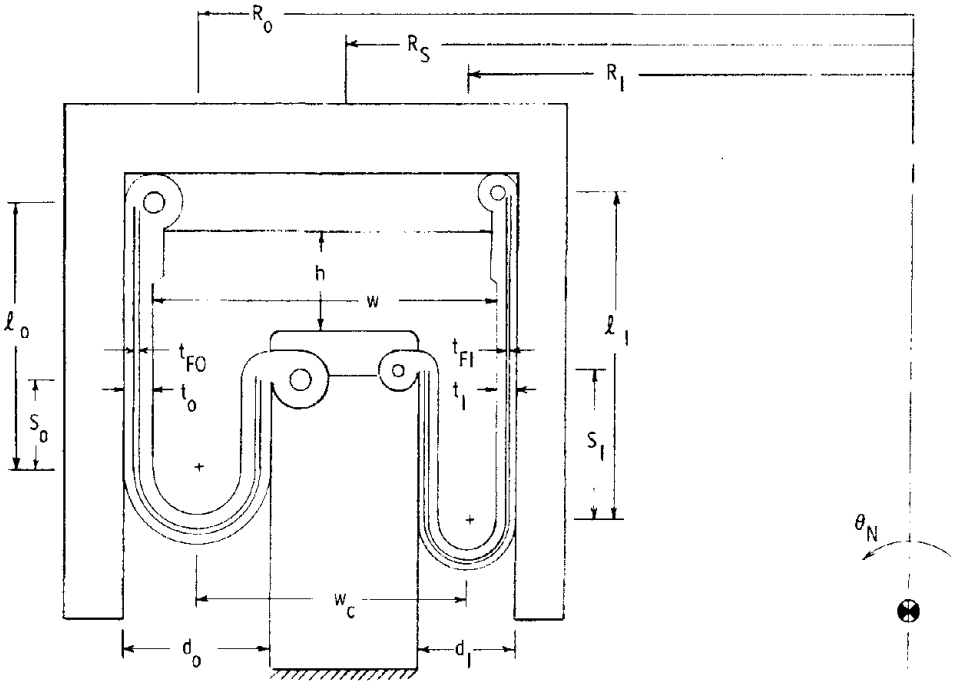

Figure 118. TECHROLL Seal Dimensions

TABLE XI

TECHROLL GEOMETRY DIMENSIONS

Geometry Dimension	Relationship
Seal mean radius (R_S), in.	$\frac{1}{2}(R_O+R_I)$
Convolute center radius, outer (R_O), in.	---
Convolute center radius, inner (R_I), in.	---
Long sidewall length, outer (ℓ_O), in.	---
Long sidewall length, inner (ℓ_I), in.	---
Short sidewall length, outer (S_O), in.	---
Short sidwall length, inner (S_I), in.	---
Convolute diameter, outer (d_O), in.	---
Convolute diameter, inner (d_I), in.	---
Convolute thickness, outer (t_O), in.	---
Convolute thickness, inner (t_I), in.	---
Fabric thickness, outer (t_{FO}), in.	---
Fabric thickness, inner (t_{FI}), in.	---
Main cavity height (h), in.	---
Main cavity width (w), in.	$R_O + \frac{1}{2}d_O - t_O - R_I + \frac{1}{2}d_I - t_I$
Convolute centers width (w_C), in.	$R_O - R_I$
Total sidewall length, outer (L_O), in.	$\ell_O + S_O + (\pi/2)d_O$
Total sidewall length, inner (L_I), in.	$\ell_I + S_I + (\pi/2)d_I$
Seal ring area (A_S), in.^{2}	$\pi(R_O^2 - R_I^2)$
Seal fluid volume (V_S), in.^{3}	$\sim 2\pi(whR_S + s_O d_O R_O + S_I d_I R_I)$
Elastomer volume (V_E), in.^{3}	---
Gas volume (V_G), in.^{3}	---
Nozzle blowoff area, effective (A_N), in.^{2}	---

TABLE XII

TECHROLL MATERIAL PROPERTIES

Material Property	Typical Value
Fluid bulk modulus (β_F), psi	150,000
Fluid viscosity (μ), lb-sec/in.^{2}	49.5×10^{-6}
Fluid density (ρ), lb-sec^2/in.^{4}	91.0×10^{-6}
Fabric elastic modulus (E_F), psi	87,600
Fabric shear modulus (G_F), psi	35,100
Elastomer bulk modulus (β_E), psi	---
Structure bulk moduls (β_S), psi	---
Combined bulk modulus (β_C), psi	60,000

Rotational damping (theoretical)

For $w \geq h$

$$B_{SR} = 12\pi\mu\epsilon\left(\frac{w_c^2}{wh^3}\right) R_S^5 \underbrace{\left[\left(\frac{1}{1-\left(\frac{R_S\theta_N}{h}\right)^2}\right)^{3/2} + \frac{2h}{w}\frac{1}{\left(\frac{R_S\theta_N}{h}\right)^2}\left[\left(\frac{1}{1-\left(\frac{R_S\theta_N}{h}\right)^2}\right)^{1/2} - 1\right]\right]}_{\sim (1+\frac{h}{w}) \text{ for small } \theta_N}$$

$$\epsilon \simeq 1-0.4\left(\frac{h}{w}\right) + 0.645\left(\frac{h}{w}\right)^2 - 0.06\left(\frac{h}{w}\right)^3 \quad \text{(figure 119)}$$

For $h \geq w$

$$B_{SR} = 12\pi\mu\epsilon\left(\frac{w_c^2}{w^3h}\right) R_S^5 \underbrace{\left[2\left[\frac{1-\left(1-\left(\frac{R_S\theta_N}{h}\right)^2\right)^{1/2}}{\left(\frac{R_S\theta_N}{h}\right)^2}\right] + \frac{2w}{h}\frac{1}{\left(\frac{R_S\theta_N}{h}\right)^2}\left[\left(\frac{1}{1-\left(\frac{R_S\theta_N}{h}\right)^2}\right)^{1/2} - 1\right]\right]}_{\sim (1+\frac{w}{h}) \text{ for small } \theta_N}$$

$$\epsilon \simeq 1-0.4\left(\frac{w}{h}\right) + 0.645\left(\frac{w}{h}\right)^2 - 0.06\left(\frac{w}{h}\right)^3 \quad \text{(figure 119)}$$

Rotational spring rate (empirical)

$$K_{SR} = C_S\,(d_O R_O^3 + d_I R_I^3) P_I$$

Spring coefficient, $C_S = 10^{-3}$/deg-in.

Rotational hysteresis (empirical)

$$T_{HR} = C_H \left(\frac{Roto}{d_o} + \frac{R_I t_I}{d_I} \right)^3 (850 + 0.55\ P_I)$$

Hysteresis coefficient, $C_H = f(t_F)$ (see figure 120)

Rotational offset (empirical)

$$T_{OR} = C_o \left(\frac{t_{Fo}}{do} R_o + \frac{t_{FI}}{dI} R_I \right) \left(3000 + P_I \right)$$

Offset coefficient, $C_O = 0.06$ in.^{2}

Axial stiffness (theoretical)

$$K_{SA} = \frac{A_S}{\frac{\pi}{2}\left[\left(\frac{L_o}{t_{FO}} \right) d_o{}^2 \left(1 + \frac{2t_o}{d_o} \right) \left(1 - \frac{A_S}{A_N} \right) R_o + \left(\frac{L_I}{t_{FI}} \right) d_I{}^2 \left(1 + \frac{2t_I}{d_I} \right) R_I \right]}{E_F} + \frac{V_S}{\beta_C}$$

$$\frac{1}{\beta_C} = \frac{1}{\beta_F} + \frac{1}{\beta_S} + \left(\frac{V_E}{V_S} \right) \frac{1}{\beta_E} + \left(\frac{V_G}{V_S} \right) \frac{1}{(1.4) P_I}$$

Lateral stiffness (theoretical)

$$K_{SL} = \left(\frac{\pi}{2} + \frac{\pi^2}{4} \right) \left[\left(1 - \frac{A_S}{A_N} \right) R_o + R_I \right] P_I$$

$$- \frac{\pi}{4} \left(\frac{1}{E_F} \right) \left[\left(\frac{L_o}{t_{Fo}} \right) \left(1 - \frac{A_S}{A_N} \right)^2 R_o + \left(\frac{L_I}{tFI} \right) R_I \right] P_I{}^2$$

$$+ \pi\, G_F \left[\left(\frac{t_{Fo}}{L_o} \right) R_o + \left(\frac{t_{FI}}{L_I} \right) R_I \right]$$

Torsional stiffness (theoretical)

$$K_{ST} = 2\pi\, G_F \left[\left(\frac{tFO}{L_o} \right) R_o{}^3 + \left(\frac{tFI}{L_I} \right) R_I{}^3 \right]$$

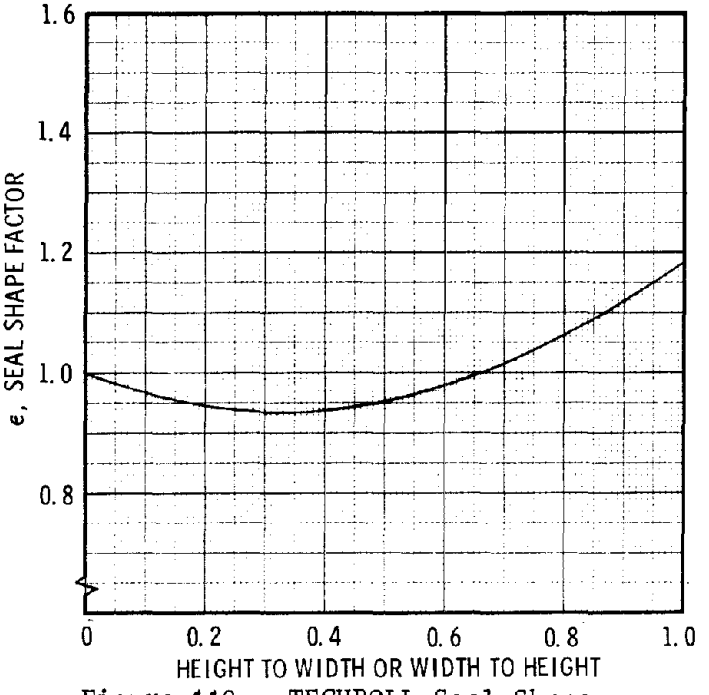

Figure 119. TECHROLL Seal Shape Coefficient vs Seal Geometry

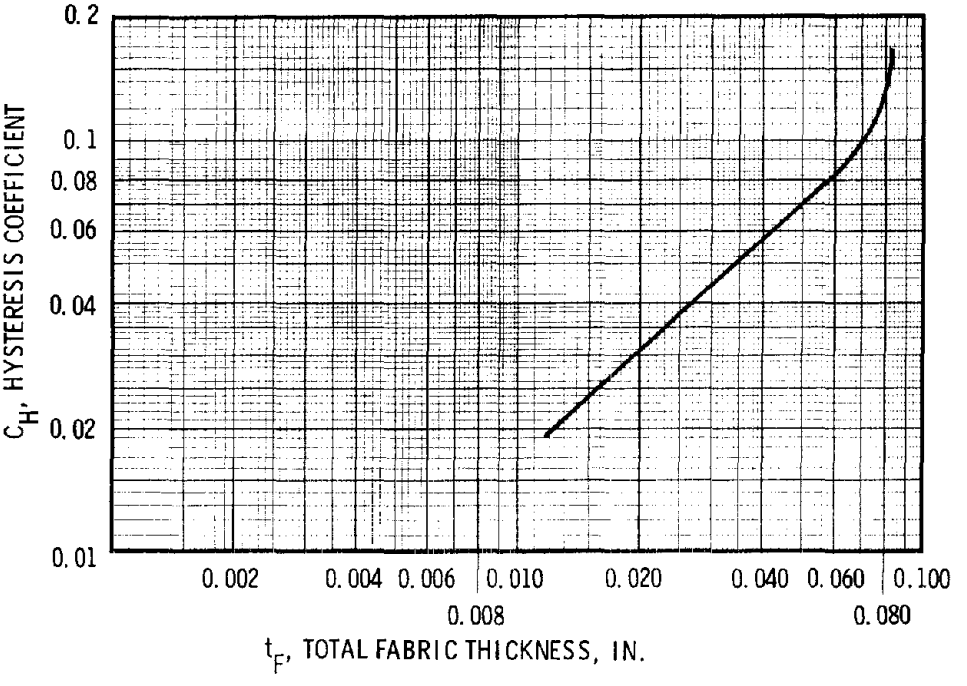

Figure 120. Hysteresis Coefficient vs Fabric Thickness

(3) Comparisons

Using the equations previously discussed, analytical predictions were made for eight different seal parameters for each of seven different TECHROLL configurations. These predictions are compared with available static firing and bench test data in table XIII at seal pressures observed during the firings. It is obvious that some parameter predictions correlate well with test data, while others do not.

c. Limitations and Conclusions

A limited data bank (especially for rotational inertia and damping, and for lateral and torsional stiffnesses) and a limited theoretical understanding of rotational hysteresis and spring rate have resulted in a restricted but useful set of TECHROLL parameter prediction equations. These equations should be adequate for preliminary design studies or computer simulations using the generalized model. When hardware is built, bench test and static firing test data would naturally be substituted for the predicted parameters.

The following restrictions apply to the prediction equations:

A. Motor sizes can vary from small tactical to medium ICBM; however, extrapolation to large boosters must be verified

B. Seal configurations can include any straight-sided cylindrical sidewall) designs (see figure 118); however, application to spherical (spherical sidewall) or canted (conical sidewall) designs could degrade their accuracy.

TABLE XIII

TECHROLL SEAL PARAMETERS*

Parameter	Minuteman	HIPPO All-Boost	HIPPO Boost/Sustain	HIPPO High Pressure†	HIPPO Miniseal†	8-In.-Diameter Demonstrator	Poseidon C-3
Rotational inertia (I_S), in.-lb-sec^2	--- 9.8	--- 0.41	--- 0.41	--- 0.41	--- 0.68	--- 0.022	--- 65.2
Rotational damping (B_S), in.-lb-sec	--- 136	--- 2.39	390‡ 410‡	--- 2.39	--- 6.64	--- 0.361	1,003 649
Rotational spring rate (K_S), in.-lb/^{o}	0 558	62.5 242	62.5 88	488 400	138 175	11 8	1,800 1,676
Rotational hysteresis (T_{HT}), in.-lb	1,250 1,041	1,450 1,193	1,000 683	3,500 3,932	2,300 1,906	275 302	1,245 2,676
Rotational offset (T_O), in.-lb	160 ±211	750 ±314	450 ±219	-500 ±633	-650 ±868	±29 ±261	580 ±328
Axial stiffness (K_{SA}), psi/in.	5,250 5,260	15,600 10,350	13,700 10,350	14,500 13,450	50,600 43,000	50,000 34,800	9,210 10,700
Lateral stiffness (K_{SL}), lb/in.	--- 56,600	26,000 45,900	--- 29,300	--- 68,400	--- 29,800	--- 21,200	--- 73,700
Torsional stiffness (K_{ST}), in.-lb/^{o}	--- 30,500	5,200 7,220	--- 7,220	--- 10,820	--- 4,520	--- 862	--- 74,100
Seal pressure (P_I), psi	1,050 ---	2,900 ---	2,320/1,050 ---	4,800 ---	4,200 ---	2,550 ---	1,450 ---
Comments	---	---	---	No static firing	---	---	---

* Actual test values appear above the line; predicted test values appear below the line. Values apply at zero deflection angle unless otherwise noted.
† High pressure seal
‡ High viscosity (60,000 ctks) silicone fluid

SECTION IV

EXPLORATORY MATERIALS DEVELOPMENT

INTRODUCTION

The materials information produced during the UTC in-house development program was used as a foundation for the materials development task performed during phase I. The materials development activity was oriented primarily toward support of the demonstration testing of a tactical air-launched type TECHROLL® seal system that was demonstrated in both phase I and phase II of this program. The Minuteman TECHROLL seal used basic materials technology which were a result of the UTC prototype program.

1. OBJECTIVES

The primary objectives of the materials development task were:

A. To develop techniques necessary to quantitatively evaluate the acceptability of various seal composite materials.

B. To derive a seal material capable of satisfying the following requirements at 75°F:

(1) Linear tensile strength of 1,500 lb/in. (minimum)

(2) Burst strength of 4,100 psi (minimum)

(3) 1,000-cycle roll flexibility compatible with 0.5-in. seal convolute

(4) Maximum thickness of 0.14 in.

(5) Axial elongation of 15% to 25%

(6) 1,000-hr minimum compatibility with associate seal composite materials

Secondary objectives of the materials development task include:

A. Derivation of a composite seal material capable of satisfying the following requirements of a TECHROLL seal for a 3,000-psi chamber pressure tactical motor over a temperature range of -65° to +165°F:

(1) Linear tensile strength of 2,500 lb/in. (minimum)

(2) Burst strength of 5,500 psi (minimum)

(3) 1,000-cycle roll flexibility compatible with 0.5-in. seal convolute

(4) Maximum thickness of 0.14 in.

(5) Axial elongation of 15% to 25%

(6) 1,000-hr minimum compatibility with associate seal composite materials

B. Development of basic materials input data that can be used in an analytical model for system design and performance predictions.

An additional design goal was to develop a single seal composite material for use on all program air-launch motor tests (chamber pressures of 2,000 and 3,000 psi).

2. ACCOMPLISHMENT SUMMARY

Primary material development objectives were satisfied, and a two-layer nylon-neoprene coated composite material capable of satisfying 2,000-psi motor requirements was developed and demonstrated.

Simplified material evaluation techniques were developed to permit ranking of candidates and a first order approximation of composite material capability in a TECHROLL seal configuration. Correlation between specimen test results and seal performance was achieved to the extent that a relative comparison of specimen to seal performance was predictable.

Secondary objectives were satisfied partially. A three-layer nylon-neoprene coated composite material meeting ambient temperature operating requirements for a 3,000-psi motor chamber pressure was developed and tested. However, this material was not tested at the required -65°F seal operation temperature because of the -40°F glass transition temperature of the neoprene elastomer.

The goal of a single combination of materials capable of satisfying TECHROLL seal requirements for both 2,000- and 3,000-psi chamber pressure nozzles was met partially. The materials and methods of construction used in both seals are essentially the same, and the composite is identical except for the number of fabric plies used.

a. Selection Criteria

To select a composite capable of meeting TECHROLL seal requirements, candidate materials in (1) reinforcement fabrics, (2) elastomer coatings, seal internal fluids, and (3) thermal protective greases were reviewed and evaluated. The spatial interrelationship among these components is shown schematically in the typical seal cross section presented in figure 121.

Candidate materials in each of the four categories were selected on the basis of requirements determined from analyzing seal construction and preliminary designs of tactical TECHROLL seal movable nozzles to be tested in both phase I and II. Maximum use was made of material information generated during the UTC in-house prototype development program.

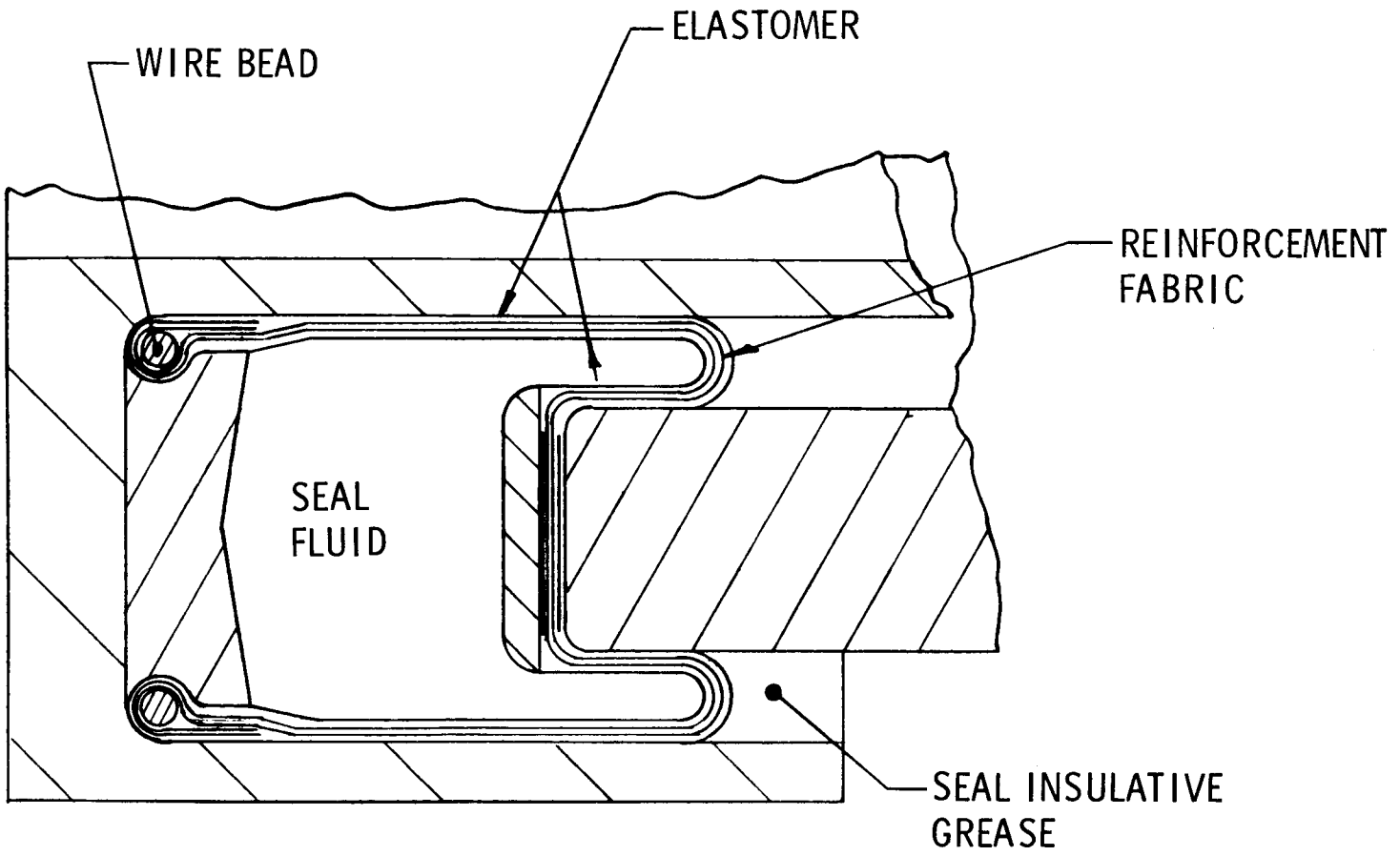

Figure 121. Material Relationship for TECHROLL Seal

Past experience and properties data gathered during a literature survey were used in compiling initial lists of candidates. Availability, cost, and producibility factors were applied in reducing the initial list to the prime candidates for each category shown in table XIV.

Final selection of elastomers was accomplished by evaluating each candidate in a simple composite with the standard nylon (J. P. Stevens style 34102) fabric. Specimens were subjected to the following tests:

Test	Success Criteria
Tensile strength (width), lb/in.	750 (minimum)
Elongation, %	25 (maximum)
Burst strength in 0.5-in. convolute, psi	2,000 (minimum) after 1,000 cycles
Grease and fluid compatibility	retention of 75% original burst strength and 10% maximum weight and volume change.

The same type of specimen (see figure 122) was used to evaluate fabrics as that used for elastomers, with each candidate fabric molded into a standard neoprene elastomer (Burke Rubber Co. 5026). Fabrics were subjected to the following quantitative tests:

Test	Success Criteria
Tensile strength (width), lb/in.	1,500 (minimum)
Elongation, %	25 (maximum)
Burst strength in 0.5-in. convolute, psi	4,100 (minimum after 1,000 cycles), 5,500 psi as design goal

Seal fluids and greases were selected on the basis of compatibility with the elastomers.

b. Candidate Materials

Based on considerations discussed in subsection a, the materials listed in table XIV were tested. Material suppliers' data and certification sheets were used as supportive factors in the material selection. A butyl elastomer compound was included in early testing, but was eliminated after burst tests produced a result of less than 1,000-psi burst strength. The first silicone rubber material procured, Burke 2107, could not be calendered uniformly. Because silicone rubber was a prime candidate for low-temperature applications, an acceptable, uniform-calendered sheet was obtained from General Electric Co. for use in the test program.

TABLE XIV

CANDIDATE MATERIALS

Material	Type	Manufacturer	Product Designation
Elastomer	Neoprene	Burke Rubber Co.	5026
	Silicone	General Electric Co.	No. 1
	Silicone	Burke Rubber Co.	2107
	EPDM	Uniroyal, Inc.	5616
	Fluorosilicone	Burke Rubber Co.	SX 8201
Nylon	2 x 2 basket weave 0.027-in. thickness 42.5 (warp) x 41.0 (fill)	J. P. Stevens & Co., Inc.	34103
	2 x 2 basket weave 0.061-in. thickness 64 (warp) x 32 (fill)	Prodesco, Inc.	F-5017-001
	2 x 2 basket weave 0.084-in. thickness 216 (warp) x 58 (fill)	Prodesco, Inc.	F-5017-002
	2 x 2 basket weave 0.084 thickness 64 (warp) x 28 (fill)	Prodesco, Inc.	F-5017-003
Fluid	Silicone	General Electric Co.	SF 96, 350 ctks
	Fluorosilicone	Dow Corning Corp.	FS 1265
	Modified silicone	General electric Co.	SF-1147
Grease	Silicone	Dow Corning Corp.	DC-55M
	Silicone	Dow Corning Corp.	DC-40M
	Fluorosilicone	Dow Corning Corp.	FS 1281

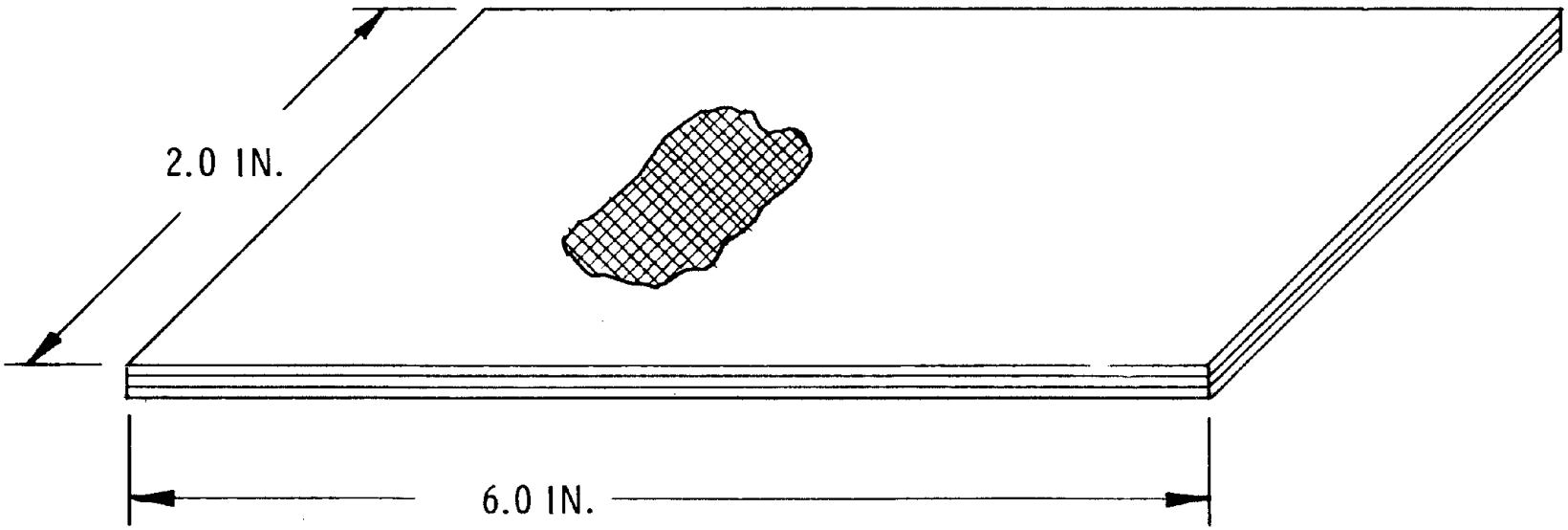

Figure 122. Elastomer/Reinforcement Fabric Specimen

During the selection of fabric reinforcements to be tested, it became evident that weave construction of a fabric had a much greater effect on its load-carrying capability than the chemistry of its fiber. Therefore, the reinforcement fabric test was directed toward a comparison of different weaves and fabric thickness using nylon as the candidate material. No comparison between different generic materials was made.

c. Material Testing

Material tests and results are discussed in detail in the following paragraphs.

(1) Elastomer Testing

Tensile properties of a nylon/elastomer composite obtained during a test series is shown in table XV. The objective of these tests was to measure the effect of temperature on the candidate elastomers. It was predicted that the fabric reinforcement would carry the major tensile load with the elastomer contributing relatively little. However, the results appeared to indicate that the elastomer had a significant effect on the load-carrying capability of the composite. The room temperature properties correlated with predicted values of tensile strength for the elastomer generic types.

Two additional test series were then conducted. Table XVI which shows results of the first tests, lists test data from two sources, the original manufacturer, and UTC laboratories. The manufacturer had tested and reported values for untreated fabric without elastomer. UTC repeated these tests for the standard J. P. Stevens 34103 nylon and for the Prodesco fabrics. In addition, a series of composite specimens in which the standard neoprene elastomer was combined with the J. P. Stevens fabric and processed was carefully constructed through: (1) a normal cure cycle of 1 hr at 310°F and (2) an abnormal cure cycle of 16 hr at 310°F. After cure, the elastomer was removed from the specimens. The specimens were then tested in identical fashion to the uncoated fabrics.

Two conclusions were drawn from the test results shown in table XVI. First, the UTC tensile tests consistently produced results which were significantly lower than those of two outside test sources. Second, cure cycle temperatures, even when applied for excessive periods of time, do not significantly reduce the tensile strength of the reinforcing fabric.

Table XVII shows the results of a series of burst strength and cycling tests of composite samples of each elastomer with J. P. Stevens 34103 nylon. These tests were performed in a 0.5-in. convolute test fixture (figure 123) and a flex-cycling fixture (figure 124) which were developed by UTC to simulate the pressure application mode of a seal assembly for materials screening purposes. Table XVII shows the burst strengths achieved by the candidate

TABLE XV

EFFECT OF TEMPERATURE ON TENSILE STRENGTH AND ELONGATION

	Burke Neoprene	Burke Silicone	General Electric Silicone	Uniroyal EPDM	Burke Fluorosilicone
	Room Temperature				
Tensile strength, lb/in.	597	462	334	528	403
Elongation, %	29.7	21.8	14.4	21.3	15.2
	$-65^{\circ}F$				
Tensile strength, lb/in.	766	473	486	905	637
Elongation, %	40.5	29.5	24.5	23.3	20.5
	$+165^{\circ}F$				
Tensile strength, lb/in.	244	323	292	275	398
Elongation, %	27.7	22.6	21.3	20.8	23.0

NOTE: Test specimens were 2 by 6 by 0.100 in., sandwich construction with single ply of J. P. Stevens 34103 nylon, covered on both sides with candidate elastomer. Each value represents an average of five test specimens.

elastomers at room temperature, $-65^{\circ}F$, and $165^{\circ}F$. Generally, these values agreed with the predicted values for seals containing a single ply of reinforcement. From these data, it can be concluded that the burst strength test was more relevant and more consistent than the tensile strength evaluations. Tensile testing of a composite does not appear to represent the apparent material strength. Its usefulness is as a factor in relating the relative strengths of various composites.

Having established relevancy of the composite burst strength tests, the next series of tests were conducted to evaluate the compatibility of the candidate elastomers with the appropriate internal seal fluids and external thermal protection greases. The test criteria were based upon physical changes and degradation of burst strengths with increasing time exposure to these media. The test results are summarized in tables XVIII through XXII. The same test series was used to accomplish the desired accelerated aging tests required by the program, since specimens were exposed continuously to candidate fluids and greases at $165^{\circ}F$ for 10, 100, and 1,000 hr.

TABLE XVI

COMPARISON OF MANUFACTURER AND UTC TEST DATA
ON TENSILE STRENGTH AND ELONGATION OF FABRIC

	Vendor Data				UTC Data			
	Tensile Strength, lb/in.		Elongation, %		Average Tensile Strength, lb/in.		Elongation, %	
	Warp	Fill	Warp	Fill	Warp	Fill	Warp	Fill
J. P. Stevens 34103 Nylon								
No Cure	950	950	22	22	634	675	19.4	20.6
Rubber (standard cure)*	---	---	---	---	---	654	---	34.5
Rubber (16-hr cure)*	---	---	---	---	670	---	36.5	---
Prodesco								
Item No. 1	1,779	---	78.0	---	1,243	---	24.0	---
(Prodesco 2)	---	1,462	---	36.0	---	1,094	---	---
Item No. 2 (Prodesco 5)	2,635	---	47.0	---	1,711	---	31.9	---
Item No. 3	2,500+	---	---	---	1,108	---	39.8	---
	---	300	---	---	---	247	---	550.0+

* Specimens were 2 by 6 in. by single ply of fabric. Specimens were fabricated using neoprene rubber on both sides, cured under pressure in normal manner, then the rubber was removed for test. Each value represents an average of five test specimens.

TABLE XVII

EFFECT OF TEMPERATURE ON BURST STRENGTH

	Burst Strength, psi				
	Burke Neoprene	Burke Silicone	General Electric Silicone	Uniroyal EPDM	Burke Fluorosilicone
		Room Temperature			
No cycles	2,500	2,200	2,000	2,600	2,400
1,000 cycles	2,400	2,200	1,800	2,800	2,200
		-65°F			
No cycles	4,600	4,000	4,800	3,600	2,900
1,000 cycles	(-30°F)*	2,200	3,200	(-36°F)*	3,000
		+165°F			
No cycles	1,000	1,000	1,500	1,200	1,000
1,000 cycles	1,000	1,800	1,400	1,200	1,000

* Would not cycle below this temperature

Note: Specimens were 2 by 6 by 0.100 in. sandwich construction with single ply of J. P. Stevens 34103 nylon covered on both sides with candidate elastomer. Each value represents an average of three specimens.

After completion of elastomer testing, the various candidates were ranked as shown in table XXIII.

On the basis of this ranking, any of the elastomers tested would satisfy most of the TECHROLL seal system requirements. Because of its low cost, availability, processability, and previous experience, neoprene was selected as the prime material for use in seal construction.

(2) Reinforcement Fabric Testing

It was apparent that the HIPPO seal required a reinforcement of greater strength than the standard fabric (J. P. Stevens 34103 nylon) used in the UTC development program. Therefore, it was decided to try the simplified approach of achieving the increased strength by use of multiple layers of the 34103 nylon. This approach proved successful, both in terms of laboratory specimen testing and in fabrication of actual seals.

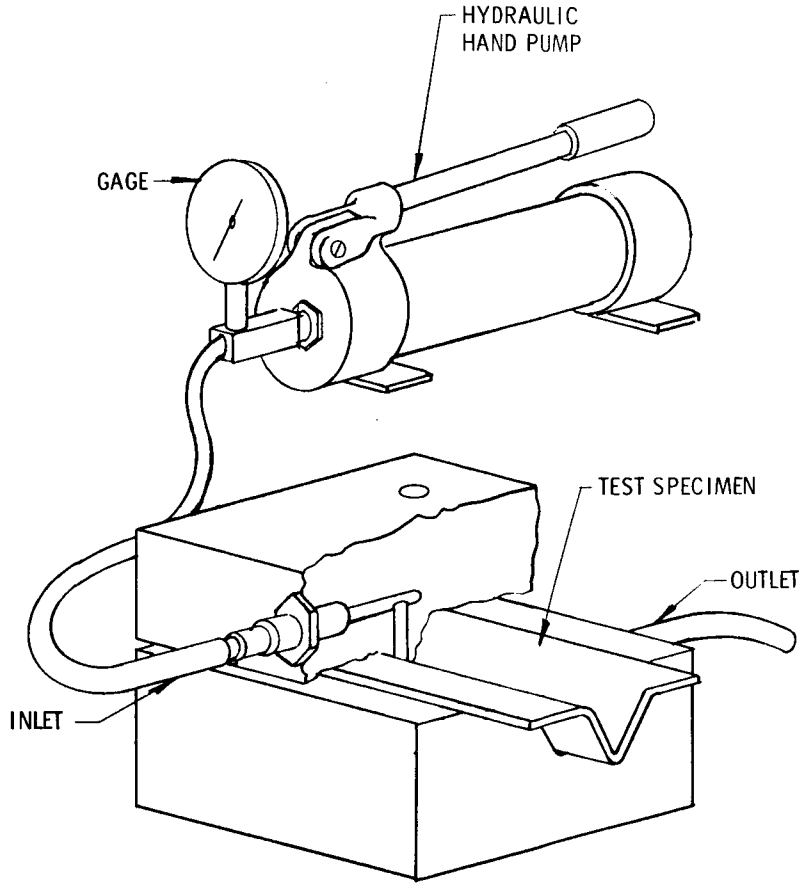

Figure 123. Burst Test Fixture for 0.5-In. Convolute

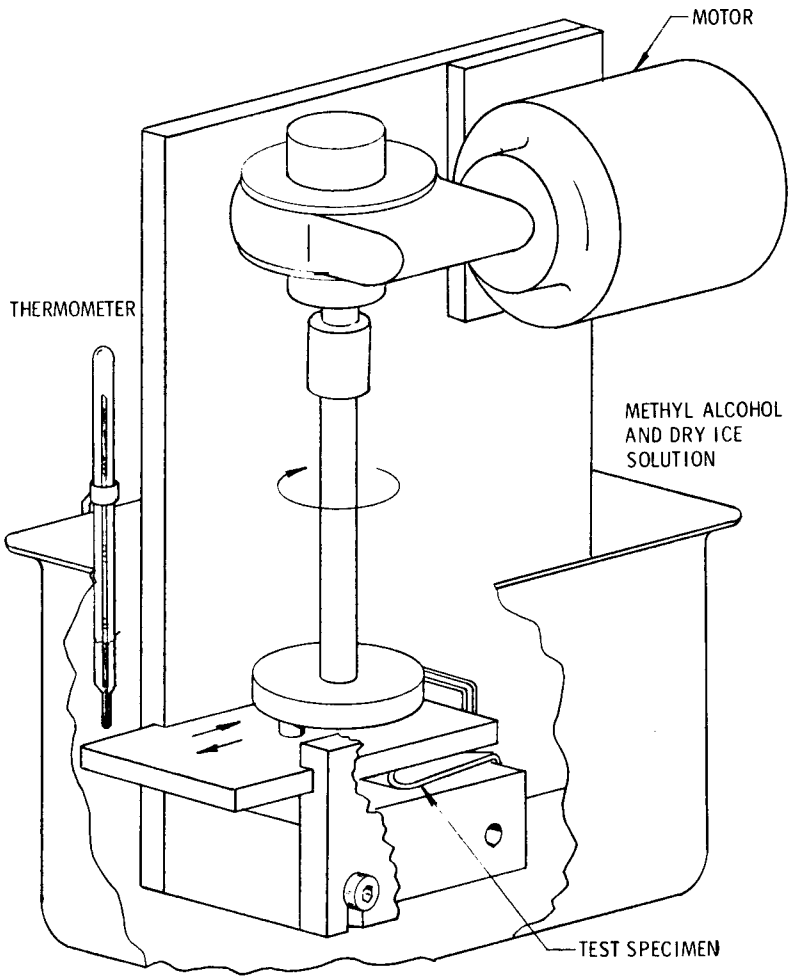

Figure 124. Flex Cycle Test Fixture

TABLE XVIII

ELASTOMERS: ACCELERATED AGING AND COMPATIBILITY WITH CANDIDATE FLUIDS — PHYSICAL CHANGE

Test Time, hr	General Electric SF 96 Silicone Fluid			General Electric SF-1147 Modified Silicone Fluid		Dow Corning FS 1265 Fluorosilicone Fluid		
	Burke 5026 Neoprene	Uniroyal 5616 EPDM	Fluoro-silicone	Burke 5026 Neoprene	General Electric No. 1 Silicone	Burke 5026 Neoprene	Burke 2107 Silicone	General Electric No. 1 Silicone
	Volume Change, %							
10	-3.53	-2.93	-0.68	-3.62	+7.02	-2.11	-0.06	-0.53
100	-7.19	-7.39	-0.95	-7.44	+11.02	-3.26	-0.08	-0.04
1,000	-8.92	-10.48	-1.23	-8.63	+12.51	-5.30	+0.07	+0.10
Aged 1,000 hr (no exposure)	-1.11	+0.06	+0.47	-1.11	+0.56	-1.11	+0.93	+0.56
	Weight Change, %							
10	-2.59	-2.93	-0.49	-2.84	+5.77	-1.66	+0.26	+0.31
100	-5.42	-5.12	-0.84	-5.77	+10.39	-2.27	+0.85	+0.29
1,000	-6.40	-8.27	-1.25	-6.46	+10.56	-3.88	+0.24	+0.14
Aged 1,000 (no exposure)	-0.70	+0.09	+0.13	-0.70	+0.47	-0.70	+0.67	+0.47
	Hardness Before and After Test							
10	54 to 55	68 to 69	55 to 52	55 to 54	73 to 67	55 to 53	54 to 55	72 to 70
100	55 to 57	67 to 72	55 to 56	55 to 57	72 to 65	55 to 54	54 to 54	73 to 73
1,000	55 to 65	67 to 79	54 to 56	55 to 65	73 to 66	55 to 64	53 to 56	72 to 72
Aged 1,000 hr (no exposure)	55 to 56	68 to 70	55 to 55	55 to 56	73 to 74	55 to 56	54 to 56	73 to 74

NOTE: Test specimens were 2 by 6 by 0.100 in., sandwich construction with single ply of J. P. Stevens 34103 nylon, covered on both sides with candidate elastomer. Each value represents one test specimen.

TABLE XIX

ELASTOMERS: ACCELERATED AGING AND COMPATIBILITY WITH CANDIDATE FLUIDS — BURST STRENGTH

Test Time, hr	General Electric SF-96 Silicone Fluid			General Electric SF-1147 Modified Silicone Fluid		Dow Corning FS-1265 Fluorosilicon Fluid		
	Burke 5026 Neoprene	Uniroyal 5616 EPDM	Burke SX8201 Fluoro-Silicone	Burke 5026 Neoprene	General Electric No. 1 Silicone	Burke 5026 Neoprene	Burke 2107 Silicone	General Electric No. 1 Silicone
	Burst Strength (No Cycles), psi							
No exposure	2,500	2,600	2,400	2,500	2,000	2,500	2,200	2,000
10	---	---	---	---	---	---	---	---
100	2,350	2,600	2,300	2,500	1,400	1,800	1,600	1,600
1,000	2,300	2,400	2,000	2,200	1,300	2,200	1,500	1,600
Aged 1,000 hr (no exposure)	2,400	2,800	2,200	2,400	1,700	2,400	1,600	1,700
	Burst Strength (1,000 Cycles), psi							
No exposure	2,400	2,800	2,200	2,400	1,800	2,400	2,200	1,800
10	---	---	---	---	---	---	---	---
100	2,600	2,100	2,300	2,500	1,200	2,300	2,000	1,800
1,000	1,900	2,500	2,200	2,200	1,300	2,200	1,500	1,600
Aged 1,000 hr (no exposure)	2,600	2,600	1,700	2,600	1,200	2,600	1,400	1,200

NOTE: Test specimens were 2 by 6 by 0.100 in., sandwich construction with single ply of J. P. Stevens 34103 nylon, covered on both sides with candidate elastomer. Each value represents one test specimen.

TABLE XX

ELASTOMERS: ACCELERATED AGING AND COMPATIBILITY WITH CANDIDATE GREASES — PHYSICAL CHANGE

Test Time, hr	Dow Corning DC-55M Silicone Grease			Dow Corning DC-40 Silicone Grease				Dow Corning FS 1281 Fluorosilicone Grease		
	Burke 5026 Neoprene	Uniroyal 5616 EPDM	Burke SX8201 Fluoro-silicone	Burke 5026 Neoprene	General Electric No. 1 Silicone	Uniroyal 5616 EPDM	Burke SX8201 Fluoro-silicone	Burke 5026 Neoprene	Burke 2107 Silicone	General Electric No. 1 Silicone
					Volume Change, %					
10	+4.05	+3.45	+2.01	-1.59	+12.09	-1.71	-0.59	-1.17	-0.10	+0.21
100	+8.70	+4.91	+1.09	-5.39	+28.26	-4.00	-0.90	-2.83	+0.30	+0.27
1,000	+15.81	+0.58	-1.09	-8.76	+36.99	-11.30	-2.01	-4.76	+0.81	+0.81
Aged 100 hr (no exposure)	-1.11	+0.06	+0.47	-1.11	+0.56	+0.06	+0.47	-1.11	+0.93	+0.56
					Weight Change, %					
10	+2.78	+2.51	+0.23	-1.82	+11.22	-1.12	-0.12	-0.92	+0.24	+0.44
100	+6.40	+4.84	+0.18	-3.83	+25.62	-2.89	-0.70	-2.01	+0.47	+0.64
1,000	+11.25	+0.34	-1.92	-6.40	+33.51	-8.94	-1.98	-3.56	+0.79	+0.80
Aged 1,000 hr (no exposure)	-0.70	+0.09	+0.13	-0.70	+0.47	+0.09	+0.13	-0.70	+0.67	+0.47
					Hardness Before and After Test					
10	55 to 51	66 to 66	54 to 48	55 to 54	73 to 65	68 to 70	55 to 54	56 to 54	54 to 53	73 to 70
100	55 to 47	67 to 58	55 to 49	55 to 57	73 to 55	66 to 60	55 to 54	55 to 56	53 to 54	73 to 72
1,000	56 to 51	67 to 70	55 to 59	55 to 63	73 to 57	66 to 76	54 to 57	55 to 64	54 to 57	72 to 71
Aged 1,000 hr (no exposure)	55 to 56	68 to 70	55 to 55	55 to 56	73 to 74	68 to 70	55 to 55	55 to 56	54 to 46	73 to 74

NOTE: Test specimens were 2 by 6 by 0.100 in., sandwich construction with single ply of J. P. Stevens 34103 nylon, covered on both sides with candidate elastomer. Each value represents one test specimen.

TABLE XXI

ELASTOMERS: ACCELERATED AGING AND COMPATIBILITY WITH CANDIDATE GREASES — BURST STRENGTH

Test Time, hr	Dow Corning DC 55M Silicone Grease			Dow Corning DC 40M Silicone Grease				Dow Corning FS 1281 Fluorosilicone Grease		
	Burke 5026 Neoprene	Uniroyal 5616 EPDM	Burke SX8201 Fluoro-Silicone	Burke 5026 Neoprene	General Electric No. 1 Silicone	Uniroyal 5616 EPDM	Burke SX8201 Fluoro-silicone	Burke 5026 Neoprene	Burke 2107 Silicone	General Electric No. 1 Silicone
	Burst Strength (No Cycles), psi									
No exposure	2,500	2,600	2,400	2,500	2,000	2,600	2,400	2,500	2,200	2,000
10	---	---	---	---	---	---	---	---	---	---
100	1,350	2,400	2,000	2,100	1,000	2,700	2,300	2,000	1,800	1,500
1,000	1,600	2,200	2,100	2,200	800	2,400	2,300	2,300	1,600	1,600
Aged 1,000 hr (no exposure)	2,400	2,800	2,200	2,400	1,700	2,800	2,200	2,400	1,600	1,700
	Burst Strength (1,000 Cycles), psi									
No exposure	2,400	2,800	2,200	2,400	1,800	2,800	2,200	2,400	2,200	1,800
10	---	---	---	---	---	---	---	---	---	---
100	2,300	2,400	2,400	2,400	1,000	2,600	2,000	2,500	1,900	1,800
1,000	1,600	2,300	2,000	2,300	1,000	2,400	1,900	2,300	1,600	1,400
Aged 1,000 hr (no exposure)	2,600	2,600	1,700	2,600	1,200	2,600	1,700	2,600	1,400	1,200

NOTE: Test specimens were 2 by 6 by 0.100 in., sandwich construction with single ply of J. P. Stevens 34103 nylon, covered on both sides with candidate elastomer. Each value represents one test specimen.

TABLE XXII

ELASTOMER MATERIAL RANKING

Criteria	First	Second	Third	Fourth
Percent volume	Fluorosilicone	Neoprene	EPDM	Silicone
Percent weight	Fluorosilicone	Neoprene	EPDM	Silicone
Hardness	Fluorosilicone	Neoprene	EPDM	Silicone
Burst strength at RT* without cycles	EPDM	Neoprene	Fluorosilicone	Silicone
Burst strength at RT after 1,000 cycles	EPDM	Neoprene	Fluorosilicone	Silicone
Burst strength at -65°F without cycles	Silicone	Neoprene	EPDM	Fluorosilicone
Burst strength at -65°F after 1,000 cycles	Silicone	Fluorosilicone	EPDM	Neoprene
Burst strength at 165°F after 1,000 cycles	Silicone	EPDM	Neoprene or fluorosilicone	Neoprene or fluorosilicone

*RT = room temperature

Concurrently with the testing of multiple plies of conventional fabric, the Prodesco Co. was contracted to produce specially woven fabrics of higher strengths, greater uniformity between warp and fill strengths, void-free construction, and the capability to be woven into seamless cones or cylinders in the event that joints in seal walls proved unacceptable for high-pressure applications. Figure 125 summarizes the comparison of these various reinforcement approaches in terms of convolute burst strength. All specimens were 2 by 6 in., with the thickness dependent upon the reinforcement. The curve illustrates that a linear relationship exists between fabric thickness and composite burst strength. Figures 126 through 129 illustrate the different weave characteristics of the Prodesco fabrics compared to the J. P. Stevens 34103 nylon.

At the beginning of the program, nylon had been selected as a satisfactory fabric reinforcement for the high-pressure TECHROLL seals. As a result of the materials evaluation tests, multiple layers of J. P. Stevens 34103 nylon were considered acceptable for use in fabrication of the test seals.

(3) Candidate Fluids and Greases

Comparison of seal fluids and thermal protection greases was conducted in terms of their effect on the properties of the seal elastomer. Candidates had been selected with the required physical properties to function adequately in the seal system, in terms of viscosity, compressibility, and density. The data presented in tables XIX through XXII demonstrate quantitatively the effects of long-term exposure of fluids and greases on elastomer performance under stringent conditions.

(4) Accelerated Aging

A prime factor in the function of an operational TECHROLL seal is its capability to withstand long term storage without degradation of performance. A series of accelerated aging tests was conducted to assess this capability. The most likely failure mode in long term storage is the progressive chemical degradation of the protective elastomer film caused by the fluid and/or grease. An extremely aggressive test environment was created in which composite specimens of the candidate elastomers with a single internal ply of nylon fabric were immersed in the appropriate fluids or greases and maintined at the highest required service temperature of 165^{o}F. The specimens were then evaluated for changes in weight, volume, hardness, or burst strength after 10, 100, and 1,000 hr of exposure.

These results are shown in tables XIX through XXII as part of the elastomer evaluation. The results confirm prior predictions that the candidate elastomers have good age resistance in the anticipated environments.

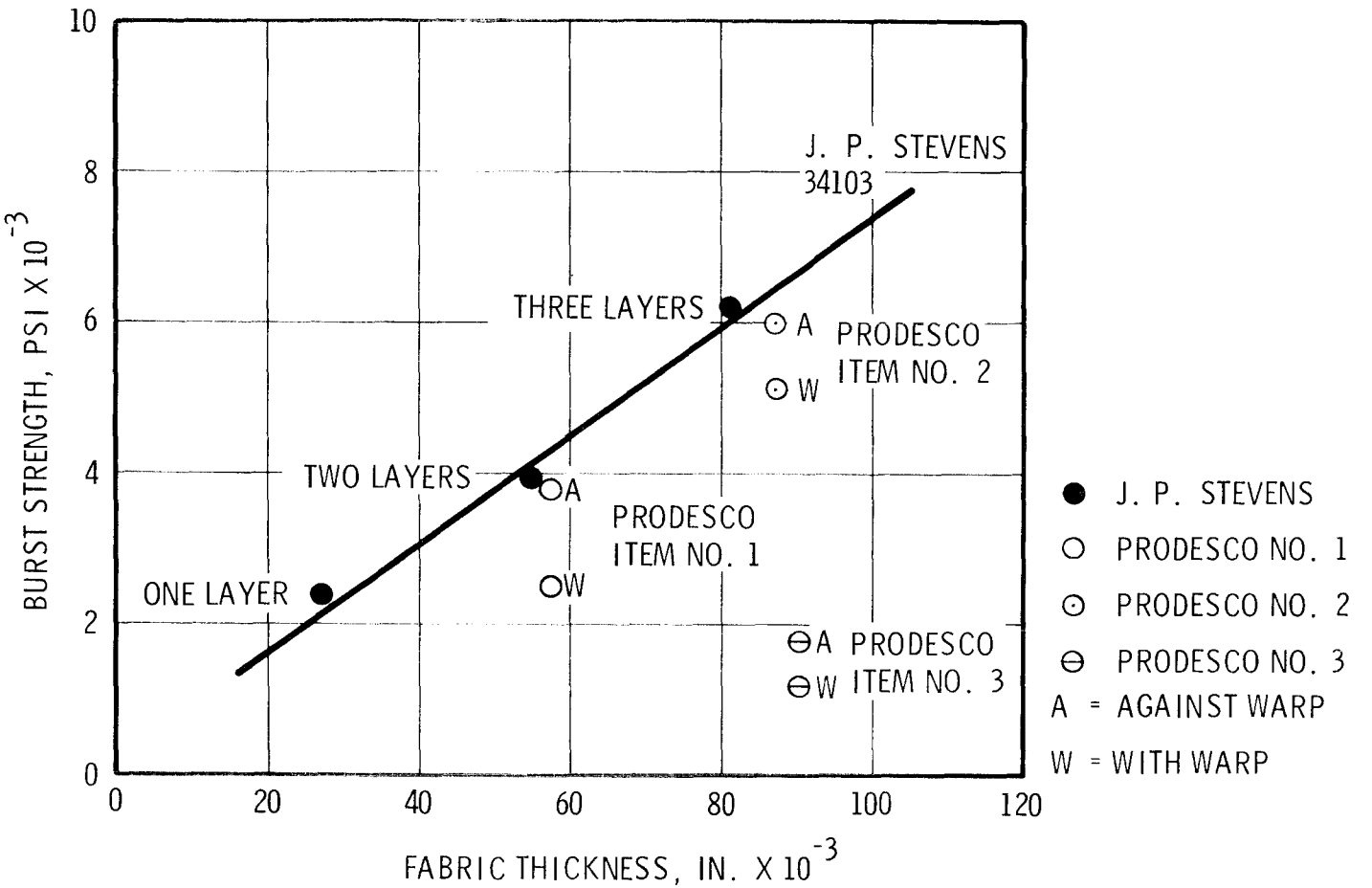

NOTE: EACH SPECIMEN IS 2 BY 6 IN., SANDWICH CONSTRUCTION, WITH NEOPRENE ELASTOMER ON BOTH SIDES OF THE REINFORCEMENT. EACH VALUE REPRESENTS AVERAGE OF FIVE SPECIMENS.

Figure 125. Burst Strength vs Thickness for Candidate Nylon Fabrics

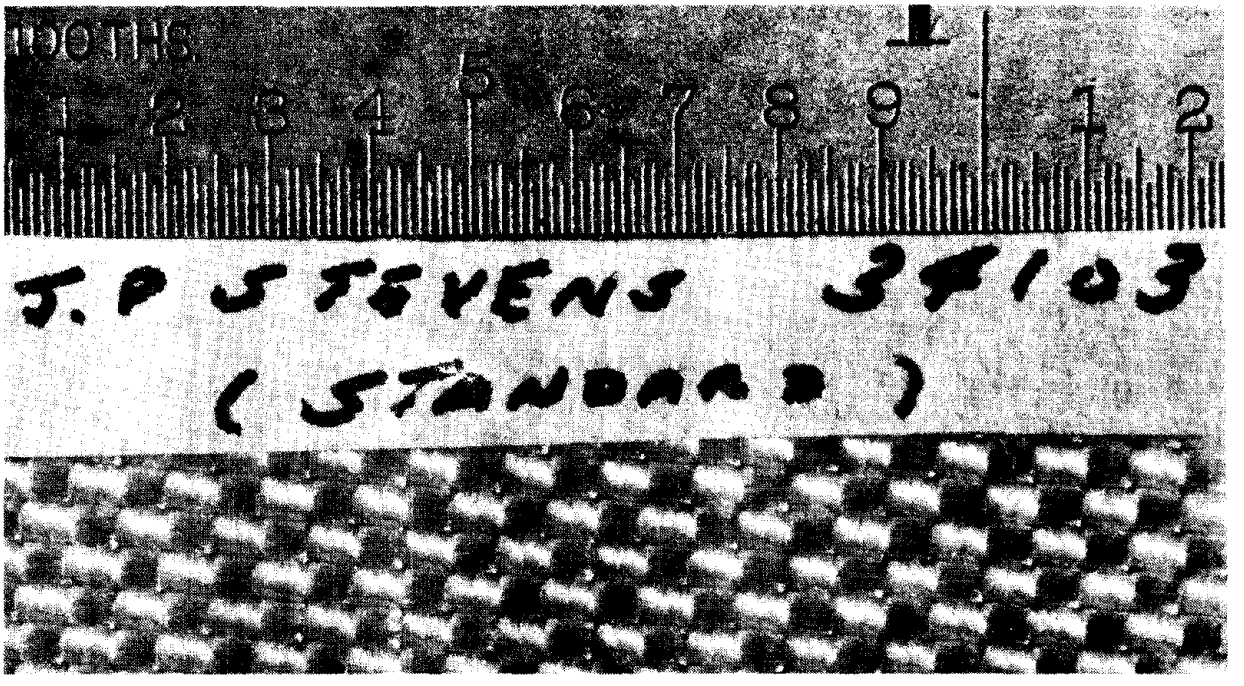

Figure 126. Sample of J. P. Stevens Fabric

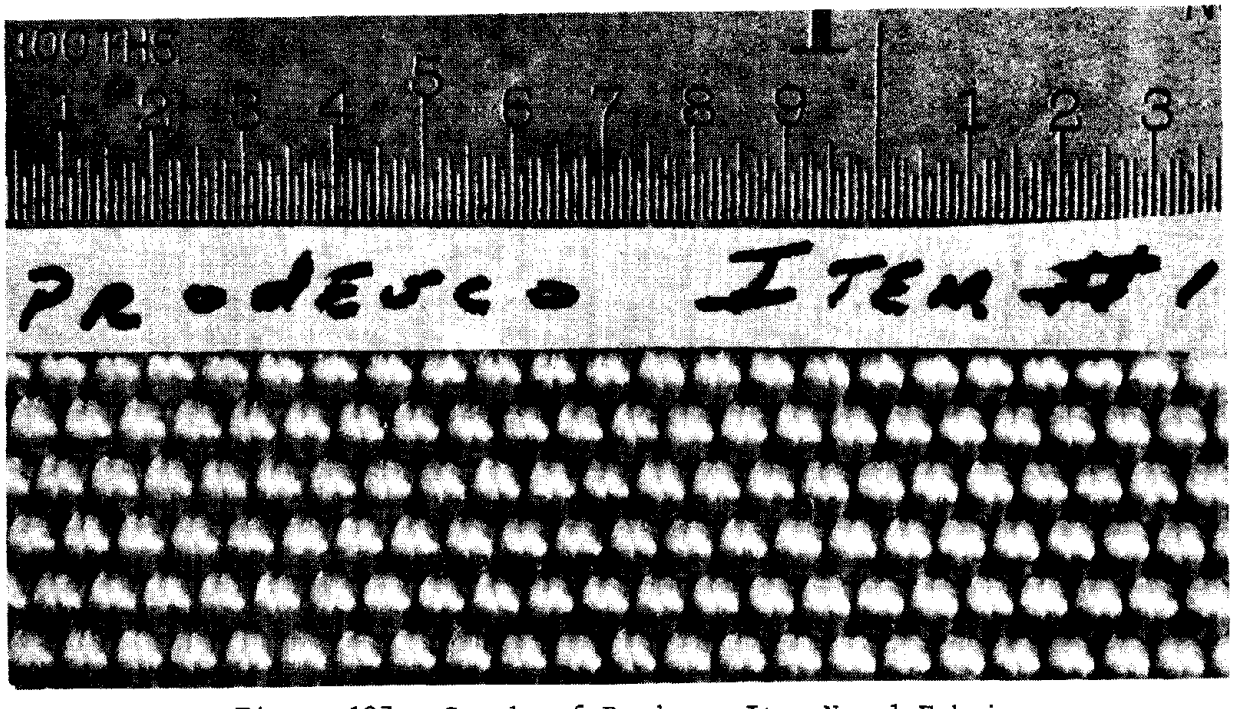

Figure 127. Sample of Prodesco Item No. 1 Fabric

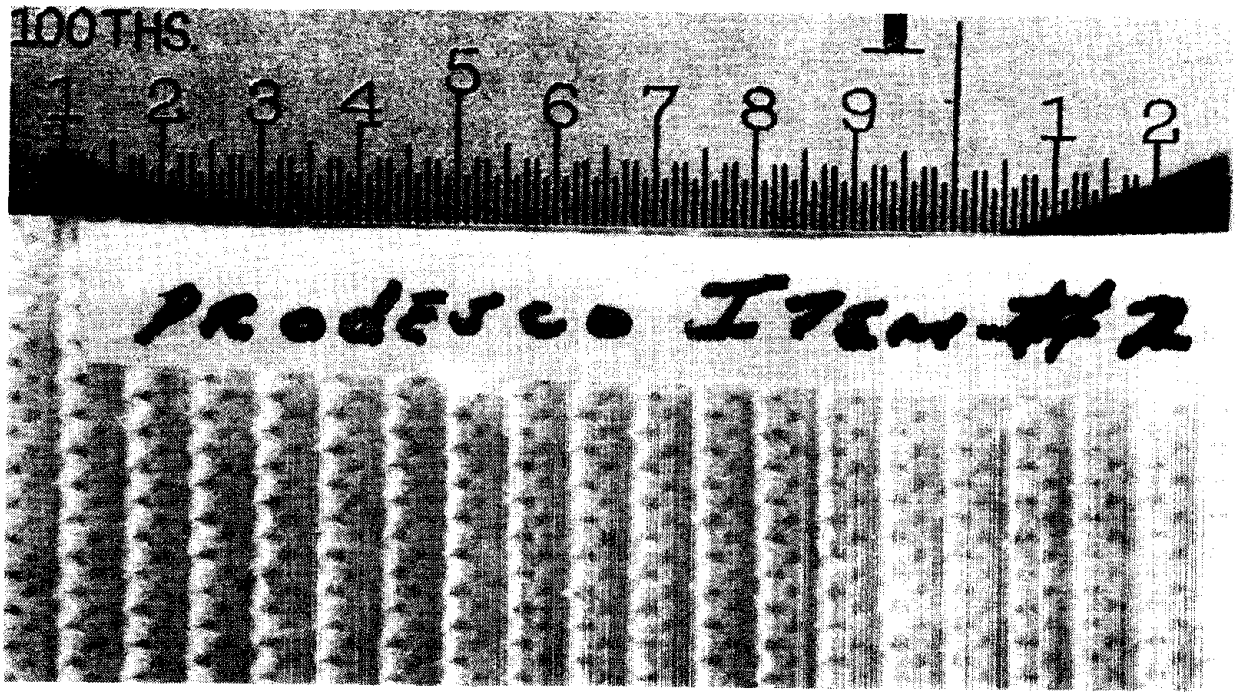

Figure 128. Sample of Prodesco Item No. 2 Fabric

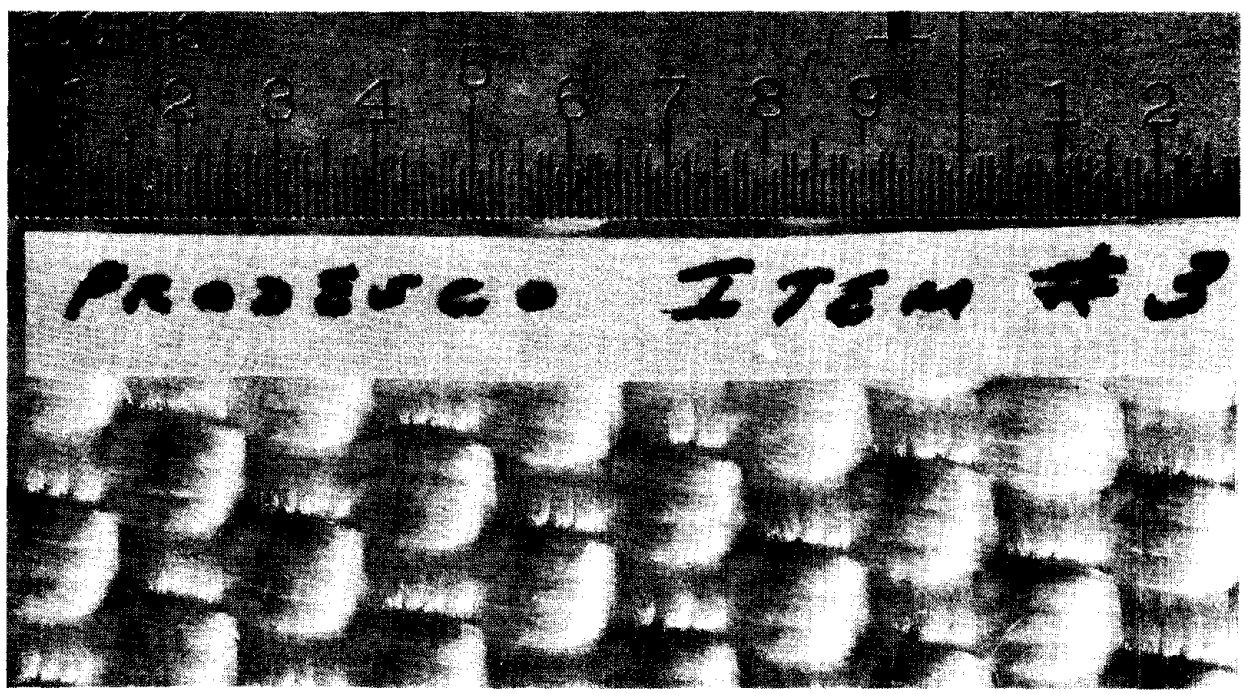

Figure 129. Sample of Prodesco Item No. 3 Fabric

d. Composite Selection and Testing

Based on the materials evaluation program previously described, the materials recommended for use in tactical seal system are as follows:

A. Elastomer: Neoprene, Burke Rubber No. 5026

B. Reinforcement: Nylon fabric, J. P. Stevens, Style 34103, 2 x 2 square weave, in multiple layers

C. Fluid: General Electric Silicone Oil, SF 96

D. Grease: Dow Corning Silicone Grease, DC 40.

This combination of materials was used in fabrication of seals for characterization, bench testing, and demonstration firings in both program configurations.

e. Testing AFRPL-Furnished Specimens

A series of composite samples consisting of multiple layers of fabric and elastomer were furnished by AFRPL for parallel testing, using the same laboratory techniques as those used for the candidate materials described earlier. Specimens were 2 by 6 in. of various thicknesses and differed from UTC specimens in that the fabric layers were either impregnated heavily or interspersed with multiple layers of elastomer. The samples were tested for burst strength in a 0.5-in. convolute and the results are shown in table XXIII. Some difficulty was experienced in cycling the thicker specimens at lower temperatures, but this probably could have been accomplished with a more powerful flexing fixture.

For direct comparison of these specimens with the multiple-ply UTC specimens which most closely resemble them, figure 130 shows the same linear thickness relating to burst strength as that shown in figure 128 resulting from the UTC specimen tests. Figure 131 through 134 show the burst strength specimens after test.

3. SEAL DEVELOPMENT

a. Design

(1) Minuteman Seal

The goal of delivering the Minuteman TECHROLL seal nozzle assembly to AFRPL approximately 5 months after contract go-ahead necessitated the direct use of seal materials, processes, and design techniques developed on the UTC prototype program. The Minuteman seal was fabricated from flat-sheet J. P. Stevens 34103 nylon fabric and coated with Burke 5026 neoprene elastomer with two seam joints, 180^{o} apart. The seal assembly was designed to withstand tensile loads imposed by a 1,000-psi chamber pressure for eventual use on the AFRPL C-3 demonstrator program.

TABLE XXIII

AFRPL-FURNISHED SPECIMENS

Specimen	Panel Thickness in.	Approximate Ply Thickness in.	Number of Plies	Approximate Total Fabric Thickness in.		Burst Strength, psi → Room Temperature No Cycles	Room Temperature 1,000 Cycles	-65°F No Cycles	-65°F 1,000 Cycles	+165°F No Cycles	+165°F 1,000 Cycles
Set I	0.072	0.030	2	0.060		3,900	4,050	3,500	6,900	2,800	*
						4,400	2,600	4,900	5,600	2,400	2,000
					Average	4,150	3,300	4,200	6,250	2,600	2,000
Set II	0.054	0.015	2	0.030		1,800	2,100	2,900	1,700	2,000	1,200
						2,100	2,200	2,500	2,200	2,100	900
					Average	1,950	2,150	2,700	1,950	2,050	1,050
Set III	0.137	0.030	4	0.120		6,800	5,500	5,900	---	5,400	6,000
						6,700	6,500	10,000	---	5,900	6,000
					Average	6,750	6,000	7,950	---†	5,650	6,000
Set IV	0.122	0.015	6	0.090		4,900	5,700	5,350	---	5,700	5,000
						4,000	5,800	5,500	---	5,000	5,400
					Average	4,750	5,750	5,425	---†	5,350	5,200

NOTE: Specimens were 2 by 6 in., with alternate layers of rubber and fabric or impregnated fabric layers internally, and external layers of elastomer.

*No results were recorded because of poor sample.
†Would not cycle below -55°F.

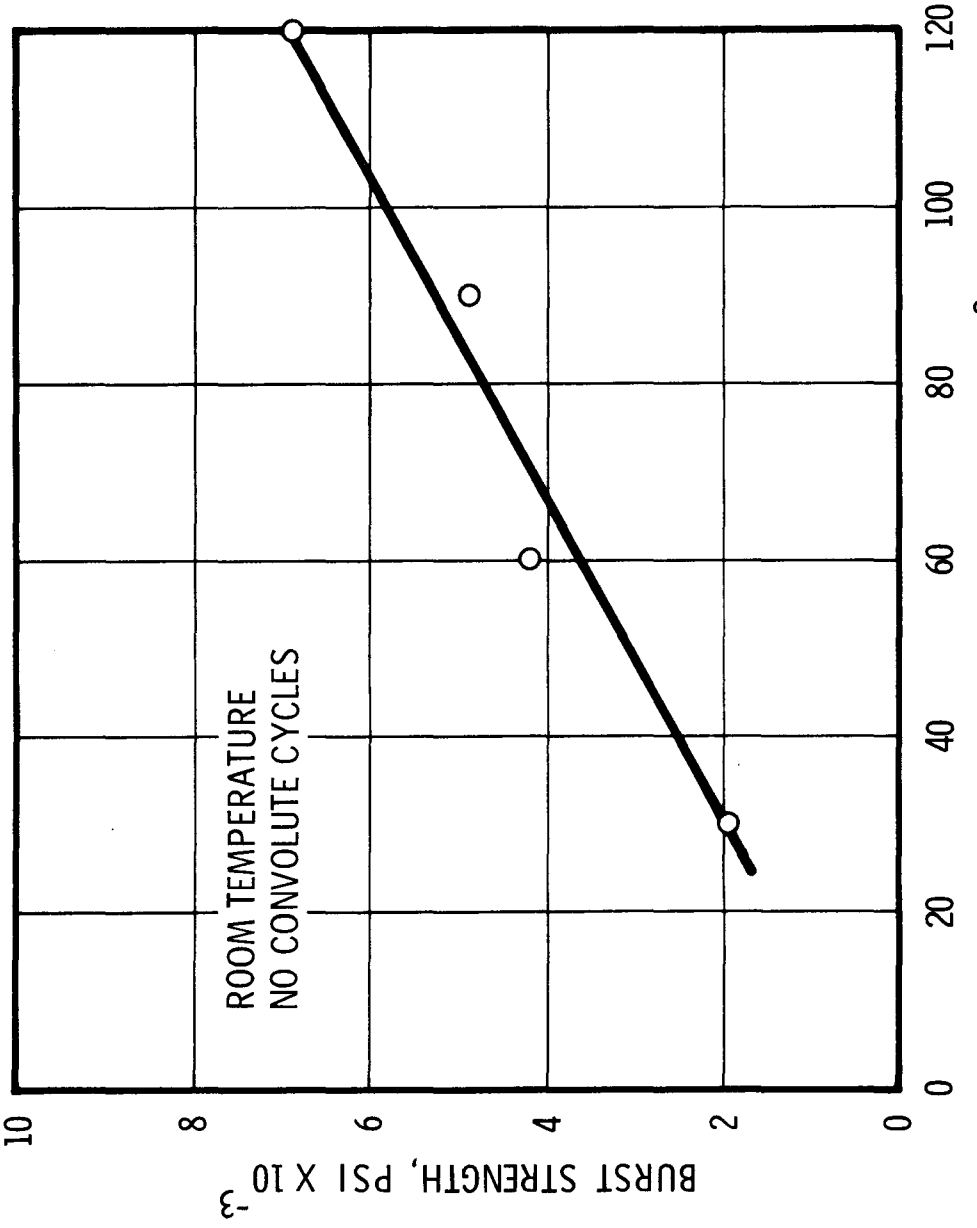

Figure 130. Burst Strength vs Thickness for Specimens Furnished by AFRPL

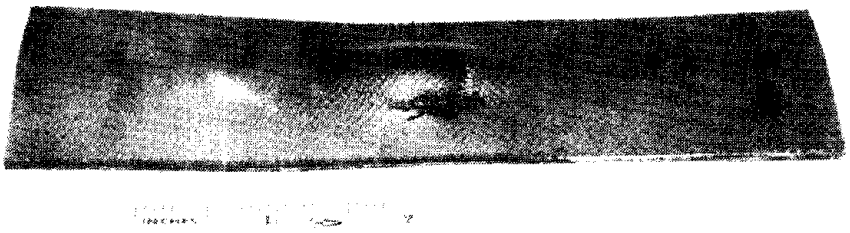

Figure 131. Burst Specimen, Set I

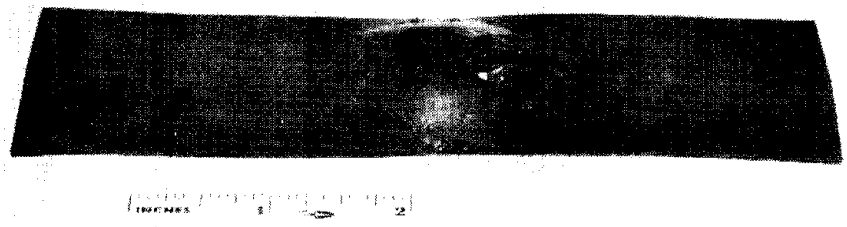

Figure 132. Burst Specimen, Set II

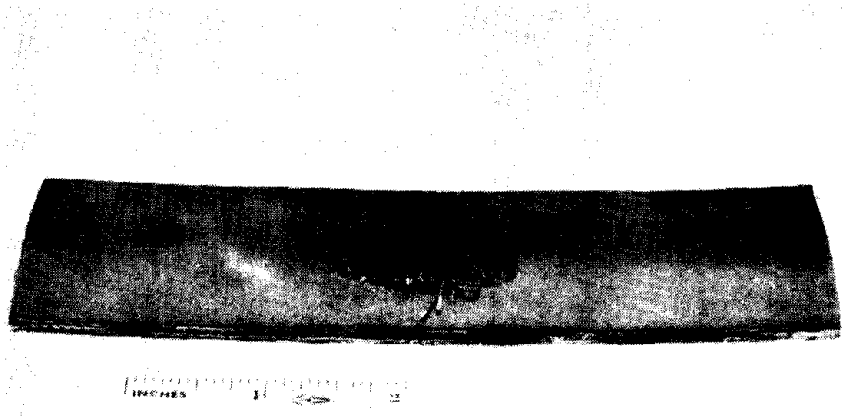

Figure 133. Burst Specimen, Set III

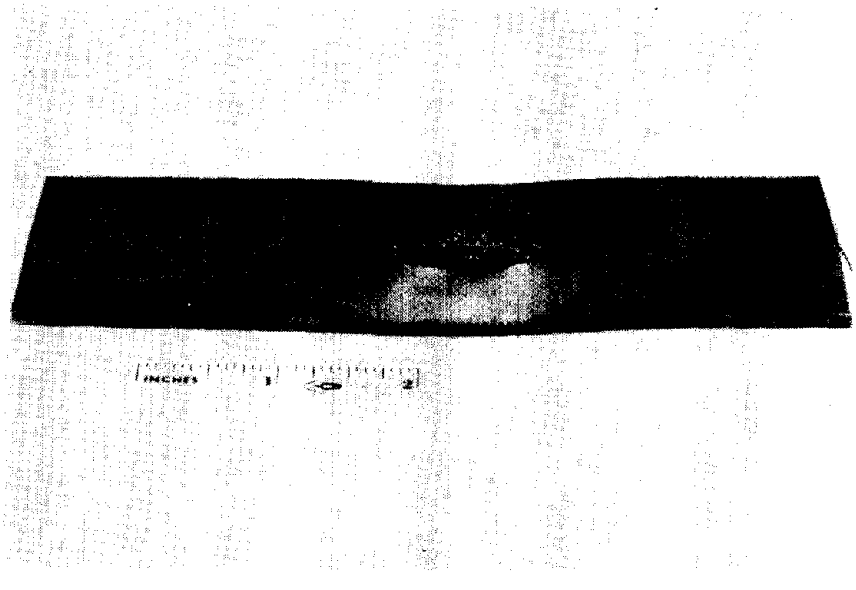

Figure 134. Burst Specimen, Set IV

(2) HIPPO Seal

As a result of the materials evaluation effort, a dual layer of flat-sheet J. P. Stevens 34103 nylon fabric/Burke 5026 neoprene elastomer composite with four seam joints, 90° apart, proved adequate to meet the tensile loads imposed by the 2,000-psi chamber pressure firing. The immediate advantage of the use of the flat stock was the ease of procurement, design flexibility, and avoidance of setup costs and leadtime associated with the procurement of special fabric weaves. UTC still considers the seamless reinforcement to be preferable for omniaxis deflections because seams in the fabric reinforcement necessitate material overlay that increases seal thickness locally and can result in nonlinear torque characteristics.

b. Fabrication

The techniques used for the prototype seal were used for fabrication of both the Minuteman and HIPPO seals. No process development studies were conducted during seal fabrication. Initial calendered elastomer thickness, fabric hold-down tension, and molding cure temperature were varied until fabrication of an acceptable part was achieved. The fabrication steps are outlined briefly as follows:

1. The fabric pattern is laid out on a 45° bias using flat patterns shown in figure 135. The bias layup is required to allow for pantographing of the seal walls as they roll.

2. The fabric is cut, and the inner and outer wire beads are prepared as shown in figure 136. For the HIPPO seal, metal rings are required on the flat portion of the seal that is bolted to the seal housing to prevent tearout at high pressures. The addition of the rings are shown in figure 137.

3. The breakaway matched-die mold shown in figure 138 is cleaned and inspected for irregularities in the Teflon coating.

4. A preform of the reinforcement fabric is laid up on the male portion of the mold shown in figure 139. The wire beads are stitched in place. For the HIPPO seal, the tearout rings are bonded on the outer fabric surface and between fabric layers as shown in figure 140.

5. While the preform is off the mold, a layer of elastomer is laid up on the inner side of the preform. The preform is replaced on the mold, and the inner and outer bead retention rings are put in place as shown in figure 141. If the fabric is cut and laid up properly, the proper tension in the part should be attained when the retention rings are bottomed out.

6. A bleeder cloth and vacuum bag is placed over the mold and a vacuum drawn to tighten up the entire part as shown in figure 142.

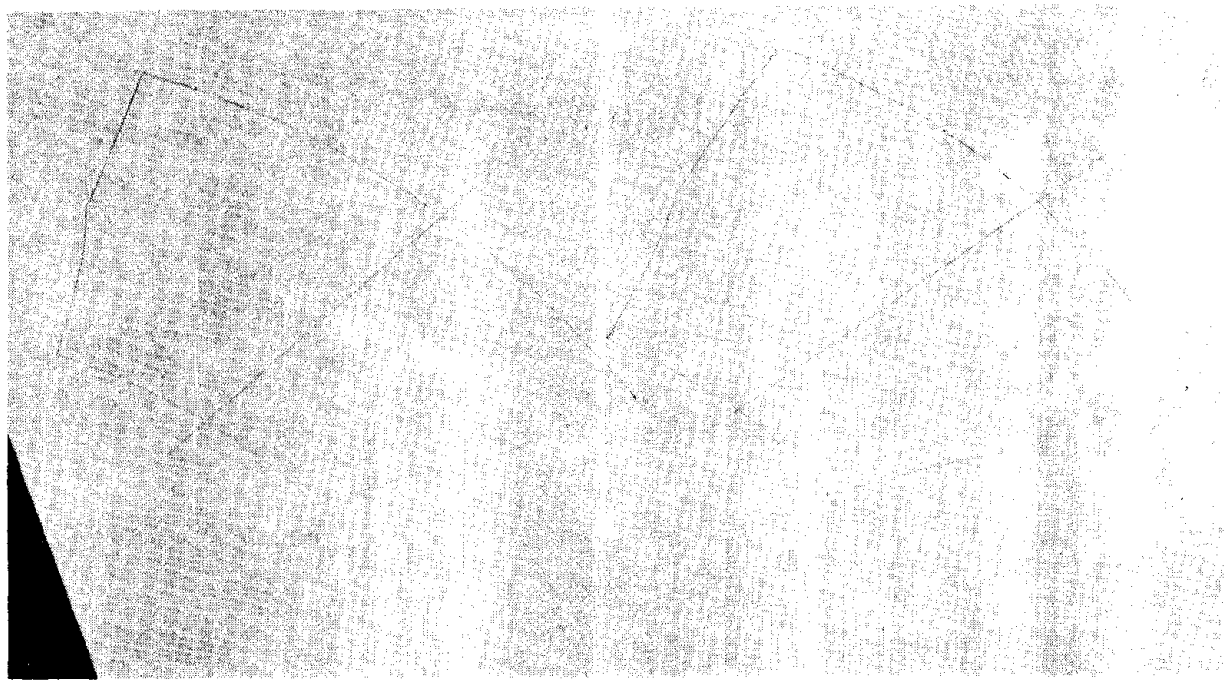

Figure 135. Pattern on 45° Bias Flat Stock Fabric

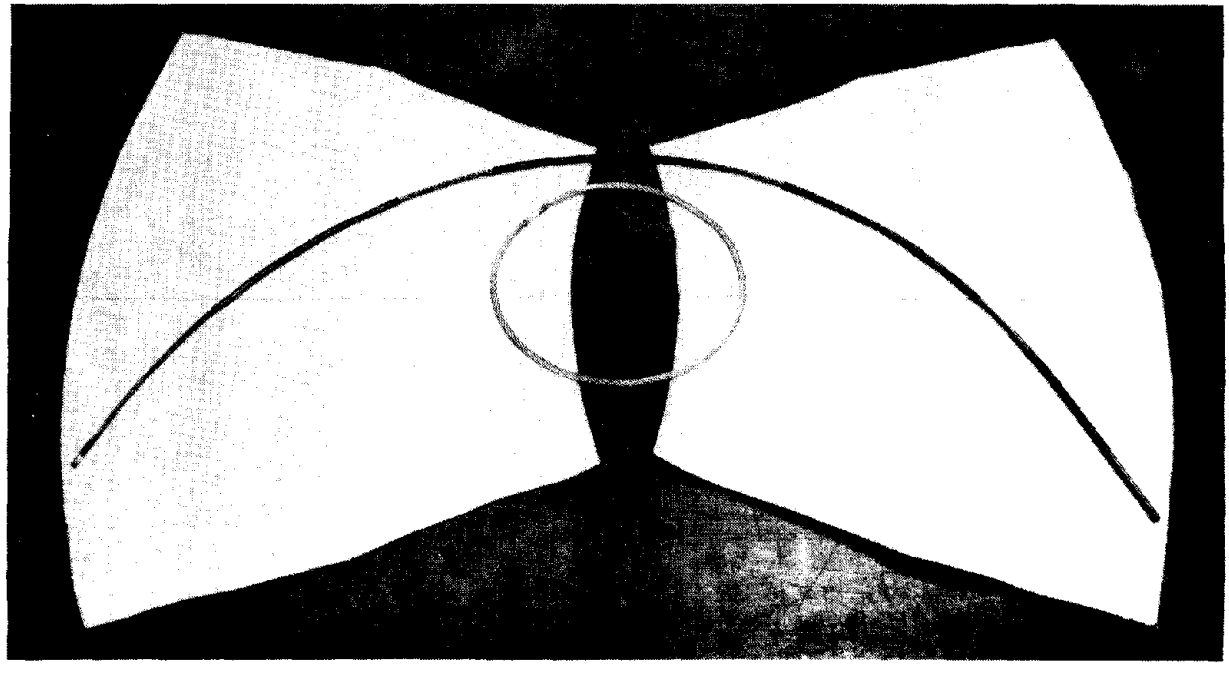

Figure 136. Cut Fabric and Bead Wires

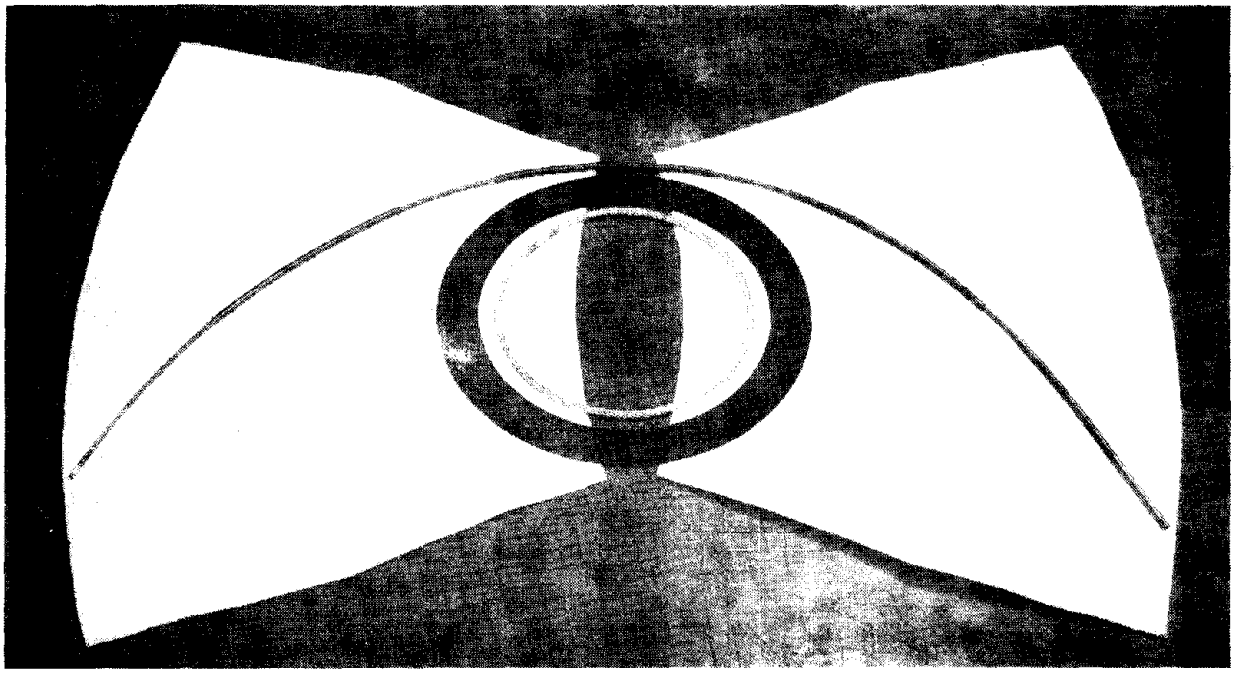

Figure 137. Cut Fabric, Bead Wires, and Metal Reinforcement Rings for HIPPO Motor

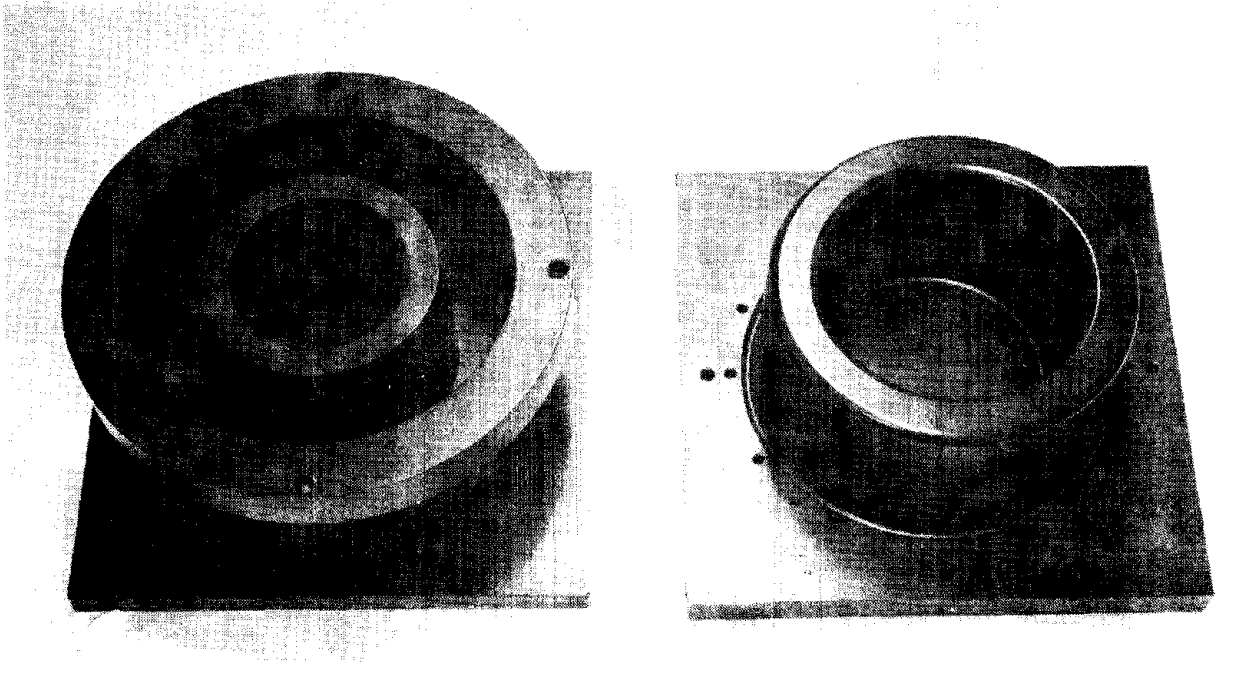

Figure 138. Matched-Die Mold

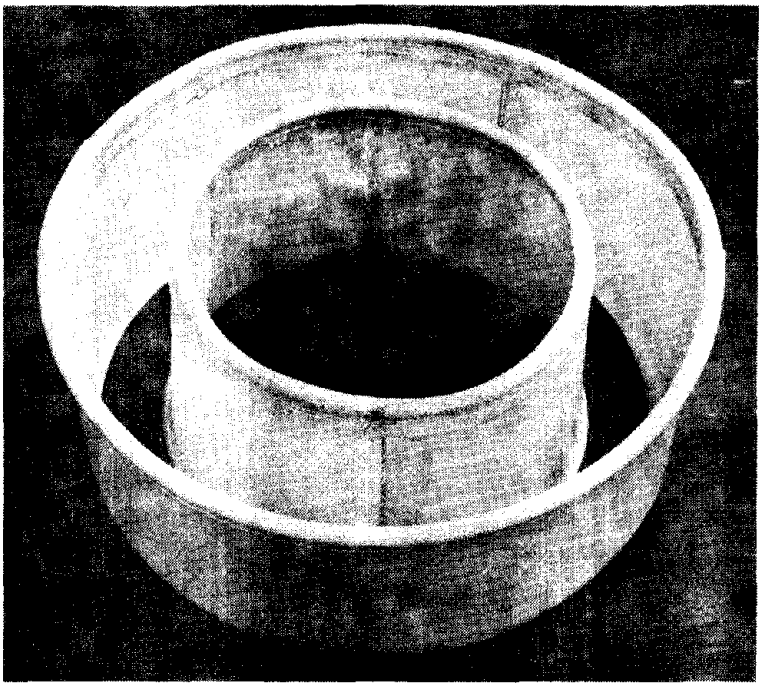

Figure 139. Fabric Reinforcement Preform

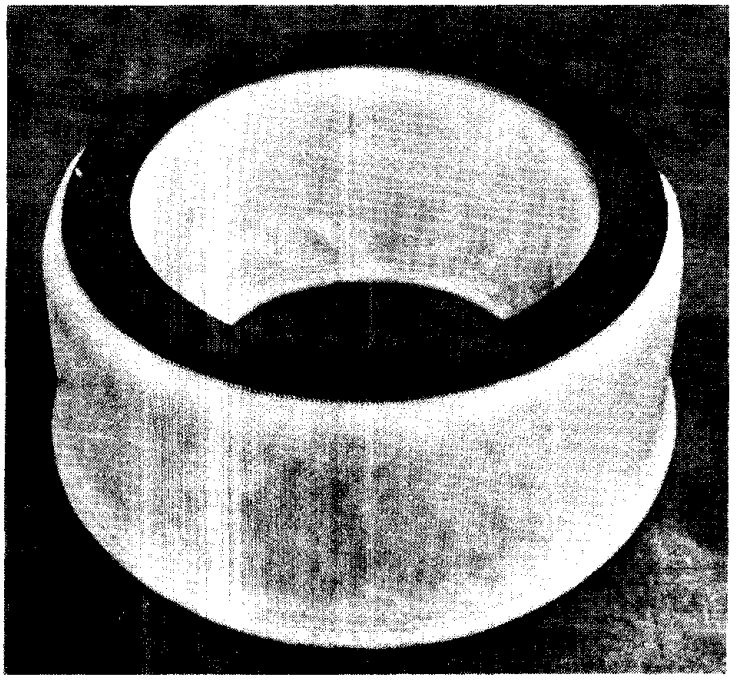

Figure 140. Fabric Preform with Reinforcement Ring

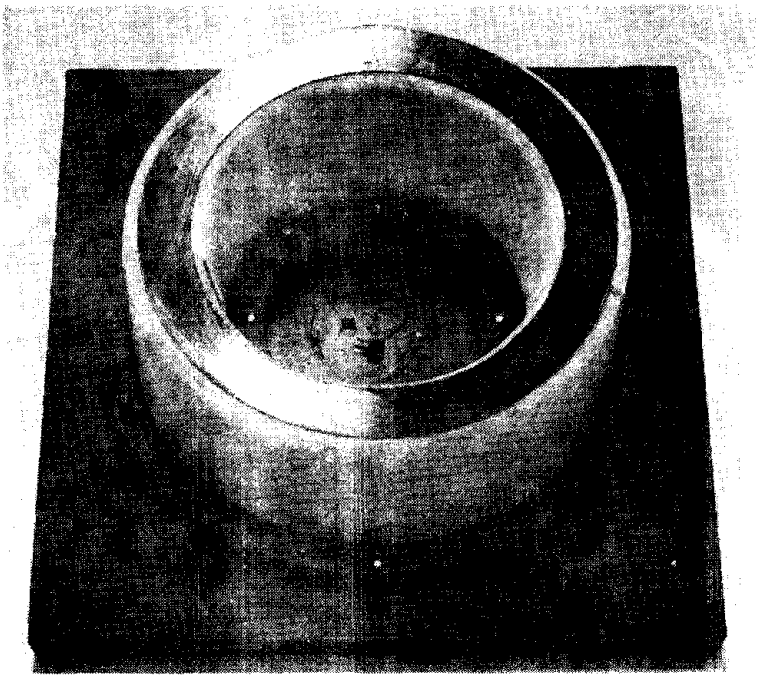

Figure 141. Layup on Mold with Bead Holddown Rings in Place

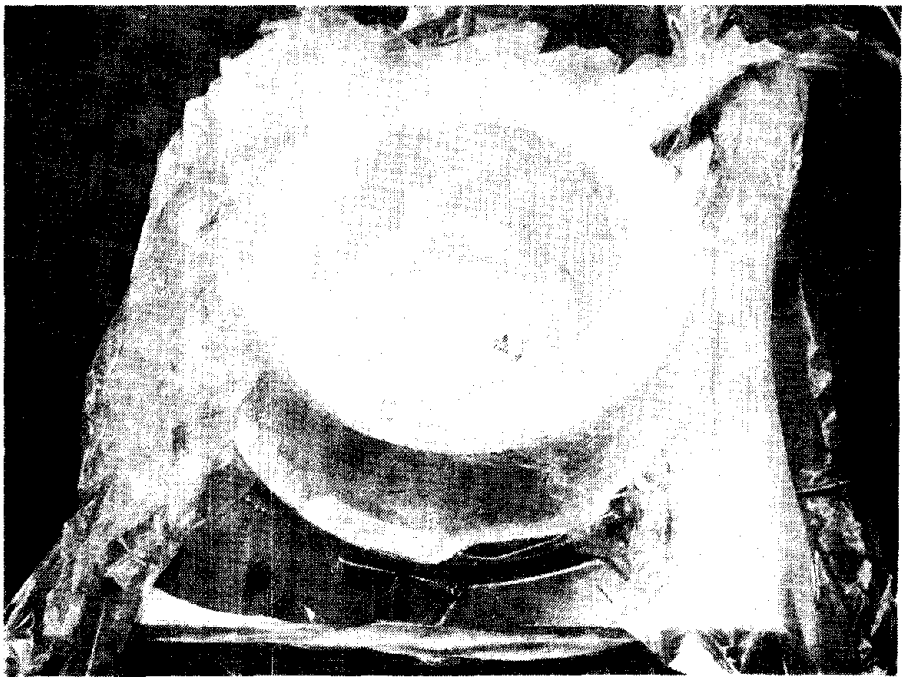

Figure 142. Layup Under Vacuum

7. The outer layer of elastomer is placed on the part as shown in figure 143.

8. The male and female portions of the mold are placed in a heated platen hydraulic press as shown in figure 144. The mold segments are preheated and then closed at a predetermined pressure as shown in figure 145.

9. The part is heat and pressure cured in the matched-die mold to allow the elastomer to reach its cure state and then is removed. The finished part still on the male mold is shown in figure 146.

10. A typical HIPPO seal after removal from the mold and before the flashing is removed is shown in figure 147 and 148.

11. The finished, ready-to-use 17-in. Minuteman and 12-in. HIPPO seals are shown in figure 149.

Each completed seal was visually inspected for flaws and surface irregularities. If the seal passed the visual inspection, it was assembled into the seal housing, filled with fluid and pressure checked to a predetermined pressure, and all assembly bolts were torqued. If the seal held pressure during this operation, it was considered acceptable to be used for the next phase of testing. This NDT process is described in the next section.

c. Nondestructive Testing

During the Minuteman TECHROLL seal fabrication phase, the finished seal was evaluated initially by visual and radiographic inspection. The material composite wall section of the seal was radiographically inspected using a low kilo voltage range (60 to 150 kv) and slow-speed, high-contrast film. The goal of this NDT process was to reveal the separations, buckling of the reinforcement fabric, nonuniform coverage of the fabric material, and discontinuities in overlap and seam areas.

The radiographic appraoch proved to be useful in identifying flaws associated with the fabric reinforcement system; however, in almost every instance these flaws also could be discerned by careful visual scrutiny. In no case was a discrepancy of sufficient magnitude to cause rejection of the seal discovered solely by X-ray techniques. Additionally, failures of early seals were experienced during proof test where both visual and radiographic inspection did not uncover an anomaly.

The major failure modes that went undetected until pressure test were "pinhole" leak paths through one or both layers of elastomer. A pinhole leak on the pressure surface permits seal oil to penetrate to the fabric, and seal leakage may then occur through nonopposed pinhole leaks in the nonpressure surface of the seal.

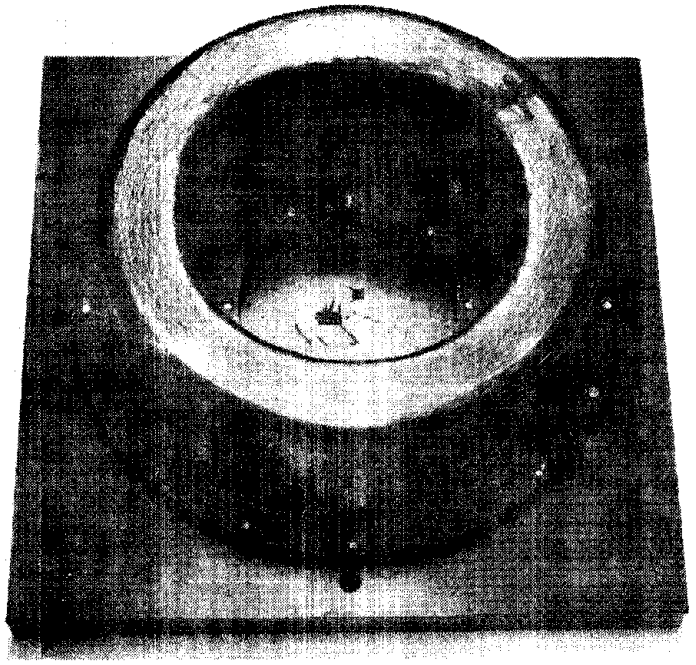

Figure 143. Completed Layup Ready for Molding

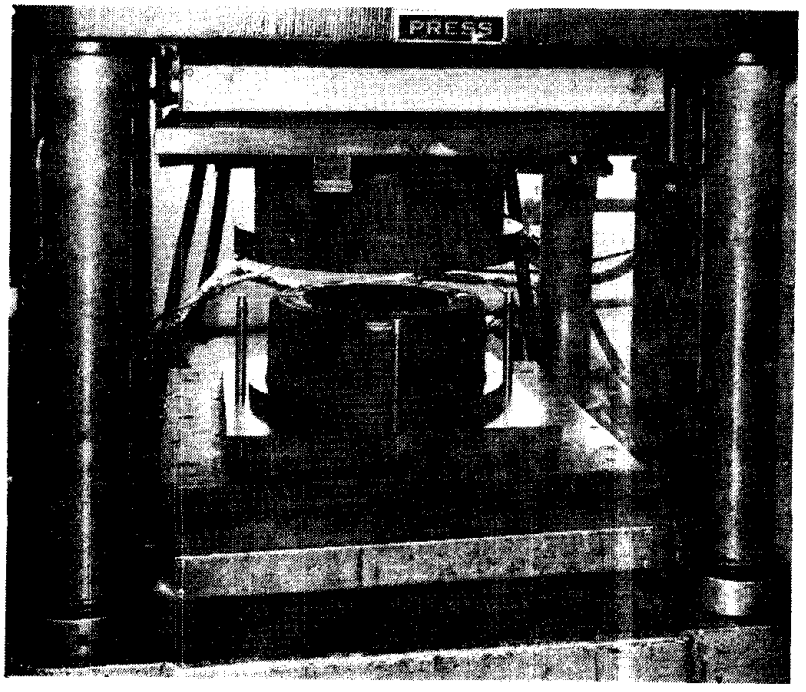

Figure 144. Mold Loaded in Heated Hydraulic Press

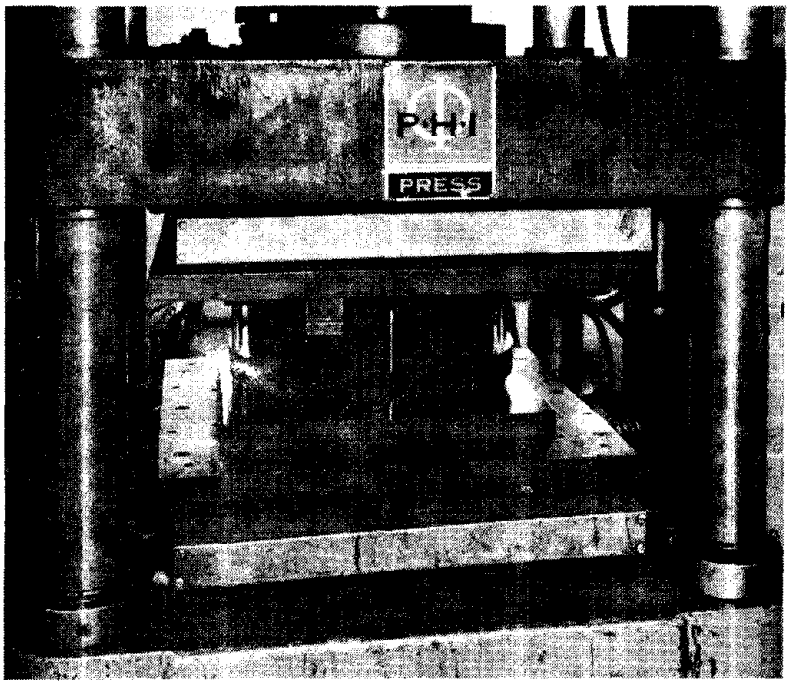

Figure 145. Molding the Seal

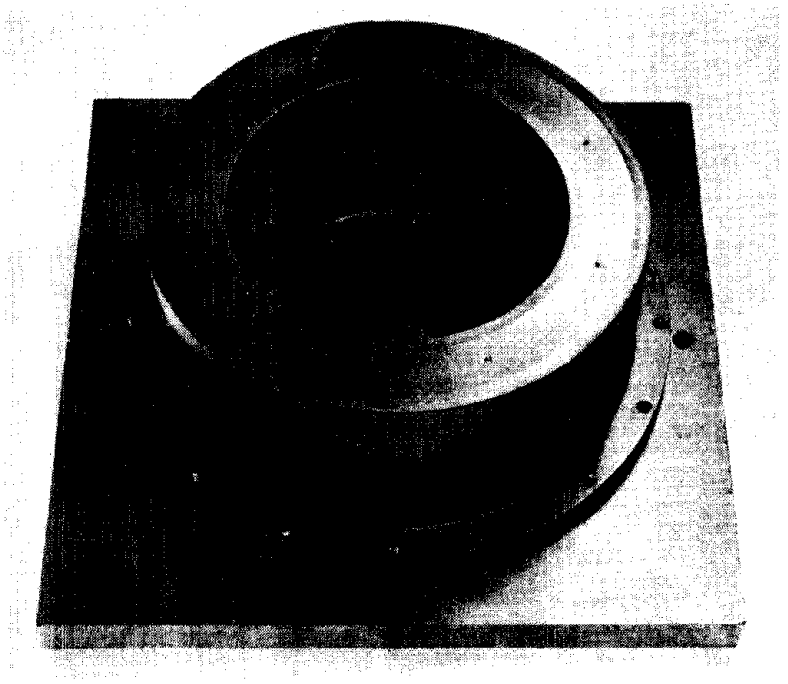

Figure 146. Finished Seal Attached to Male Part of Mold

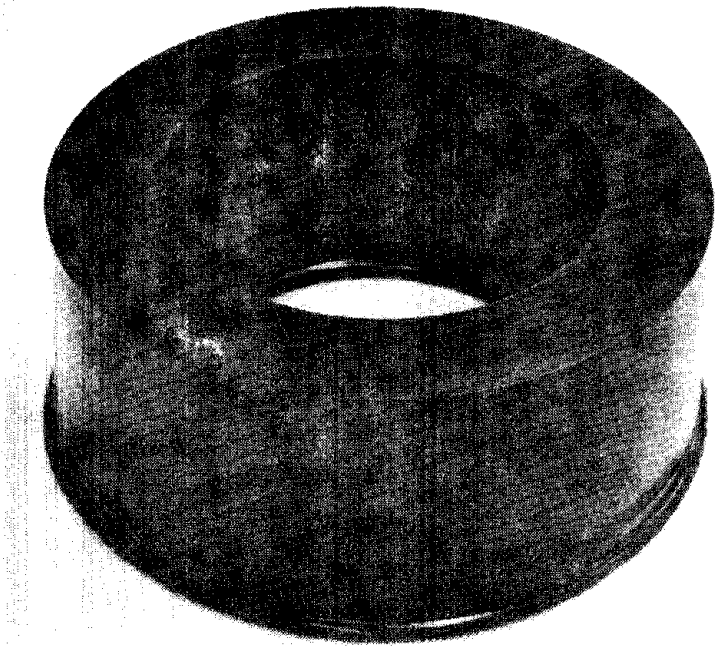

Figure 147. Finished Seal with Flashing on Outer Surface

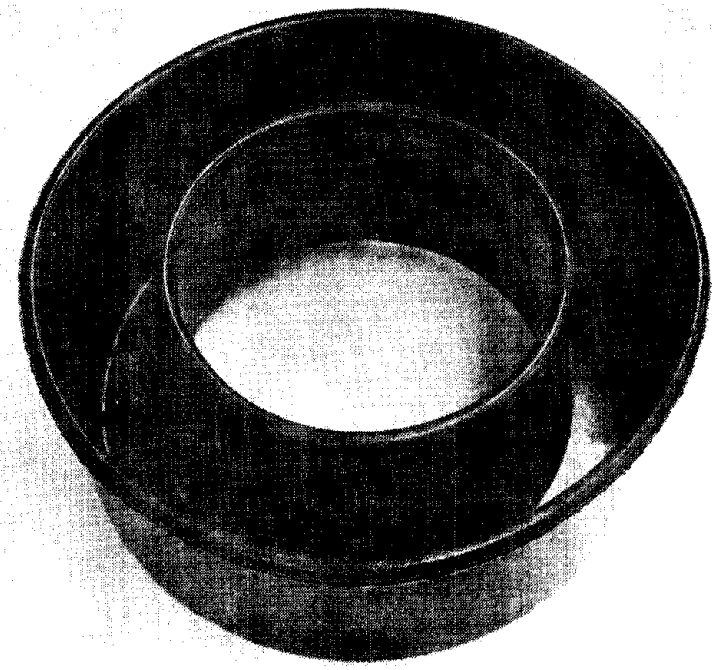

Figure 148. Finished Seal with Flashing on Inner Surface

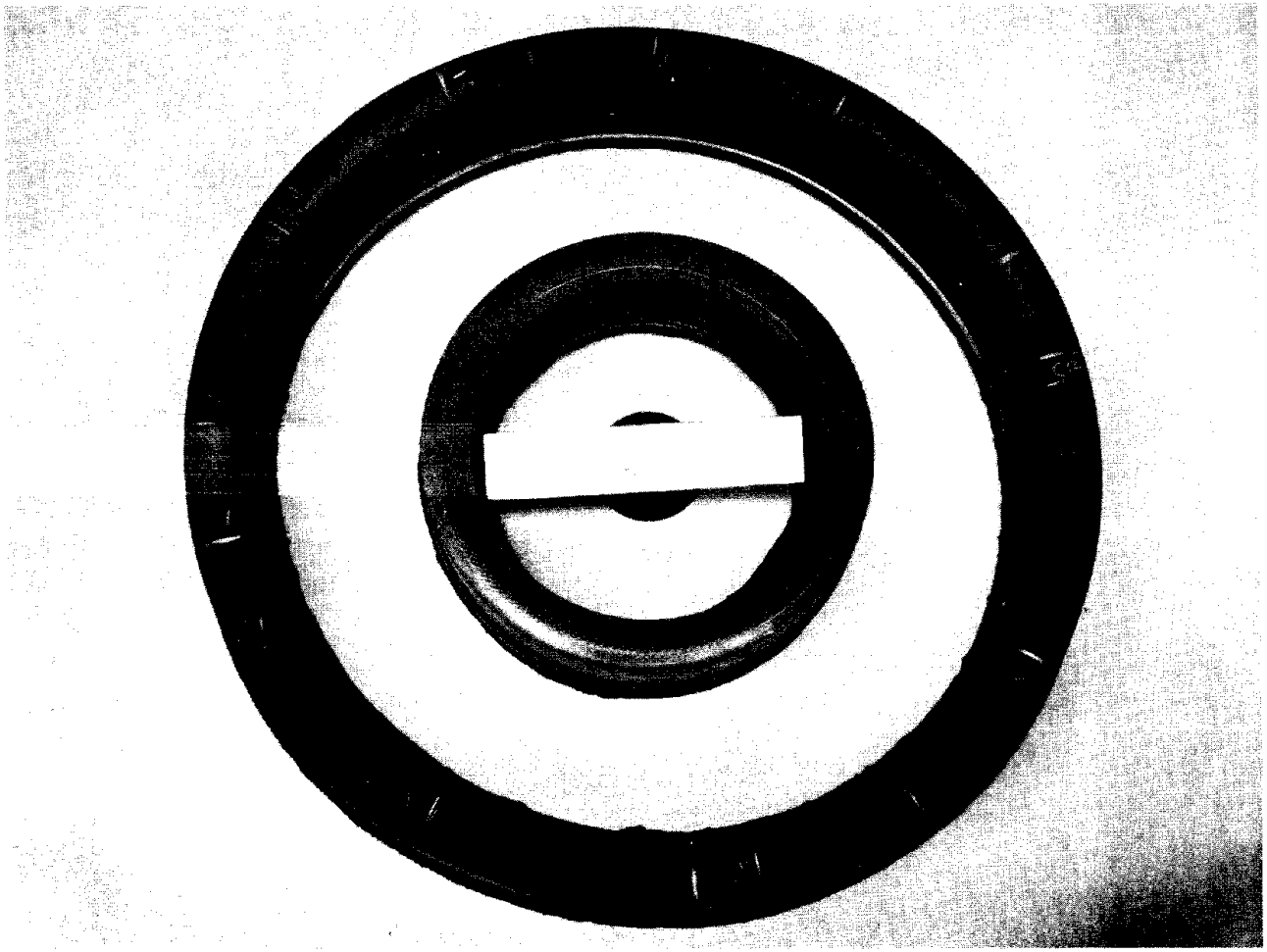

Figure 149. TECHROLL Seal for Minuteman and HIPPO Motors

Radiographic inspection appears to be a potentially useful production screening technique and is considered to be valuable during evaluation of fabrication techniques of new seal configurations. Further investigation of radiography is now under consideration.

Primary NDT techniques used with all demonstration test seals were critical visual inspection using magnifying devices followed by proof pressure and axial hysteresis tests.

Comparison of axial deflection characteristics of a seal before, during, and after exposure to proof pressure appears to be a reliable means of screening out seals including production defects.

SECTION V

COMMERCIAL SOURCE OF SUPPLY

1. INTRODUCTION

Companies having capabilities for manufacturing fabric-reinforced elastomeric seals were surveyed for interest in developing assembly line fabrication techniques. A company was then selected to fabricate the conventional air-launched TECHROLL seal configuration and to provide manufacturing plans, techniques, and cost for both the air launch and Minuteman seal configurations.

2. VENDOR SELECTION

Proposals were solicited from 17 companies whose products and approach to manufacturing were primarily commercial rather than aerospace oriented. Only two companies, B. F. Goodrich Co., and Uniroyal Inc., bid by the 30 June 1971 closing date.

Based primarily on cost and a better understanding of technical accomplishments, B. F. Goodrich was selected as the commercial source, and a contract was let in August 1971.

3. FABRICATION AND TEST RESULTS

From the requirements established by the envelope drawings for the two seals (figures 150 and 151), B. F. Gooodrich submitted a program and fabrication plan in September 1971. Later that month, the B. F. Goodrich program manager met with UTC personnel to discuss the plan. Also, he delivered samples of the proposed elastomer/fabric composite. UTC burst-test these samples and the results were poor. The B. F. Goodrich tire-cord approach resulted in a too widely spaced reinforcement fabric and the cord separated under load. UTC recommended that the polyester tire-cord approach be modified to reduce the spacing between strands and possibly to cover the strands with a thin layer of fabric to keep the strands from separating under load.

The operating requirements shown in figure 151 resulted in a seal proof pressure of 5,500±50 psi for the air-launched configuration. The samples which were tested burst at pressures less than 1,000 psi.

In October 1971, B. F. Goodrich sent UTC a second set of sample specimens. These specimens consisted of two plies of tire cord and one ply of a fabric covering. This time the specimens burst at slightly below 2,000 psi.

In November 1971, B. F. Goodrich changed the elastomer from neoprene to silicone SE-7565 to meet the -65° to +165°F temperature required for an air-launched system. Four 2 in. by 6 in. specimens using the silicone elastomer were transmitted to UTC for testing. The results were as follows:

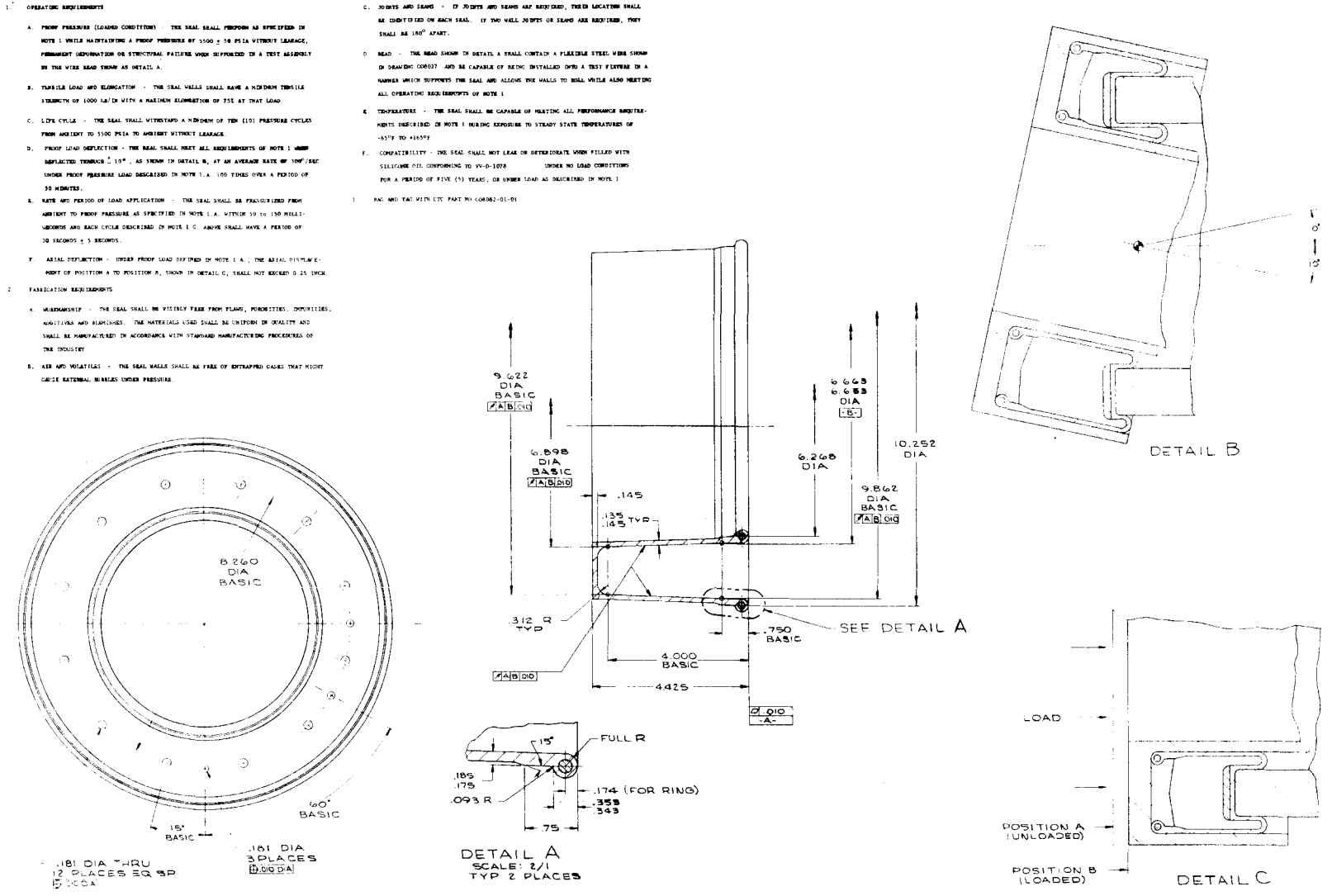

Figure 150. TECHROLL Seal Assembly, HIPPO Envelope Drawing

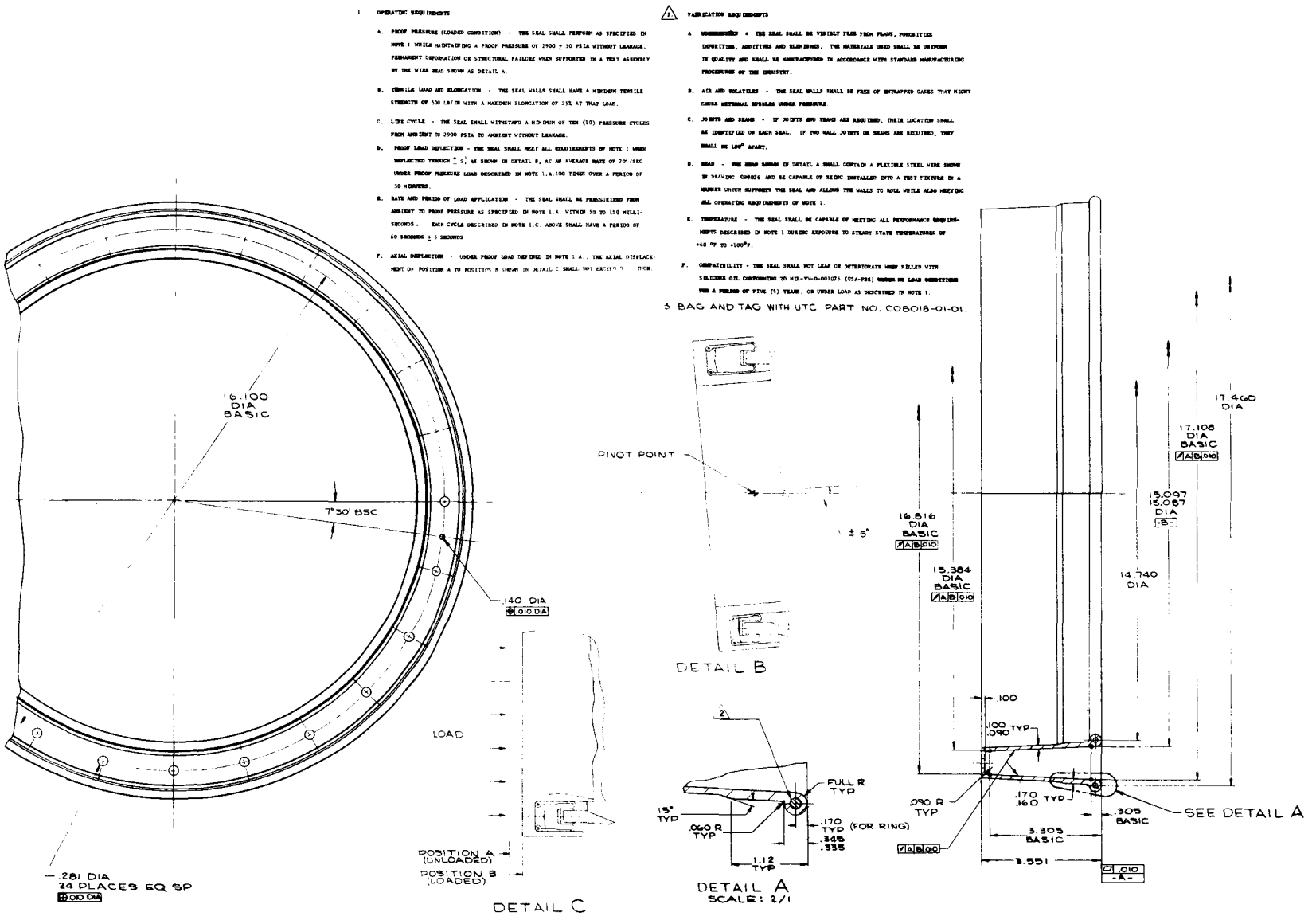

Figure 151. TECHROLL Seal Assembly, Minuteman Envelope Drawing

Sample	Maximum Burst Pressure, psi	Wall Thickness, in.
Two-ply tire-cord, one-ply tricot fabric	2,425	0.169
Two-ply tire-cord, one-ply plain weave fabric	2,300	0.180
Two-ply tire-cord, one-ply plain weave fabric, 600 lb/in. tensile strength	2,800	0.180
Four-ply tricot fabric, no cord	2,900	0.109

In January 1972, B. F. Goodrich in an effort to meet the burst test requirements, built a burst fixture similar to the UTC burst fixture and tested samples with the following results:

Sample	Thickness, in.*	Burst Pressure, psi
Nylon 34103		
two ply	0.108	3,200
three ply	0.154	4,900
four ply	0.200	5,400
Nylon 3 x 4 basket weave		
two ply	0.125	3,500
three ply	0.185	5,000 (No burst, slipped in fixture)
Nylon tricot		
four ply	0.128	1,000 (No burst, slipped in fixture)

* Envelope drawing requires wall thickness to be 0.135 to 0.145 in.

During a technical status review of the program held with the Air Force program office and UTC personnel at UTC on 13 and 14 January 1972, it became apparent that attempts to establish a commercial source for TECHROLL seals would not be successful within the constraints of this project. Subsequently, a TWX was received from the AFRPL contracting officer to terminate this effort.

To close out the contract, B. F. Goodrich agreed to deliver three HIPPO seals as originally intended but not to the stated requirements. In April, after discussions concerning the format and the method, UTC advised B. F. Goodrich to build three seals on a best effort basis.

The first two seals, using three-ply square woven 1,000 lb/in. nylon and silicone elastomer, were oversized in the bead areas. These seals did not fit the test hardware and could not be tested.

A third seal was fabricated in May 1972 using nylon tricot and silicone rubber. Both the bead areas and wall thickness were over tolerance. This part was rejected.

Another seal was made with the silicone replaced by neoprene rubber. This seal was also out of tolerance in the bead area. No further testing was performed.

4. QUANTITY MANUFACTURING COSTS

The following production costs were quoted by B. F. Goodrich for the air launch and Minuteman seals assuming that they were successful in meeting the technical requirements.

Air Launch Seal

Quantity	Cost per Seal, dollars	Tooling, dollars
3	3,189	8,655 (soft)
10	1,112	11,462 (production, 10 per month)
100	770	8,300 (production, 25 per month)
500	664	
1,000	643	

Minuteman Seal

10	2,200	9,167 (soft)
100	879	11,766 (production, 10 per month)
500	764	8,700 (production, 25 per month)
1,000	731	

5. FABRICATION METHOD

The seal composite was layed up on a preform tool covered with a bleeder cloth and a vacuum bag. The assembly underwent a curing cycle in an autoclave and then a hot air postcure cycle in the unconstrained position.

SECTION VI

CONCLUSIONS AND RECOMMENDATIONS

The TECHROLL seal development program conducted under this contract has resulted in the successful demonstration of this advanced, low torque, movable nozzle bearing in both high pressure tactical and ballistic motor configurations.

Adequate knowledge was obtained during this program to permit design of TECHROLL seal movable nozzle systems for a variety of potential applications.

The complete success of the multifiring demonstration program, and the empirical and analytical data base which it produced, indicates that the TECHROLL seal movable nozzle is ready for engineering development for ballistic systems applications.

The performance of the TECHROLL seal concept for use in high pressure tactical air-launched systems was determined; however, all work was conducted in the ambient temperature range since all seals were fabricated from nylon-neoprene composite materials. The TECHROLL seal was not evaluated in the air-launched missile vibration environment.

Development work to date on the TECHROLL seal also has indicated some highly attractive actuation techniques, alternate seal geometries, and fabrication approaches that could result in further improvements in movable nozzle system performance.

TECHROLL seal storage and aging characteristics have been demonstrated based largely on material samples tests and proven long term compatibility of components. Long term real time aging/performance studies have not been conducted.

Additional work is recommended in the following areas:

A. Demonstrate a ballistic motor TECHROLL seal movable nozzle using high pressure (miniseal) technology and an integrated actuation system. This would represent the TECHROLL seal state of development on completion of this program

B. Develop and evaluate elastomer-fabric composite seals capable of operation from -65° to $+165^{\circ}F$

C. Evaluate a tactical configuration TECHROLL seal movable nozzle system in the air-launched missile vibration environment

D. Develop and evaluate seamless weave fabric preforms for TECHROLL seals to improve seal integrity and uniformity of operating characteristics in all axes

E. Evaluate the effects of long term storage and aging on the performance of a TECHROLL seal configured for tactical system application

F. Develop, evaluate and test fire an advanced state-of-the-art movable nozzle tactical motor TVC system using an optimized TECHROLL seal.

APPENDIX I

DATA COLLECTION AND REDUCTION

A discussion follows of the bench and static testing techniques used for this program.

1. BENCH AND ACCEPTANCE TEST DATA

During the early phase of bench testing, data were recorded on an oscillograph recorder. These data were transferred to digital data by use of a Gerber digital data reduction system. The digital data along with transducer calibration data were then transferred to a digital engineering units tape.

Subsequent bench/acceptance test data were recorded on FM tape, and then digitized with the UTC digitizer. The digital tape along with transducer calibration information was then transferred to a digital engineering units tape. This was the input to computer program TRS/Angle, which calculates the nozzle movement and torque data. Listings and plots of these data were then transmitted to the cognizant engineers for analysis. Figures 152 and 153 show the data reduction flow charts for these processes.

2. STATIC TEST DATA

Data from the static tests were provided by AFRPL on a digital engineering units tape. After conversion to a Burroughs compatible format, these tapes were input to computer program TRS/Angle. The resultant nozzle movement and torque data were then transmitted to the cognizant engineers for analysis. Figure 154 shows the data reduction flow chart for this process.

3. VISCOUS FLUIDS TEST DATA

The data from the fluid pumping tests were initially handled in the same manner as the acceptance test data. The data were recorded on FM tape, and the digital conversion of this FM data was then converted to engineering units. The resultant data were then calculated using computer program MA27ZDZ.

The data were digitized at both 100 and 500 samples/sec. The 100 sample/sec data did not provide enough data points during the dynamic portion of the duty cycles. The resolution of the 500 samples/sec data was such that meaningful acceleration and velocity data could not be obtained.

The data were then digitized at 1,600 samples/sec using a frequency multiplier to retain some of the resolution of the original data. At the same time, a high speed oscillograph was made of the data. The resolution of the digital data was still not good enough to provide automatic data reduction. The data were then sent to the engineer in the form of 30- by 40-in. plots. Using these plots and the high speed oscillograph, the desired data were obtained.

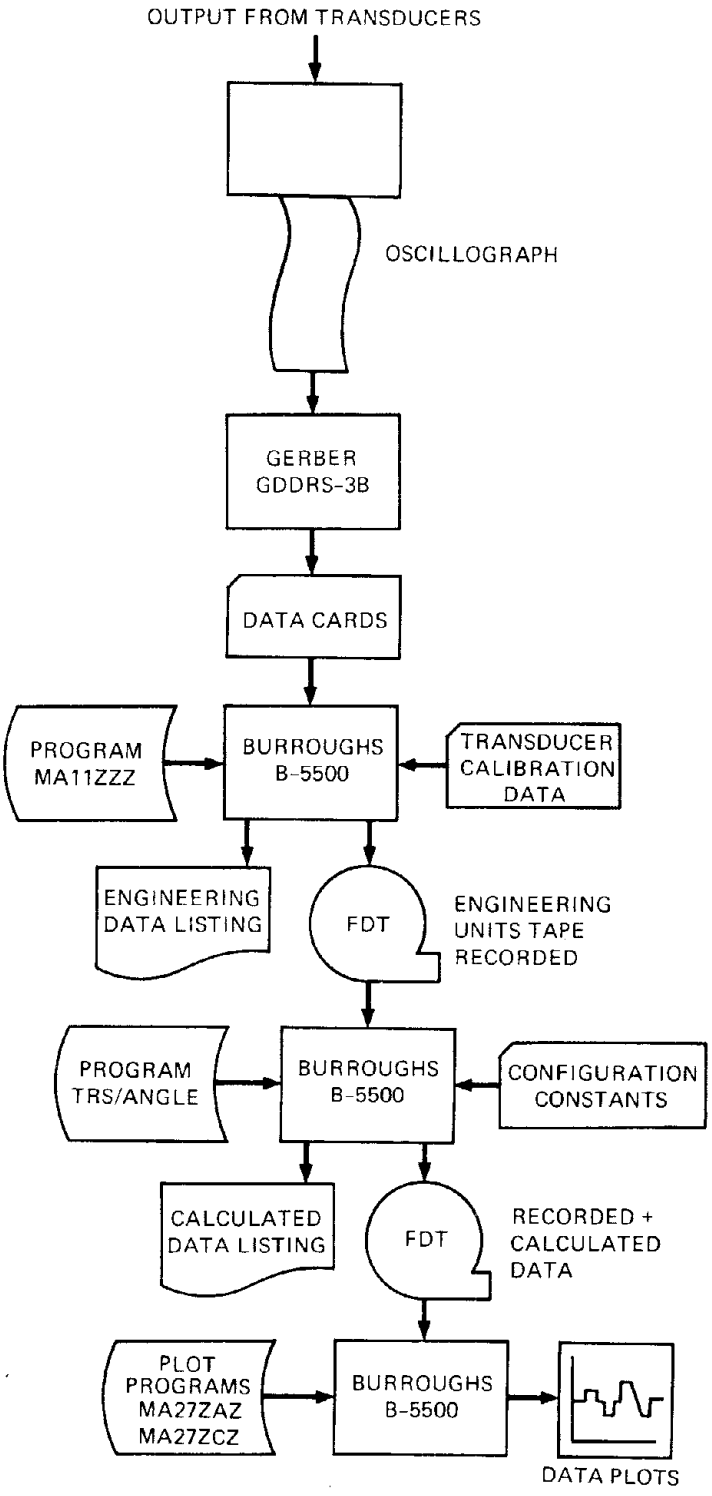

Figure 152. Early Bench Test Data Reduction Technique

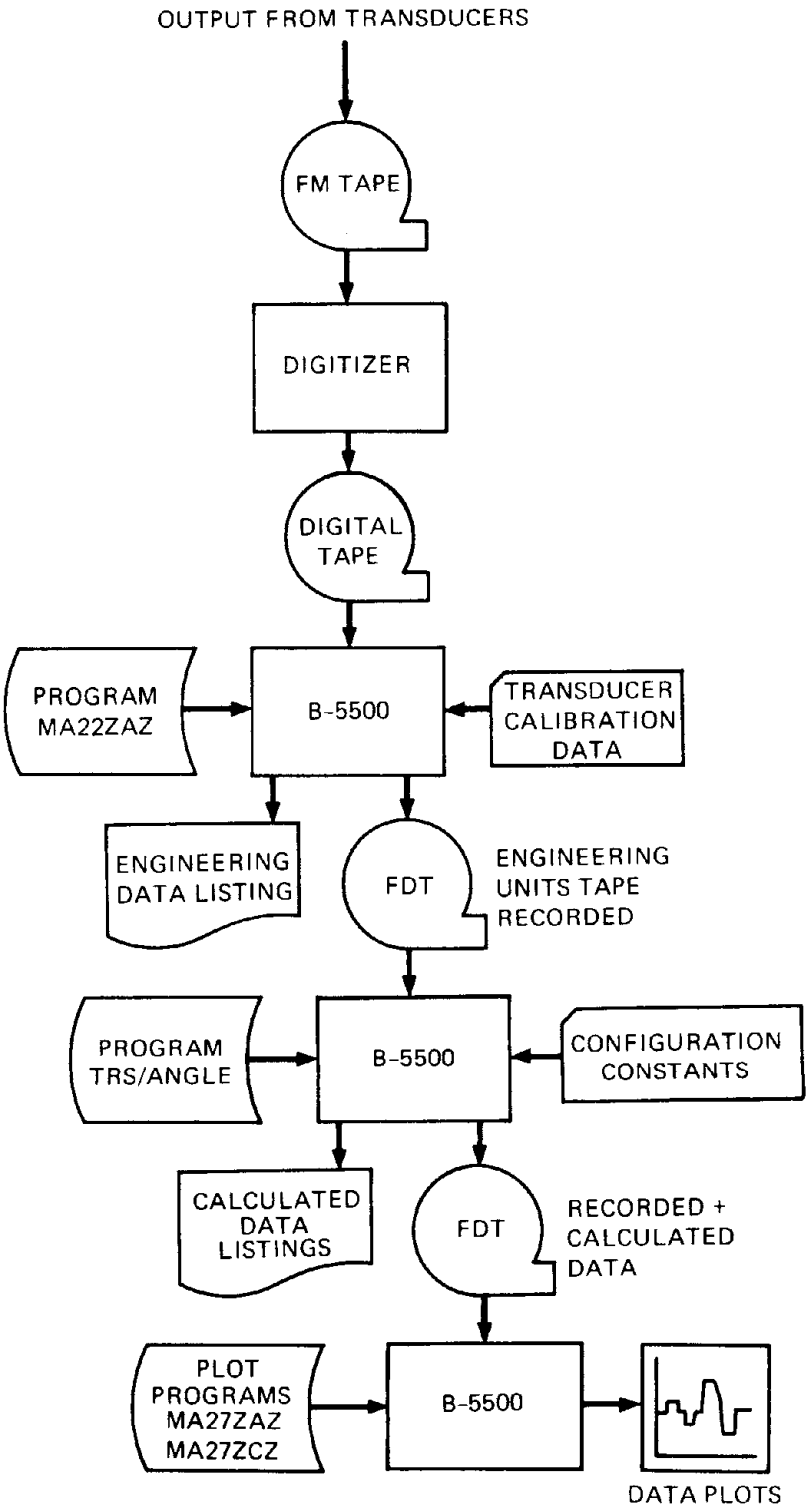

Figure 153. Later Bench Test Data Reduction Technique

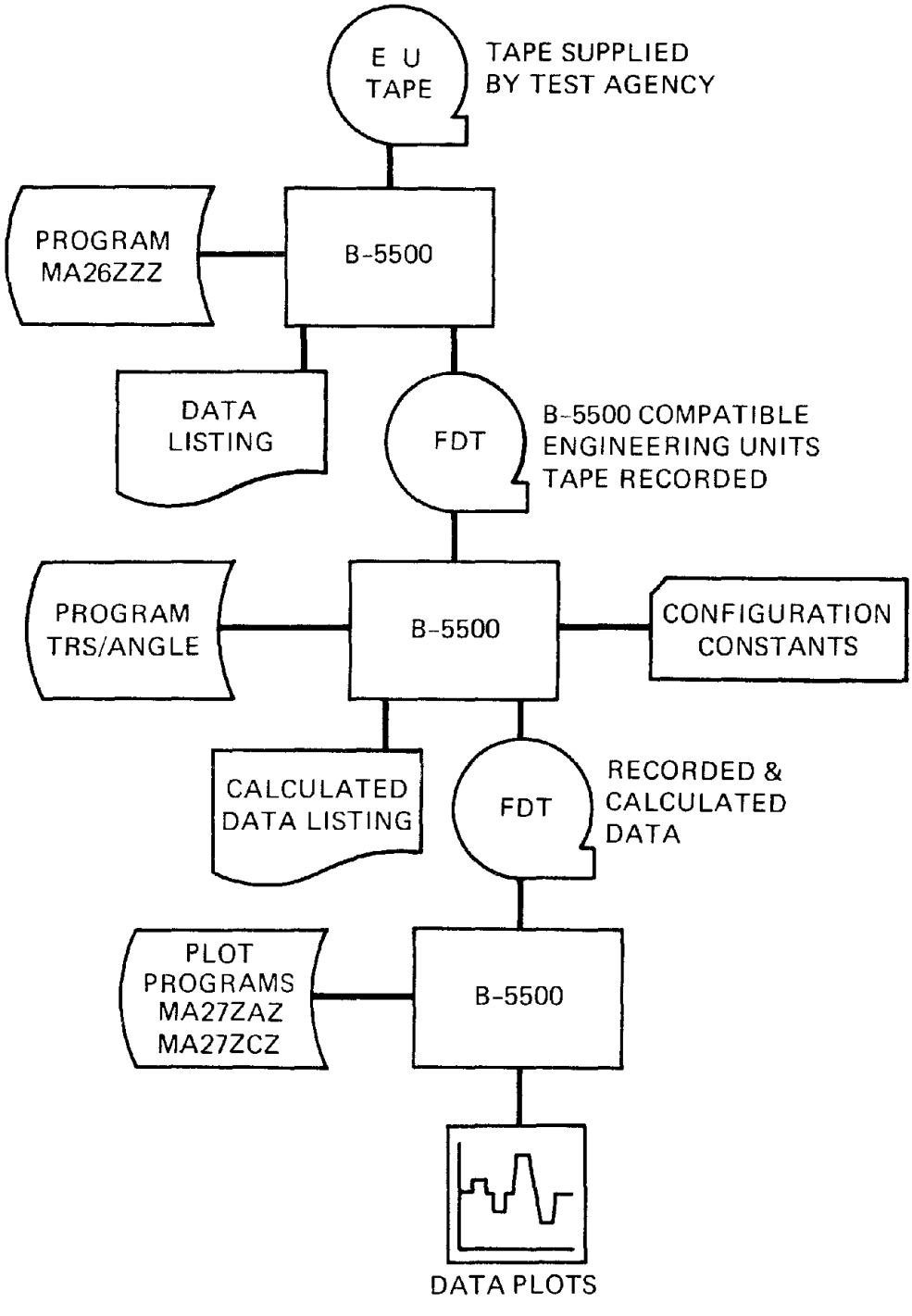

Figure 154. Static Test Data Reduction Technique

4. DATA REDUCTION SYSTEM AND COMPUTER PROGRAMS

A. Gerber digital data reduction system (GDDRS-3B)

B. Computer program MA11ZZZ

C. Digitizer

D. Computer program MA22ZAZ

E. Computer program MA26ZZZ

F. Computer program TRS/Angle

G. Computer programs MA27ZAZ and MA27ZCZ

H. Computer program MA27ZDZ

a. Gerber Digital Data Reduction System

The Gerber digital data reduction system contains three basic pieces of equipment: The Gerber digital reader, the IBM typewriter, and an IBM 026 keypunch.

Figure 155 shows the Gerber digital reader. The positions of the movable hairlines are displayed on the Nixie tubes. This position data can be

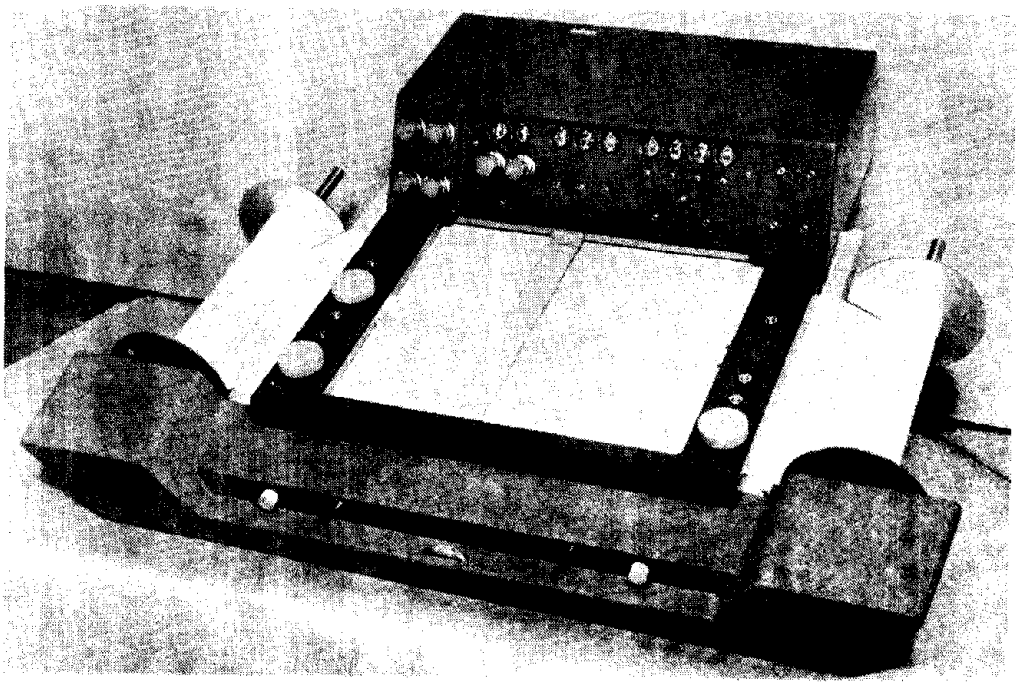

Figure 155. Gerber Digital Reader

output to the typewriter and the keypunch. The oscillograph is read by adjusting the hairlines until they cross at the desired point. The output control is then activated. Prior to running a test sequencer, calibration data for each measurement channel are recorded on the oscillograph.

b. Computer Program MA11ZZZ

This computer program uses the output data cards from the Gerber digital data reduction system along with the calibration information recorded prior to each test. The input is of the following form:

DATA:

	CHANNEL 1	CHANNEL 2		CHANNEL n
TIME,	COUNTS,	COUNTS,	. . . ,	COUNTS

CALIBRATIONS:

VALUE STEP 1,	VALUE STEP 2
COUNTS STEP 1,	COUNTS STEP 2

Two cards for each parameter.

The engineering units data are then calculated in the following manner:

$$EU_i = (COUNTS_i - COUNTS_1)\left(\frac{VALUE_2 - VALUE_1}{COUNTS_2 - COUNTS_1}\right)$$

where: EU_i = Engineering unit value

$COUNTS_i$ = Data count (read from Gerber output)

$COUNTS_1$ = Counts for calibration step 1

$COUNTS_2$ = Counts for calibration step 2

$VALUE_1$ = Value of calibration step 1

$VALUE_2$ = Value of calibration step 2

The engineering unit values are then written on an output data tape.

c. Digitizer

The digitizer reads the FM recorded tape and writes an output digital tape. The digital values written on this tape are directly proportional to the voltage output of the transducers. The UTC digitizer is an integration digitizer (i.e., the input frequency is summed for the entire sample time). Prior to each test sequence, calibration data for each measurement are recorded on the tape.

d. Computer Program MA22ZAZ

This computer program is similar to MA11ZZZ. The major difference is that the input data are on magnetic tape instead of computer cards.

e. Computer Program MA26ZZZ

This program converts the data tape from the IBM 7044 36-bit, floating point word mode into Burroughs-5500 48-bit, floating point word mode, and writes the data on a UTC standard floating data tape.

f. Computer Program TRS/Angle

This program reads the engineering unit floating data tape and calculates the nozzle position, angle, and actuation torque.

The equations used in this program are as follows:

Nozzle Displacements

Axial: $X = K_3 V_3$

where K_3 = potentiometer gain, in./v

V_3 = linear potentiometer 3 displacement from null position

Lateral: $Y = V_1 + V_2 - (K_2)\ (V_1 - V_2)/K_1\ /2 - Y_o$

where V_1 = linear potentiometer 1 displacement from null position

V_2 = Linear potentiometer 2 displacement from null position

$K_2 = R_1 + R_2$

$K_1 = R_1 - R_2$

R_1 = distance from (null) theoretical nozzle intercept point to potentiometer 1

R_2 = distance from (null) theoretical nozzle intercept point to potentiometer 2

Y_o = Value of Y at t = 1 sec

Deflection Angle (Radians)

$$\theta = \text{arc tan } (V_1 - V_2/K_1)$$

Actuation Torque

$$T = L\ (P_1 A_1 - P_2 A_2)$$

where L = moment arm (actuator to nozzle theoretical intercept point)

P_1 = hydraulic inlet pressure

A_1 = small area of hydraulic piston

P_2 = hydraulic outlet pressure

A_2 = large area of hydraulic piston.

g. Computer Programs MA27ZAZ and MA27ZCZ

These computer programs read a floating data tape and write an output tape compatible with the CalComp plotter.

h. Computer Program MA27ZDZ

This computer program is a multipurpose calculation program modified for the equations provided by engineering. Angular velocity and accelerations are obtained by differentiating the calculated angle data using the three point second order Lagrange derivation method.

The following equations were used to reduce the data.

$$\theta = 15.58\ (U_1 - U_2)$$

$$\dot{\theta} = \frac{d\theta}{dt}$$

$$\ddot{\theta} = \frac{d^2\theta}{dt}$$

$$T_A = 9.0\ (.626\ Pr - 1.227\ Pc)$$

$$B_F = \frac{T_A - (I_N + I_{F1})\ (\ddot{\theta}/57.3) - (U_S(\theta) - T_H\left(\frac{\dot{\theta}}{1\dot{\theta}1}\right) - T_O}{(\dot{\theta}/57.3)}$$

$$I_F = \frac{T_A - B_{F1}\ (\theta/57.3) - U_S(\theta) - T_H\ \left(\frac{\dot{\theta}}{1\dot{\theta}1}\right) - T_O - I_N}{(\ddot{\theta}/57.3)}$$

where θ = angular deflection, degree

$\dot{\theta}$ = angular velocity, degree/sec

$\ddot{\theta}$ = angular acceleration, degree/sec^2

T_A = actuation torque, in.-lb

B_F = fluid damping, in.-lb-sec

I_F = fluid inertia, in.-lb-sec^2

I_N = nozzle inertia

U_S = seal spring rate

T_H = seal hysteresis

T_0 = seal offset

U_1 = potentiometer 1 output

U_2 = potentiometer 2 output

Pr = actuator pressure rod (psig)

Pc = actuator pressure cylinder (psig)

i. Data Format for the HIPPO Miniseal Static Firing Tape from AFRPL

Contents and Sequence of Data on Tape:

Physical Record No.	Logical Record No.	Parameter Name on Tape
1	1	NUMA, NUMB, NUMC
1	2	ITEMA1 through ITEMA150
1 and 2	3	IHEADA1 through IHEAD600
2	4	ISEQA1 through ISEQA150
2 and 3	5	ICALA1 through ICALA150
3	6	DATA1 through DATA150
3	7	Repeat logical record 6 format for all data values
.	.	
.	.	
.	.	End of tape mark.

Tape Specifications:

A. Seven track

B. Binary tape

C. 556 BPI

D. 150 parameters/logical record

E. CDC floating point for data values.

APPENDIX II

EQUATION DERIVATIONS

This appendix contains the derivations of equations (section II) which describe some of the key TECHROLL seal performance parameters.

1. SEAL FLUID INERTIA AND DAMPING EQUATIONS

Derivation of TECHROLL seal fluid torques was performed in several stages. The number of variables and complexity of the result increased with each successive stage. Only the initial derivation is presented in detail; followup efforts are briefly summarized.

a. Derivation

A cross-sectional sketch of the TECHROLL seal (figure 156) shows it is divided into three rectangular fluid cavities. Fluid in the convolute cavities was assumed to move only axially while in the main cavity the fluid was assumed to move only tangentially around the seal circumference. Fluid flowing between the cavities was neglected. The basic equations were derived at zero deflection and for a seal whose cross-sectional width is much greater than its height. The other assumptions listed below are followed by the result of this first derivation. The equations are derived in detail on pages 188 through 193.

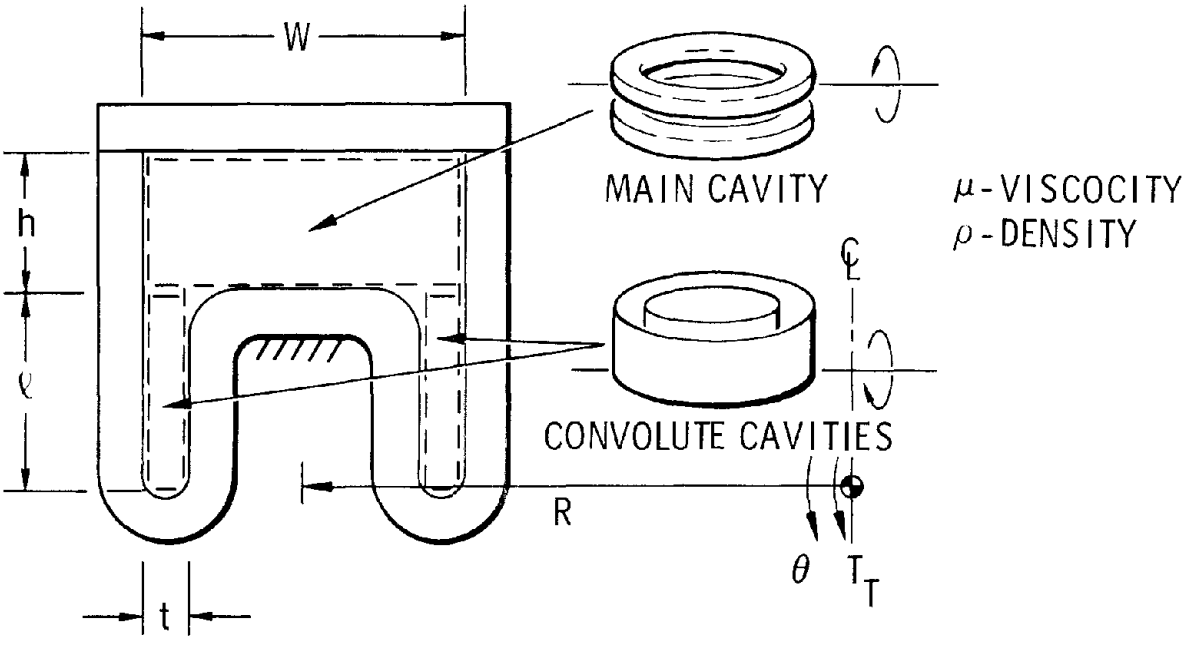

Figure 156. Diagram of TECHROLL Seal Fluid Torque

Assumptions

Fluid - massive, viscous, incompressible

Convolute cavities - damping and inertia torques due to axial fluid motion

Main cavity - damping and inertia torques due to tangential fluid motion

Dimensions - $R >> W >> h >> t$

Angle - small θ; $\sin\theta \approx \theta$

Flow - laminar $\frac{\rho W R^2}{\mu(W+h)}$ $\dot{\theta} < 1{,}000$, quasi one-dimensional

Results

$$T_T = \left[\pi \frac{\rho W R^5}{h} + \pi \rho \ell t R^3\right] \ddot{\theta} + \left[12\pi \frac{\mu W R^5}{h^3} + 2\pi \frac{\mu \ell R^3}{t}\right] \dot{\theta}$$

Derivation

(1) Velocity Torque: $\dot{\theta} > 0$, $\ddot{\theta} = 0$, $W >> h$, $\theta \approx 0$

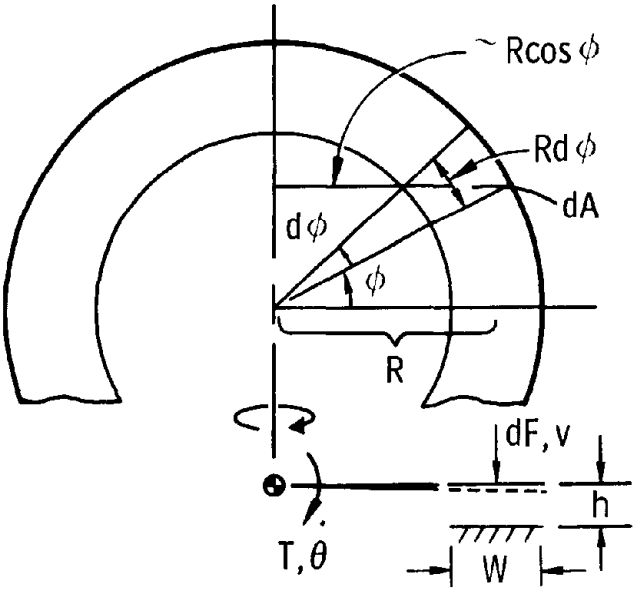

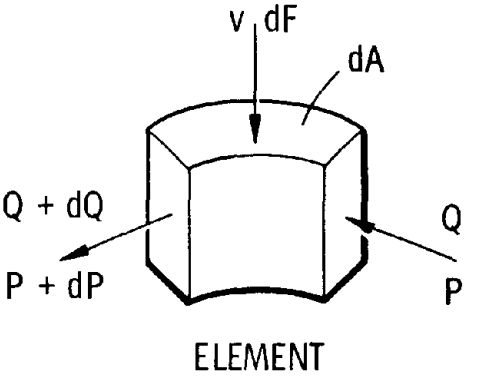

FLOW VELOCITY IN MAIN CAVITY

Fluid conservation in element

$$Q + dQ = Q + vdA$$

$$dQ = vdA$$

$$v = R \cos \phi \, \theta$$

$$dA = WRd\phi$$

$$dQ = WR^2\theta \cos \phi \, d\phi$$

Integrate to get flow as function of angle (ϕ)

$$Q = WR^2 \sin \phi\dot{\theta} + Q_o$$

BC - Q = 0 when $\phi = 0$ due to symmetry; therefore $Q_o = 0$

$$Q = WR^2 \sin \phi\dot{\theta}$$

Pressure distribution due to flow velocity in main cavity

Pressure difference required for laminar flow of a viscous (μ) fluid through a rectangular cross-sectional passage of length (L), width (W), and small height (h)

$$\Delta P = 12 \frac{\mu L}{Wh^3} Q \quad \text{general expression}$$

$$P - (P + dP) = 12 \frac{\mu R d\phi}{Wh^3} \frac{Q + (Q + dQ)}{2}$$

Product of differentials $\left(d\phi \frac{dQ}{2}\right)$ neglected

$$-dP = 12 \frac{\mu R^3}{h^3} \dot{\theta} \sin \phi \, d\phi$$

Integrate to get pressure as function of angle (ϕ)

$$P_I = 12 \frac{\mu R^3}{h^3} \cos \phi \, \dot{\theta} + P_o$$

BC – when $\dot{\theta} = 0$ (regardless of ϕ), $P = P_s$ where P_s is the static pressure caused by thrust on the seal; therefore, $P_o = P_s$

$$P_I = 12 \frac{\mu R^3}{h^3} \cos \phi\dot{\theta} + P_s$$

Torque due to flow velocity in main cavity

$$dT = R \cos \phi \, dF$$

$$dF = PdA$$

$$dA = WRd\phi$$

$$dT = 12 \frac{\mu WR^5}{h^3} \dot{\theta} \cos^2 \phi \, d\phi + WR^2 P_s \cos \phi \, d\phi$$

Integrate from $\phi = 0$ to $\phi = 2\pi$ to get total torque

$$T_{VM} = 12\pi \frac{\mu WR^5}{h^3} \dot{\theta}$$

Two cavities combined to form one at radius R

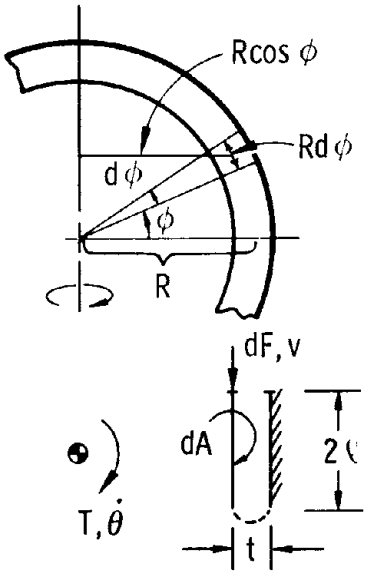

$$dF = \mu \frac{v}{t} dA \quad \text{shear expression}$$

$$v = R \cos \phi \dot{\theta}$$

$$dA = 2\ell Rd\phi$$

$$dT = R \cos \phi \, dF$$

$$dT = 2 \frac{\mu \ell R^3}{t} \dot{\theta} \cos^2 \phi \, d\phi$$

Figure 157. Torque Due to Fluid Shear in Convolute Cavities

Integrate from $\phi = 0$ to $\phi = 2\pi$ to get total torque

$$T_{VC} = 2\pi \frac{\mu \ell R^3}{t} \dot{\theta}$$

(2) Acceleration Torque $\ddot{\theta} > 0$, $\dot{\theta} = 0$

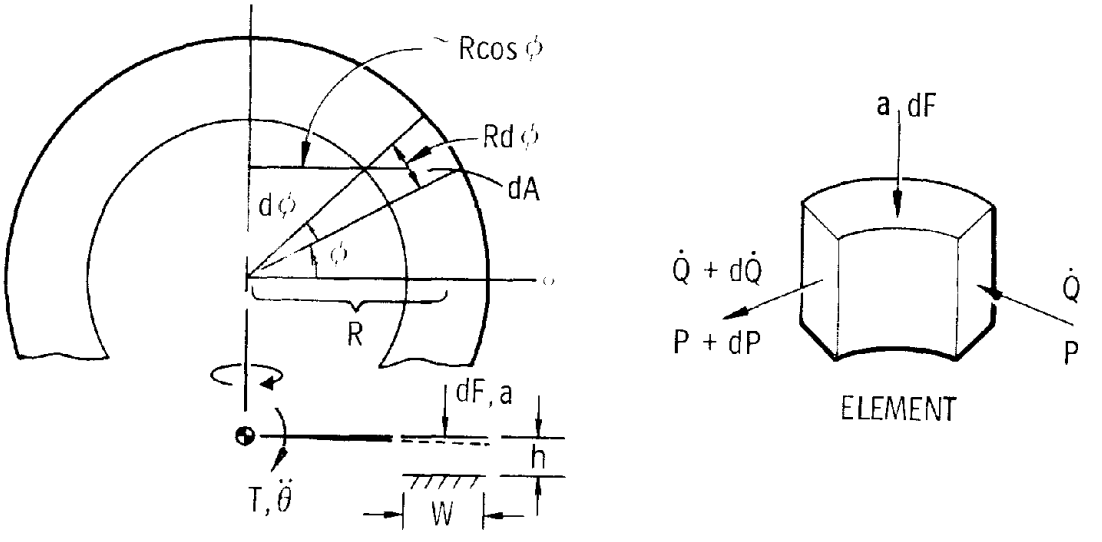

FLOW ACCELERATION IN MAIN CAVITY

Differentiate the velocity expression with respect to time

$$d\dot{Q} = adA$$

$$a = R \cos \phi \ddot{\theta}$$

$$dA = WRd\ \phi$$

$$d\dot{Q} = WR^2\ \ddot{\theta} \cos \phi\ d\phi$$

Integrate to get flow acceleration as function of angle (ϕ)

$$\dot{Q} = WR^2 \sin \phi \ddot{\theta} + \dot{Q}_o$$

BC - $\dot{Q} = 0$ when $\phi = 0$ due to symmetry; therefore, $\dot{Q}_o = 0$

$$\dot{Q} = WR^2 \sin \phi \ddot{\theta}$$

Pressure distribution due to flow acceleration in main cavity

Pressure difference required for acceleration of a massive (ρ) fluid in a rectangular cross-sectional passage of length (L), width (W), and height (h); from F = ma

$$\Delta P = \frac{\rho L}{Wh} \dot{Q} \qquad \text{general expression}$$

$$P - (P + dP) = \frac{\rho R d\phi}{Wh} \frac{\dot{Q} + (\dot{Q} + d\dot{Q})}{2}$$

Product of differentials $\left(d\phi \frac{d\dot{Q}}{2}\right)$ neglected

$$-dP = \frac{\rho R^3}{h} \ddot{\theta} \sin \phi \, d\phi$$

Integrate and apply boundary conditions $P = P_s$ when $\ddot{\theta} = 0$, same as velocity expression.

$$P_I = \frac{\rho R^3}{h} \cos \phi \ddot{\theta} + P_s$$

Torque due to flow acceleration in main cavity

Use same area and moment arms as velocity expression

$$dT = \frac{\rho W R^5}{h} \ddot{\theta} \cos^2 \phi \, d\phi + WR^2 P_s \cos \phi \, d\phi$$

Integrate from $\phi = 0$ to $\phi = 2\pi$

$$T_{AM} = \pi \frac{\rho W R^5}{h} \ddot{\theta}$$

Two cavities combined form one at radius R

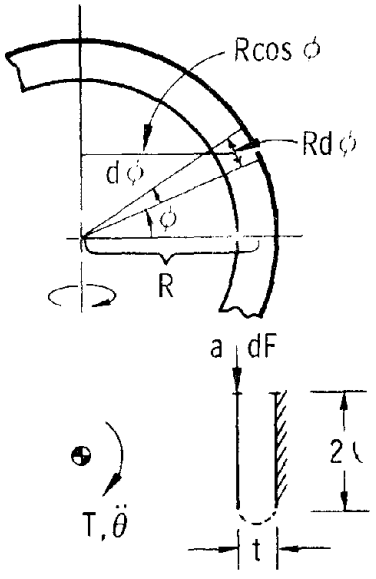

$dF = adm$ Newton's law

$dm = \rho 2\ell t R d\phi$

$a = \frac{1}{2} R \cos \phi \ddot{\theta}$

$dT = R \cos \phi \, dF$

$dT = \rho \ell t R^3 \ddot{\theta} \cos^2 \phi \, d\phi$

Figure 158. Torque Due to Fluid Acceleration in Convolute Cavities

Integrate from $\phi = 0$ to $\phi = 2\pi$ to get total torque

$$T_{AC} = \pi \rho \ell t R^3 \ddot{\theta}$$

When numerical values for several seals were substituted into the basic equations, the convolute expressions proved to be insignificant compared to the main cavity expressions. For simplicity, the convolute expressions were dropped at this point.

The basic derivation presented on pages 188 through 193 is restricted to small deflection angles and a limited number of seal geometries. The derivation was then improved to cover more applications.

The cross sectional shape of the main cavity can vary greatly for different seal geometries. The derivation was modified to include seals with various height-to-width ratios. This affects only the velocity expression not the acceleration expression. The effect resulted in the coefficient of figure 159.

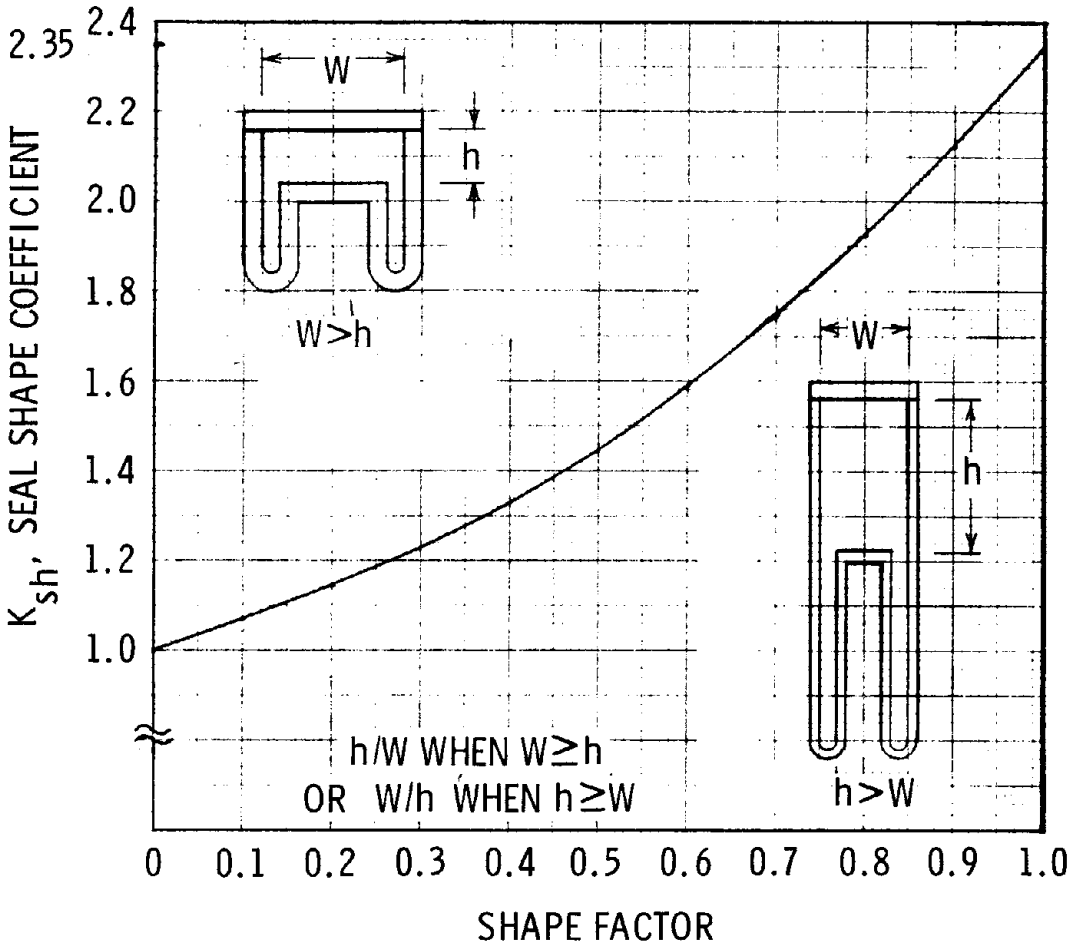

Figure 159. Shape Coefficient for Fluid Pumping Torque

As the deflection angle (θ) varies, so does the main cavity height (h). A variable height ($h-R\theta \cos \phi$) was substituted in the pressure expressions before integrating (with respect to ϕ). The resulting equations indicate a significant magnification of both velocity and acceleration torques at large deflections (figures 160 and 161).

The shape factor obtained should be included as a variable in the deflection expression. An analysis was made by including a linearized shape factor as a variable before the integrations. The results from two cases ($h/w = 1/2$ and $h/w = 2$) agreed favorably with the results from using a constant shape factor. For simplicity, the variable shape factor analysis was not pursued further.

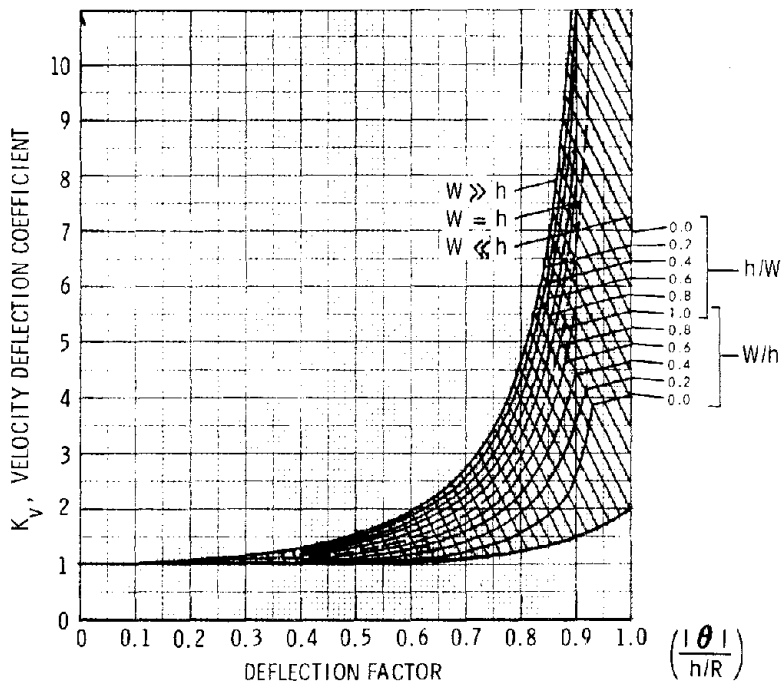

Figure 160. Velocity Coefficient for Fluid Pumping Torque

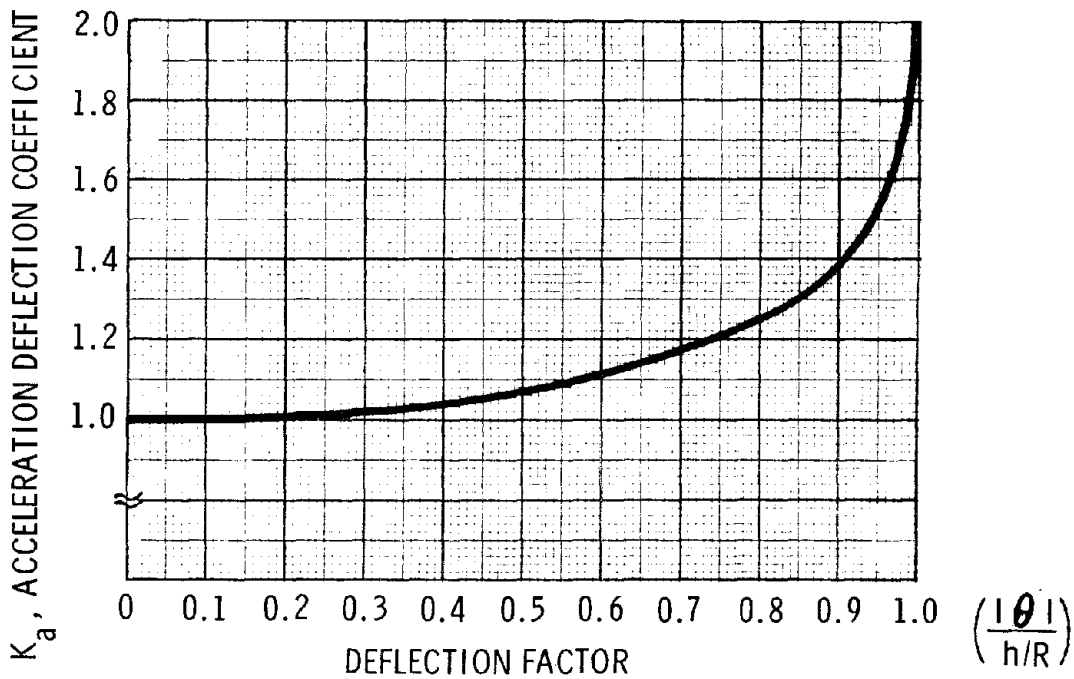

Figure 161. Acceleration Coefficient for Fluid Pumping Torque

Because all seals do not have sidewalls parallel to the centerline, a cone angle factor was included (figure 162). This effect produces a different length along an element ($R\sin\psi d\phi$) and element area ($WR\sin\psi d\phi$). The moment arms remain the same ($R\cos\phi$). Increasing the cone angle reduces the torque slightly but may cause complications (i.e., seal stretch under deflection). This cone angle effect resulted in the coefficient shown in figure 163.

b. Resulting Expressions for Determining Seal Fluid Inertia and Damping Coefficients

Generalized expressions for analytically determining seal fluid inertia and damping are presented below. Numerical values are determined by first establishing seal geometry parameters and then obtaining amplification coefficients (figures 157, 160, 161, and 163).

The fluid used to fill the TECHROLL seal cavity imposes torques during angular acceleration and angular velocity motions of the nozzle due to density and viscosity. The equation used to determine the torque coefficient during angular acceleration is:

$$I_S = \pi K_c K_a \frac{\rho W R^5}{h}$$

where:

K_c = seal cone angle coefficient, 1→0 (figure 5)

K_a = acceleration deflection coefficient, 1→2 (figure 6)

ρ = fluid density, lb-sec^2/in.^{4}

W = seal cavity width, in.

R = seal cavity height, in.

h = seal cavity, height, in.

The equation used to determine the torque coefficient during angular velocity is:

For $W \geq h$

$$B_S = 12\pi K_c K_{sh} K_v \frac{\mu W R^5}{h^3}$$

For $h \geq W$

$$B_S = 12\pi K_c K_{sh} K_v \frac{\mu R^5}{Wh}$$

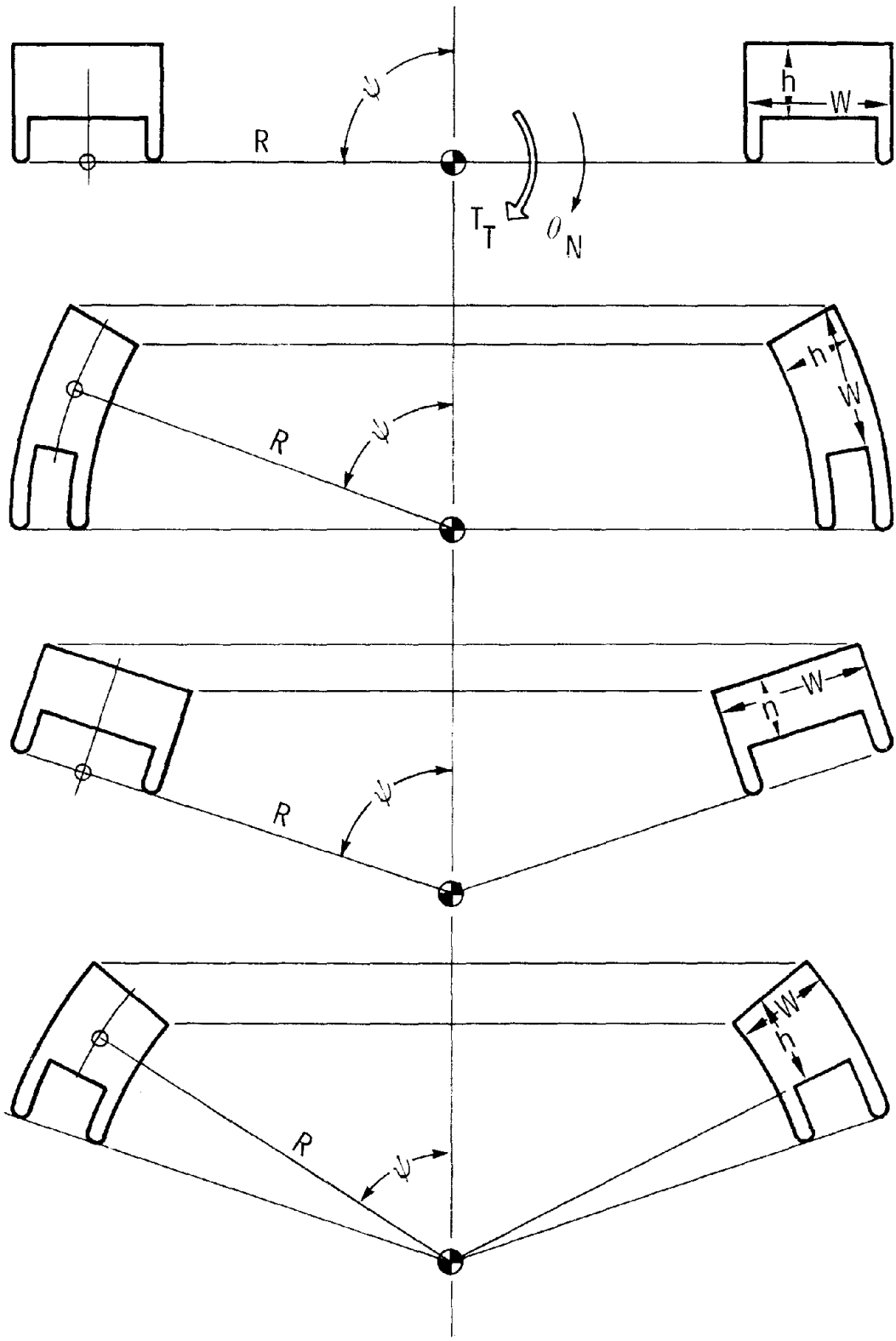

Figure 162. Seal Cone Angle Factor

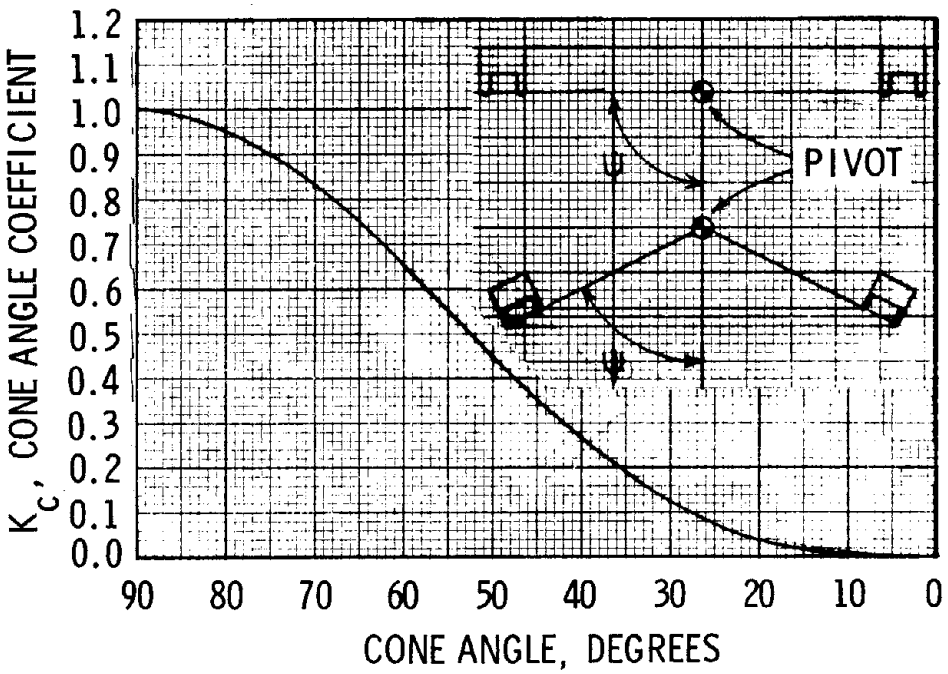

Figure 163. Cone Angle Coefficient for Fluid Pumping Torque

where:

K_{sh} = seal shape coefficient, 1→2.35 (figure 157)

K_v = velocity deflection coefficient, 1→∞ (figure 160)

The density and viscosity of silicone oil, the baseline TECHROLL seal fluid, are given below for ambient temperature conditions:

$$\rho = 90 \times 10^{-6} \text{ lb-sec}^2/\text{in.}^4$$

$$\mu = 50 \times 10^{-6} \text{ lb-sec/in.}^2$$

The above equations were derived prior to the initiation of this program. Further refinements were made during the program. The most recent equations are presented in section III, subsection 4 of this report.

TABLE XXIV

NOMENCLATURE

Symbol	Definition	Unit
R	seal radius	in.
W	seal main cavity width	in.
h	seal main cavity height, $\theta=0$	in.
ℓ	seal convolute cavity height, $\theta=0$	in.
t	seal convolute cavity width	in.
ρ	fluid density	$lb\text{-}sec^2/in.^4$
μ	fluid viscosity	$lb\text{-}sec/in.^2$
$\ddot{\theta}$	angular acceleration	rad/sec^2
$\dot{\theta}$	angular velocity	rad/sec
θ	angular deflection	rad
ψ	cone angle	degree
ϕ	circle angle, $\phi=0 \perp$ to pivot axis	rad
$\dot{Q}$	fluid flow acceleration at ϕ	$in.^3/sec^2$
$\dot{Q}_o$	fluid flow acceleration, integration constant	$in.^3/sec^2$
Q	fluid flow velocity at ϕ	$in.^3/sec$
Q_o	fluid flow velocity, integration constant	$in.^3/sec$
P_I	fluid pressure at ϕ	psi
P_o	fluid pressure, integration constant	psi
P_s	fluid static pressure, $\ddot{\theta}=\dot{\theta}=0$	psi
F	seal force at ϕ	lb
T_T	seal torque, total	in.-lb
T_A	seal acceleration torque, $\dot{\theta}=0$	in.-lb
T_V	seal velocity torque, $\ddot{\theta}=0$	in.-lb
a	boundary acceleration at ϕ	$in./sec^2$
v	boundary velocity at ϕ	in./sec
T_{VM}	torque due to fluid velocity in main cavity	in.-lb
T_{VC}	torque due to fluid velocity in convolutes	in.-lb
T_{AM}	torque due to fluid acceleration in main cavity	in.-lb
T_{AC}	torque due to fluid acceleration in convolutes	in.-lb

2. SUBSONIC SPLITLINE TECHROLL SEAL INTERNAL PRESSURE EQUATIONS

To determine an expression for the pressure in a TECHROLL seal during a test firing, it is necessary to know the entrance cap pressure force and exit cone pressure force.

a. Derivation

(1) Entrance Cap Pressure Force

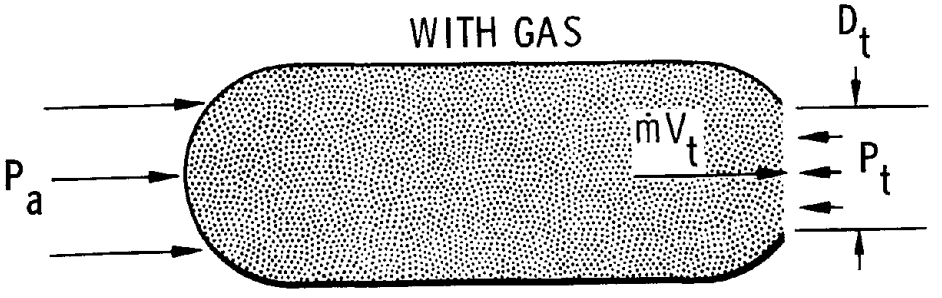

From the sketch above

$$\text{The force due to } \dot{m}V_t = C_{F\ opt} \cdot P_c \frac{\pi D_t^2}{4} \qquad (1)$$

$$\Sigma F_x = 0, \text{ Thrust } F_1 = C_{F\ opt} \cdot P_c \frac{\pi}{4} D_t^2 + (P_t - P_a) \frac{\pi}{4} D_t^2 \qquad (2)$$

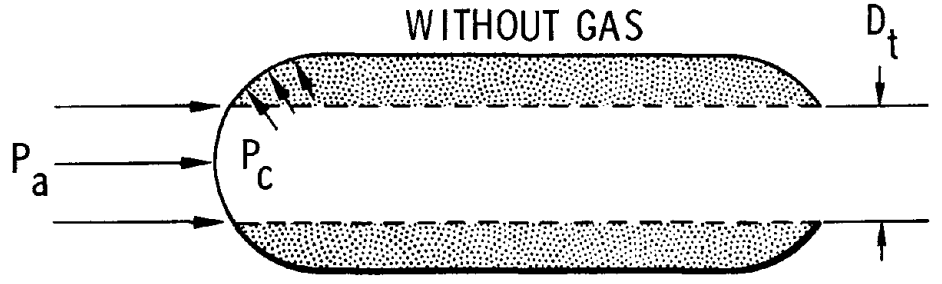

From the sketch above

$$\Sigma F_x = 0, \text{ Thrust } F_1 = (P_c - P_a) \frac{\pi}{4} D_t^2$$

$$+ \text{ entrance cap pressure force} \qquad (3)$$

From equations 2 and 3

$$C_{F\ opt} \cdot P_c \frac{\pi}{4} D_t^2 (P_t - P_a) \frac{\pi}{4} D_t^2 = (P_c - P_a) \frac{\pi}{4} D_t^2$$

$$+ \text{ entrance cap pressure force} \qquad (4)$$

or entrance cap pressure force = $P_c \frac{\pi}{4} D_t^2 \left(C_{F\ opt} - 1\right) P_t \frac{\pi}{4} D_t^2$ (5)

(2) Exit Cone Pressure Force

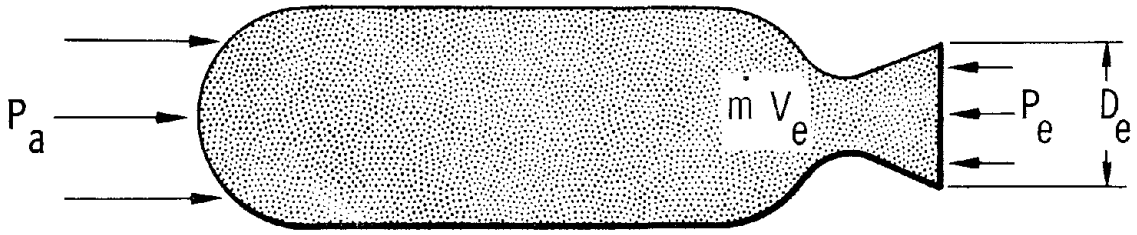

From the sketch above

The force due to $\dot{m}V_e = \eta_{F\ opt_e} P_c \frac{\pi D_t^2}{4}$ (6)

where η_e is the efficiency due to the nozzle divergence loss

$\Sigma F_x = 0$, thrust $F_2 = P_c \frac{\pi D_t^2}{4} \eta_e C_{F\ opt_e} + (P_e - P_a) \frac{\pi}{4} D_e^2$ (7)

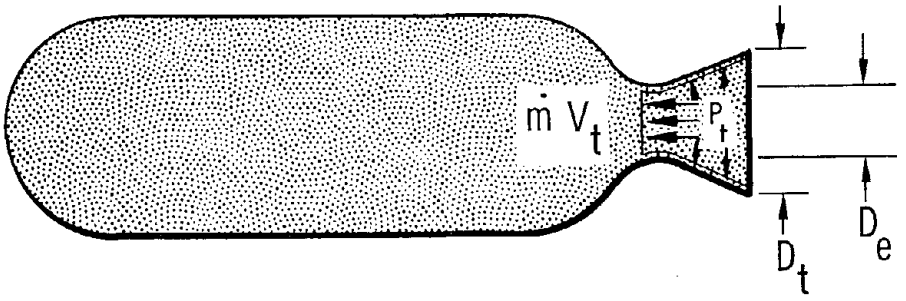

From the sketch above

$\Sigma F_x = 0$, thrust $F_2 = P_c \frac{\pi}{4} D_t^2 C_{F\ opt_t} + P_t \frac{\pi}{4} D_t^2$

$- P_a \frac{\pi}{4} D_e^2$ + exit cone pressure force (8)

From equations 7 and 8; $P_c \frac{\pi D_t^2}{4} \eta_e C_{F\ opt_e} + (P_e - P_a) \frac{\pi}{4} D_e^2$

$$= P_c \frac{\pi}{4} D_t^2 C_{F\ opt_t} + P_t \frac{\pi}{4} D_t^2$$

$$- P_a \frac{\pi}{4} D_e^2 + \text{exit cone pressure force} \quad (9)$$

Therefore, exit cone pressure force $= P_c \frac{\pi}{4} D_t^2 \left[\eta_e C_{F\ opt_e} - C_{F\ opt_t}\right]$

$$+ P_e \frac{\pi}{4} D_e^2 - P_t \frac{\pi}{4} D_t^2 \quad (10)$$

(3) TECHROLL Seal Pressure

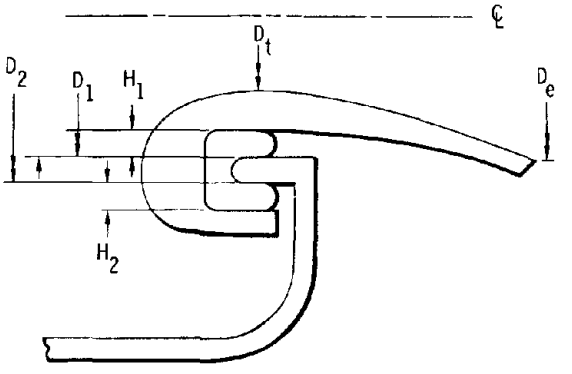

From the sketch above, a free body diagram for the seal and nozzle can be constructed which eliminates seal tensile forces in the X-direction.

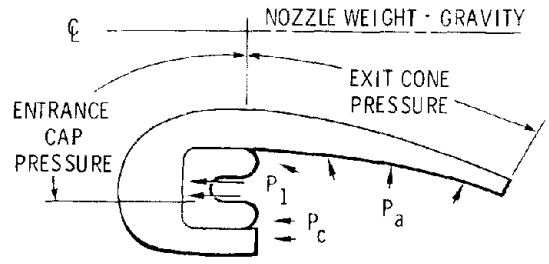

From the sketch above and from equations 5 and 10,

$$\Sigma F_x = 0, \underbrace{P_c \frac{\pi}{4} D_t^2 \left[\eta_e C_{F\ opt_e} - C_{F\ opt_t}\right] + P_c \frac{\pi}{4} D_e^2 - P_t \frac{\pi}{4} D_t^2}_{\text{Nozzle Thrust}}$$

$$+ P_I \frac{\pi}{4}\left[\left(D_2 + H_2\right)^2 - \left(D_1 - H_1\right)^2\right] \qquad (11)$$

$$= \underbrace{P_c \frac{\pi}{4}\left[\left(D_2 + H_2\right)^2 - D_t^2\right] - P_c \frac{\pi}{4} D_t^2 \left[C_{F\ opt_t} - 1\right] - P_t \frac{\pi}{4} D_t^2}_{\text{Blowoff Loads}}$$

$$+ P_a \frac{\pi}{4}\left[D_e^2 - \left(D_1 - H_1\right)^2\right] + Noz \cdot W_t(g)$$

reducing equation 11

$$P_I = \frac{P_c \left(D_2 + H_2\right)^2 - \eta_e C_{F\ opt_e} D_t^2 + P_a \left[D_e^2 - \left(D_1 - H_1\right)^2\right] - P_e D_e^2 + Noz \cdot wt \cdot g \cdot \frac{4}{\pi}}{\left(D_2 + H_2\right)^2 - \left(D_1 - H_1\right)^2} \qquad (12)$$

or

$$P_I = \frac{P_c \left\{\left(D_2 + H\right)^2 - \eta_e C_{F\ opt_e} D_t^2 + \frac{P_a}{P_e}\left[\varepsilon D_t^2 - \left(D_1 - H_1\right)^2\right] - \frac{P_e}{P_c} \varepsilon D_t^2\right\}}{\left(D_2 + H\right)^2 - \left(D_1 - H\right)^2}$$

where $\varepsilon = \frac{D_e}{D_t}$ (13)

APPENDIX III

TEST METHODS

The following test methods were used to perform the bench and static tests discussed in section II.

1. BENCH TESTS

a. Hysteresis/Seal Deflection Test

This test was performed using the configurations shown in figures 164 and 165. After pressurizing the hydrotest fixture, the seal was slowly deflected by a turnbuckle and cable until maximum deflection was attained. The load was measured with the load cell. Deflection angle, radial displacement, and axial displacement were derived from the feedback of potentiometers 1, 2, and 3. The HIPPO miniseal and HIPPO three-layer conventional seals were tested by commanding a closed loop actuation system through a $\pm 10^{\circ}$ triangular wave command of frequency of 0.01 Hz. The actuation torque was obtained from the differential pressures in the equal area actuator.

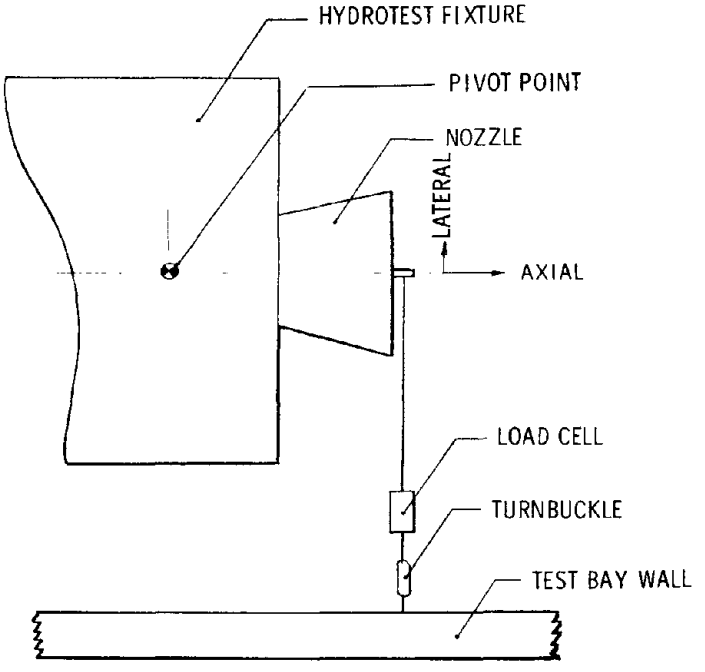

Figure 164. Test Schematic for Determining Minuteman Nozzle Hysteresis/Seal Deflection Torque

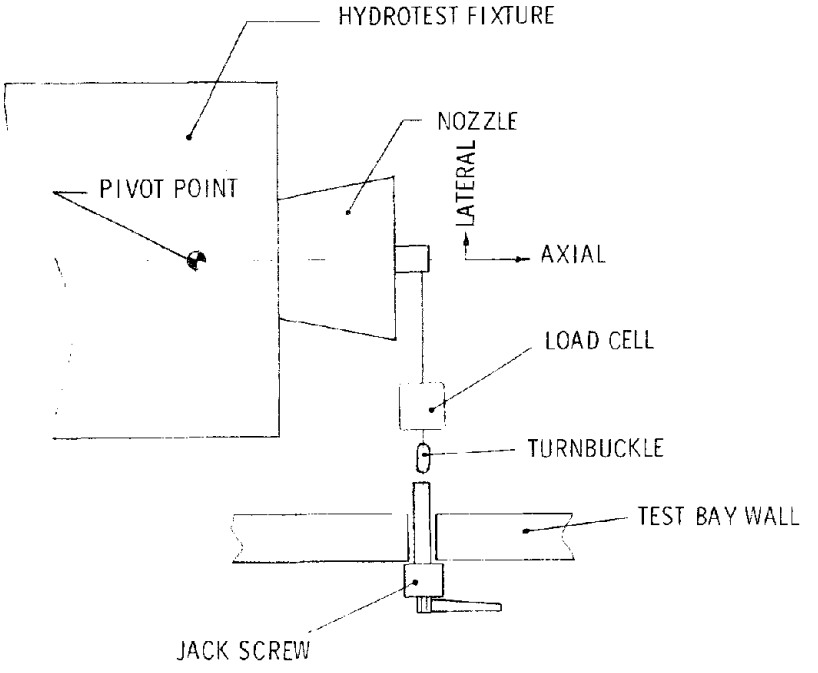

Figure 165. Test Schematic for Determining HIPPO Nozzle Hysteresis/Seal Deflection Torque

b. Axial Spring Rate Test

This test was performed by pressurizing the hydrotest fixture using a GN_2 bottle and hand valve to create a load on the seal. The internal seal pressure from this load was measured. The nozzle axial movement was monitored with potentiometer 3 (figure 166) during pressurization and depressurization to develop a spring rate relationship between internal pressure and axial movement and to determine the axial hysteresis of the seal.

c. Ignition Shock Test

This test was performed using a precharged accumulator with a solenoid valve vented to the hydrotest fixture. At the beginning of the test, the solenoid valve was actuated to produce a shock load simulating motor ignition. The same instrumentation was used as in the axial spring rate test, and the same parameters were monitored.

d. Safety Margin Test

This test was performed in the same manner as the axial spring rate test, but the seal internal pressure was increased until the seal failed or, in the case of the high pressure seals, an upper limit on hardware deformation was reached.

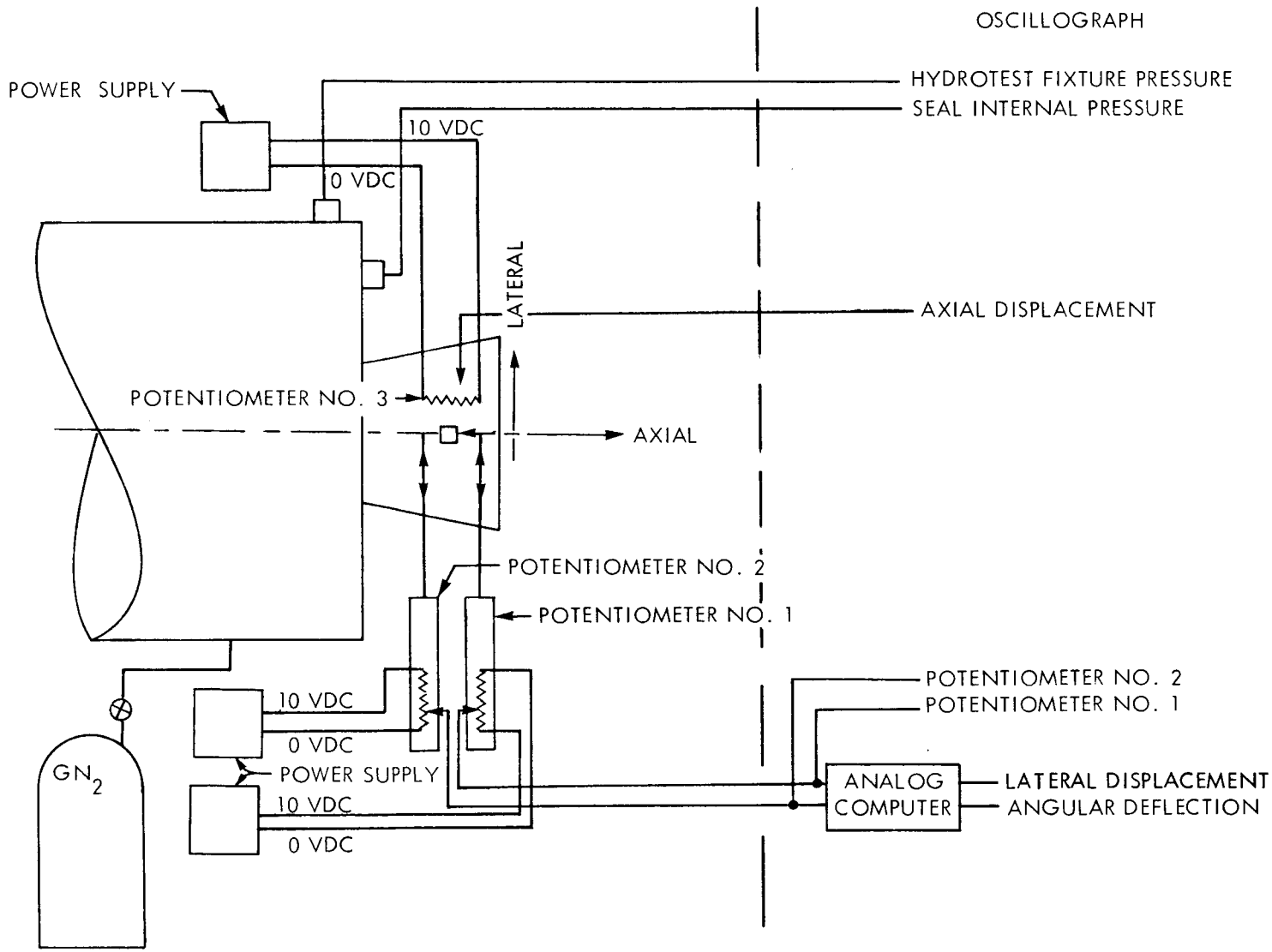

Figure 166. Instrumentation and Retrieval Data Test Setup

e. Simulated Duty Cycle Test

This test was performed using a configuration consisting of the instrumentation and hardware shown in figures 166, 167, and 168. Programmed operation of the solenoid valves for the open-loop test and closed-loop operation using a flow control servovalve provided repeatable nozzle actuation. Deflection angle, axial and radial displacement, and seal internal pressure were monitored as in the previous tests. Hydraulic actuation loads were derived from the differential pressures and area of the actuator piston.

f. Lateral and Torsional Spring Rate

During bench testing of the conventional HIPPO TECHROLL seal in preparation for static firing at AFRPL, testing was conducted to determine the lateral and torsional spring rates of the thick-walled, 0.5-in.-diameter convolute seal. Testing was performed using the setup shown in figures 169 and 170. To determine the nozzle radial stiffness, it was necessary to deflect the nozzle in a purely translative motion. As shown in figure 169, two hydraulic actuators were used to create this motion. Hydraulic actuator loads were derived from the inlet and outlet pressures of the two actuators and the motion from the position potentiometer voltages. To determine the rotational stiffness of the seal about the nozzle major axis, it was necessary to restrain the nozzle from angular deflection with a ball bushing (figure 170). Load was applied with a hydraulic actuator, and deflection was measured with a potentiometer at the end of a beam.

g. Viscous Fluids Special Test

Tests were conducted on a HIPPO TECHROLL seal to determine experimentally the viscous fluid velocity and acceleration related torque parameters and to compare the results with previously derived analytical equations. HIPPO test equipment is shown in figure 171. An existing, unequal area, open loop, hydraulic actuator was used to vector the nozzle in a prescribed duty cycle. Two distinct data acquisition techniques were planned to obtain experimental damping and inertia parameters.

(1). Primary Data: (a) instrument nozzle angle and three seal pressures, (b) compute angular velocities and accelerations, (c) calculate seal pressure/velocity and pressure/acceleration coefficients, (d) compare with theoretical data.

(2). Secondary Data: (a) instrument nozzle angle and two actuator pressures, (b) compute torques, velocities, and accelerations, (c) calculate damping and inertia parameters, (d) compare with theoretical data.

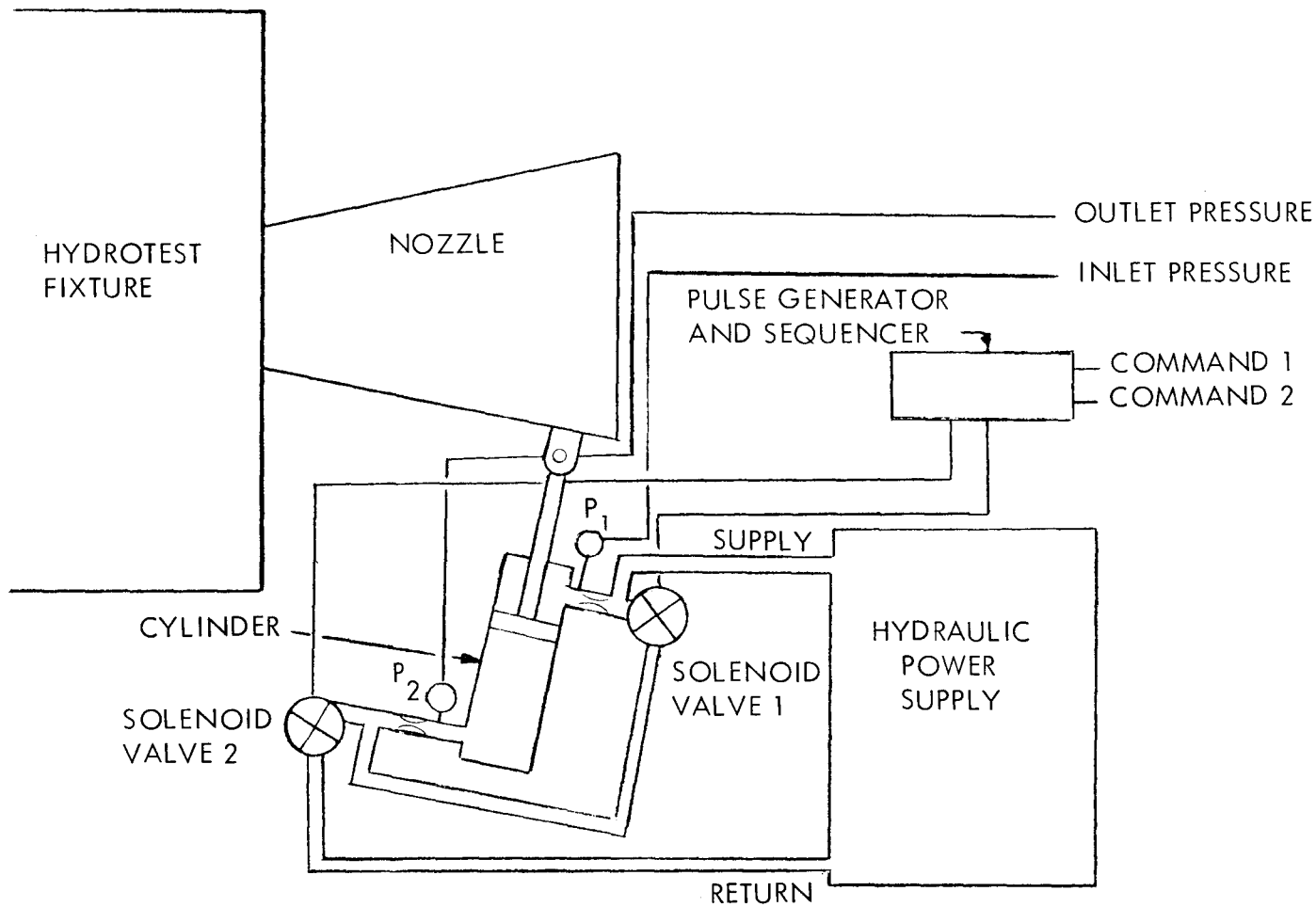

Figure 167. Open Loop Duty Cycle Test Setup
for Minuteman and Conventional HIPPO Nozzles

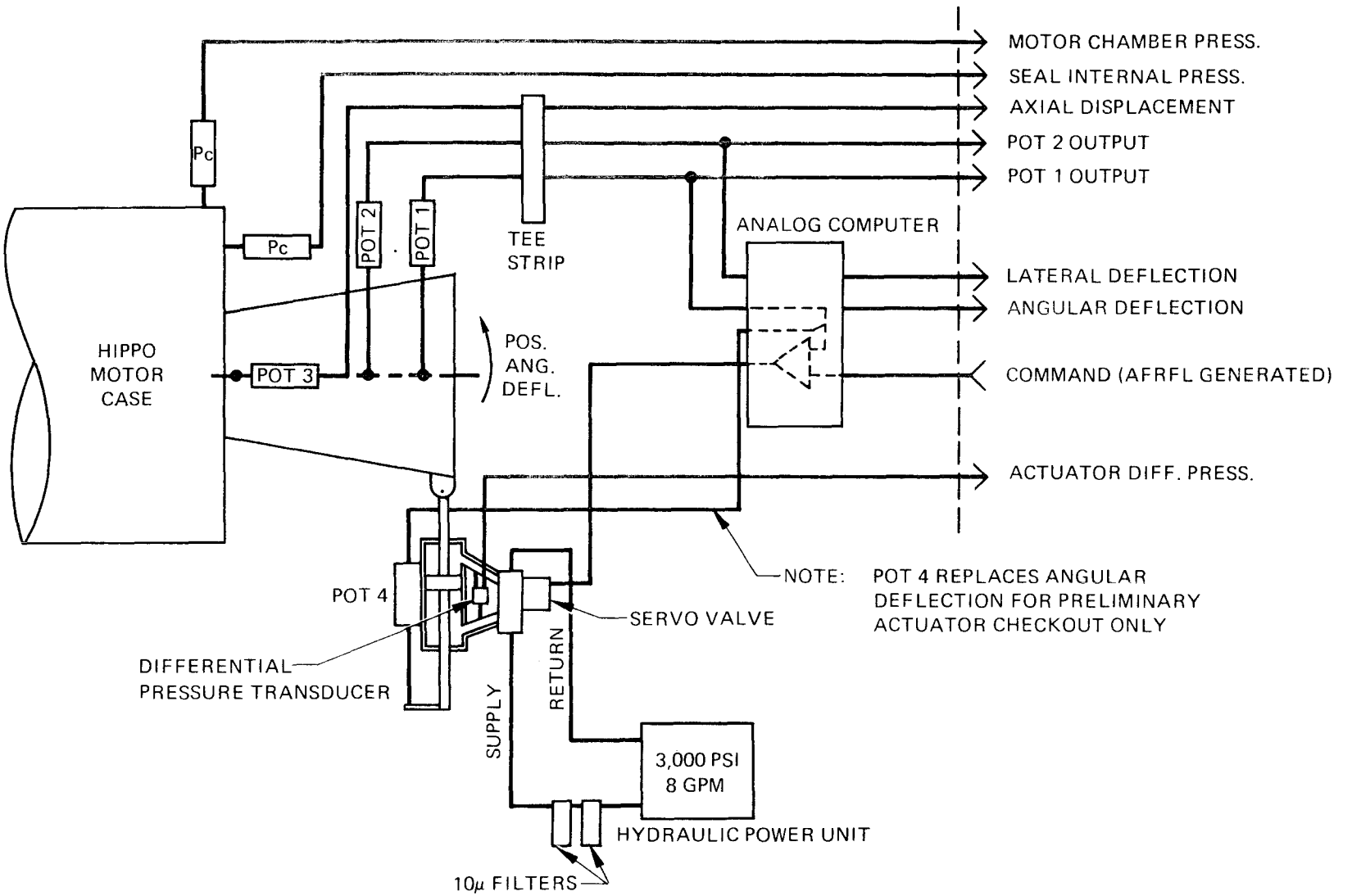

Figure 168. Closed Loop HIPPO (Miniseal) Nozzle Duty Cycle Test Setup

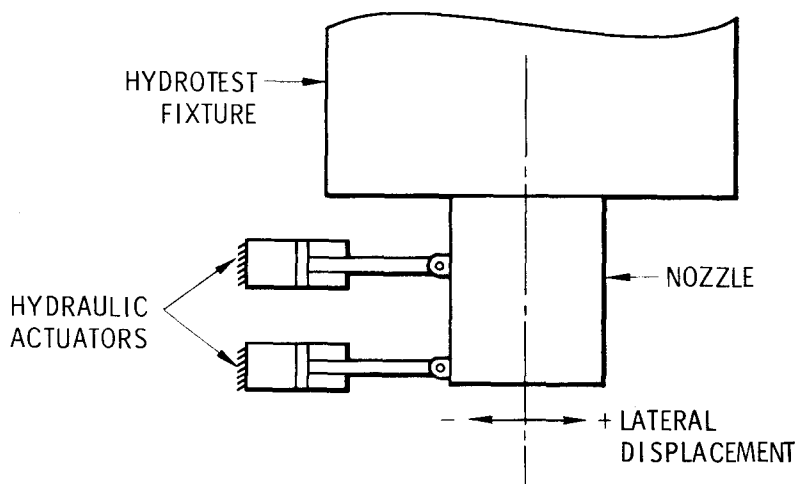

Figure 169. Radial Stiffness Test Setup, HIPPO TECHROLL Seal

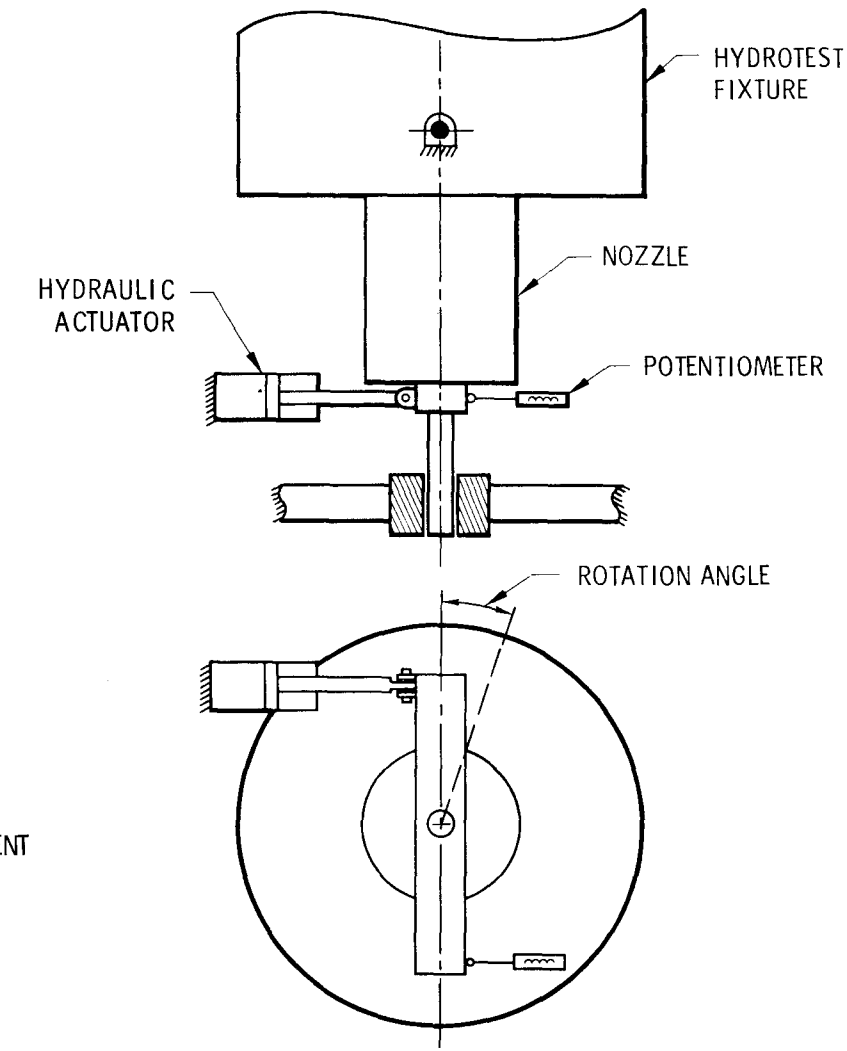

Figure 170. Torsional Stiffness Test Setup, HIPPO TECHROLL Seal

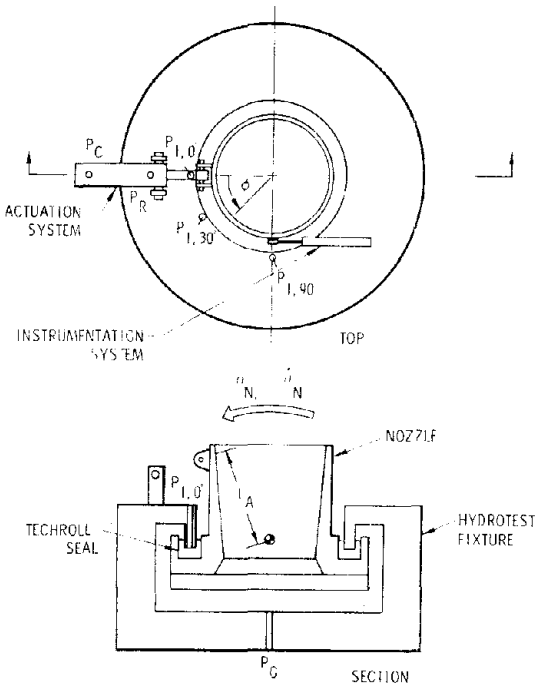

Figure 171. HIPPO Fluid Pumping Test Setup

Midway through the test effort, it became evident that seal pressure measurements were not responding dynamically (probably due to the small size of the passages connecting the transducers to the seal cavity). Therefore, the primary data reduction method was abandoned in favor of the secondary method involving torque measurements.

2. STATIC TESTS

The Minuteman TECHROLL seal movable nozzle system was installed on the Wing 1 stage 2 Minuteman motor in the horizontal test bay at AFRPL. The plane of nozzle actuation was vertical with the actuator at top dead center (figure 172). HIPPO TECHROLL seal movable nozzle systems were installed on the HIPPO motor in the vertical test bay at AFRPL. The plane of nozzle actuation was horizontal (figure 173) and the instrumentation and actuation systems for the conventional HIPPO seals were connected identically to the Minuteman system schematic (figure 174). Table XXV presents the instrumentation specification sheet for the Minuteman and the conventional HIPPO seal tests. The instrumentation and the actuation system for the HIPPO miniseal were connected according to figure 175. Table XXVI presents the instrumentation specification sheet.

As shown schematically in figures 174 and 175, two potentiometers were mounted on different radii from the nozzle pivot point to measure the nozzle deflection angle and pivot point radial movement. A third potentiometer measured the axial movement of the nozzle. The actuation torques

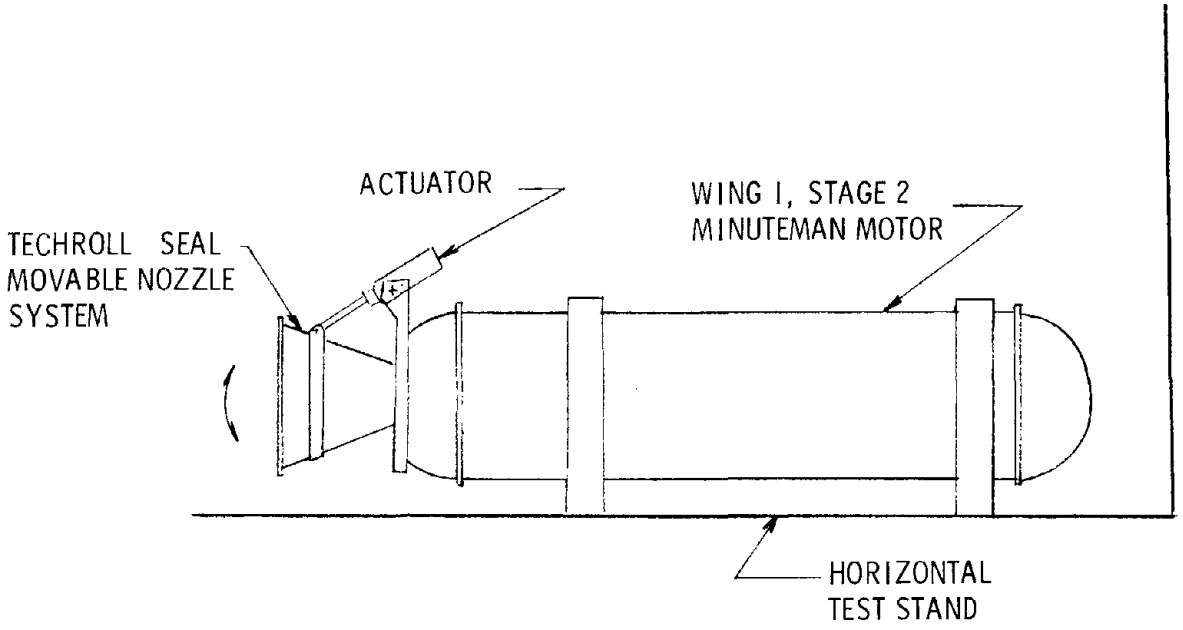

Figure 172. Minuteman Motor Static Firing Configuration

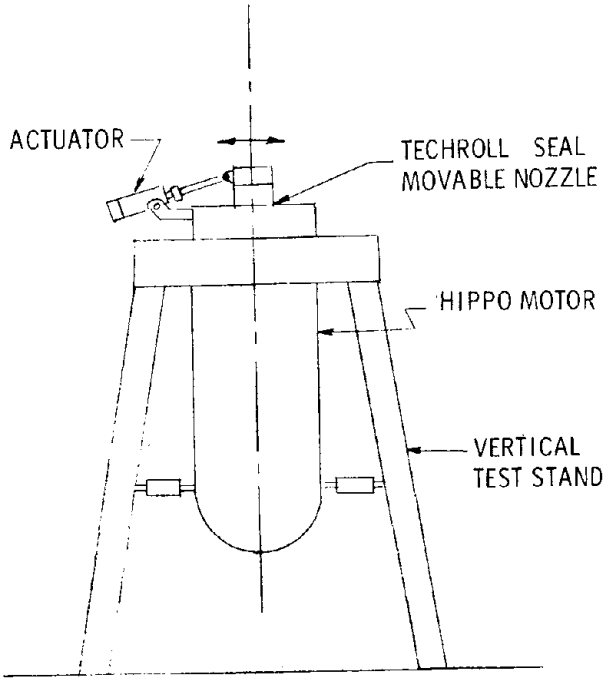

Figure 173. HIPPO Motor Static Firing Configuration

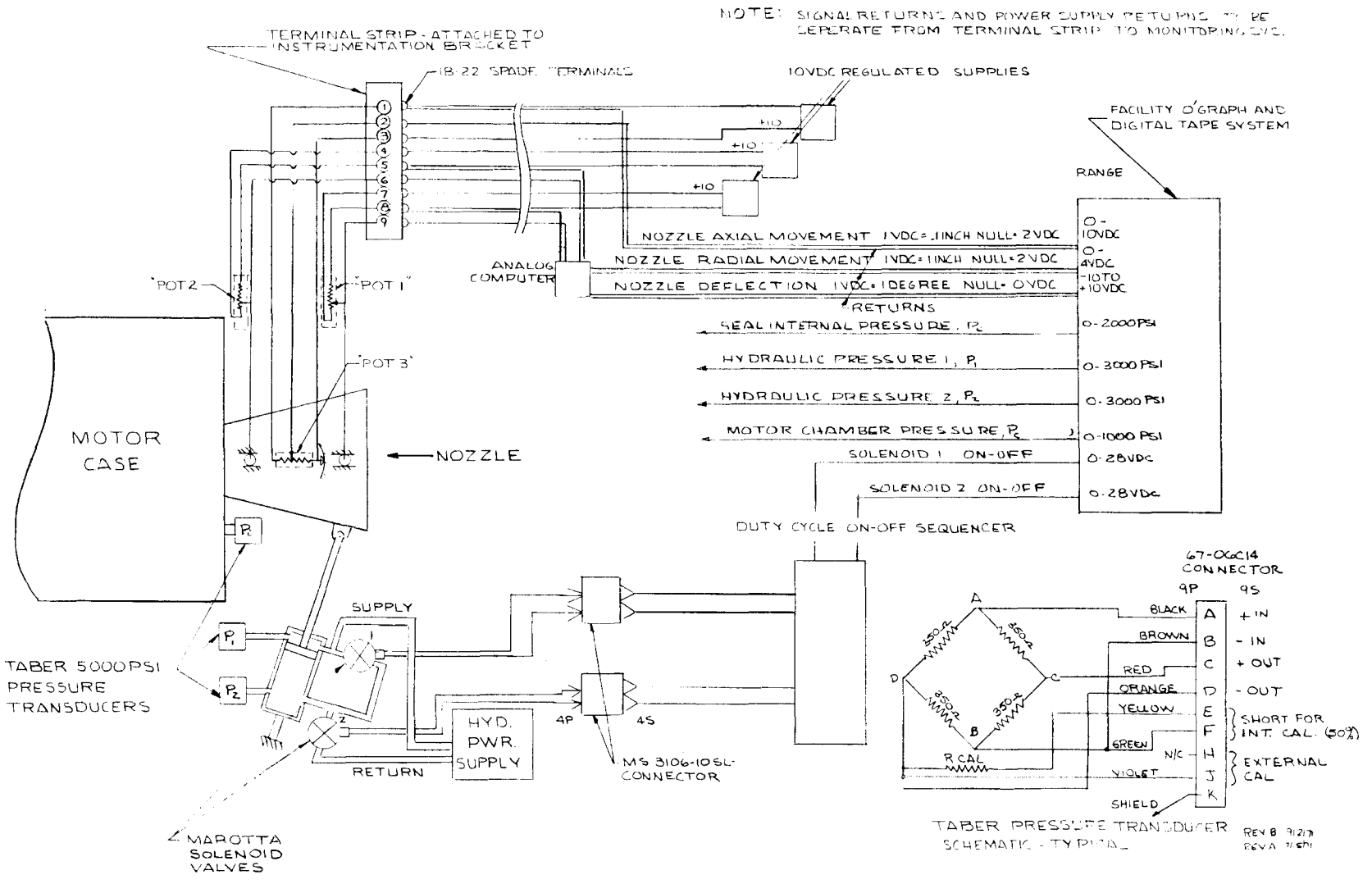

Figure 174. Conventional Nozzle Seal Open Loop Actuation Static Test Schematic

TABLE XXV

INSTRUMENTATION LIST-
OPEN-LOOP ACTUATION

Parameter	Range	Hz	Symbol	Remarks
Digital Tape				
Seal internal pressure	5,000 psi	2,000	PI	---
Pressure, hydraulic No. 1	5,000 psi		P1	---
Pressure, hydraulic No. 2	5,000 psi		P2	---
Voltage (position), potentiometer No. 1	0 to 5 vdc		X1	---
Voltage (position), potentiometer No. 2	0 to 5 vdc		X2	---
Voltage (position), axial	0 to 5 vdc		X3	---
Voltage, solenoid command No. 1	0 to 30 vdc		CMD1	---
Voltage, solenoid command No. 2	0 to 30 vdc		CMD2	---
Pressure, motor chamber	1,000 or 5,000 psi		PC	---
Excitation voltage, potentiometer No. 1	0 to 5 vdc		EX1	---
Excitation voltage, potentiometer No. 2	0 to 5 vdc		EX2	---
Excitation voltage, potentiometer No. 3	0 to 5 vdc	2,000	EX3	---
Oscillograph				
Seal internal pressure	5,000 psi	50	PIO	---
Pressure, hydraulic No. 1	5,000 psi		P10	---
Pressure, hydraulic No. 2	5,000 psi		P20	---
Voltage, position, angular	-5 to +5 vdc		ANGO	0.5 vdc = 1° Null = 0 vdc
Voltage, position, radial	0 to 2 vdc		XRADO	0.5 vdc = 1 in. Null = 1 vdc
Voltage, position, axial	0 to 5 vdc		X30	0.5 vdc = 1 in. Null = 1 vdc
Voltage, solenoid, command No. 1	0 to 30 vdc		CMD10	---
Voltage, solenoid, command No. 2	0 to 30 vdc		CMD20	---
Pressure, motor chamber	0 to 5,000 psi	50	PCO	---

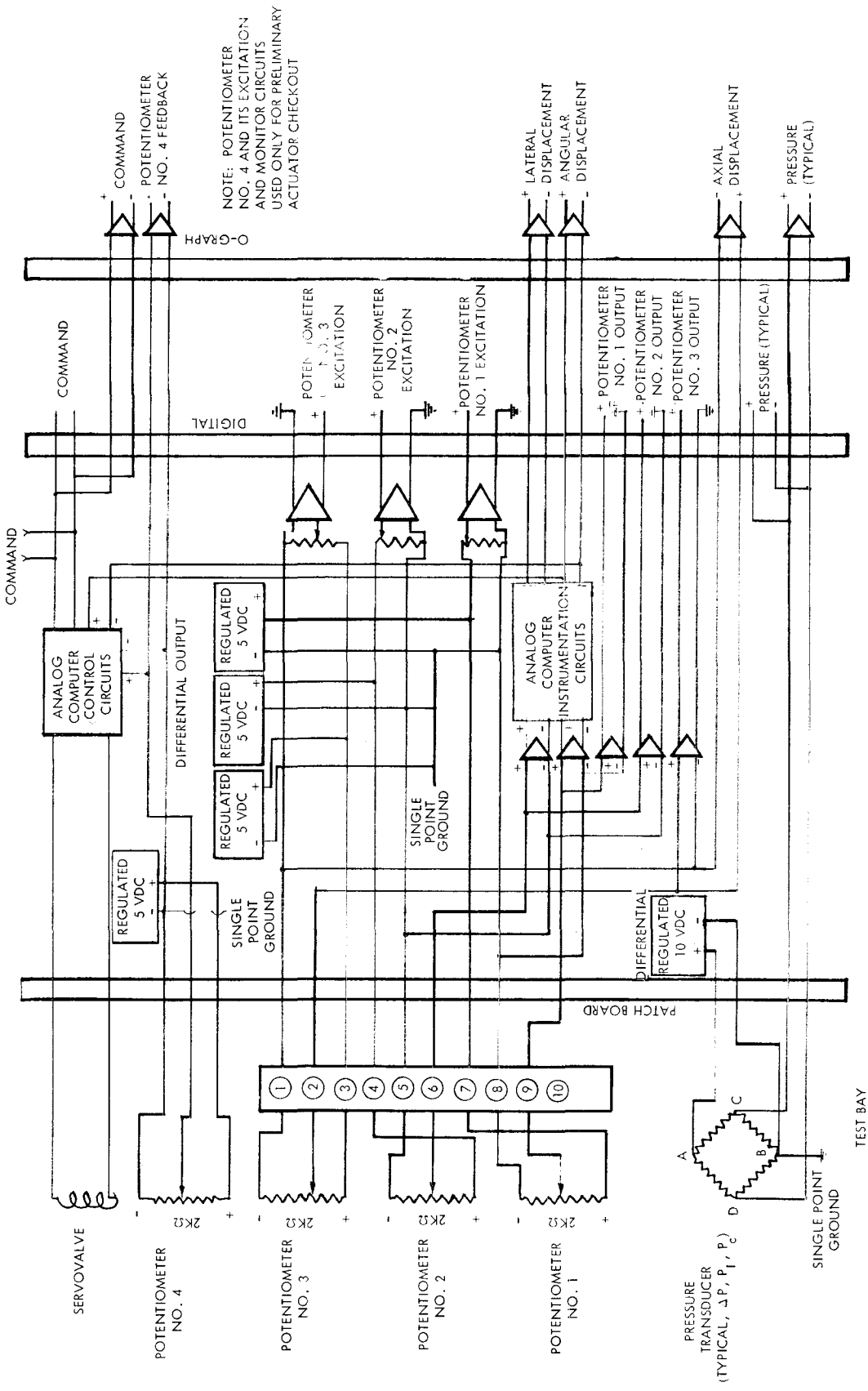

Figure 175. HIPPO Nozzle Closed Loop Instrumentation and Control Schematic

TABLE XXVI

INSTRUMENTATION LIST-
CLOSED-LOOP ACTUATION

Parameters	Range	Response Samples/ sec	Symbol	Remarks
Digital Tape				
Seal internal pressure	6,000 psig	290	PI	---
Pressure, differential	5,000 psid	290	ΔPP1	---
Voltage (position), potentiometer-1	0→5 vdc	290	X1	---
Voltage (position), potentiometer-2	0→5 vdc	290	X2	---
Voltage (position), axial	0→5 vdc	290	X3	---
Pressure, motor chamber	TBS	290	PC	---
Excitation voltage, potentiometer-1	0→5 vdc	290	EX1	---
Excitation voltage, potentiometer-2	0→5 vdc	290	EX2	---
Excitation voltage, potentiometer-3	0→5 vdc	290	EX3	---
Oscillograph				
Seal internal pressure	6,000 psig	50 Hz	PIO	---
Pressure, differential	5,000 psid	50 Hz	DP	1 psid ~ 5.17 in.-lb
Voltage (position), angular	-5→+5 vdc	50 Hz	ANGO	0.5 vdc = 1° Null = 0
Voltage (position), radial	0→2 vdc	50 Hz	XRADO	0.5 vdc = 1 in. Null = 1 vdc
Voltage (position), axial	0→5 vdc	50 Hz	X30	1 v null 0.5 vdc = 1 in.
Pressure, motor chamber	TBS	50 Hz	PCO	---

were determined by measuring the hydraulic pressures on both sides of the actuator piston. These pressures were multiplied by the piston areas and the actuator moment arm to determine actuation torque. To assure a large safety margin of actuation torque, the hydraulic supply pressure was set at 3,000 psi. For the open-loop system duty cycle, the length of time each solenoid valve remained open was controlled precisely by a special sequencer and pulse generator.

A postshipment integrity check was performed prior to each motor firing by pressurizing the seal to approximately 30 psi with a hand pump and monitoring the pressure on the oscillograph.

The output data were converted into nozzle lateral displacement, nozzle axial displacement, nozzle deflection angle, and actuation torques using the relationships and data reduction techniques shown in appendix I.